Cyclin B1 regulation and APC/C processivity in mouse oocyte meiosis I

Scott Thomas Kerridge

160160648

Thesis submitted in accordance with the requirements for the degree of

Doctor of Philosophy

Biosciences Institute

September 2024

Newcastle University

Abstract

Chromosome alignment is orchestrated by the activity of CDK1 bound to its coactivator cyclin B1. Equally important, chromosome segregation is orchestrated by termination of CDK1 activity, driven by cyclin B1 destruction. Both events must be precisely timed by APC/C (Anaphase Promoting Complex/Cyclosome) activity, an E3 ligase that targets cell cycle proteins for destruction via the ubiquitin-proteasome pathway. In mitosis, this system is rapid, robust, and well-studied. Critically, through oocyte chromosome alignment, CDK1 and APC/C activities must be regulated differently, over substantially longer time frames. Specifically, the APC/C must first be dampened to prevent cyclin B1 destruction and CDK1 activity loss as chromosomes begin aligning. This is followed by a period of non-CDK1-bound cyclin B1 destruction during final alignment stages, followed by CDK1-bound-cyclin B1 destruction once fully aligned. This ordering is vital to minimise errors that otherwise cause the cell to arrest (infertility) or produce an embryo that is incompatible with life (miscarriage). However, little is published regarding the molecular mechanism of cyclin B1 targeting in oocytes, or indeed the wider landscape of any APC/C substrate ordering. To address this, I have expressed fluorescent versions of cyclin B1 and APC/C substrates in live mouse oocytes, utilising time-lapse fluorescence microscopy to map their levels and movements through meiosis I. Additionally, I mutated short linear motifs within these substrates, as well as APC/C subunit knockdowns to obtain mechanistic insight into substrate targeting. I reveal that cyclin B1 harbours a motif which boosts its affinity for a specific form of the APC/C during chromosome alignment. This form of the APC/C does not exist globally across the cell, but likely in high priority areas across this spindle zone. This and other insights, describe novel aspects of cell cycle regulation that are critical to produce healthy eggs

Acknowledgements

First and foremost, I would like to thank my friends and family for their unwavering faith and support throughout the past 4-years. I absolutely could not have done this without the constant advice from my parents who have always encouraged me to try my hardest and not give up on anything I do.

I would like to give a massive thanks to my supervisor Dr. Suzanne Madgwick for her constant advice, support and feedback. Suzanne, I could not have asked for a better PhD supervisor. You have kept me encouraged, motivated and determined and you have (many times) gone out of your way to ensure that I have the support I needed. I will always have fond memories of our scientific discussions which always seemed to go way off-topic, owing to our collective love of science. This maintained the momentum of the project and made my PhD a thoroughly engaging and enjoyable experience.

My thanks extend to all members of the Madgwick lab: Dr. Ben Wetherall, the soon to be Drs. Lexy Sarginson, Hania Fiaz and Hammed Takur. We were a great team and it was a pleasure working alongside all of you. Of course, I must also thank our honorary lab member Ava-James Cook.

I would also like to thank all members of the Higgins, Wollman and Rodriguez labs. The shenanigans that went down in our office are too many to mention, from daily game time to movie night and office badminton. When moral hit a low for any of us, we always collectively found ways to reverse it. This is the key to completing a PhD. Without you this would not have been possible.

Additionally, I would also like to thank other labs at Newcastle University that have supported me throughout my entire time at Newcastle University. Namely the Endicott, Gaughan and Perkins labs. I would also like to thank the staff at the Comparative Biology Centre for taking great care of the animals used in this project.

Table of Contents

Table of Figures

List of tables

Chapter 1 – Introduction

1.0 Overview

Oocytes are female germ cells produced in-utero, lying dormant until they are prepared for ovulation and potential fertilisation. Along with male germ cells (spermatozoa), these are the only cells in mammals produced by meiosis. Meiosis is a specialised form of cell division which consists of two rounds of cell division without an intervening S-phase. The goal of meiosis is the production of a haploid cell which is genetically diverse to somatic cells, owing to the homologous recombination of maternal and paternal chromosomes. This both primes the cell with the correct ploidy for fertilisation as well as increases the diversity of the gene pool in the population.

Proper segregation of chromosomes during meiosis is critical, as errors in chromosome segregation often results in cells with an incorrect number of chromosomes, or 'aneuploidy'. Aneuploidies seriously increases the chance of cell line death and are the leading cause of miscarriage and infertility as well as chromosomal disorders in babies which reach term. Importantly, the oocyte only has one attempt at meiosis and lacks apoptotic pathways. This means that erroneously developed oocytes are unable to correct any mis-segregation errors that arise and are also unable to self-destruct. Together, this highlights the importance of meiotic regulation mechanisms which serve to prevent cell cycle progression until correct events occur.

Cyclin B1 is a coactivator for Cyclin Dependent Kinase 1 (CDK1), a kinase which targets a plethora of substrates to drive a significant number of events in meiosis. After the alignment of homologous chromosomes in metaphase of meiosis I, cyclin B1 is thought to be targeted for destruction to inactivate CDK1 and permit chromosome segregation. The Anaphase Promoting Complex/Cyclosome (APC/C) is an E3 Ubiquitin ligase which targets cyclin B1 bound to CDK1 for destruction at this timepoint. The APC/C can be described as a highly efficient runaway destruction machine which absolutely must be halted to prevent cyclin B1 destruction and allow time for chromosomes to be aligned. A number of regulatory

mechanisms exist to prevent the APC/C from targeting substrates during the alignment stage of meiosis. However, meiosis and the oocyte biology are error prone by nature and APC/C slippage does occur.

In 2019, our group discovered that cyclin B1 in mouse oocytes exists in two forms, either bound to CDK1 or unbound. The unbound pool of cyclin B1 is targeted for destruction in late prometaphase I, at a timepoint at which the substrate targeting capabilities of the APC/C are thought to be inhibited. This provides a mechanism which preserves CDK1 activity, subsequently prolonging prometaphase I by preferentially targeting free cyclin B1 over the bound form. The group showed that by removal of this pool of free cyclin B1 substantially increases the frequency of cell division errors. Understanding how this form of non-CDK1 bound cyclin B1 is targeted for destruction will provide substantial insight into APC/C processivity in mammalian oocytes.

This thesis details a series of studies designed to explore APC/C activity in mouse oocyte meiosis I with particular interest in understanding the interaction of cyclin B1 with the APC/C. Briefly, I express fluorescent reporters of cyclin B1 in live mouse oocytes and utilise time-lapse fluorescence microscopy to quantify their destruction over the course of meiosis I. Utilising mutagenesis of APC/C substrates, knockdown of APC/C subunits and protein fusions, I aim to gain further insights into the molecular basis of the interaction between cyclin B1 and the APC/C.

1.1 The key events of oocyte meiosis

Meiosis is a specialised cell division which produces haploid gametes, sex cells which are genetically diverse compared to somatic cells. The haploid cell produced via this process is primed for fertilisation. At fertilisation, haploid sperm and egg combine genetic material and subsequently produce a zygote. This then undergoes multiple rounds of embryonic mitosis to form a blastocyst and eventually the foetus. Meiosis consists of one round of DNA replication followed by two distinct rounds of cell division without an intervening DNA synthesis phase. These division events are termed Meiosis I (MI) and Meiosis II (MII) (Figure 1.1). Male and

female meiosis posess significant differences, going forward in this document ‘meiosis’ will refer to female mammalian meiosis. MI is described as a reductional division whereby one of each homologous chromosome pair (held together by recombination sites called chiasmata) is discarded by the extrusion of the first polar body (PB1) at anaphase I (AI) with the remaining pair being retained in the MII oocyte. The oocyte (often now termed an egg) then arrests in MII until it is fertilised. MII, described as an equational division, is much more analogous to mitosis. Here, sister chromatids segregate but again, half of the genetic material is discarded in a second polar body (PB2). Therefore, unlike spermatogenesis which results in four haploid progeny, oogenesis produces a single viable cell. This strategy is essential for the oocyte to maintain the huge cellular volume necessary for multiple rounds of mitotic divisions in the first stages of zygote development[1].

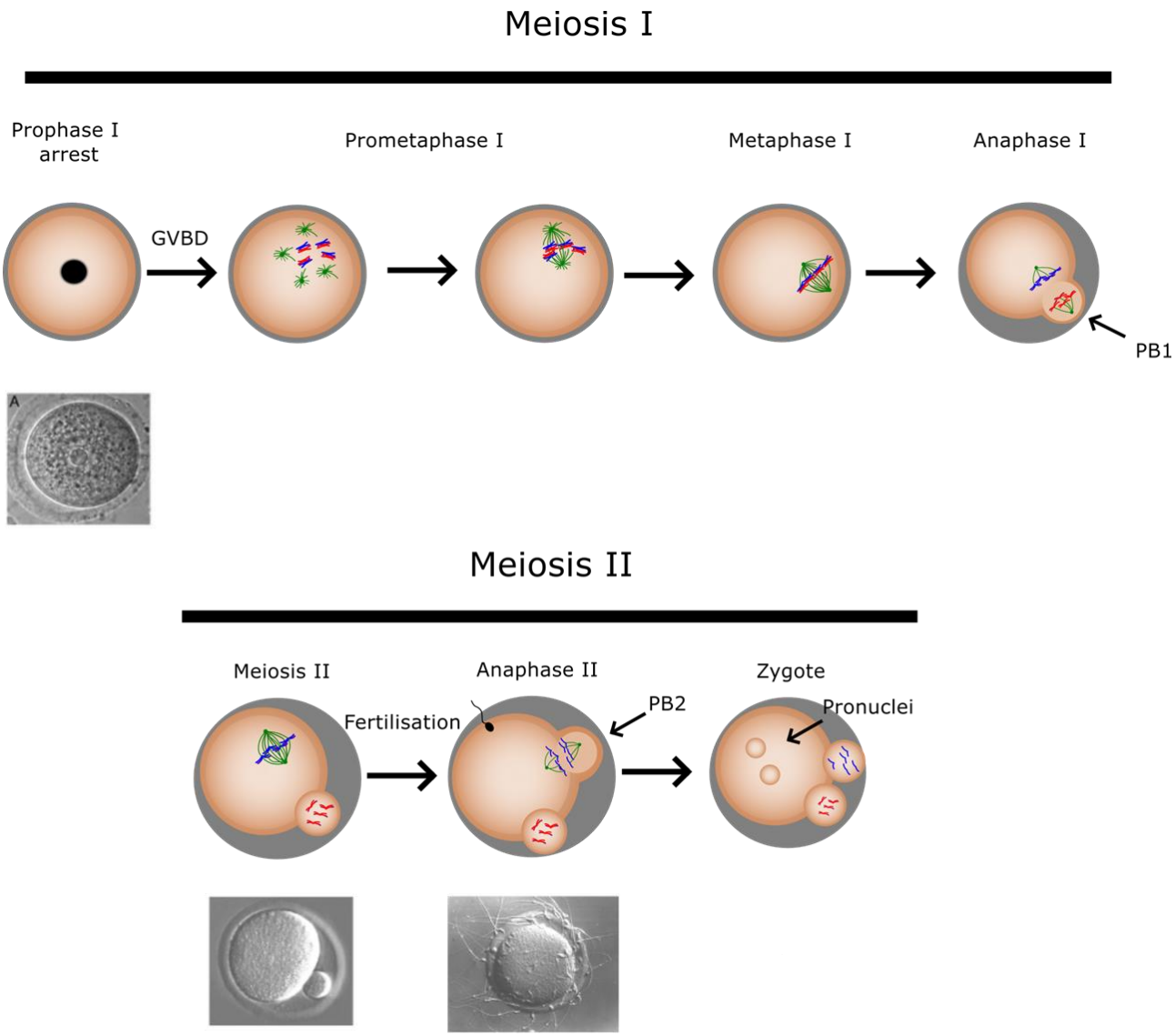

Figure 1.1. Outline of female mammalian meiosis I and meiosis II.

Oocytes are arrested in prophase I until ovulation when periodically a select few oocytes complete their growth and resume meiosis and undergo GVBD. The oocyte enters a lengthy period of chromosome. After successful chromosome alignment and spindle attachments to chromosome kinetochores, the chromosomes are segregated with half of the genetic material being retained in the oocyte, and the other half being extruded in the first polar body, described as a reductional division. The oocyte enters meiosis II and begins a second period of chromosome alignment in where chromosomes fully align in metaphase II and the oocyte awaits fertilisation to occur. Introduction of a second complement of genetic material from the spermatozoa results in anaphase II occurring and the extrusion of a second polar body via a equational division. Subsequently, a zygote is produced which harbours two pronuclei, one maternal and one paternal, which undergoes multiple mitotic events to produce a blastocyst and early embryo

1.1.1 Oogenesis to prophase arrest

Prior to meiosis, gametogenesis must occur. In female mammalian species, gametogenesis produces oogonia, diploid pre-cursor oocytes. Oogenesis begins with undifferentiated sexually dimorphic primordial germ cells in foetal ovaries. These differentiate into oocytes in the 12th week of gestation (between E12.5 and E13.5 in mouse oocytes) which results in the transition from mitosis to meiosis. The newly formed oocytes harbour two homologous copies of each chromosome, one from each parent, which replicates to form two sister chromatids during the pre-meiosis S-phase[1,2].

The first stage of meiosis I is prophase I, which occurs in the ovaries of the foetus while *in-utero*. Here, chromosomes pair as homologs and recombination occurs to increase genetic diversity in the resulting egg. Prophase I can be further divided further into substages (Figure 1.2) [3]:

- Leptotene: chromosomes condense and form long thread like structures and the process of recombination begins. At this stage, the chromosomes gather towards one side of the nucleus in a bouquet arrangement, aligning towards the centrosome[4].
- Zygotene: homologous chromosomes pair and begin to form bivalents. The chromosome axes begin to close together and form a synapse.
- Pachytene: full synapsis occurs between homologs via the formation of the synaptonemal complex. During this stage recombination occurs. In most but not all mammals, recombination is initiated by the formation of DNA recombination hotspots. These sites are marked by a DNA-binding Zinc finger domain protein, PRDM9, which trimethylates histone H3 on lysine 4 (H3K4Me3) and associates them with the chromosome axis. A portion of these hotspots, undergo double-strand breaks by topoisomerase-like protein, SPO11[5]. Synapsis and double-strand break repair occur via the action of recombination-processing proteins such as RAD51, DMC1, RPA and MSH4/MSH5 which form recombination nodules, located on the synaptonemal complex. The double-strand breaks formed at this stage are mostly resolved by non-crossovers whereby no exchange of sequences occur. However, a

small subset are resolved as crossovers, where maternal and paternal DNA are exchanged [6]. Ultimately, this process results in a mixture of alleles and increases genetic diversity between sister gametes. This ultimately provides the foundation for uniqueness between individuals and is a driving force for evolution.

- Diplotene is the final stage of Prophase I. This stage typically occurs around the time of birth. During this stage, chromosomes desynapse in preparation for the first meiotic division. Importantly homologous chromosomes remain together as single bivalent units due to the chiasmata produced during crossover events during pachytene, acting as physical connections[6]. Each oocyte at this stage becomes surrounded by pre-granulosa cells in a structure referred to as the primordial follicle. One of the more prominent features of the oocyte at this stage is the presence of a central Germinal Vesicle (GV), which contains chromatin and is akin to the nucleolus of a mitotic cell (Figure 1.1).

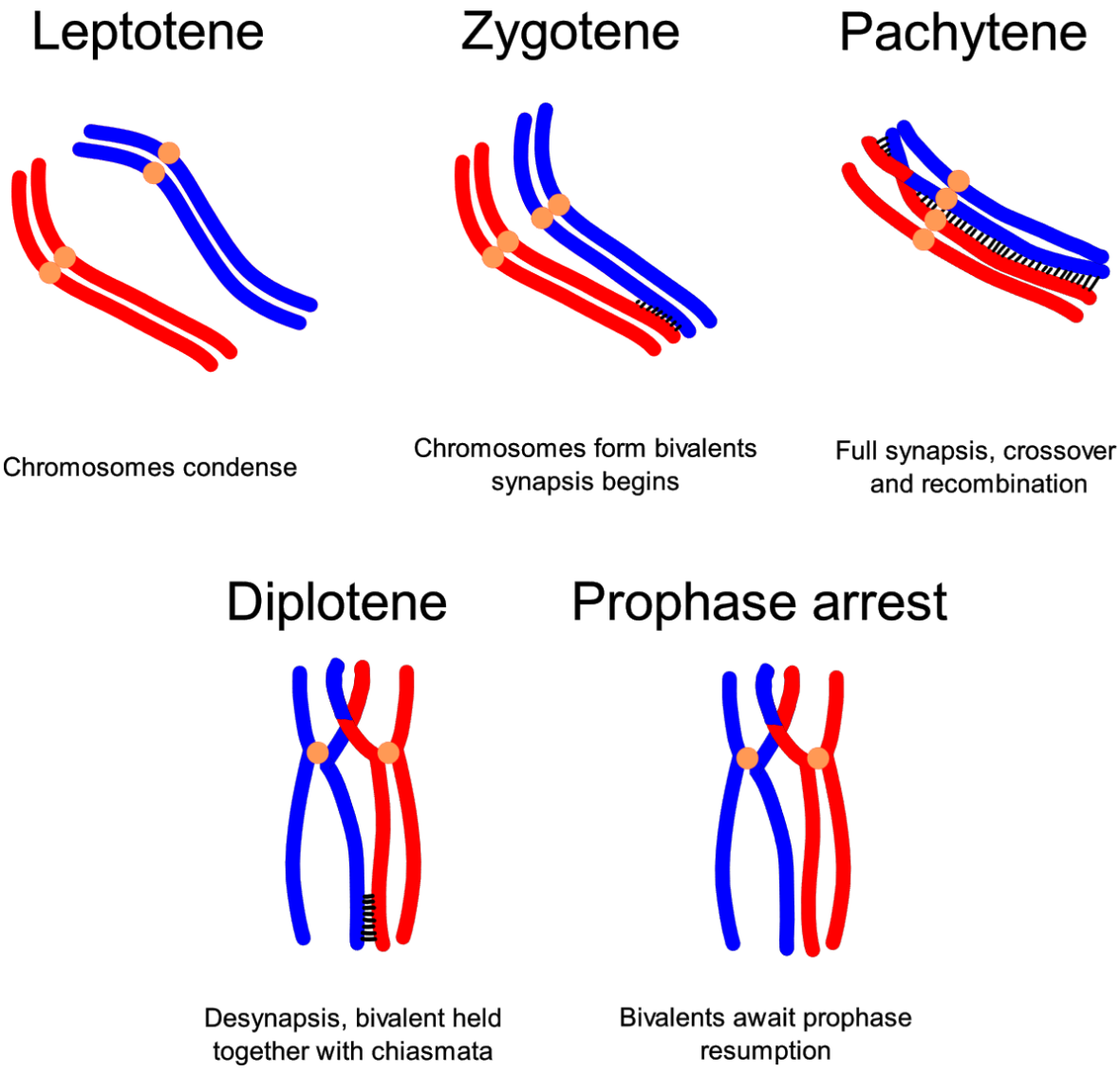

Figure 1.2. Chromosomal arrangements in prophase I

Prophase I begins with the Leptotene stage whereby chromosome condense, marked by the chromosomes forming long thread-like structures. In zygotene, homologous chromosomes pair to form structures called bivalents, held together by the formation of the synaptonemal complex. In pachytene the synaptonemal complex occupies the full length of the bivalent structure. Cross-over and recombination occurs which ultimately increases genetic diversity in sister gametes and eventual offspring. This produces regions of crossover called chiasmata which hold the bivalents together after desynapsis in Diplotene. After the formation of bivalents linked by chiasmata, the cell enters a lengthy period of prophase I arrest until ovulation. Figure adapted from:[7].

Oocytes then arrest at this stage, in diplotene of prophase I for an extended period of time depending upon the species. For example, decades in humans, and months in mice. This arrest is sustained due to elevated intracellular cyclic AMP (cAMP) levels, which are maintained via endogenous cAMP production via its synthesis from adenylyl cyclase by phosphodiesterases. Intercellular communications via gap junctions with granulosa cells, which surround the oocyte at this stage, also provide a source of exogenous cAMP to maintain arrest[8,9].High levels of cAMP activate protein kinase A which in turn inactivates Cyclin Dependent Kinase 1 (CDK1). CDK1, a kinase referred to as 'the master regulator of the cell cycle', coordinates hundreds of cellular processes and drives chromosome alignment. cAMP induced inhibition of CDK1 therefore prevents meiosis resumption[10]. The importance and function of CDK1 will be discussed extensively in later sections.

By this point in development there has been a substantial loss of oocyte number. In the foetal stage, millions of primordial germ cells occupy the ovaries, and by the time of birth, over two-thirds are lost in humans[11]. One significant reason is due to the difficulty of completing crossover in prophase I and being unable to successfully repair or resolve double-stranded breaks or defects in synapses, leading to apoptosis. Most oocytes die before their surrounding of pre-granulosa cells in diplotene (attrition) or at a later stage in development as follicles break down (atresia). By the end of diplotene, the oocyte has changed significantly from its parental somatic cell, not only in terms of ploidy and genetic diversity. The oocyte is transcriptionally inactive as chromosome condensation significantly perturbs transcription capabilities. Translation of proteins relies on massive stores of mRNA in the oocyte which have accumulated throughout its development[12]. Fully grown oocytes also present with a decreased capacity to respond to apoptotic signals from diplotene going forward, owing to a decrease in TAp63 expression which prevents the activation of the DNA-damage response pathway. This means that oocytes are able to develop with DNA damage, with only high levels of damage able to activate a response[13].

Notably, though prophase I arrest is a pause in the cell cycle. Oocytes still grow in size, most importantly over periods prior to ovulation once sexual maturity is reached. Ovulation is

then induced by hormonal cues, such as a rapid increase in luteinizing hormone and follicle stimulating hormone where many more oocytes are prepared than are actually ovulated. For example, typically in each human menstrual cycle 10-20 arrested oocytes resume meiosis with only one being ovulated[14].

1.1.2 Meiosis resumption

In response to hormonal cues, intracellular cAMP reduces and the cAMP induced inhibition of CDK1 is relieved, permitting meiosis resumption. The now active CDK1 phosphorylates and inhibits PP1 phosphatase, resulting in the maintenance of phosphorylation on laminin A/C leading to Germinal Vesicle Breakdown (GVBD)[15]. The MI microtubule spindle forms and migrates to the cortex of the oocyte. Herein 'spindle' refers to the microtubule spindle that captures and aligns chromosomes by kinetochore microtubule attachments.

After GVBD, the oocyte enters prometaphase, a lengthy period of spindle establishment and chromosome alignment. The goal of this stage is to organise chromosomes in such a way that an equal division of chromosomes can occur. In MI chromosomes are organised as pairs of homologous chromosomes, linked by chiasmata. Sister kinetochores are paired in this arrangement. To segregate properly, two sister chromatid kinetochores must co-orient and the kinetochores of homologous chromosomes must attach to spindle from opposite poles[16]. This attachment style ensures that one of each pair of homologous chromosomes segregate to each daughter cell, producing a daughter with the correct ploidy. Most strikingly, prometaphase operates over a completely different time frame in meiosis compared to mitosis. While prometaphase only lasts a matter of-minutes in mitosis, in the mouse oocyte this can last 12 hours, 24-hours in a human oocyte. The reasons for this significant length difference are owed to the key events in prometaphase which will be discussed further below. Importantly this significant time difference of prometaphase and the challenges of this process in the oocyte require different cell cycle regulation.

Following GVBD, during the initial events of prometaphase, a "wait-anaphase" signal is produced by the Spindle Assembly Checkpoint (SAC). It is important to state that our current

understanding regarding the SAC is largely derived from studies in mitosis. While it can be thought that there will be substantial similarities between the SAC in mitosis and meiosis, there will undoubtably be differences, owing to the properties of the oocyte. The SAC will be detailed extensively in a later section, but briefly, the SAC acts to produce 'Mitotic Checkpoint Complexes' (MCCs). MCCs are constantly produced at unattached kinetochores lacking tension, which diffuse across the cytoplasm to reach their target, the Anaphase Promoting Complex/Cyclosome (APC/C). This is a massive multi-subunit E3 Ubiquitin ligase which targets cell cycle proteins for destruction via the ubiquitin-proteasome system to drive the cell towards anaphase[17,18]. MCC binding to the APC/C manipulates the APC/Cs substrate recognition capabilities, altering the speed of cell cycle progression and ultimately preventing its ability to target the substrates which are required to be degraded to permit anaphase I (for example cyclin B1)[19]. As an essential stoichiometric activator of CDK1, cyclin B1 stabilisation by the MCCs action on the APC/C maintains CDK1 activity and permits prometaphase I progression. The result is that while chromosomes are still establishing proper microtubule-kinetochore attachments, cyclin B1-CDK1 activity is preserved to prevent premature anaphase (Figure 1.3). The name "Mitotic checkpoint complex" highlights how we understand this structure, that is its formation and function has largely only been explored in mitotic cells. Yet those who have explored this complex in oocytes have discovered differences in how it operates.

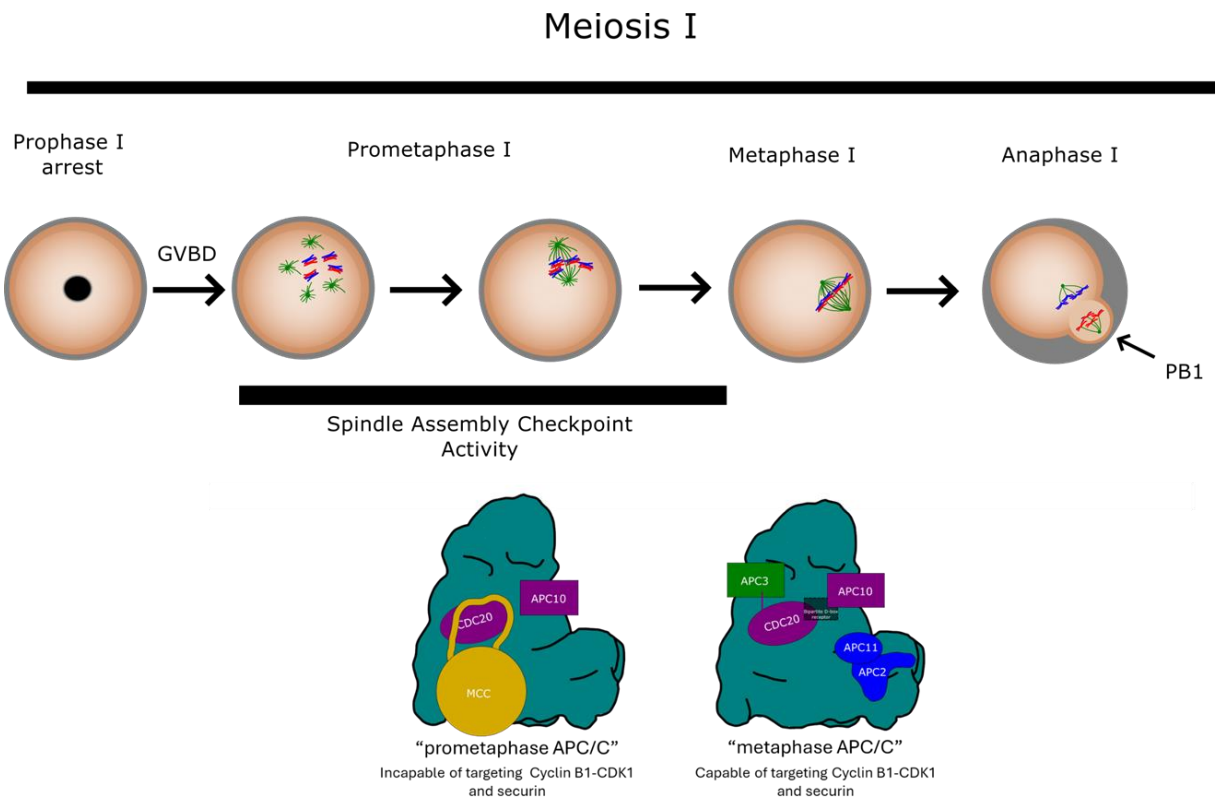

Figure 1.3. Outline of female mammalian meiosis I and a simplified structure of the APC/C with and without the MCC present

The oocyte enters a lengthy period of prophase I arrest in-utero, maintained by elevated intracellular cAMP levels. At this stage chromosomes exist as bivalents held together by chiasmata. A surge in hormones during ovulation results in the resumption of meiosis I, marked by germinal vesicle breakdown (GVBD). The oocyte enters a lengthy period of chromosome alignment which is orchestrated by cyclin B1:CDK1 and sustained by the Spindle Assembly Checkpoint (SAC). When the SAC is active, in response to kinetochores unattached to spindle microtubules, the Mitotic Checkpoint Complex (MCC) is produced, which associates with the Anaphase Promoting Complex/Cyclosome (APC/C) forming the APC/C-MCC ("prometaphase APC/C") and prevents its targeting of cyclin B1. This maintains prometaphase I on account of continued cyclin B1:CDK1 activity. Upon stabile microtubule-kinetochore attachments and chromosome alignment, the SAC diminishes and the MCC dissociates with the APC/C. This allows the APC/C to target cyclin B1, causing the inactivation of CDK1 and allows anaphase I to occur. Chromosomes are segregated with half of the genetic material extruded in the first polar body (PB1). The oocyte now enters meiosis II where it again arrests, until fertilisation. Graphical representations of the APC/C complexes are adapted from images by the Barford group[20].

1.1.3 Key events of prometaphase I

As mentioned earlier, prometaphase in oocyte meiosis is significantly lengthy, taking hours to complete chromosome congression before division. There are numerous reasons for this but are ultimately owed to the significant differences between somatic cells and the oocyte which will be discussed in further detail in a later section.

In mitosis, spindle is formed to align chromosomes using a widely accepted 'search and capture' mechanism[21]. In brief, spindle microtubules are nucleated from centrosomes, composed of centrioles, using their growing plus end until a kinetochore is reached which ultimately connects kinetochores to centrosomes on opposing poles of the cell and their alignment is orchestrated. Additionally, microtubules nucleated from chromosomes also contribute to mitotic spindle assembly. Any erroneous attachments are detected, and removed, allowing for new attachments to occur[22].

During oogenesis, developing oocytes degrade their centrioles. Instead of centrioles, fully grown oocytes contain large, acentriolar MicroTubule Organising Centres (MTOCs) which surround the nucleus in prophase, then fragment into many smaller MTOCs upon GVBD. In mouse oocytes MTOCs are scattered throughout the cell while in humans these centres are initially located on chromosomes[23]. Each produce spindles which surround individualised chromosomes to form a ball structure approximately 1-hour post GVBD in mouse oocytes. Hours are spent throughout prometaphase I moving chromosomes along the surface of the microtubule ball to form what is described as a 'prometaphase belt', given that they arrange initially as a ring around the microtubule ball. Following this, chromosomes invade the centre of the belt to form the metaphase plate. At the same time, MTOCs distribute towards opposite poles utilising spindle-associated HURP protein which coordinates spindle elongation. Elongation occurs 3-4 hours post-GVBD and critically requires antiparallel microtubule sliding motor protein kinesin-5.

The structure of MTOCs located at poles that is connected to aligning chromosomes via spindle microtubules is described as "barrel" shaped (notably very different to the shape of a

mitotic spindle), and in mouse oocytes this barrel is approximately 30 µm long[24]. In oocytes kinetochore-microtubule attachments accumulate gradually, coinciding with the increase in CDK1 activity. Whereas in mitotic cells, entry into mitosis is characterised by a rapid increase in CDK1 activity. This can mean that even in late stages of meiosis, aligned and bioriented chromosomes sometimes lack stable kinetochore-microtubules attachments.

Up to this point all spindle formation and chromosome positioning has taken place in the centre of the oocyte where the GV broke down. However, to permit polar body extrusion, prior to anaphase I, the spindle must migrate to the cortex. During spindle migration, kinetochore microtubule attachments are still in a state of flux and it is readily apparent that chromosomes are still aligning and attempts are being made to resolve erroneous attachments. This period of error correction is incredibly important. In fact, most attempts at kinetochore microtubule attachments are erroneous and these multiple rounds of correction by successive attachments increases the number of successes over time[16,25]. Without the ability to detect erroneous attachments and depolymerise incorrectly attached microtubules, the risk of cell division errors increases dramatically.

In mitotic cells, Aurora-B kinase mediates microtubule turnover at kinetochores which ultimately maintains SAC signalling and allows for the production of new microtubule-kinetochore attachments. In mammalian oocytes, Aurora-C provides this role. Inhibition or knockdown of Aurora-C in oocytes has been shown to result in accumulation of attachment errors[26]. Upon the establishment of stable microtubule-kinetochore attachments, the rate of MCC produced at kinetochores, and therefore SAC signalling, begins to diminish[27]. MCC complexes are short-lived within the cytoplasm, therefore cessation of production quickly relieves the inhibitory hold on the APC/C. The APC/C is then free to target substrates whose destruction initiates and coordinated anaphase, for example cyclin B1 (Figure 1.4).

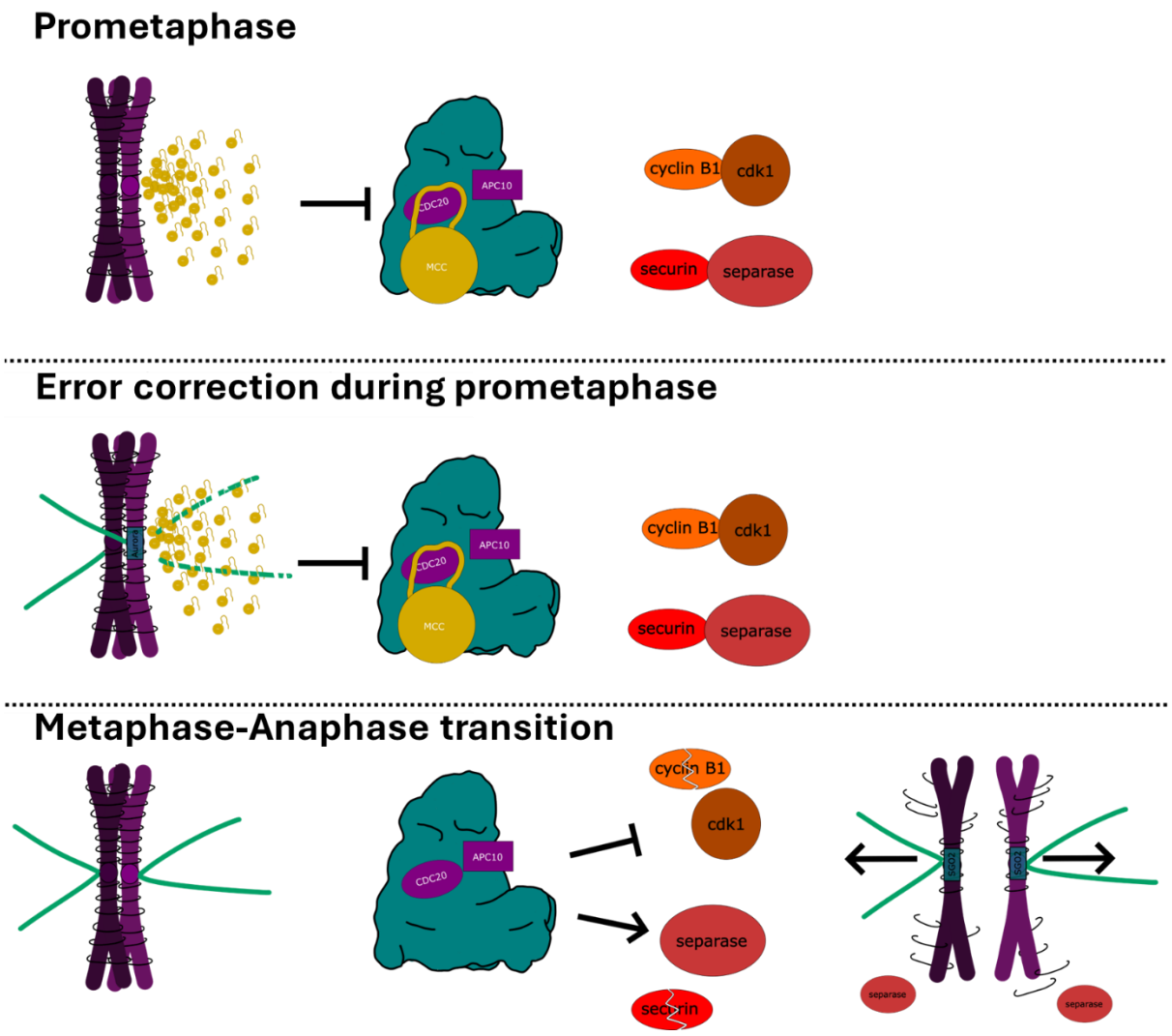

Figure 1.4. Generation of the MCC and its action on the APC/C during meiosis I.

In prometaphase I, kinetochores are unattached to spindle microtubules resulting in the activation of the spindle assembly checkpoint (SAC). During an active SAC, Mitotic Checkpoint Complexes (MCCs) are continuously produced at unattached kinetochores which act as a diffusible signal and associates with the Anaphase Promoting Complex (APC/C). Primarily, the MCC blocks the substrate recognition capabilities of the APC/C, particularly towards substrates which inhibit Anaphase (cyclin B1 and securin). The SAC remains active during the process of error-correction whereby Aurora C (Aurora B in mitosis) causes the destabilisation of erroneous spindle microtubule, which keeps the SAC active. When kinetochores are attached to spindle microtubules correctly, the SAC is turned off and MCCs are no longer produced. As the MCC is continuously disassembled from the APC/C, the diminishing SAC no longer provides MCCs and the APC/C is no longer inhibited towards cyclin

B1 and securin. The destruction of securin permits separase to cleave cohesin which hold bivalents together. Importantly SGO2 maintains centromeric cohesin which maintains homologous chromosomes. Cyclin B1 destruction by the APC/C inactivates CDK1 and anaphase I is permitted. Graphical representations of the APC/C complexes are adapted from images by the Barford group[20].

1.1.3 The Metaphase-Anaphase transition

The APC/C mediated destruction of cyclin B1 and subsequent CDK1 inactivation initiates anaphase I. Simultaneously, the APC/C coordinates the destruction of securin, an inhibitory pseudo-substrate of the protease separase that acts to digest the cohesin, ring-like structures that hold homologous chromosomes together[28]. Very importantly, chromosome cohesin at centromeres is protected to preserve sister chromosome attachments that must remain intact until the second meiotic division[29]. Here shugoshin2 (Sgo2), a scaffold protein at the centromere and kinetochore, is essential. Sgo2 recruits phosphatase PP2A-B56 which is thought to dephosphorylate cohesin at centromeric regions, rendering it non-cleavable by separase[30]. Centromeric cohesin protection is also further promoted by meikin, a meiosis specific kinetochore protein which is also present at centromeres and stabilises shugoshin[31].

Following arm cohesin degradation in meiosis I, homologous chromosomes segregate, pulled apart by microtubules which then disassemble. One of each pair is retained by the oocyte while the other is extruded in the first polar body (PB1) which eventually degenerates. The entire process of MI lasts approximately 7-11 hours in mice and 24-36 hours in humans[32]. Following this, immediate progression into MII sees the now ovulated oocyte relocate to the oviduct where it awaits possible fertilisation by the spermatozoa.

1.1.4 Meiosis II and the zygote

Like MI resumption, entry into MII is driven by a rapid increase in cyclin B1-CDK1 activity. This division is more analogous to mitosis compared to MI. Prometaphase II consists of a period of extraordinary rearrangement as mono-oriented sister chromatids now bi-orient to form the meiosis II spindle. This spindle is also barrel shaped and orchestrated by MTOCs. However, there are significant differences. For instance, Miss and Doc1R are proteins specifically key in producing a MII spindle, but are not required in MI[33]. Second, high levels of cyclin A2 are maintained through this stage and is essential to minimise mis-attachments and segregation errors (note cyclin A2 will be introduced and discussed in detail in later sections)[34]. Third, MII spindles are highly defective in the absence of Ran-GTP, a GTPase key in the spatial control of spindle formation, which is not the case in meiosis I[35]. In addition, SGO2 redistributes in MII, thought to permit the removal of centromeric cohesin during the second metaphase to anaphase transition if the oocyte is fertilised[36]. In Anaphase II separase is now able to degrade centromeric cohesin, allowing for the separation of sister chromatids. SGO2 itself has been reported to be an APC/C target, thus degradation via the ubiquitin-proteasome pathway removes the protection of cohesin on centromeres, ultimately permitting segregation of sister chromatids[37].

A further unique feature of MII is an activity known as cytostatic factor (CSF). CSF (largely mediated by the protein Emi2) adds a second layer of APC/C inhibition alongside the SAC. Emi2 however, is not satisfied by chromosome alignment, and its destruction is instead triggered by spikes in intracellular Ca^{2+} as a result of a sperm cell entering the oocyte[38,39]. This ensures that even if all chromosomes are aligned in MII, the oocyte waits for fertilisation before the APC/C directs the second wave of cyclin B1 and securin destruction (along with other important metaphase proteins).

Anaphase II marks the segregation of sister chromatids, in which half of the genetic material is extruded in the second polar body (PB2). The pronuclei of the sperm head fuses with the female pronuclei resulting in the reformation of 23 maternal and 23 paternal chromosomes to form a single cell embryo called a zygote. Following this is entry into the first mitosis and

subsequent embryonic cell division. The first few rounds of mitosis are different to the canonical mitosis of a non-embryonic somatic cell. These first mitotic events are significantly more time consuming and error prone, however are compatible with live birth[40,41]. Indeed the switch from meiosis to mitosis is complex and includes significant chromatin remodelling; switch from acentrosomal to centrosomal spindle assembly and a change in gene expression[42].

1.2 Factors contributing to high rates of Aneuploidy

Oocytes, particularly those of larger mammals, are error prone by nature. It is well documented that oocyte quality significantly reduces with maternal age. However, even at peak fertility in humans, a staggering number of oocytes are thought to not be viable for fertilisation. In women under the age of 35, up to 30% of zygotes are aneuploid, with 80-90% of these errors thought to originate in oocyte MI due to segregation errors[43]. This section outlines a number of factors associated with high instances of aneuploidy in oocytes and failure to produce a healthy egg.

1.2.1 Age related challenges

Aneuploidy is the leading cause of miscarriage and birth defects in humans[43]. The rate of non-viable oocytes is difficult to measure however In-Vitro Fertilisation (IVF) success rates can be indicative of this. Those undergoing IVF between the ages of 35-37 have a success rate of 33% which decreases to 6% for 43- to 44-year-olds (Human Fertilisation & Embryology Authority, 2021). On top of this, the maternal age effect is a well-documented phenomenon whereby oocyte quality and number decline rapidly with age[44]. In humans this has serious negative impact for couples looking to conceive over a maternal age of 35 years since not only is the egg pool depleting, but where conception is successful, the frequencies aneuploidy, miscarriage, birth defects, and problems associated with higher risk pregnancies are all increasing. Furthermore, as discussed earlier, IVF is not a good solution. This procedure is often misconceived as a “silver bullet” to conception however it generally takes 6-cycles to stand a greater chance of having a baby via this method than not. Age related

fertility decline occurs rapidly. Women below 30-years old have an 85% chance to conceive within 1-year which decreases to 44% by the age of 40. Similarly, miscarriage rates increase from approximately 16% before the age of 30 to 27% by the age of 45[45,46]. This coincides with the increased prevalence of aneuploidy. There are multiple reasons for this, ultimately stemming from the biology of the oocyte[43,44].

A major source of this error is thought to be loss of the oocyte's capacity to maintain bivalent chromosome structures. In humans, this structure must be held together for many years from the diplotene stage in prophase I *in-utero* until the point of ovulation. During this lengthy period, bivalent structures weaken, which can lead to sister chromatids splitting and the formation of univalents in MI. Related to this, over time, a weakening of the bonds holding sister chromatids together is lost, in a process referred to as "cohesin fatigue"[47]. Inefficient separase inhibition is one factor compounding this. It may be possible that low level separase activity over the course of a long period of time gradually degrades cohesin, increasing the instances of premature separation[47–49]. There is also evidence for a similar mechanism occurring to SGO2, where gradual loss predisposes cohesin for premature destruction[50]. In addition to this, slow cohesion deterioration can occur due to oxidative damage or spontaneous hydrolysis of peptide bonds, however little is known about these mechanisms[6].

Furthermore, telomeres, which are tandem repeats of DNA sequences which occupy the end of chromosomes, shorten with age in the majority of cell types, including oocytes. In oocytes, telomeres begin to shorten in oogenesis and continue to do so during their lifespan. Women who experience recurrent miscarriage and/or IVF failure have been determined to harbour oocytes with shortened telomeres, in a process identified by Keefe et al. named "telomere-mediated oocyte aging"[51].

1.2.2 Challenges associated with the oocyte biology

An additional insult to the quality of oocytes is that SAC in oocytes is not as effective as that in somatic cells. This is thought to be owing to the large size of the oocyte (although this is

controversial). Studies have shown that the diffusible MCC signal produced from few unattached kinetochores becomes too dilute in the large cytoplasmic volume of the oocyte, and is not able to prevent premature activation of the APC/C. Consequently, slippage into anaphase can occur before proper chromosome alignment. Indeed, a study by Heasley et al. whereby mitotic cells were fused with interphase cells showed that the "wait anaphase" signals produced by the mitotic cells were diluted and resulted in premature exit of mitosis[52]. Similarly, Kyogoku et al. showed that if the cytoplasm of an oocyte is artificially doubled, time to anaphase I was accelerated, and therefore inferred SAC strength is lower. Conversely, removal of half of the volume of the cytoplasm, prolonged the time to anaphase I and thus inferred SAC strength was increased[53]. This could be one explanation as to why mouse oocytes (3-4x smaller than human oocytes) present with far fewer aneuploidies than human oocytes, as the cytoplasm:nucleus size ratio is smaller[32].

An additional challenge for oocytes, contributing to high rates of failure, is the lack of canonical DNA damage response pathways, and the fact that these cells can progress through meiosis even with significant DNA damage. A rudimentary DNA damage response does occur, but this involves the accumulation of SAC proteins (which for the reasons above can be ineffective at low levels) and result in an arrest at metaphase I. In this case, the SAC protein MAD2 has been shown to accumulate at kinetochores in response to DNA damage. Mihajlović and Fitzharris in their 2018 review suggest that this could indicate a mechanism whereby kinetochores can sense damage on chromosome arms or centromeres and act as "sentinels for broader chromosome damage"[32].

In mitosis, erroneous kinetochore-microtubule attachments are detached via the activity of Aurora B kinase, which phosphorylates substrates on the kinetochore and contributes to the removal of attachments. This acts to maintain the SAC and prevents chromosome segregation. One model for this mechanism suggests that when an attachment is correct, tension spatially separates kinetochores from a subpopulation of Aurora B, reducing the extent of its phosphorylation and results in the stabilization of these correct attachments[25]. In contrast to mitotic cells, oocytes in meiosis I lack a mechanism to coordinate bivalent

stretching and subsequent inhibition of Aurora B/C. It has been suggested that this is due to Aurora B/C abundance and activity remaining high on stretched bivalents. This results in correct kinetochore-microtubule attachments becoming unstable and increases the instances of erroneous attachments[54]. Additionally, oocytes treated with Aurora B/C inhibitor AZD1125 during the stretching phase significantly increased the instances of correct kinetochore-microtubule attachments. Taken together, this further highlights that the robust mechanisms underlying cell division in mitotic cells is less robust in the context of oocyte meiosis[55].

In addition to the challenges faced by the oocyte which contribute to the high rate of aneuploidies and failure to develop into an embryo, there are also significant challenges in performing research in female mammalian meiosis which contributes to a significant lack of understanding of the biology for this cell type. Most significantly, the oocyte pool is a finite resource, and donation of human oocytes for research is both invasive and expensive. Animal models such as mice provide a useful alternative, however they are not completely analogous to human models. For example the rates of aneuploidy are significantly different to that in humans (1-4% in mice and 20-30% in humans at reproductive age)[56]. Conducting biochemical experiments on this cell type is also challenging. Because of the low cell number obtained from either human donation or mouse harvests, experiments are generally restricted to single cells. Protocols which require larger amounts of protein for instance, such as Western blotting, require cell numbers to be accumulated over the course of multiple experiments, which is time consuming.

1.4 The importance of CDK1 and its roles in mitosis

Not surprisingly, meiosis cell cycle literature cites many mitotic studies when describing the mechanistic detail surrounding proteins key to both types of cell division. Often this is sensible and well caveated. However, over several re-cites, some assumptions (albeit sensible assumptions) have become presumed as fact without confirmation in context, the origins of these experiments are left behind as the field moves over years. This has the potential to be problematic, propagating misinformation. While it is expected that the basic function of each protein is similar between mitosis and meiosis, we know from our own research and that of

others, that functional conservation does not always mean proteins are regulated or employed in the same way. Indeed, a goal of our lab is to reveal these differences. Using mitotic cell cycle regulation knowledge as a framework and comparator gives an outstanding point of reference provided it is acknowledged as such. Therefore, to detail fundamental cell cycle processes underpinning cell division, the following sections draw information from many experiments using mitotic cell lines, many *in-vitro* investigations into protein-protein interactions, and some confirmations in oocyte meiosis as indicated.

1.4.1 CDK1 activation and feedback mechanisms

Initiation of mitosis and oocyte meiosis resumption are both driven by a sharp increase in the activity of CDK1 which requires both cyclin B1 association and post-translational modification. Prior to this each cell type is primed for CDK1 activity. In mitosis CDK1 is found in abundance as a monomer at the end of G1, inactivated by inhibitory phosphorylations on threonine-14 and tyrosine-15 by WEE1 and MYT1 kinases [57]. This large abundance of CDK1 in its inactive form primes the cell for rapid CDK1 activation and entry into mitosis. Similarly, cyclin B1 levels peak in late G2 under the regulation of transcription factors such as NF-Y, FoxM1 and B-Myb stimulated by cyclin A2-CDK2 (an S-phase kinase) activity[58].

In S-phase and early G2, cyclin B1 is mostly exported outside of the nucleus, but as G2 progresses nuclear shuttling of cyclin B1 predominates and it begins to localise specifically at the centrosomes[59]. Here, cyclin B1 binds to CDK1 as a coactivator. Cofactor binding is essential for CDK1 to function as a kinase. Alongside cyclin B1 association, cdc25 phosphatase removes the inhibitory phosphorylations on threonine-14 and tyrosine-15 of CDK1[60]. CDK1 also gains an activatory phosphorylation on threonine-161 (Figure 1.5A) [61]. After cyclin B1 association, and changes in its phosphorylation status, CDK1 is active and its activity is herein referred to as “cyclin B1-CDK1 activity”. CDK1 can interact with both A and B type cyclin proteins however cyclin B1 is the primary CDK1 activator regulating mitosis entry and exit[62].

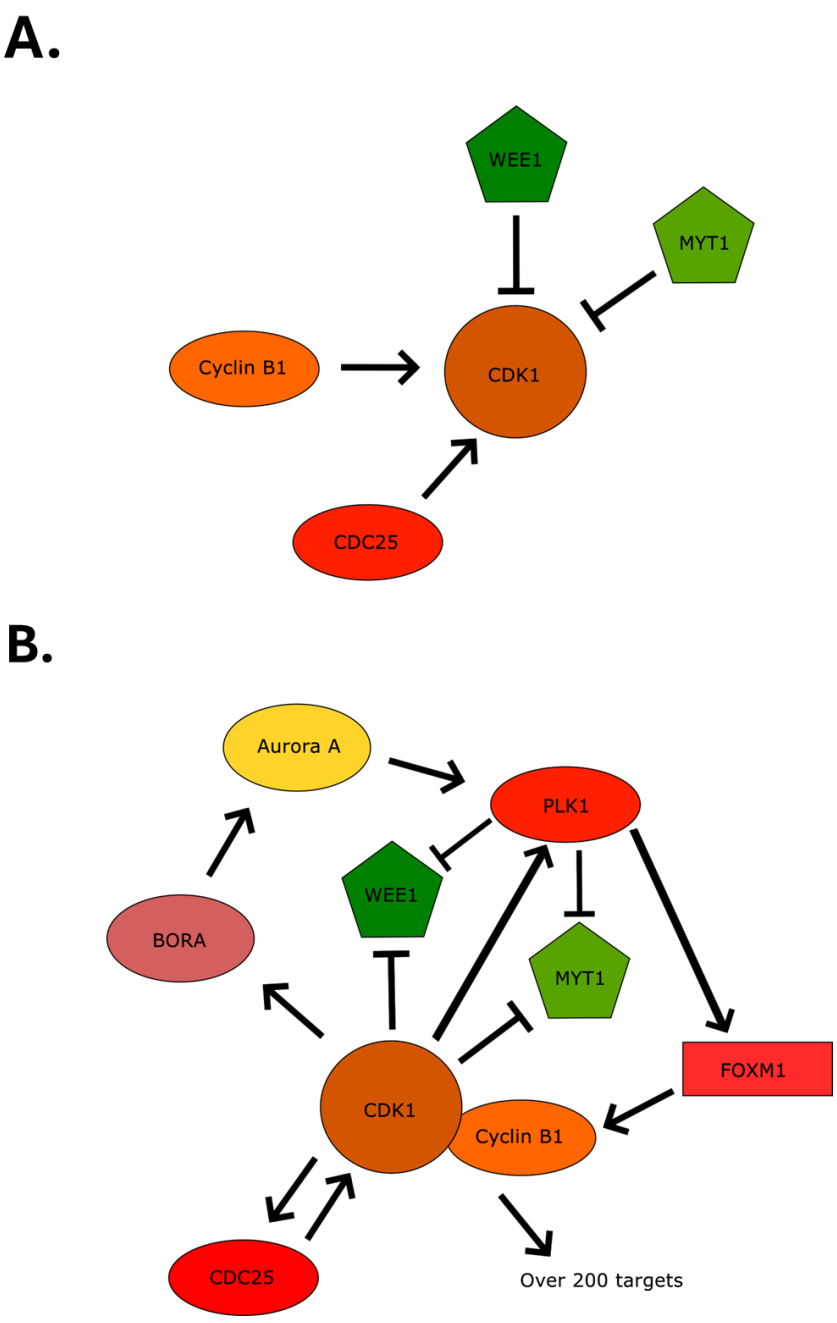

Figure 1.5. Mechanism of cdk1 regulation and it's positive feedback activation loop

A) Prior to mitosis/meiosis cdk1 is maintained in its inactive state on account of phosphorylations by WEE1 and MYT1 kinases. Cyclin B1 association alongside the removal of inhibitory phosphorylations by cdc25 phosphatase activate cdk1. B) Upon activation of cdk1, its activation is amplified by a positive feedback loop. CDK1 activates cdc25 which removes inhibitory phosphorylations on CDK1. Cdk1 phosphorylates and inactivates wee1 and myt1 kinases as well as activating PLK1 which also inactivates wee1

and myt1. PLK1 also activates transcription factor FOXM1 which upregulates cyclin B1. Finally, CDK1 activates BORA which in turn activates Aurora A which subsequently activates PLK1. This figure is adapted from: Lindqvist et al.

On entry into mitosis CDK1 activation is further promoted by several additional mechanisms that amplify activity (Figure 1.5B). Firstly, cyclin B1-CDK1 phosphorylates and inactivates its own inhibitors (Wee1/Myt1) as well as activating cdc25 phosphatase, which promotes CDK1 activation. Second, cyclin B1-CDK1 substrates develop a PLK1 docking site in response to phosphorylation by CDK1 which permits phosphorylation events by PLK1[63–65]. PLK1 targets include WEE1/ Myt1 as a further mechanism of their suppression. Cyclin B1-CDK1 can also activate PLK1 by phosphorylating BORA, which results in the activation of Aurora A kinase and further activation of PLK1[66,67]. In turn, Aurora A is able to phosphorylate and promote the activity of CDK1. Finally, PLK1 (activated by cyclin B1-CDK1 phosphorylation), activates transcription factors such of FoxM1 which, not only increases the expression of mitotic proteins, but also cyclin B1[65,68,69]. Thus, cyclin B1-CDK1 activity is initiated rapidly and then vastly amplified. Clearly many positive feedback loops exist to promote and accelerate CDK1 activity which highlights its importance during prometaphase.

CDK1 is the main acting CDK in mitosis and is often referred to as the 'mitotic master regulator'. Searching the Signor database, a database of causal relationships between biological entities, Massacci et al. suggest that CDK1 phosphorylates approximately 200 proteins. In addition, GO-term enrichment analysis indicates that CDK1 substrates broadly populate many different pathways ranging from signal propagation, gene expression, apoptotic pathways, protein transport and Golgi organisation[70]. Further, CDK1 also phosphorylates several transcription factors responsible for the modulation of over 8,000 mitosis specific genes, as well as pro-survival and proliferation enhancing signalling cascades such as MAP, ERK, and mTORC pathways[71]. By various points of control, CDK1 activity coordinates entry into mitosis, nuclear envelope breakdown (NEBD), DNA condensation, production of spindle, remodelling of endoplasmic reticulum and Golgi apparatus as well as checkpoint modulation[72–76].

1.4.2 CKS proteins and their role in CDK activity

CDK proteins also associate with small accessory subunits called CKS (Cyclin-dependent kinase subunit) proteins. These are small accessory subunits of which there are two types in human cells CKS1 and CKS2. Removal of both CKS proteins is lethal however removal of only one is tolerable. These proteins are conserved through evolution and bind both CDK1 and CDK2. CKS proteins harbour an anion binding site which has been shown to bind residues which have been phosphorylated by CDK proteins. This is thought to enhance the activity of CDK proteins by associating to a phosphorylated CDK target and facilitating further CDK mediated phosphorylation of surrounding residues[77].

CKS proteins also play a role in facilitating the destruction of cyclin proteins and thus the termination of CDK activity. Studies have shown that depleting CKS1 and CKS2 prevents cyclin A2 destruction[78]. Therefore, CKS proteins provide a dual role, both enhancing local CDK activity as well as enhancing the efficiency of destruction. Here, CKS proteins associate with phosphorylated APC/C subunit APC3 which recruits the cyclin-CDK complexes to the APC/C. This also occurs for cyclin B1-CDK1-CKS in prometaphase however because of the inhibitory role of the SAC on the APC/C, cyclin B1 destruction does not occur. This seemingly premature binding of cyclin B1-CDK1-CSK renders it a better APC/C substrate come metaphase[78].

1.4.2 CDK1 driven processes in mitotic progression

Clearly cyclin B1-CDK1 activity is very important for driving essential processes in mitosis and meiosis. However, while cyclin B1-CDK1 may coordinate many of these processes, there are a significant number of other players involved more directly. Here I will briefly describe some of the key processes that cyclin B1-CDK1 coordinates and some of the key factors involved (Figure 1-6).

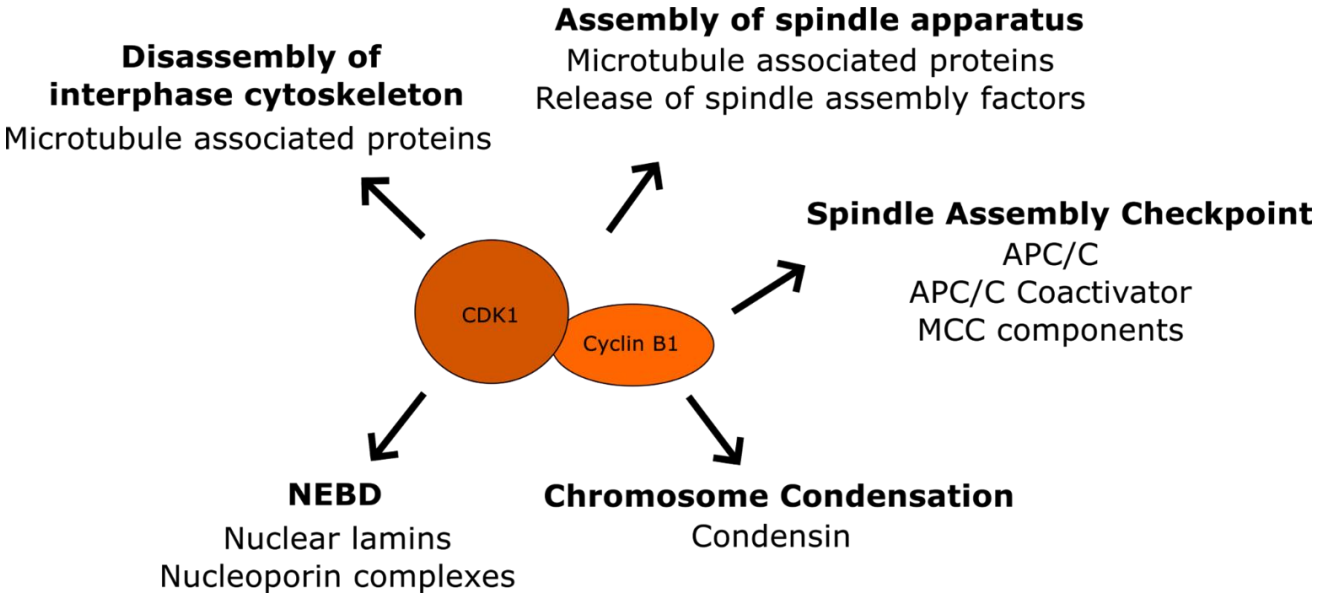

Figure 1-6. Cyclin B1:CDK1 has a number of roles throughout mitosis/meiosis

Cyclin B1:CDK1 functions as an active kinase which phosphorylates over 200 target proteins, driving a significant number of functions throughout prometaphase. Cyclin B1:CDK1 phosphorylates nuclear lamins and nucleoporin complexes leading to the breakdown of the nuclear envelope (or germinal vesicle in meiosis), marking the entry into prometaphase. Alongside this, cyclin B1:CDK1 also plays roles in chromosome condensation. It also plays a key role in the assembly of spindle apparatus which permits chromosome alignment in prometaphase. Cyclin B1:CDK1 also regulates the APC/C as well as maintaining the mitotic checkpoint complex.

Prophase marks the first stage of mitosis. One of the processes defining the end of prophase and the initiation of prometaphase is Nuclear Envelope Breakdown (NEBD). Cyclin B1-CDK1 is an essential kinase coordinating this event, however other kinases are also involved, including Aurora A and PKC. Briefly, cyclin B1:CDK1 phosphorylates nuclear lamins, filaments critical for nuclear stability, causing them to depolymerise as a result. Alongside this nucleoporin complexes located on the nuclear envelope and nuclear membrane proteins such as Lap2α are phosphorylated resulting in their disassociation. As nuclear pore complexes disassemble, the envelope is reabsorbed into the endoplasmic reticulum and complexes disperse into the cytoplasm[79–82]. Approximately 15-minutes before NEBD completion, Cyclin B1:CDK1 drives chromosome condensation in preparation for division,

phosphorylating condensin to promote interactions with proteins that cause condensation[72]. Interestingly at the onset of mitosis, CDK1 signalling also promotes the disassembly of the microtubular interphase cytoskeleton thought to prevent chromosome damage during spindle assembly. CDK1 exerts this function by either stabilising or destabilising microtubule-associated proteins (MAPs) such as ch-Tog and Map4 that promote microtubule growth[83,84].

In prometaphase, key events include the completion of the formation of the spindle apparatus responsible for locating and binding kinetochores, and for orchestrating movement, alignment and subsequent segregation of chromosomes. Critical to the accuracy of this, the breakdown of erroneously attached microtubules is equally important and CDK1 has been shown to have dynamic roles in this. As discussed earlier, microtubules can be destabilised by CDK1 signalling as well as its role in promoting spindle formation. Here cyclin B1:CDK1 phosphorylates importin-α1, which forms an inhibitory complex of spindle assembly factors[85]. Cyclin B1:CDK1 phosphorylation of importin- α1 causing its dissociation from importin-β which permits the release of spindle assembly factors such as TPX2, TACC3 and NUMA. Alongside this, RCC1 localised at chromatin catalyses the conversion of RanGDP to RanGTP at chromosomes, providing a signal for further spindle production[85,86]. Cyclin B1:CDK1 activity also has a critical role in prolonging the length of prometaphase to ensure adequate spindle assembly and kinetochore-microtubule attachments. This is achieved by promoting the SAC which works in synergy with cyclin B1-CDK1 activity to safeguard the fidelity of anaphase[87].

In prometaphase, cyclin B1:CDK1 plays a key role in maintaining the SAC at unattached kinetochores to prolong prometaphase via the MCC induced inhibition of the APC/C[74]. In contrast, cyclin B1:CDK1 also activates the APC/C[88]. This provides a mechanism whereby CDK1 is activating the APC/C while simultaneously inactivating it by promoting SAC signalling. The SAC is maintained by CDK1 phosphorylation of the APC/Cs coactivator Cdc20, which prevents its incorporation into the APC/C as well as phosphorylating other MCC components[89]. This seemingly counterintuitive inactivation/activation tempers APC/C activity, promoting the destruction of some proteins (for example cyclin A2), yet still prevents

the Anaphase-promoting destruction of other proteins that are required for longer. For example, it is known that cyclin A2 must be destroyed by the APC/C in prometaphase, ahead of cyclin B1 while the SAC is active to enable stable kinetochore-microtubule attachments necessary for chromosome segregation[90,20]. This state of selective activation/inactivation of the APC/C supports this and will be discussed later. In addition, the activation/inactivation balance primes the APC/C for a rapid switch upon diminishing MCC production in response to successful kinetochore-microtubule attachments. Importantly, alongside Cdc20 phosphorylation, cyclin B1:CDK1 also contributes to the localisation of the SAC protein MPS1 to unattached kinetochores which primes the production of MCC complexes[91]. Further phosphorylation of MCC complexes, mainly by CDK1- and MPS1- recruits further MCC components to accelerate MCC formation.

Upon silencing of the SAC, brought about by chromosome alignment (or at least occupied kinetochore-microtubule attachments), CDK1 must be rapidly inactivated to initiate anaphase. This is of upmost importance, constitutively active CDK1 would causes a metaphase arrest and slow inactivation results in stalling or a reactivated SAC[87]. CDK1 inactivation is mediated by the rapid APC/C targeting of cyclin B1 and subsequent destruction via the proteasome. Alongside inactivation of CDK1, securin is targeted to release separase to permitting dissociation and segregation of sister chromatids.

1.4.3 The significance of cyclin B1

The epithet of CDK1 being the ‘master regulator’ of mitosis is certainly befitting considering its ability to drive cells into mitosis, alongside its vast role in signalling cascades concerning many aspects of division. Also considering that inactivation of CDK1 kickstarts the completion of mitosis. However, it must not be forgotten that there can be no CDK1 activation without cyclin proteins, and in regard to mitosis, cyclin B1 is of upmost importance. While it isn’t described as “the master regulator of the master regulator” this description is nevertheless fitting. Progression through the cell cycle ultimately depends upon cyclical abundances of

cyclin B1 to drive CDK1 activity and inactivation. Thus, fluctuations of cyclin B1 abundance drive key stages of mitosis (Figure 1.7). Entry into mitosis is driven by an increase in cyclin B1, exit out of metaphase is driven by a rapid decrease in cyclin B1.

The cyclin B1 driven spatial and temporal regulation of CDK1 and its activity is multidimensional. Firstly, binding of cyclin B1 to CDK1 results in its activation. Second, Cyclin B1 activation of CDK1 drives the nuclear retention of cyclin B1-CDK1 to trigger mitosis[87]. Third, cyclin B1 provides a suitable surface for the docking of kinases and phosphatases required for CDK1 post-translational modifications. Finally, cyclin B1 association provides a docking site for CDK1 substrates[92].

Cyclin B1 levels begin to increase in S-G2 phase and molecules shuttle between the cytoplasm and nucleus, however it is generally found accumulating in the cytoplasm as export rates exceed import rates. In late G2 the inverse predominates with cyclin B1 levels peaking at the G2/M transition to initiate mitosis[93]. Nuclear import of cyclin B1:CDK1 is immediately triggered upon activation and import during prophase appears to be a result of a change in the nuclear transport machinery instead of modifications to cyclin B1. Work by pines et al. utilised a biosensor for cyclin B1-CDK1 to disprove previous models of cyclin B1 nuclear import whereby PLK1 phosphorylates cyclin B1 in its N-terminal nuclear export sequence, resulting in nuclear retention[93,94]. Indeed, they found no evidence that changes in nuclear export rates contribute to cyclin B1 CDK1 nuclear accumulation[94].

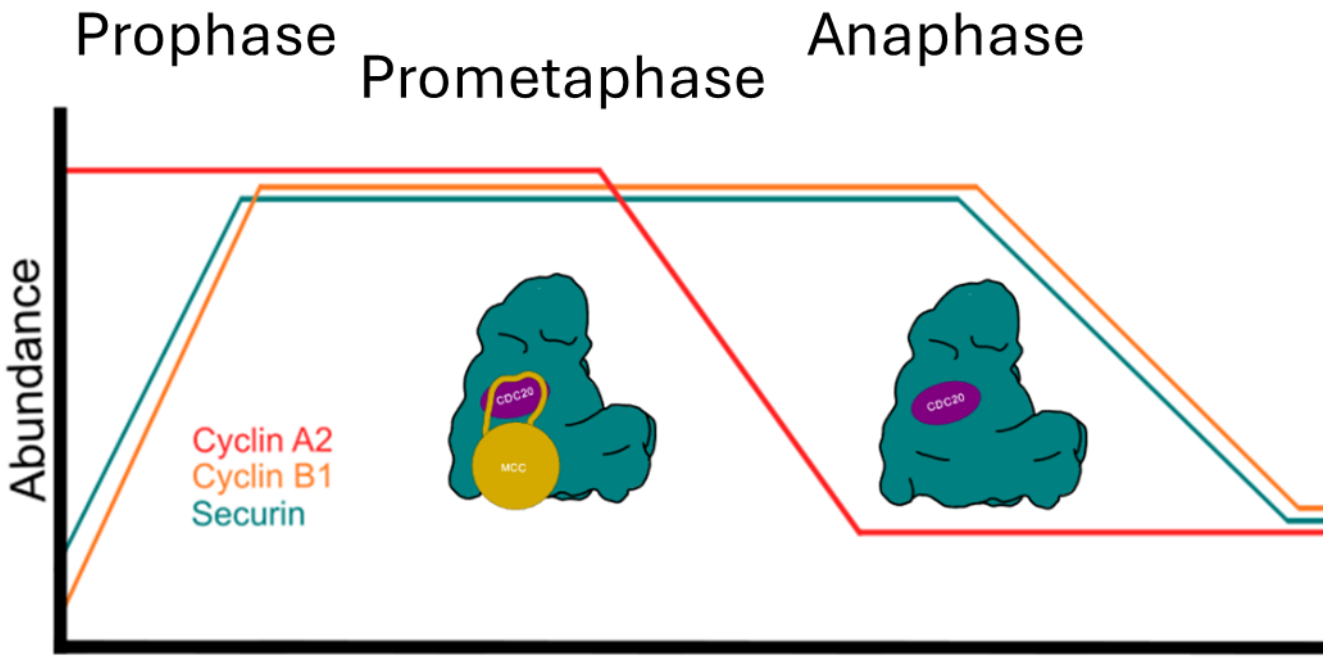

Figure 1.7. The fluctuations in abundance of key cell cycle proteins through mitosis.

The relative abundance (not to scale) of a subset of key APC/C substrates in respect to the stages of meiosis and mitosis. Images of the APC/C indicate that the MCC is in complex with the APC/C when the SAC is active in prometaphase. When the SAC is not active, the MCC disassociates and the targeting of anaphase-inhibiting substrates such as cyclin B1 and securin can be achieved. Interestingly, cyclin A2 can be targeted by the APC/C-MCC in prometaphase in a mechanism described in detail in a later section. Graphical representations of the APC/C complexes are adapted from images by the Barford group[20].

At the point of chromosome alignment and SAC signal reduction, the APC/C becomes active and targets cyclin B1:CDK1 for destruction. This destruction must occur rapidly to ensure that CDK1 becomes inactivated promptly in order to permit chromosome segregation (Figure 1.7).

1.5 Substrate recognition motifs

The processes that take place through the cell division cycle are ultimately coordinated by oscillations in the activity of kinases, controlled by many regulatory pathways, including the ubiquitination and subsequent destruction of coactivator proteins, as is the case for CDK proteins (Figure 1.7). Through the active stages of division, ubiquitination events are largely directed by the APC/C, a massive 1.2 MDa multi-subunit complex, which acts as a scaffold to bring together an E2 ubiquitin conjugating enzyme and a substrate[19,95–97]. It is incredibly important that the correct substrate is targeted at the right time point but also that the rate of destruction is tightly controlled. For instance, at the end of prometaphase, cyclin B1 must be targeted for destruction very rapidly to put an end to CDK1 activity and permit chromosome segregation. One way in which the APC/C orchestrates substrate specificity is by the presence of a coactivator, either Cdh1 or Cdc20, which bestow substrate recognition capabilities[98]. It has been determined that Cdc20 binds to fewer substrates compared to Cdh1 which targets a larger range[99]. The structure of the APC/C and the precise mechanisms of substrate binding will be discussed in a later section. However, note that the substrates themselves harbour structural sequences which play a significant role in regard to how and when the APC/C targets them.

It is important to note at this stage that there is well established nomenclature for the different structures of the APC/C which are being referred to in text. Most notably, superscript text indicates which coactivator is associated with the APC/C being referred to e.g. "APC/C^{Cdc20}" and "APC/C^{Cdh1}". Additionally, MCC associated APC/C is referred to as "APC/C-MCC". Finally, the APC/C not containing a coactivator is referred to as the "apo-APC/C".

The vast majority of APC/C substrates associate with the APC/C by binding to highly conserved, WD40 repeat containing coactivators Cdc20 and Cdh1, each associating with the APC/C at different stages of the cell cycle. The WD40 domains provide multiple recognition sites that are specific to Short Linear Motifs (SLiMs) on APC/C substrates[100–103]. Specifically SLiMs are amino acid sequences present on APC/C substrates, which either confer

destruction capability or enhance the timing and rate of destruction. Many of these motifs are also referred to in the literature as “degrons”, however the degrons and their distinction to SLiMs are somewhat inconsistent in literature as the terms are often used interchangeably. Generally, degrons are motifs which confer destruction capabilities without the requirements for accessory motifs, for example the well-known destruction box (D-box) motif[104].

1.5.1 SLiMs and degrons

The D-box is defined by a nine-residue linear sequence of amino acids with the consensus sequence RxxLx[D/E][Ø]xN[N/S][105]. Many studies have shown that the presence of this motif alone (alongside adequately spaced ubiquitinatable lysine residues) is sufficient to turn a peptide into an APC/C substrate, and in many cases, removal of a substrates D-box obliterates APC/C dependent ubiquitination[104,106]. High resolution structural studies have revealed that the D-box associates with a binding pocket located between two blades of the coactivator WD40 domain and a second site on closely located 10th subunit of the APC/C, APC10 (Figure 1.8)[101]. This site is often referred to as the “bipartite D-box receptor”, bipartite referring to the two subunits which compose it[101]. The D-box binding site is conserved between both Cdc20 and Cdh1 and therefore D-box containing substrates may be targeted by both coactivators[104].

Structural insights into the binding sites of SLiMs describe reasonings for specific residues at each site of the consensus sequences. For instance, the N-terminal arginine (in position 1 – P1) of the D-box binds to an acidic patch on the surface of the coactivator and the leucine in P4 is inserted into an aliphatic pocket nearby. A proline or alanine residue in P3, and a small residue in P5 of a D-box sequence are likely present given that the D-box must turn to accommodate the leucine in P4. A P6 acidic residue forms a hydrogen bond with an arginine residue on the activator surface. A non-polar region on the coactivator surface also explains a hydrophobic residue in P7. Alongside this, the C-terminal hydrophilic region of a D-box is generally composed of a serine, threonine or asparagine at P8 and an asparagine at p9 that associates with a hydrophilic surface on APC10 on its 80s and 140s loop[105,107,108].

The KEN-box is another SLiM which fits the definition of degron. This motif is defined by the consensus sequence KENxxxD/N and, unlike the D-box, the KEN box is slightly structured as this sequence often forms an underwound helix. The KEN-box is often found in combination with the D-box however their presence in respect to each other is not mutually exclusive[107,109]. The KEN-box binding site is located in a depression on the top surface of the WD40 domain of both Cdc20 and Cdh1. The underwound helical section of a D-box wraps around a glutamate residue in this region and charged residues of this KEN-box contact a binding pocket (Figure 1.8) [107,108].

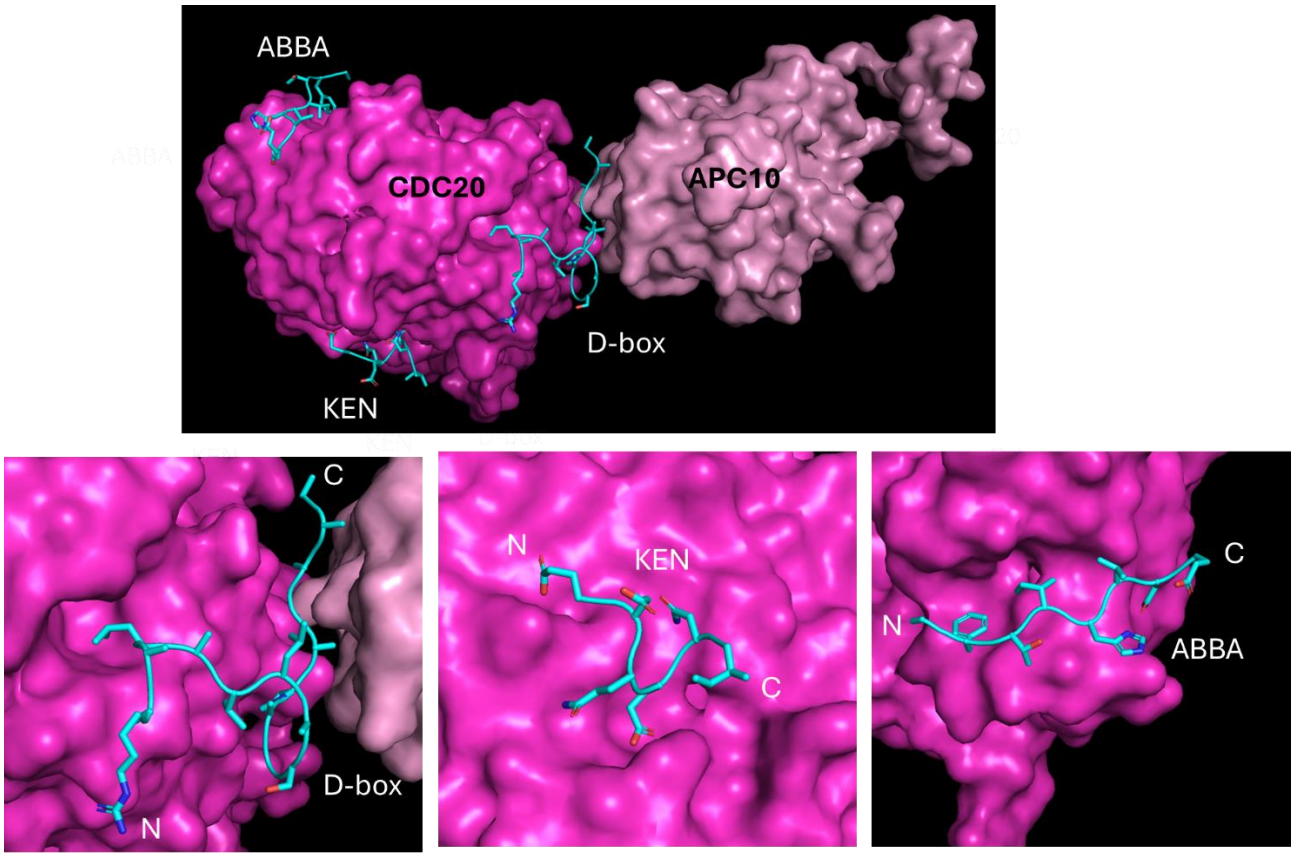

Figure 1.8. APC/C coactivator Cdc20 and its association with various SLiMs

Various orientations displaying the structure of Cdc20 (surface, magenta) in proximity to to APC10 (surface, light pink) associating with various cyclin A2 SLiMs (cartoon, cyan) including

the D-box motif; ABBA-motif; KEN-box. Alongside closeups of these motifs interacting with Cdc20 (and APC10 in the case of the D-box) with orientation described by labelling the C- and N-termini of these motifs. These are cryo-EM images of the APC/C in complex with cyclin A2 SLiMs solved by the Barford group, accessed using the Protein Data Bank (PDB:6Q6G[20]) and adapted (isolated and colorised) using PyMOL[20].

The ABBA motif is an example of a SLiM which does not fit the definition of a degron, as the presence of an ABBA motif alone will not result in a substrate being targeted by the APC/C for destruction. Identified by Pines et al in 2015, the name 'ABBA' refers to the fact that it was first identified in APC/C substrates cyclin A, BubR1, Bub1 and Acm1[102]. The ABBA motif consensus sequence is [ILVF]x[ILMVP][FHY]x[DE] and it occupies a hydrophobic groove between blades 2 and 3 on the WD40 domain of both APC/C coactivators[102,107]. This site is located on the opposite surface of the coactivator to the KEN box binding site. P1 and 3 of the ABBA motif are buried into a binding pocket whereas the residue in P4 rests against blade 3 of the coactivator WD40. While the ABBA motif does not confer APC/C targeting suitability alone, it does enhance the rate of substrate destruction in some contexts. As discussed briefly in section 1.4.2**,** cyclin A2 is able to be targeted for destruction in prometaphase. The ABBA motif appears to enhance the rate of APC/C mediated destruction during its prometaphase destruction, but not outside of this context. This is likely via a mechanism whereby the presence of an ABBA motif provides an increase in the binding affinity of a substrate to the coactivator, and will be discussed further in a later section[102].

Aside from the degron and non-degron characterisation of SLiMs, they can be further categorised into being canonical or non-canonical, as many motifs do not fit the consensus sequences described earlier while still being able to occupy the same binding sites[99,108]. The canonical sequences however do tend to describe the sequences with the highest binding affinities to their respective binding sites, which will have a substantial impact on the rate of destruction for a given substrate. There are exceptions to this though, for example the second identified D-box of cyclin A2 (D2-box) which has the sequence "VAPLKDL" compared to the canonical D1-box, "RAALAVL". Curiously Zhang et al. suggest that the non-canonical D2

box is the principal D-box as it is the only degron of cyclin A2 which is self-sufficient to allow ubiquitination by APC/C^{Cdc20}. This does however suggest that alterations to canonical sequences likely provide substrates differential destruction dynamics[20].

The three motifs discussed here are perhaps the most understood SLiMs in literature, however, there exists many more across a wide range of substrates, and there are expected to many more. One additional SLiM to note is the CRY-box since it seems to exclusively operate in meiosis. Specifically, the CRY-box is a degron identified in Cdc20 which contributes to its degradation in GV-stage oocytes by APC/C^{Cdh1}.

1.5.2 Regulation of SLiMs

Degrons are also often subject to post-translational modifications. The residue on position 2 of a D-box, which in some instances is a serine, can be phosphorylated and result in substrate stabilisation, as is the case for plus-end microtubule based motor protein KIF1C[110]. Conversely, dephosphorylation of these sites can enhance the degradation of the substrate. An acidic residue in D-box P6 enhances ubiquitination of a substrate due to an increase in affinity to the D-box receptor and a phosphate group on this site in place of an acidic residue has the same effect[30].

Motifs themselves can be negatively regulated without modifications via the binding to other proteins resulting in their inaccessibility. This is referred to as 'degron masking' and can occur whereby the association of another protein masks, or blocks access to a degron. Such as is the case for TPX2, which protects Aurora A from APC/C^{Cdh1}. Guharoy et al. found that degron regions extensively overlap with protein-protein interaction sites[111].

1.6 Structure of the APC/C and mechanism of action

Considerable progress has been made dissecting the fine details of the APC/C structure and mechanism of action. This is significantly aided by the fact that individual APC/C subunits can be expressed in insect cells and reconstituted as a single complex, subsequently purified using size exclusion chromatography for downstream analysis[112].Importantly, this purified complex retains *in-vitro* ubiquitination capability, which has permitted its use in ubiquitination assays as well as structure determination. Mutations can be induced in individual subunits as well as exclusion of whole subunits to determine their impact on ubiquitination ability and impact on structure. These techniques have been used extensively by David Barford's group to produce an outstanding degree of insight into the structure and function of the APC/C in a range of contexts[20,107,113,114]. In 2016 this group used cryo-EM to determine the structure of the APC/C bound to a high affinity D-box substrate at sub-nanometre resolution, revealing the complete secondary structure of the APC/C and subsequent positioning of subunits[115].

The apo-APC/C is a massive 1.2 MDa multi-subunit complex at its core which adopts a triangular shape. It is composed of distinct organised structures; the TPR lobe, the catalytic module and the platform scaffolding complex (Figure 1.9). Auxiliary components, including E2 ubiquitin conjugating enzymes and coactivators also associate with the APC/C which permit ubiquitination and substrate docking capabilities respectively, as well as modulating activity of the APC/C depending on the context of the cell cycle[105,114]. In general, the APC/C can be thought of as a platform which facilitates the interactions between substrates and ubiquitinating units.

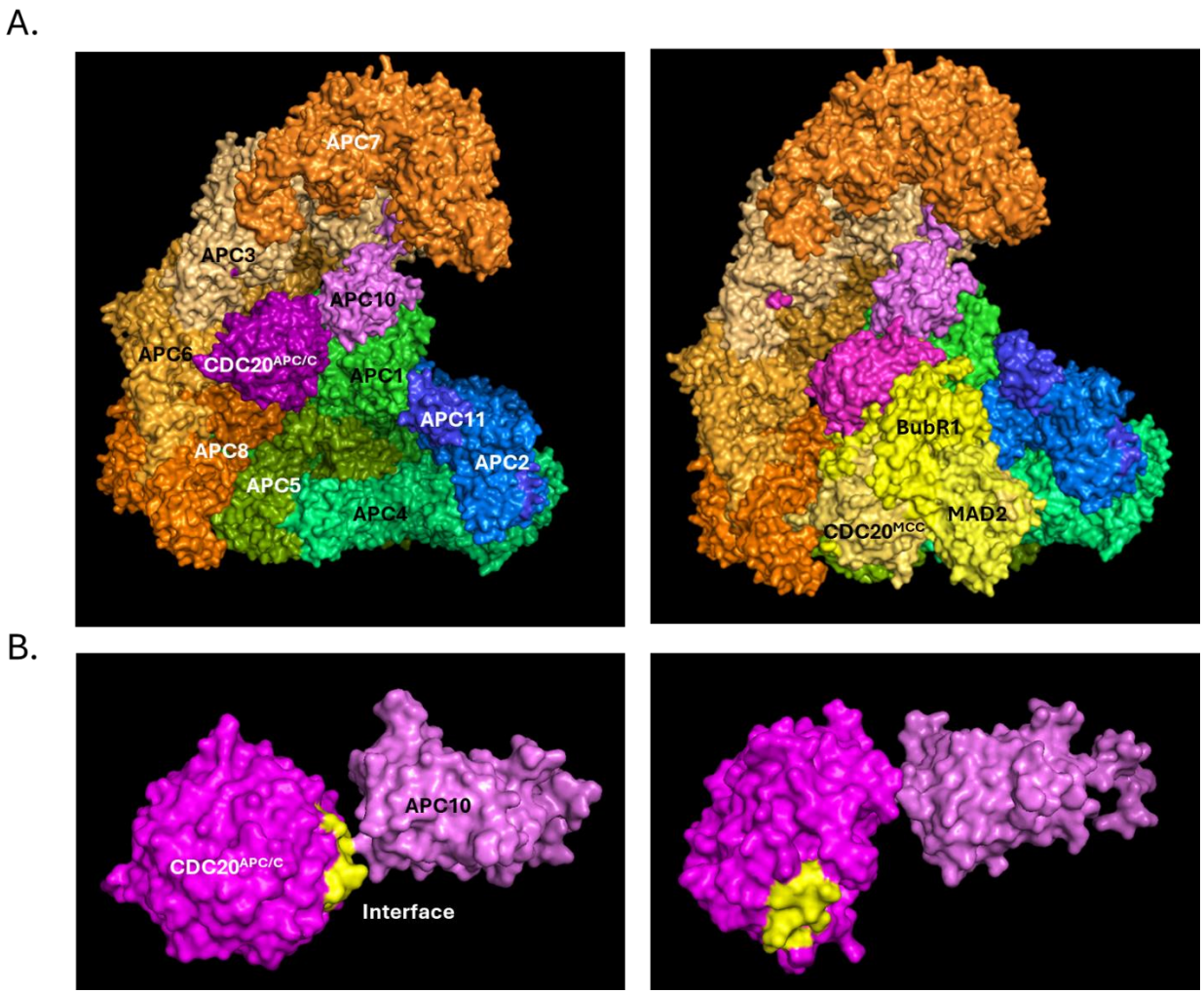

Figure 1.9. Structure of the APC/C^{Cdc20} and APC/C^{Cdc20}-MCC showing the various substructures and the movement of Cdc20$^{APC/C}$ induced by MCC binding.

Structure of the APC/C^{Cdc20} without (left) and with (right) the MCC present, coloured by different substructures and labelled by subunit. The catalytic core (blue shades), TPR subunit (orange shades), substrate recognition module (purple shades), scaffold subunit (green shades) and the Mitotic Checkpoint Complex (yellow shades). These are cryo-EM structures solved by David Barford's group and accessed using the ProteinDataBank (PDB:5G04, left; PDB:6TLJ, right;)[115,116] . Structures were adapted by isolating the individual protein chains and colourising them dependent on the substructure using pyMOL. B. Positioning of Cdc20$^{APC/C}$ (dark purple) relative to APC10 (light purple) when the MCC is (left, PDB:5G04[115]) and is not (right, PDB:6TLJ[116]) in complex. Cdc20 residues 168-176, which are located on the interface to APC10, has been highlighted in yellow to display the movement of Cdc20 upon MCC binding.

The tetratricopeptide repeat (TPR) lobe forms the substrate recognition complex of the APC/C. It consists of subunits APC3, APC6, APC7 and APC8. Each of these subunits exist as homodimers in the APC/C and are composed of highly repetitive 34-amino acid repeats called TPRs[114,117]. TPR repeats form helices which provide protein binding capabilities, for instance APC6 interacts with APC12 via its TPR repeat. This structure is incredibly important for the docking of key substrate recognition subunits including WD40 repeat containing coactivators (Cdc20/Cdh1) and APC10, all of which interact with APC3 TPR motifs using their C-terminal Isoleucine-Arganine (IR) tails. Coactivators also rely on APC8 binding utilising their conserved C-box motifs. APC10 and the coactivator are referred to as the "sub recognition module" as these two components are critical for substrate docking forming the bipartite D-box receptor as discussed earlier[105,105,108,114].

The coactivators themselves (essential for substrate recognition to bestow a key regulatory role for the APC/C) are highly conserved, composed of seven WD40 domain beta-propeller blades which forms a torus shape with an enclosed centre towards its C-terminus. The N-terminus is a long unstructured region which harbours a number of motifs which facilitate binding to interaction partners, as well as the APC/C for incorporation and their own destruction[118]. Notably, the WD40 domain is one of the most abundant protein interaction structures in the eukaryotic genome. The multiple WD40 repeats of these coactivators provide the potential to bind multiple peptides at once. This ultimately provides the substrate recognition capabilities of coactivators and the APC/C as a whole, and plays roles in temporal destruction differences[100,119]. Incorporation of APC/C coactivators (Cdc20 or Cdh1) is dependent on the stage of mitosis/meiosis as their specificity to substrates are slightly different and they are sensitive to different regulation mechanisms e.g. CDK1 phosphorylation.[120].

The coactivators associate with the APC/C by utilising a C-terminal dipeptide IR tail to bind the hyperphosphorylated loop of APC3 as well as binding to APC8 using their C-box motif via electrostatic interactions[115]. The binding of both Cdh1 and Cdc20 to the APC/C are not identical, however. The N-terminal KILR motif of Cdh1 engages APC1 using a hydrophobic

interface whereas this motif in Cdc20 contacts APC8 by inserting the Isoleucine and Leucine residues into a hydrophobic pocket of the TPR motif of APC8. It has been suggested that KILR motif binding stabilises C-box association. Interestingly, the differences between the KILR motif interactions between Cdc20 and Cdh1 suggest that Cdc20 binds to the APC/C with lower affinity than Cdh1[115]. The C-box interaction between coactivator and APC1 plays an important role in coactivator binding and thus is an important regulatory mechanism in terms of APC/C activation. APC1 harbours a disordered loop segment which blocks the C-box binding site on APC8 and prevents Cdc20 C-box binding. Upon phosphorylation of the disordered loop on APC1, the C-box binding site is liberated and Cdc20 incorporation becomes possible[114,115,121]. Importantly Cdc20 binds to the APC/C in close proximity to APC10 to form the substrate recognition module. Alongside permitting substrate recognition of the APC/C, coactivator association also causes the repositioning of the catalytic subunits APC2 and APC11 upwards, positioning them near the substrate-recognition module and aiding in ubiquitination[122].

Importantly, APC/C structure, and in particular the coactivators associated with it, is highly dynamic. A most prominent change is that at the onset and through mitosis Cdc20 is the primary coactivator of the APC/C. While Cdh1 becomes the primary coactivator following CDK1 inactivation through to G1[123,124]. In oocyte meiosis the pattern is somewhat different and further APC/C inhibitors become more critical to facilitate oocyte arrest points. Prior to meiosis initiation (prophase I-prometaphase I transition) the APC/C^{Cdh1} is inhibited by Emi1 which ultimately allows for the accumulation of cyclin B1. At GVBD, Emi1 is then targeted for destruction by another E3 ubiquitin ligase, $SCF^{beta\text{-}TrCP}$, which relieves the Emi1 inhibition of the APC/C and promotes its activation and subsequent Cdc20 incorporation[125,126]. After the metaphase-anaphase transition the APC/C is re-inhibited now by Emi2 to prevent the APC/C^{Cdc20} from triggering anaphase until fertilisation. The increase in Ca^{2+} which arises post-fertilisation results in the $SCF^{beta\text{-}TrCP}$ mediated destruction of Emi2 enabling the activation of APC/C^{Cdc20} [67,126].

The platform scaffolding complex of the APC/C consists of APC4 and 5 which associate with the APC/C as a heterodimer alongside APC1. This links the catalytic module and TPR lobe, as well as providing a key interaction for APC10 docking[114,127]. APC1 harbours a WD40 domain which contains phosphorylation sites for cyclin B1-CDK1 which, upon phosphorylation by this complex, moves away from APC8 and subsequently permits Cdc20 C-box association, as discussed earlier[128].

The catalytic module subcomplex consists of APC11 and APC2 which form a highly flexible ubiquitinating core. It is thought that this flexibility is very important for ubiquitination. APC11 and APC2 are essential for the binding of E2 ubiquitin conjugating enzymes UBCH10 which conjugate multiple monoubiquitins on substrate lysine residues, as well as Ube2S which is responsible for chain extension[129,130]. To achieve this the APC/C adopts a closed conformation, permitting a single substrate lysine residue to attack the E2-ubiquitin thioester bond, resulting in the transfer of ubiquitin. APC/C subunits that are critical to this include APC2, 4 and 11. Ube2S is recruited to the APC/C by coactivators and binds APC2 utilising its LRRL tail motif as well as associating with APC4. Ube2S then extends the mono-ubiquitin molecules on substrates via K11 and/or K48 linkages. This is aided by APC11 which positions the acceptor ubiquitin appropriately for this extension[122,131,132].

1.7 Regulation of APC/C targeting

The APC/C must be highly regulated in a number of different ways, to ensure that the correct substrates are being destroyed at the correct time and to prevent the destruction of unintended substrates (Figure 1.11). This is of upmost importance specifically in oocyte meiosis.

The capability of the APC/C to bind to a coactivator provides an incredibly robust mechanism of regulation as coactivators are essential for substrate recognition and APC/C activation. The presence of a coactivator is required for; the activation of UbCH10, substrate recognition and

subsequent ubiquitination. Indeed, coactivators are absolutely essential for substrate targeting and APC/C activity. However, it is not the case that different coactivators target different substrates, largely due to the high level of conservation between Cdc20 and Cdh1, meaning that the vast majority of substrates can be targeted by both coactivators. It is thought that APC/C^{Cdh1} can target all known APC/C^{Cdc20} substrates and select additional substrates. All of the known degron binding sites are shared between Cdc20 and Cdh1[105,108]. However it is plausible that to-be-discovered degron binding regions exist which could differ between these two coactivators and it also is possible that non-conserved regions could result in differences in targeting of substrates. For example Davey and Morgan suggest that since Cdc20 primarily targets securin and cyclin B1 to promote anaphase, and Cdh1 is surprisingly not essential for cell viability, that Cdc20 interacts with key substrates while Cdh11 "tidies up afterwards"[99].

The SAC is key regulator of the APC/C during prometaphase by preventing the APC/C^{Cdc20} targeting substrates that are otherwise involved in coordinating chromosome alignment and bivalent maintenance. The SAC is a signal which is constantly produced by kinetochores lacking microtubule attachments or often erroneously attached microtubules (Figure 1.4). Indeed, treating cells with microtubule depolymerising agents such as nocodazole has been shown to result in constitutively active SAC signalling[133,134]. The SAC exerts its effects by producing the MCC composed of BubR1; Bub3; Cdc20 and MAD2. This complex binds to the APC/C^{Cdc20} and exerts its inhibitory roles in a number of ways as described below[107]. First the MCC sequesters Cdc20 by introducing a second Cdc20 molecule its structure. The pre-existing Cdc20 coactivator molecule is referred to as $Cdc20^{APC/C}$ and the Cdc20 molecule incorporated into the MCC is referred to as $Cdc20^{MCC}$ (Figure 1.10A). The MCC utilises BubR1 and its cassette of ABBA/KEN/D-box motifs to bind to the $Cdc20^{APC/C}$ which both occupies the motif binding sites on $Cdc20^{APC/C}$ and shifts the positioning of $Cdc20^{APC/C}$ away from the co-receptor APC10 (Figure 1.10B). This both provides strong competition for substrate binding and places Cdc20 in a position which prevents its canonical D-box binding modes (utilising APC10). In addition to this, BubR1 contains TPR motifs that interact with APC2 providing a steric hinderance for mono-ubiquitin conjugating enzyme UbcH10 access to the catalytic core

(APC2 and11)[107]. Interestingly Kelly et al. determined that MCC incorporation into the APC/C^{Cdc20} did not however prevent the association of E2-ubiquitin conjugating enzyme Ube2S and the elongation of any existing mono-ubiquitins were still permitted[135].

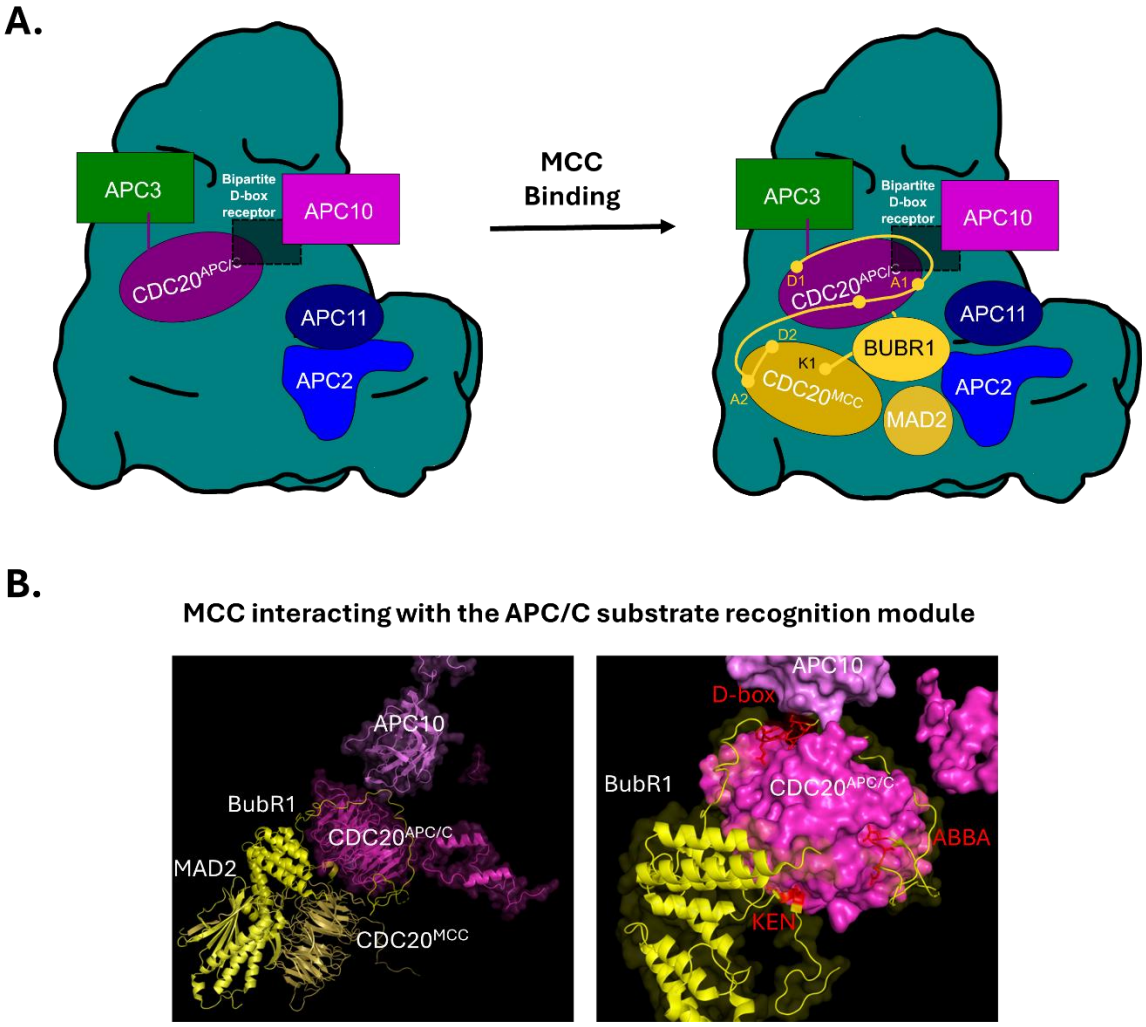

Figure 1.10. Structural changes of the APC/C upon MCC binding showing BubR1 occupying the SLiM binding sites of Cdc20

Structural of APC/C^{Cdc20} showing the catalytic module composed of Cdc20 and APC10 (purple) alongside APC3 (green) which is essential for Cdc20 incorporation into the APC/C. The catalytic subunit, composed of APC11 and APC2 (blue) provides the ubiquitin ligase

capabilities of the APC/C. Upon MCC binding, Cdc20 positioning is shifted and the bipartite D-box receptor (formed between $Cdc20^{APC/C}$ and APC10) is disrupted. BubR1 physically prevents the reformation of the bipartite D-box receptor and its SLiMs occupy the SLiM binding sites on $Cdc20^{APC/C}$ and $Cdc20^{MCC}$. Graphical representations of the APC/C complexes are adapted from images by the Barford group[20]. B) Cryo-EM images, solved by the Barford group (PDB:6TLJ[116]) and isolated/colourised using PyMOL, showing the structure of the APC/C substrate recognition module composing of $Cdc20^{APC/C}$ (purple) and APC10 (pink) in complex with the MCC, composing of BubR1 (yellow), $Cdc20^{MCC}$ (dark yellow), MAD2 (light yellow). BubR1 D-box, ABBA and KEN motifs are highlighted in red. BubR1 uses its unstructured N-terminal to wrap around Cdc20 APC/C and utilises its cassette of SLiMs to engage with the SLiM receptors of the $Cdc20^{APC/C}$ and $Cdc20^{MCC}$.

The disassociation of the MCC from the APC/C is also an important regulatory mechanism (Figure 1.11). This provides a way to monitor SAC activity and detect when the SAC switches off as a result of sufficient chromosome alignment and kinetochore-microtubule attachment. By consistently disassociating the MCC, newly formed MCC can take its place if the SAC is still signalling. And if the SAC is switched off, no MCC will be readily available to replace it. This constant flux of APC/C-MCC to APC/C^{Cdc20} allows a rapid response to induce anaphase upon SAC switching off. To permit this, the APC/C-MCC adopts two conformations, either open or closed, driven by APC15[105,107,113]. In the open state, the MCC is rotated away from the catalytic module which permits UbCH10 binding to the APC/C and subsequent autoubiquitination of $Cdc20^{MCC}$, resulting in its disassociation. In the closed conformation MCC blocks UbCH10 binding[135–137]. More detail into the formation of the MCC and specifically how this complex prevents APC/C^{Cdc20} activity will be discussed in a later section.

An additional mechanism of regulation is the phosphorylation of the APC/C (Figure 1.11). As discussed earlier, coactivator association with the APC/C is dependent on the phosphorylation of TPR containing subunits, specifically APC3 and APC1. The C-box binding site on APC8 is occupied by a disordered loop of APC1, hyperphosphorylation of this loop induces a conformational change which liberates the C-box binding site. Similarly, a disordered loop of APC3 blocks its IR-tail binding site which too is liberated upon phosphorylation of this loop. Free C-box and IR-tail binding sites are essential for coactivator association to the APC/C[138].

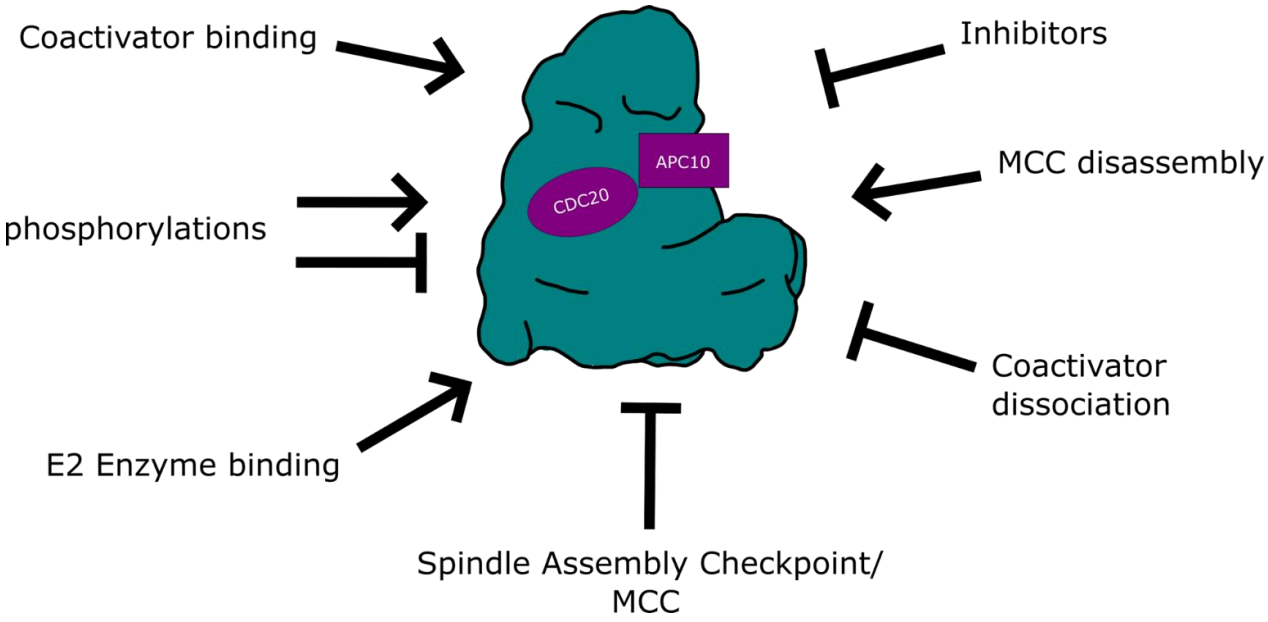

Figure 1.11. Regulation of the APC/C

Simplified structure of the APC/C labelled with positive and negative regulation factors. Coactivator association provides the APC/C with substrate recognition capabilities, and dissociation of the coactivator from the APC/C complex removes its ability to target substrates. The association of the Mitotic Checkpoint Complex, the effector molecule of the Spindle Assembly Checkpoint, regulates the destruction of substrates which prevent anaphase. Phosphorylations allow for finely tuned control of the APC/C and have various roles such as coactivator association as well as substrate docking. E2 enzyme association allows for the transfer of ubiquitin onto substrate lysine residues. Finally, inhibitors such as Emi1 can prevent the APC/C from targeting substrates. Graphical representations of the APC/C complexes are adapted from images by the Barford group[20].

Phosphorylation by CDK1 provides a key feedback loop in order to switch coactivator (Figure 1.11). As APC/C^{Cdc20} targets cyclin B1, CDK1 becomes increasingly inactive which means that Cdh1 and APC/C phosphorylation events are reduced and they exist increasingly in a dephosphorylated state. Phosphorylated Cdh1 is unable to be incorporated into the APC/C, but this dephosphorylation both activates Cdh1 and permits APC/C^{Cdh1} formation. As a result, Cdc20 becomes an APC/C^{Cdh1} target which results in a mass switch from APC/C^{Cdc20} to APC/C^{Cdh1} activity. Indeed, it has been observed that non-phosphorylatable Cdh1 mutants constitutively activate the APC/C both *in-vitro* and *in-vivo*[98].This allows the newly formed

APC/C^{Cdh1} to target Anaphase/Telophase substrates such as PLK1 and Aurora A/B as well as Cdc20, which yet further promotes the transition from APC/C^{Cdc20} to APC/C^{Cdh1} [139].

Similarly to Cdh1, Cdc20 phosphorylation by CDK1 also prevents its incorporation into the APC/C, and yet CDK1 phosphorylation activates the APC/C which appears to be contradictory. However, CDK1 phosphorylates the APC/C on serine residues and Cdc20 on threonine residues. Mitotic phosphatase PP2A has a specificity to de-phosphorylated threonine residues, thus PP2A counteracts CDK1 phosphorylation on Cdc20 which provides a mechanism that activates both APC/C and Cdc20[140,141]. Phosphorylation is incredibly plastic during the life course of the APC/C and provides finely tuned temporal regulation of APC/C activity.

1.8 MCC formation at unattached kinetochores, its action on the APC/C and disassembly

The SAC provides a mechanism for the cell to detect misaligned chromosomes and prolong the length of prometaphase until this is achieved (Figure 1.4). Insufficient signalling by the SAC can result in premature APC/C activation and therefore premature chromosome separation. In the context of meiosis this is a major contributor to aneuploidy and subsequent miscarriage or birth defects[142].

The SAC is often referred to as a surveillance mechanism composed of a signal transduction pathway. It is activated in prometaphase when kinetochores either lack microtubule connections or kinetochores not sensing tension (Figure 1.4). The signal can be described as a ‘wait anaphase’ signal as its main purpose is to prevent APC/C activity towards promoting anaphase. Upon chromosome alignment, sufficient kinetochore tension and correct kinetochore-microtubule attachments, this signal stops being produced. This is highly sensitive. It has been proposed that a single unattached kinetochore is sufficient to produce enough signal to prevent anaphase promotion across the entire area of a typical mitotic spindle[143].

Checkpoint proteins are recruited to kinetochores in response to an Mps1 driven phosphorylation cascade which assembles a catalytic scaffold. The establishment of SAC activity is complicated but I will attempt to summarise below[144].

- Mps1 kinase phosphorylates MELT motifs on Knl1, a component of the KMN (Knl1C, Mis12C, Ndc8) network located on the outer kinetochore, which provides a key microtubule-binding interface.[145]
- This results in the recruitment of MCC components BUB3 bound to Bub1:BubR1[146]. Further Mps1 and Cdk1 phosphorylation events support Bub1 binding and recruits Mad1:C-Mad2 which then associates with Cdc20[133,147]. "C-Mad2" refers to Mad2 in its "closed", active conformation and "O-mad2" refers to mad2 in its "open", inactive conformation. This forms the assembled catalytic scaffold on the kinetochore corona which promotes Mad2:Cdc20 formation. This is an inherently energetically unfavourable conversion, hence the formation of the catalytic scaffold.
- The scaffold is utilised to convert O-MAD2 to active C-MAD2 by introducing the MAD2 interacting motif of Cdc20 to O-mad2, subsequently releasing MAD2 from MAD1:C-MAD2 to Cdc20[148].
- MAD2:Cdc20 then binds BubR1:BUB3 to form the final MCC. MCC complexes assemble *in-vitro* from recombinant MAD2, BUBR1, BUB3 and Cdc20 at a much slower rate proving that association with the kinetochore is catalytic as opposed to essential for formation
- BubR1 utilises its cassette of SLiMs to occupy the SLiM binding sites of Cdc20 (Figure 1.10), which is critical to ensure that Cdc20 does not bind to APC/C substrates. The KEN1-box of BubR1 occupies the KEN-box binding site of Cdc20, alongside its ABBA2 and D2-box motifs in their respective Cdc20 inter blade groove binding sites. Cdc20 additionally binds to MAD2 utilising its KILR motif[107].

This model satisfies the findings that individual subunits bind each other individually, for instance Cdc20:MAD2, Cdc20:BUBR1, BUBR1:MAD2 have all been established to interact independently of the MCC structure as a whole[149–151]. Indeed, many sub-complexes of the

MCC have been determined and verified *in-vitro* as being inhibitors of the APC/C such as the BBC, consisting of BubR1:BUB3:Cdc20 as well as BubR1:Bub3 and MAD2:Cdc20[98]. These individual complexes could act as less potent APC/C inhibitors before the prometaphase increase in MAD2. Proposed mechanisms of MCC assembly have been debated throughout literature. Another proposed method of assembly is the initial formation of the BBC complex which then incorporates C-MAD2 in prometaphase.

Once formed, the MCC complex acts as a diffusible inhibitor of the APC/C^{Cdc20}. The MCC occupies the central cavity of the APC/C forming the APC/C-MCC complex. BubR1, as part of the MCC, exerts its role to control substrate binding to the APC/C by binding as a pseudo-substrate. It utilises its disordered region containing SLiMs to engage Cdc20$^{APC/C}$ motif binding regions while still maintaining contact with Cdc20$^{MCC.}$ Specifically, BubR1s D1-box, ABBA-1 and KEN-2 motifs associate with the respective binding sites on Cdc20$^{APC/C}$ while simultaneously utilising its ABBA-2 and D2-box motifs to occupy the binding sites of Cdc20^{MCC} (Figure 1.10). However, studies have shown that mutation of BubR1s ABBA2 and D2-box motifs do not entirely prevent MCC mediated APC/C inhibition, suggesting that interactions between BubR1 and Cdc20$^{APC/C}$ are sufficient to retain MCC docking into the APC/C complex.

Upon MCC binding, Cdc20$^{APC/C}$ is tilted ~40° and rotated 90° about its central axis, thus positioning it away from co-receptor APC10, disrupting the bipartite D-box receptor. Interestingly, this movement also appears to disrupt the IR tail of Cdc20$^{APC/C}$ interacting with APC3 which may permit this movement. The interaction between Cdc20$^{APC/C}$ and APC8 remains. Alongside acting as a pseudo-substrate for the APC/C, BubR1 prevents the mono-ubiquitination ability of the APC/C by interacting with APC2 utilising its TPR domain, providing a steric hinderance to UbcH10 binding[105,107,108,114].

Importantly, the consensus across many excellent cell cycle groups is that the spindle assembly checkpoint is not an ‘all or nothing’ signal but rather provides a gradient, concentration dependent response where difference APC/C populations may exist simultaneously[27].

To enable rapid termination of the MCC induced substrate targeting inhibition of the APC/C, the MCC complex is auto-ubiquitinated by the APC/C-MCC in which an open state of the APC/C-MCC is induced to permit MCC release followed by ubiquitination. When the SAC is active, the APC/C-MCC exists as two different populations at any one time, either in the APC/C-MCC-open or APC/C-MCC-closed configuration, with the majority in closed mode. In the APC/C-MCC-open configuration, $APC15^{NTH}$ binds to $APC5^{NTD}$, subsequently $APC5^{NTD}$ and $APC4^{HBD}$ are moved downwards, displacing $Cdc20^{MCC}$ and permitting the release of the MCC. $Cdc20^{MCC}$ is then ubiquitinated which contributes to MCC dissociation and inactivation (demonstrating constant turn over and flux)[107,152]. Furthermore, there is increasing evidence for BubR1 being targeted for destruction in the APC/C-MCC-open configuration as the D-box and ubiquitinatable lysine residues are in close proximity to UbCH10 and the APC2-11 catalytic module in this mode[152,153].

1.9 Substrate recognition of the APC/C

Perhaps a most important capability of the APC/C is to recognise substrates with high affinity, a property which is owed to the coactivators of the APC/C and specifically their WD40 domains.

The Cdh1 D-box binding site is located between blades 1 and 7 of its WD40 domain. This was determined by Kraft et al. who utilised chemical crosslinking to identify residues of Cdh1 responsible for D-box binding[154]. This site is conserved between Cdc20 and Cdh1 alongside ABBA and KEN-box binding regions[101,155]. The D-box binding site is composed of a hydrophobic binding pocket to which the leucine of the D-box consensus sequence binds (Figure 1.8). In this study, the group mutated this pocket and ubiquitination capability was perturbed. Investigating this further, this group also identified a second conserved surface which favours electrostatic interactions with the arginine of the D-box[154].

The non-MCC associated APC/C, APC/C^{Cdc20}, targets substrates utilising a bipartite D-box receptor formed between Cdc20 and APC10 which are located in close proximity (Figure 1.8). The D-box binding site of Cdc20 faces a peptide binding region of APC10. In this mode, N-

terminal residues of a substrates D-box associate with Cdc20 and C-terminal hydrophilic residues of the D-box associate with APC10. This region is important for targeting substrates such as cyclin B1 and securin. MCC association prevents the formation of the bipartite D-box due to a positional change of Cdc20 and BubR1 incorporation. This ultimately prevents the destruction of anaphase inhibiting substrates during an active SAC[107,156].

Perhaps the best understood APC/C substrate targeting mechanism is that of cyclin A2. Considerable work by the Pines and Barford labs have provided the best insight into the destruction of this protein[20,157]. Cyclin A2 is a fascinating APC/C substrate as it is able to be targeted by the APC/C regardless of whether the MCC is present, however the mechanism of targeting is different depending on the mode the APC/C is in. This is essential. Throughout mitosis and meiosis cyclin A2 levels need to remain low in prometaphase, while chromosomes are still aligning, so it makes sense that the APC/C is permitted to efficiently target this protein even while the SAC is active. The following describes targeting in both modes (Figure 1.12).

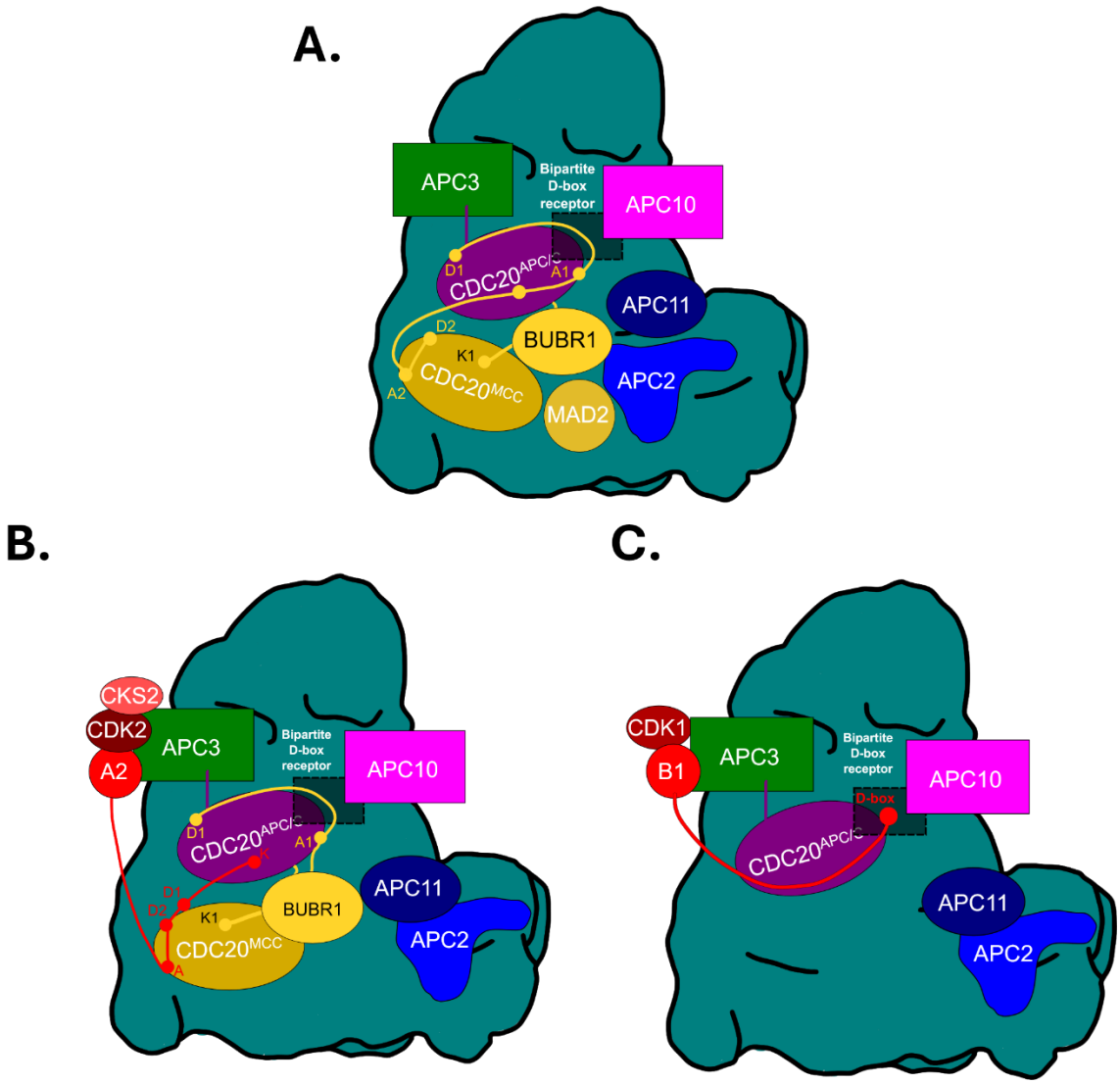

Figure 1.12. Mechanisms of cyclin A2 and cyclin B1 destruction by the APC/C

A) Simplified structure of the APC/C bound to the MCC during an active SAC (adapted from a study by the Barford group[20]). MCC binding introduces a second Cdc20 molecule ($Cdc20^{MCC}$) alongside the existing APC/C coactivator ($Cdc20^{APC/C}$). MCC incorporation induces a positional change of $Cdc20^{APC/C}$ which disrupts the bipartite D-box receptor. BubR1 utilises its SLiMs to block the substrate recognition sites of both CD20 molecules. B) Cyclin A2 destruction by the APC/C-MCC during an active SAC (adapted from a study by the Barford group[20]). Cyclin A2 utilises its high affinity SLiMs to displace the SLiMs of BubR1 and allow its ubiquitination. Importantly the bipartite D-box receptor remains unformed which prevents cyclin B1 destruction. C) Proposed mechanism of cyclin B1 destruction by APC/C^{Cdc20}. Thus far, no cryo-EM analysis has been conducted on cyclin B1 destruction by the APC/C. However, the D-box of cyclin B1 is known to interact with the bipartite D-box receptor after MCC dissociation in

metaphase[158]. Graphical representations of the APC/C complexes are adapted from images by the Barford group[20].

Cyclin A2-CDK2-CKS2 localises to the APC/C by utilising CKS2s ability to associate with phosphorylated APC3 which docks this substrate into position. Studies have shown that CKS2 and the N-terminal 165 residues of cyclin A2 are required for destruction by APC/C^{MCC} in prometaphase[78,157,159].

The unstructured N-terminal tail of human cyclin A2 contains two D-box motifs, D1 and D2 (canonical and non-canonical respectively), an ABBA motif and a KEN motif[99,102]. As described earlier, when the MCC is bound to the APC/C, BubR1 binds to both Cdc20 coactivator molecules (one coactivator as part of the APC/C and the other, a subunit of the MCC) by binding to all six degron binding sites across both Cdc20 molecules (D-box, ABBA and Ken box sites). This is ultimately to prevent substrates from freely binding to these sites thought to be owed to the higher binding affinity of BubR1s motifs. However, analysis of the motifs, and their respective binding sites on coactivators, suggests that cyclin A2 is able to outcompete BubR1 for these binding sites due to more favourable residues which give better binding affinities. As such, Cyclin A2s ABBA motif displaces the ABBA2 motif of BubR1 for binding onto $Cdc20^{MCC}$. Cyclin A2 then also uses its KEN box to bind the KEN box binding site of $Cdc20^{APC/C}$. The Barford group predicts that cyclin A2s KEN box is able to compete for BubR1s KEN2 motif because of a C-terminal PRO and ASP at P1, which have a higher affinity for this site than the equivalent BUBR1 KEN box residues. Cyclin A2 further uses its D2-box to bind the D-box binding site on $Cdc20^{MCC}$. However, many other contacts made by BubR1 still bridge both APC/C and MCC components, holding the MCC in place. It has been suggested that the action of cyclin A2 binding both $Cdc20^{MCC}$ and $Cdc20^{APC/C}$ is also enough to hold this structure in place after outcompeting BubR1 for these sites[20,105].

Binding of cyclin A2-CDK2-CKS2 to the APC/C-MCC, this resulted in a four-fold increase in the ratio of open:closed APC/C-MCC states, suggesting that the binding of cyclin A2 induces an

open state APC/C which may result in the catalytic subcomplex to engage an E2 enzyme and permit ubiquitination of cyclin A2[20].

Importantly, substrates such as cyclin B1-CDK1 are thought to be unable to bind to the APC/C-MCC in a similar manner to cyclin A2-CDK2. Cyclin B1 does not hold an ABBA motif, or KEN-Box. Interestingly, the Barford group found that appropriately positioning an ABBA motif into cyclin B1 conferred some ability to be targeted by the APC/C-MCC, while addition of a KEN box alone had no effect. However, the addition of both KEN and ABBA motifs into cyclin B1 conferred similar ubiquitination dynamics to that of cyclin A2. Ultimately this suggests that neither motif alone bestows SAC resistance, but that this is a cooperative effect, likely boosting affinity[20].

As mentioned, Cyclin A2 is also an APC/C target in the absence of the SAC, but in this case cyclin A2 does not necessarily interact in a way that might be expected, it does not mimic metaphase cyclin B1 binding owing to the fact that it utilises the ABBA and/or KEN motifs for its destruction in this mode. The Barford group utilised cryo-EM to determine the structure of cyclin A2-CDK2-CKS2 bound to a APC/CΔAPC1-300S mutant, a constitutively active form of the APC/C without the MCC present. They found that when the MCC is not present, cyclin A2 can bind to APC/C^{Cdc20} in two different binding modes, utilising either D1 or D2 boxes. The D1 mode mechanism of destruction involves the D1 box binding to the Cdc20 D-box binding site, as well as binding to Cdc20 with both ABBA and KEN motifs. In the D2 mode, cyclin A2 D2 motif again binds to the Cdc20 D-box binding site, alongside the KEN motif binding to the KEN binding site of Cdc20. The ABBA motif is suggested not to be employed in this mode. Without the MCC present, the D-box binding site of Cdc20 is positioned in close proximity to APC10, and both binding modes appear to make contact with APC10, thus the bipartite D-box receptor is still involved. These experiments also provided further insight in to the formation of the bipartite D-Box receptor. The positioning of Cdc20 relative to APC10 appears to be dynamic in order to position D-boxes well in the bipartite D-box receptor. To facilitate the docking of the D1 box, a 20Å shift of the Cdc20 WD40 domain occurs which permits the

C-terminus of the D1 box to fold backwards and become sandwiched between Cdc20 and APC10[20].

To summarise, Cyclin A2 targeting by the APC/C^{Cdc20}, without an MCC present, uses D-boxes as well as KEN and ABBA motifs depending on which D-box is in play. However, by *in-vitro* ubiquitination assays, the Barford group determined that mutation of both KEN and ABBA motifs had no significant impact on ubiquitination of cyclin A2 compared to wildtype in the absence of the MCC, suggesting that while they use of the KEN and ABBA motif, they appear to not be essential. They only become essential when cyclin A2 is targeted by the APC/C-MCC as mutation of both resulted in no ubiquitination of the substrate in that context.

Another example of a protein able to be targeted by the APC/C-MCC during an active SAC is the protein kinase, NEK2A, essential for mitosis and spindle production in particular. Uniquely, it is able to associate with the APC/C-MCC independently of coactivator binding and instead docks with APC/C subunits directly. NEK2A associates with APC/C-MCC in its open conformation and utilises its C-terminal MR motif to bind to the APC8A TPR subunit. Interestingly, it binds in a nearly identical manner to the IR tail of $Cdc20^{MCC}$, which binds to APC8B, the other monomer of the APC8 homodimer. Another MR binding pocket exists formed between APC2 and APC4 which is not essential for NEK2A ubiquitination however likely increases the efficiency of ubiquitination. While NEK2A harbours both D- and KEN-box motifs, mutation of these does not significantly impair its ubiquitination by the APC/C[116].

1.10 APC/C mediated cyclin B1 destruction in meiosis

In 2019 our group identified a second sequence in cyclin B1 necessary for correctly timed APC/C targeting in MI oocytes. Importantly without this sequence aberrant cyclin B1 destruction resulted in many more cell division errors[160].

Our group discovered that in the mouse oocyte, cyclin B1 exists in a 6-fold excess to CDK1. This is in contrast to mitotic cells whereby CDK1 is instead in excess to cyclin B1[161]. This means that in the oocyte, cyclin B1 can be identified as either bound to CDK1 or unbound,

which is referred to herein as “free cyclin B1”. This nomenclature of “free” is in respect to CDK1 binding, as binding to other proteins has not been excluded.

Utilising mRNA encoding cyclin B1 linked C-terminally to a fluorescent protein and microinjected into GV-stage mouse oocytes, the oocytes were stimulated to continue into meiosis and express the fluorescent protein. The abundance of this construct was quantified over time to investigate how cyclin B1 is targeted for destruction over the course of MI. Interestingly, we found that in MI the fluorescent reporter of free cyclin B1 was targeted for destruction in late prometaphase, approximately 2.5-hours ahead of anaphase and before chromosomes have successfully congressed. Considering in mitosis, cyclin B1 is targeted for destruction only after chromosomes have fully aligned with correct microtubule attachments, this is a significant finding[158]. Initiating cyclin B1 destruction prior to full chromosome alignment significantly increases the risk of aneuploidy in mitosis. And yet, aneuploidy rates in mouse oocytes are very low.

Our group additionally utilised a second cyclin B1 reporter which included a Y170A mutation. An alanine mutation at this site removes the ability of cyclin B1 to bind to CDK1 and this mutant thereby reports the characteristics of the pool of free cyclin B1[162,163]. Interestingly, this non-CDK1 binding mutant was destroyed with almost identical dynamics as wildtype cyclin B1, critically in late prometaphase I and not metaphase I. Our group also reported that cyclin B1 destruction does not report CDK1 activity in oocyte meiosis, while both mirror each other in mitosis. The reason for this is suggested to be first loss of the excess of free cyclin B1 in the oocyte before CDK1-bound cyclin B1 destruction, which only then depletes CDK1 activity.

Significantly, surprising results were obtained when injecting and reporting a cyclin B1 construct which only contains the N-terminal 90 amino acids. This truncation of cyclin B1 was expected to be destroyed like wildtype cyclin B1 since it includes a D-box and lysine residues. All the ingredients thought at that time to govern cyclin B1 destruction dynamics, given the finding that the non CDK1 binding mutant is destroyed with identical timing. However,

destruction was initiated significantly later, approximately 80-90 minutes after the cyclin $B1^{Y170A}$ mutant (herein referred to as free cyclin B1), and remarkably now at a timepoint coinciding with chromosome alignment. Furthermore using nocodazole to stimulate a persistent checkpoint, our group showed that the reporter for free cyclin B1 was able to be targeted for destruction while the D-box containing truncated construct was stabilised. This ultimately suggests that full-length cyclin B1 contains an additional region, aside from the D-box, which permits destruction in late prometaphase of meiosis I, and while the SAC is signalling[160].

Further experiments extending the length of cyclin B1 revealed that this early destruction characteristic is due to the presence of a short sequence of amino acids located in the N-terminal helix of cyclin B1. Further point mutations revealed individual residues "^{173}DIY^{175}—^{177}LRQL^{181}". Our group named this sequence the "PM-motif" owing to its potential to permit destruction in prometaphase.

Ultimately, when the PM motif is unmutated, fluorescent cyclin B1 reporters are destroyed in late prometaphase. When the PM motif is mutated to alanines, the destruction occurs later, closer to the metaphase-anaphase transition. The location of this motif is critical to its ability to orchestrate this timing. The PM motif is located at the binding interface between cyclin B1 and CDK1. Therefore, a suggested degron-masking mechanism model has been proposed whereby CDK1 binding prevents access to the PM motif and results in late destruction of CDK1-bound cyclin B1. The free cyclin B1 contains an un-masked PM motif and is therefore targeted in late prometaphase I. This is detailed in Figure 1.13**.**

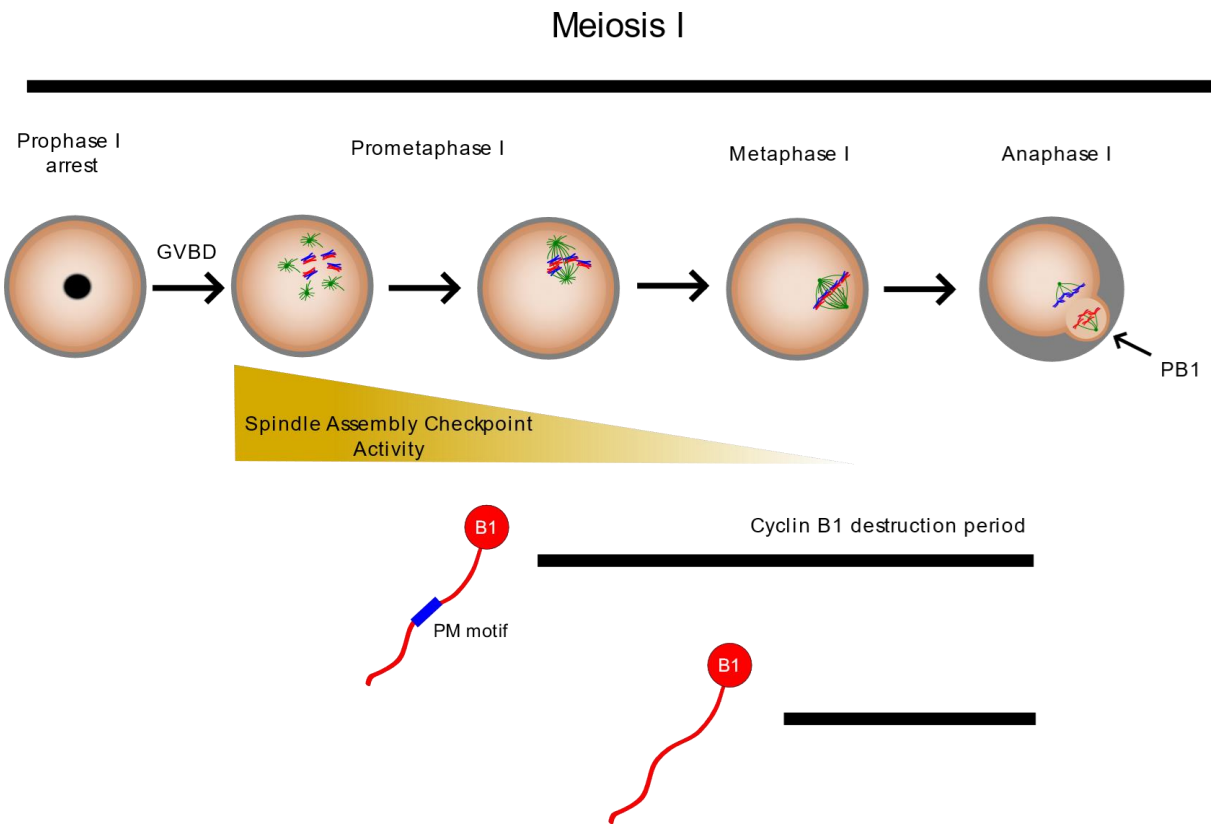

Figure 1.13. Diagram showing the timings of destruction of cyclin B1 in mouse oocyte meiosis.

Free cyclin B1, with an unmasked PM motif, is targeted for destruction in late prometaphase, prior to full chromosome alignment and at a time period when the Spindle Assembly Checkpoint will still be active. CDK1 bound cyclin B1 is targeted for destruction at the metaphase-anaphase transition, due to CDK1 masking the PM motif.

The mechanism of how the PM motif permits prometaphase destruction remains a significant question. To permit earlier destruction it seems highly likely that the PM motif binds to a region on the APC/C, most probably the coactivator Cdc20. Further, given destruction occurs during the spindle assembly checkpoint activity, it is reasonable to assume that the MCC is present in APC/C complexes destroying this form of cyclin B1. Drawing similarities to cyclin A2, it seems likely that the PM motif could displace regions of BubR1 for access to the destruction machinery. One candidate for a PM motif binding site on Cdc20 could be the ABBA motif binding site which, as discussed previously, contributes to

cyclin A2 destruction in prometaphase. While the PM motif differs significantly from an ABBA motif in both sequence and structure (the ABBA motif is linear and the PM motif is helical), the ABBA motif binding site presents as a groove on the surface of Cdc20 which could hypothetically accommodate a helix (Figure 1-14). Additionally, the PM motif is largely comprised of residues with hydrophobic side chains which could become buried in a structure like this.

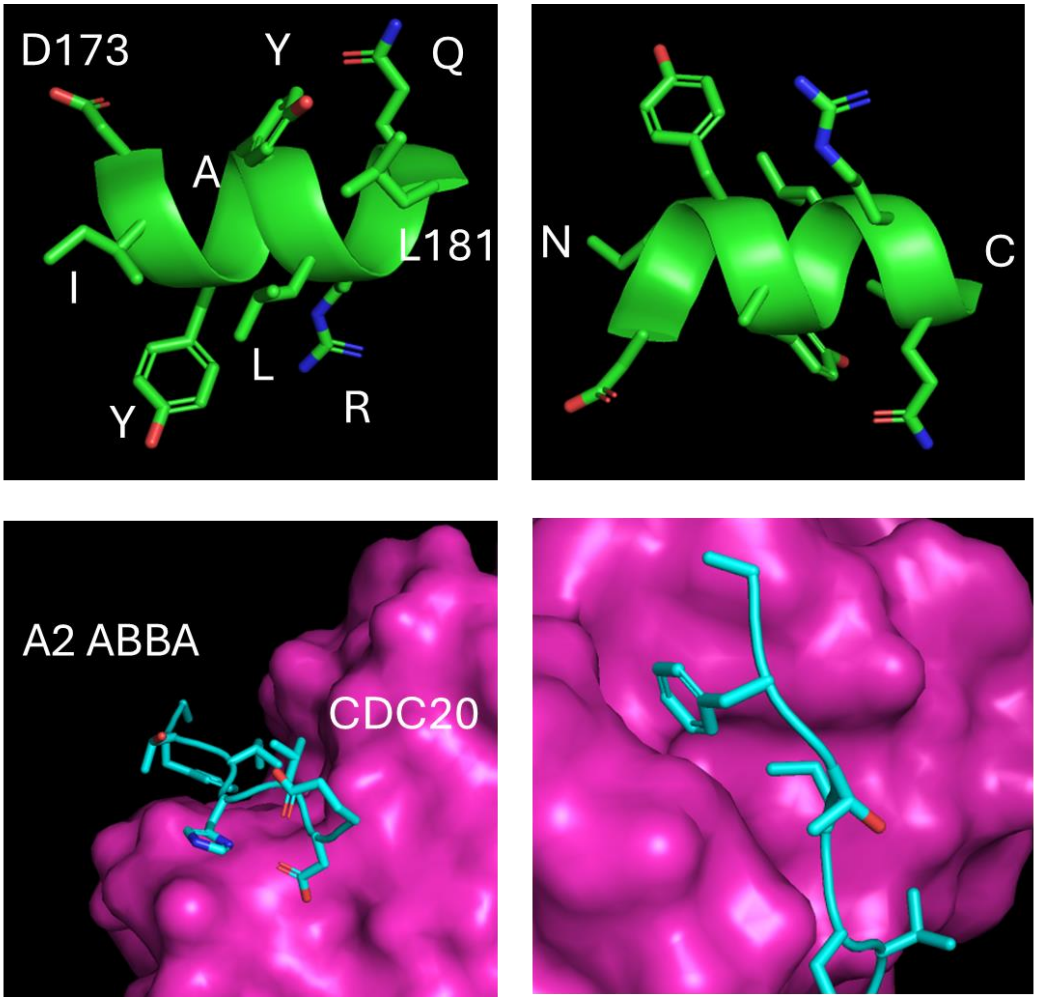

Figure 1.14 - Structure of the PM motif and ABBA motif binding site of Cdc20

The PM motif of cyclin B1 (top row; cartoon; green; PDB:2B9R[164]) shown in two orientations with residues labelled and side chains displayed. Cyclin A2 ABBA motif (bottom row; cartoon; cyan) is shown in-situ with the Cdc20 (surface; purple) ABBA motif binding site, which adopts a groove on Cdc20 surface (PDB:6Q6G[20]). Structures have been isolated and colourised using pyMOL.

The main aims of this PhD study are to reveal how free cyclin B1 is targeted for destruction in the MI oocyte. Specifically, how the PM motif of cyclin B1 permits prometaphase I targeting. Additionally, to further understand the interaction between cyclin B1 and the APC/C. As discussed throughout this introduction, there are profound differences between mitosis and female mammalian meiosis. Therefore, this study also aims to understand these differences, especially regarding APC/C substrate targeting in the context of female mammalian meiosis.

This study utilises the expression of fluorescent reporters of mutant cyclin B1 constructs, alongside other APC/C substrates, in mouse oocytes to characterise their localisation and destruction dynamics over the course of MI. This is achieved via the *in-vitro* production of mRNA which is microinjected into live oocytes and quantified using live cell fluorescence imaging over the course of MI. Localisation and destruction profiles can then be compared between mutant constructs to further understand the roles of SLiMs and their impact on APC/C targeting. Morpholino antisense oligomers are also utilised to knockdown endogenous APC/C subunits to determine their role in substrate targeting in MI oocytes. Finally, I explore the potential of a protein-protein interaction assay in live oocytes to identify interaction partners of mutant forms of cyclin B1 in MI.

Chapter 2 - Methods

2.1 Mouse oocyte collection and culture

Female 5–10-week-old CD1 mice (Charles River) were used. All animals were handled in accordance with ethics approved by the UK Home Office Animals Scientific Procedures Act 1986. However, given that mice did not undergo a 'procedure' as defined by the Act, the project did not require Home Office Licensing. The reason for animal use was instead approved and governed by Newcastle University's Comparative Biology Centre Ethics Committee; Study Plan Reference Number 699; AWERB Approval Reference Number; 663. Mice were housed in the Comparative Biology Centre at Newcastle University and culled in compliance with UK Home Office approved technique. Ovaries were harvested from a minimum of two mice per experiment were placed into petri dishes containing pools of M2 media (Sigma-Aldrich; #M7167) supplemented with penicillin/streptomycin (Pen/strep; Sigma-Aldrich; #P4458) and either 30 nM 3-isobytyl-1-methylxanthine (IBMX Sigma; #I5879; from a stock solution of 60 μM dissolved in DMSO) or 1 μM Milrinone (Sigma-Aldrich; #M4659; from a 2 mM stock solution in DMSO) as indicated depending on the extended incubation period necessary. Media pools were covered in embryo-grade mineral oil (Sigma-Aldrich; #M5310) to prevent evaporation and maintained at 37°C on a heated stage. Under a stereoscope, ovaries were shredded using a sterile needle to release GV stage oocytes which were separated from ovary tissue and cumulus cells using mouth pipettes. Briefly, mouth pipettes are fabricated by heating glass Pasteur pipettes over a Bunsen burner flame until malleable and pulled by hand to produce an internal diameter just slightly larger than that of an oocyte. Selected oocytes were transferred through further pools of clean M2 media (supplemented with IBMX, or milrinone as indicated) for washing free of cumulus cells and other ovarian debris. Dishes were transferred from the stereoscope stage to a 37°C dry bath every few minutes to ensure they remained warm. Only oocytes with a generally circular shape, centred GV and prominent zona were used in experiments. These are predicted to be the healthiest oocytes and at the correct stage of development.

2.2 Plasmid constructs

Wildtype Human Cyclin B1 (NM_031966), Securin (NM_001282382), Cyclin A2 (NM_001237) and CKS1 (EF026652) sequences were amplified from pre-existing gene targets within the Madgwick lab. C- and N- TurboID gene targets were a gift from Alice Ting (AddGene Plasmid #153004 and #153005 respectively)[165]. BioID2 gene target was a gift from Leinhard Schmitz (pTet-on-Puro-Myc-BirA). Human BubR1 gene target was a gift from Don Cleveland (AddGene plasmid #47330)[166].

Sequences of interest were amplified by PCR using KOD polymerase mastermix (NOVAGEN; # 13148426) to generate blunt-ended products. Primers used in PCR reactions contained additional sequences for restriction endonuclease recognition sites at both ends to produce a PCR product with a >15bp sequence homologous to the restriction endonuclease site of the destination vector. PCR products were purified using the GeneJET PCR purification kit (ThermoScientific; K0702) and eluted in elution buffer.

MDL9 or MDL8 plasmid vectors were used as a backbone to which genes encoding proteins of interest were inserted. MDL9 and MDL8 are pRN3 vectors containing restriction enzyme sites to which genes are inserted. This is followed by a 5 amino acid C-Terminal linker (AGAQF) to Venus Fluorescent Protein (MDL9) or Cerulean Fluorescent Protein (MDL8), respectively. Upstream of the gene insertion regions are a T3 promotor. The presence of this specific promotor is essential for downstream mRNA production. Additionally, this vector contains an ampicillin resistance gene for positive selection. In preparation for gene insertion into MDL9/MDL8, vectors were linearised utilising restriction enzyme digestion. ~1 µg of vector was diluted in Nuclease Free Water (Invitrogen #AM9937) and combined with 10x NEBuffer r3.1 (NEB; #B6003S) and BGLii enzyme (NEB; #R0144S) to a final buffer concentration of 1x. The digestion mixture was heated on a thermocycler (ThermoScientific Hybaid PCR Sprint) at 37°C for 4-hours to linearise the vector.

To purify the fraction of digestion mixture which was successfully linearised/digested, DNA fragments in the digestion mixture were separated by size using agarose gel electrophoresis.

A sample of undigested vector was also ran on this gel to confirm successful digestion, alongside an appropriate DNA-ladder (NEB; #n3232). DNA mixtures were mixed with 6X gel loading dye (NEB;#B7204S) to a final concentration of 1X. Samples were then run on a 1.5% agarose-TAE gel containing 1xSYBR-safe (ThermoFisher; #S33102) in 1x TAE buffer (50X stock; Formedium; #TAE0500) and ran at 120V until the dye-front migrated approximately 80% of the length of the gel. The gel was visualised using a UV machine and correct sized fragments were excised from the gel using a scalpel. Appropriate eyewear was used when visualising the gel on the UV machine.

Gel segments containing correctly sized DNA fragments were weighed purified using the geneJET gel Gel Extraction kit (ThermoFisher; #K0691). Briefly, gel segments were mixed with buffer QG at 1:3 w/v and heated at 50°C to melt the gel. DNA suspension was passed through a spin column from the extraction kit and followed by a series of wash steps before elution and DNA quantified using a nanodrop (ThermoScientific: #ND2000) blanked with elution buffer supplied by the extraction kit**.**

Amplified genes were inserted into linearised vector using the NEBuilder HiFi DNA Assembly kit (NEB; #E2621S). This kit contains a master mix which contains: an exonuclease which creates single-stranded 3’ overhangs which aid in the annealing of fragments with overlapping regions; a polymerase which fills in gaps within each annealed fragment; and a DNA ligase which seals the assembled DNA. On ice, 100 ng vector and a 2-fold excess of insert where added NEBuilder HiFi DNA Assembly master mix and the volume made up to 20 µl with nuclease-free water. This reaction mixture was heated in a thermocycler at 50°C for 15-minutes and subsequently cooled on ice before transformation into chemically competent e. coli.

Chemically competent NEB 5-alpha competent E. coli (NEB; C2987H) were defrosted on ice and gently flicked to resuspend cells. Assembly product was mixed with e. coli and stored on ice for 30-minutes. Following this, cells were subject to a heat-shock at 42°C for 30-seconds before storing on ice for a further 2-minutes. SOC outgrowth medium was added to the tube

containing now transformed e. coli, before plating on LB Agar supplemented with 100 µg/ml Ampicillin (100 mg/ml stock in deionized water; Sigma-Aldrich; #A5354) and incubated overnight at 37°c.

Colonies were then amplified as per section 2.4.

2.3 Mutagenesis of plasmid constructs

To create specific mutations in the various protein sequences as indicated primers for Q5 mutagenesis were designed using the NEB Base changer tool to which DNA sequences were submitted. The NCBI CCDS database was used to determine the codons to mutate for each desired point mutation and these modified sequences were submitted to the NEB Base changer tool which produced forward and reverse primer sequences as well as indicating annealing temperatures for each reaction. Primers were custom made by Invitrogen.

The Q5 mutagenesis kit (NEB; #E0554S) was followed as per manufacturers protocol. In short, a PCR reaction was performed using MDL9 or MDL8 vectors containing genes encoding proteins of interest, made using the methods in section 2.2. The PCR reaction was conducted using Q5 Hot Start High-Fidelity DNA Polymerase master mix utilising the primers, specific annealing temperatures and extension times for the construct being made. 1 µl of this PCR product was then used in a 5-minute KLD (Kinase-Ligase-Dpn1) reaction at room-temperature for circularisation of the PCR product and template removal.

5 µL of circularised product from the KLD reaction was transformed into NEB 5-alpha competent E. coli cells using the heat shock and plating method in section 2.2.

2.4 Colony amplification and Sequencing

Individual colonies were selected from transformation plates and grown in LB broth supplemented with 100 µg/ml ampicillin in an oscillating 37°C incubator overnight. Plasmid was then isolated using a Promega plasmid miniprep kit (Promega; #A1222) as per the manufacturers protocol. In brief, e.coli suspensions were lysed centrifuged to pellet cell debris. Supernatant was passed through a spin-column supplied in the miniprep kit using centrifugation and an endotoxin removal wash conducted. This was followed by further wash steps using the wash buffer supplied in the kit and eluted in 25 µl elution buffer, also supplied in the kit. 1 µl Plasmid was diluted 1:3 in nuclease-free water and sent to Eurofins Genomics for sanger sequencing and analysis. Sequence reports were analysed using nucleotide BLAST (https://blast.ncbi.nlm.nih.gov/Blast.cgi) and EXPASY translate (https://web.expasy.org/translate/). Plasmid preps containing poor quality DNA or incorrect sequences were discarded. Plasmid preps containing the correct sequences were quantified and used for cRNA preparation

Amino acid sequences of the proteins used throughout this thesis alongside their mutated residues can be found in Appendix II.

2.5 Preparation of cRNA and morpholino oligomers used in microinjection

After sequence and quality analysis, 1 µg plasmid DNA was digested with 10 U/µl SfiI in 1x Buffer G (ThermoFisher; #ER1821) for 4-hours at 50°C to linearise the vector in preparation for downstream *in-vitro* cRNA synthesis. 200 µg/µl Proteinase K (ThermoFisher; #AM2546) and 0.5% SDS was added to linearised plasmid and incubated at 50°C in a thermocycler for 1-hour. DNA was purified prior to cDNA synthesis by the following method. DNA was extracted by increasing the volume of the sample to 150 µl with nuclease-free Water (Invitrogen; #AM9937), followed by a phenol/chloroform reaction. Briefly, DNA solutions for extraction were mixed with an equal volume of phenol/chloroform/isoamylalcohol (25:24:1, v/v;

ThermoFisher; #15593031), vortexed and centrifuged at 13,000xG for 1-min. The supernatant (the DNA fraction) was aspirated, mixed thoroughly with an equal amount of chloroform (SigmaAldrich; #288306) to remove residual phenol. This was centrifuged at 13,000xG for 1-min. The supernatant (the DNA fraction) was removed before the addition of Pellet Paint (Merck; #69049), 10%v/v 3 M sodium acetate (pH 5.5; Invitrogen; #AM9740) and 100% ethanol. Now purified DNA was precipitated overnight at -20°C. The following day, a 30-minute centrifugation at 13,000xG and 4°C was performed to pellet the purified DNA. The DNA pellet was washed in 70% ethanol in nuclease-free water and re-centrifuged at 13,000xG for 20-minutes. The supernatant was removed, and the DNA pellet was resuspended in 6µl nuclease-free water.

The purified and linearised plasmid DNA was used for the input in the T3 mMessage mMachine *in-vitro* transcription kit (ThermoFisher; #AM1348) as per manufacturers instruction to produce cRNA for microinjection. The reaction mix, containing RNA polymerase; ribonucleotides; and reaction buffer was incubated for 2-hours at 37°C followed by the addition of TURBO DNase (2 U/µl supplied by the kit) for 15-mins to remove template DNA. The reaction was then terminated and RNA precipitated by the addition of nuclease-free water and Lithium Chloride Precipitation Solution (7.5 M lithium chloride, 50mM EDTA) supplied in the kit. This solution was incubated overnight at -20°C to improve yield. The following morning, cRNA was pelleted by centrifugation of the precipitation mixture at 13,000xG at 4°C for 30-minutes. The supernatant was removed and the cRNA pellet was washed in 70% ethanol in nuclease-free water and recentrifuged at 13,000xG at 4°C. The supernatant was aspirated and the cRNA was resuspended in nuclease-free water, aliquoted on ice immediately and stored at -80°C to limit freeze-thaw cycles.

The above plasmid linearisation, *in-vitro* transcription reaction and cRNA purification was performed in an area of the lab dedicated to RNA procedures. All reagents and equipment used were certified DNase/RNase free where possible. Surfaces in the RNA procedure area were wiped down with RNase*Zap* RNase decontamination wipes (ThermoFisher; #AM9780).

Morpholino antisense oligonucleotides (MO; Gene tools) were used in knockdown experiments. MOs were designed against specific endogenous mouse mRNA sequences found in Table 2.1. All MOs were diluted in water to 2mM stored at room temperature as per manufacturers protocol. Prior to use in microinjection MOs were heated for 5-mins at 65°C and diluted to a final concentration of 1 mM in Texas-red dye (1:200). Texas-red dye was used in knockdown experiments to confirm the injection of MO by visualising injected oocytes on a fluorescence microscope.

Protein	**Morpholino sequence (5'-3')**
BubR1	TCCCAATACTTGCTCTCGCCCTTCC
APC10	GCCCACAAAGCCTGAGGAGACAGCA

Table 2.1 - Morpholino sequences used for knockdown experiments

2.6 Microinjection and Imaging

For microinjection experiments, oocytes from a minimum of two mice were pooled. Microinjection was carried out in a 1 ml well of M2 media (with IBMX and Pen/strep as described in Section 2.1 on the heated stage of an inverted epifluoresence microscope (Leica Dmi8) fitted for micromanipulation. The temperature was set at 37°C and the media was covered in mineral oil to prevent evaporation. A glass holding pipette with a 30° bend (coopersurgical; #MPHMED30) connected to a injection holder set and microinjector (Narishige; IM-21 and IM-H3), back filled with mineral oil used to hold the oocytes in place at the base of the well during microinjection. Oocytes with centred GVs, of spherical structure and with prominent zona pellucida were pooled and transferred by mouth pipette to the

supplemented M2 media on the heated stage of the microscope. They were positioned on the stage and held one at a time for injection by the holding pipette, under the control of 3-axis micro-manipulation instruments (Narishige; MMO-203).

For microinjection, needles were prepared using filamented fine glass capillaries (Warner Instruments; #GC150F-10) and a needle puller (Sutter Instrument; Model P-97) which heats and draws out glass into a fine point. The pointed end of a pulled glass capillary was brushed against cotton wool to snap the end and open the needle lumen. Needles were then assessed under a light microscope (Nikon Optiphot PO1) and graded depending on needle diameter and shape for quality. For microinjection, approximately 0.2 µl of either cRNA or MO at the appropriate concentration was loaded into a needle using a fine pipette tip and Hamilton syringe. Filled needles were then stored upright with the needle pointing downwards for over 10-minutes to allow capillary action to draw the solution to the tip of the needle and allow air bubbles rise out of solution. The needle was then filled with 120 mM KCl in 10 mM HEPES pH 7.4 and fitted to a Pneumatic PicoPump (World Precision Instruments; #PV830) via plastic tubing.

Needles were positioned above the egg and again controlled using a three-way manipulator. For injection, the tip of the needle was pushed through the zona pellucida and cell membrane. A pulse of negative capacitance was then provided by a MICRO-ePORE (World Precision Instruments) to assist passage into the oolemma and subsequently increase survival rates. Injectant was then released into the oocyte by a pulse of compressed air regulated by a pneumatic picopump. Injectant volume was adjusted using the air pressure controller on the picopump and was estimated by the diameter of displaced ooplasm, estimated to be between 0.1-0.3% of total volume.

Healthy injected oocytes were isolated and maintained in a labelled petri dish with each pool of IBMX supplemented M2 media containing oocytes from one injectant group. After over two-hours of incubation at 37°C to allow for sufficient translation of cRNA, the injection stage was cleaned and prepared as an imaging stage. This involves the addition of 0.5 µL of cell-tak

(Corning;#354240) to a clean dry glass coverslip as a new stage insert, this prevents the movement of oocytes once then are reintroduced. Once the cell-tak had dried, as indicated by the formation of microscopic crystals, the stage was filled with 1 mL of M2 media (now with or without IBMX supplement as indicated) and oocytes were carefully positioned for imaging.

For oocytes injected with MOs, extended incubation times post-injection were necessary. This included incubation times of >20-hours. In this case oocytes were transferred into M16 media (Sigma-Aldrich; #M7292) supplemented with milrinone (1 µM; ApolloScientific; #BIM0128) and penicillin/streptomyocin supplemented M16 media (Sigma-Aldrich; #M7292) which had been pre-equilibrated in a CO_2 incubator at 37°C to support longer periods of culture. At the end of MO incubation, oocytes were washed into M2 media and placed onto the stage using the above method.

Images were captured on a Leica DMI8 inverted epifluoresence microscope (Leica Microsystems) and were captured every 10-minutes for 20-hours. All imaging was conducted with the heated stage maintained at 37°C.

Oocytes expressing different constructs always sat alongside a group of oocytes expressing a relevant 'control' protein as an indicator of 'normal' oocyte behaviour. The identity of control protein changed relative to the question being asked but was defined as a profile well established by previous experimentation, reporting highly reproducible results (for example the destruction profile of a cyclin B1). By confirming the destruction profile of the established construct matches that of previous experimentation, alternative constructs were compared with greater confidence. The exception to this is Figure 4.7 whereby for technical reasons the "control expressor" failed in these experiments. Importantly the 'control' expressor and 'treatment' expressors were always oocytes selected from the same pool of oocytes, randomly selected. In addition, average destruction trace lines are the sum of oocytes from at least 2 replicates across 4 mice. Unfortunately, it is not practical to always have all groups for comparison represented at the same time.

2.7 Data capture and processing

Change in fluorescence over time was recorded by the Leica LAS X software (Leica Microsystems). Regions of interest were drawn over individual oocytes and an average intensity for each region was calculated and logged over time. Data were transferred and exported as Microsoft Excel files, followed by import into Prism/Graphpad (GraphPad Prism version 10.3 for Windows, GraphPad Software, Boston, Massachusetts USA, www.graphpad.com).

Data were looked at in several forms. As the timing of meiosis I differs between individual oocytes, fluorescence traces for individual oocytes need to be aligned to a distinct, easily identifiable point of meiosis I. Therefore, fluorescence readings for individual oocytes were aligned to the extrusion of the first polar body (PB1). DIC images of individual oocytes over the course of the experiment were examined over time and the time of PB1 for each oocyte was recorded, specifically the time at which a bleb at the cortex first appears. Fluorescence readings for individual oocytes were aligned to this timepoint. Oocytes which did not produce a polar body were removed from the dataset unless otherwise indicated. Where indicated, fluorescence readings for individual oocytes were instead aligned at Germinal Vesicle Breakdown (GVBD).

Using Prism/Graphpad, fluorescence readings for individual oocytes were normalised whereby 100% is defined as the peak fluorescence prior to destruction. Per construct, normalised fluorescence readings were then collated from all experiments utilising that construct.

Following this, row means and Standard Error of Mean (SEM) of fluorescence readings were calculated for all oocytes in each injection group using Prism/Graphpad. Means were graphed and SEM displayed as error bars.

2.8 ProTAME experimentation

In ProTAME dose-response experiments, oocytes were harvested and cultured as described in section 2.1 and placed into M2 media without IBMX supplementation to resume meiosis I. After two hours, oocytes were then transferred to a petri dish containing pools of M2 media, without IBMX supplemented with varying concentrations of ProTAME (BostonBiochem #I-440). Oocytes were left overnight at 37°C and rate of polar body extrusion calculated. For experiments quantifying cyclin B1 destruction in the presence of proTAME, oocytes were injected with fluorescent cyclin B1 cDNA and fluorescence verified. Oocytes were released into M2 media without IBMX to allow the oocytes to resume meiosis. After 1.5-hours post-GVBD, oocytes were transferred onto the microscope stage containing M2 media supplemented with ProTAME (1.5 µM).

2.9 Oocyte TURBOID biotin proximity ligation

Oocytes were injected with cDNA encoding cyclin B1±PM motif linked on its C-terminus to a TurboID sequence. As previously described, oocytes were then incubated for 2-hours in M2 media supplemented with IBMX to allow protein expression and useful levels of fluorescence. Fluorescence was quantified using a Leica DMi8 epifluorescence microscope and checked to determine that they were expressing this construct to a reasonable extent. After removal of suboptimal oocytes, oocytes were washed in non-IBMX M2 media to stimulate the resumption of meiosis I, indicated by GVBD. Those that did not undergo GVBD after 2-hours were removed. Oocytes were then left to mature for a further 4.5 hours post-GVBD before washing into pools of M2 media supplemented with 100 µM biotin (Thermo Scientific:#10588733, dissolved in DMSO as a 100 mM stock). Biotin exposure lasted for 1-hour before washing through multiple pools of non-biotin supplemented media.

For banking of lysates for eventual pulldown and mass spectrometry, oocytes were then washed into pre-warmed dishes of PBS with 0.3%(w/v) polyvinylpyrrolidone (Sigma-Aldrich; #PVP10) before aspirating into Pierce IP lysis buffer (Thermo Scientific; #87787; 25 mM Tris-

HCl pH 7.4, 150 mM NaCl, 1% NP-40, 1 mM EDTA, 5% glycerol) followed by a vortex treatment. After a 5-minute room temperature incubation with intermittent vortexing, lysates were snap frozen in liquid nitrogen and stored at -80°C for later use.

For immunofluorescence experiments, oocytes underwent the immunofluorescence protocol described in section 2.11.

2.10 Confocal microscopy

For higher resolution imaging oocytes expressing fluorescent protein constructs were imaged using a Zeiss LSM800. As discussed previously oocytes were washed into non-IBMX supplemented M2 media to resume their cell cycle. For confocal imaging, oocytes were incubated first away from light for 3.5-hours post-GVBD before washing into 6.25 pM sirDNA (Spirochrome) containing M2 media for 1-hour. A droplet of cell-tak (Corning; #354240) was allowed to dry on a glass bottom dish suitable as a confocal platform and 2mL of sirDNA (6.25 pM) containing M2 media filled this dish. Oocytes were transferred to the dried celltak and briefly left to adhere. The glass bottom dish was positioned on the confocal microscope, regions of interest were set and oocytes were imaged periodically overnight as they completed MI.

2.11 Oocyte fixation and immunofluorescence

Oocytes were cultured as previously described until either prophase oocytes (incubated in M2 media supplemented with IBMX until fixation) or prometaphase (released into non-IBMX supplemented M2 media for 4.5-hours post-release from IBMX). As a quality control measure only oocytes graded as full competency potential were selected and any oocytes that did not undergo GVBD after 2-hours were discarded.

To secure oocytes for fixation a droplet of cell-tak (corning; #354240) was placed into each well of an 8-well slide (Thermo Scientific; #162600661). Cell-tak was then left to dry until crystals formed. A single rinse in 500 µl of wash buffer (PBS, 0.1% Tween-20) removed any

remaining excess acetic acid left behind by the cell-tak. Warm M2 media was placed in each well and oocytes were loaded onto the cell-tak in relevant groupings. They were then allowed to fully adhere without movement for 5-minutes. Following this M2 media was slowly aspirated and replaced with a rinse of wash buffer to remove any cell debris or excess media. A fixative (1.6% paraformaldehyde in 0.1% PBS Triton X-100) was then added to each well and the slide was incubated at room temperature for 30-minutes. Afterwards, fixing media was removed and the oocytes were washed with three-times in permeablisation buffer (0.1% PBS Triton X-100) the final wash of permeablisation buffer was left overnight.

The following day oocytes were washed 3 times into blocking buffer (3% BSA in 0.1% PBS Tween-20, filtered using a 0.22 µm filter) and incubated in the final blocking buffer addition at room temperature for 1-hour. Oocytes were then then incubated with relevant primary antibodies (Table 2.2) at 1:1000 in blocking buffer at 4°C overnight. The following day, primary antibody was washed out using three 5-minute blocking buffer washes. Oocytes were then incubated with a relevant secondary antibody (1:2000) in blocking buffer at room temperature for 1-hour. Secondary antibody was washed out 3-times with blocking buffer and 100 µl of blocking buffer was added to each well as a final step. The wall structure of the wells was removed using the well removal tool supplied by thermofisher and coverslips were applied before wiping away excess blocking buffer and sealing the unit with nail varnish. Nail varnish was left to dry and slides were imaged using the imaging protocol described in section 2.6 Microinjection and Imaging

Antibody/Conjugated fluorophore	**Dilution**	**Manufacturer/product code/Lot**	**Secondary antibody**
BubR1	1:1000 Concentration unknown	Gift from Stephen Taylor	Donkey anti-Sheep IgG (H+L) Cross-Adsorbed Secondary Antibody, Alexa Fluor™ 488 (ThermoFisher #A-11015; LOT: 1807723) 1:2000, 1 ng/mL final concentration
TACC3	1:1000 0.978 ng/mL Final concentration	Abcam; ab134154; LOT: GR179938-10	Goat anti-Rabbit IgG (H+L) Cross-Adsorbed Secondary Antibody, Alexa Fluor™ 594 (ThermoFisher #A-11012; LOT:1744751) 1:2000, 1 ng/mL final concentration
Streptavidin AlexaFluor 594	1:1000 2 ng/mL Final concentration	Molecular Probes; FisherScientific; #10626153; LOT:N/A	
SirDNA	1:1000	Spirochrome; SiR-DNA kit	

	125 nM Final concentration		

Table 2.2. List of antibodies used in experiments

2.12 Molecular structure visualisation

Protein structures were obtained from the protein database and visualised using PyMOL by Schrodinger (Version 3.0; https://www.pymol.org/). All images visualised using PyMOL were accessed from the ProteinDataBank (https://www.rcsb.org/). PDB entry IDs used are indicated in figure legends alongside the group responsible for generating the structures. Once structures were downloaded, sequences of protein subunits were displayed in "chain identifier" mode and extracted as individual objects. Structures of individual proteins were displayed as either surface or cartoon structures, and the colour changed as indicated in figures. Analysis whereby the contacting residues were determined was performed by selecting regions using the "residue codes" display mode and finding any contacts with 3A. Alignment of structures were performed by isolating the residues to be analysed, extracting as objects and using the alignment tool in PyMOL.

All graphical representations of the APC/C are based on structures from the Barford group.

Chapter 3 – The PM motif

3.1 Introduction

The APC/C targets its numerous substrates guided by a coactivator (Cdc20 or Cdh1 depending on the stage mitosis/meiosis), to recognise Short Linear Motifs on substrates referred to as 'SLiMs' which permit and time the targeting of substrates (Figure 3.1) [137]. A subset of SLiMs are referred to in the literature as 'degrons'. However there exists inconsistencies in the literature as to what defines a degron. Well established groups in the field however tend to define a degron as a SLiM which harbours destructive capability on it's own and does not require the presence of additional SLiMs on substrates to permit destruction. These degron signals are transferable as inserting a degron into a non-APC/C substrate has been shown to turn it into an APC/C target and result in its destruction, and conversely, mutating degrons in well characterised APC/C substrates results in their stabilisation which highlights the potency of these short signals[99].

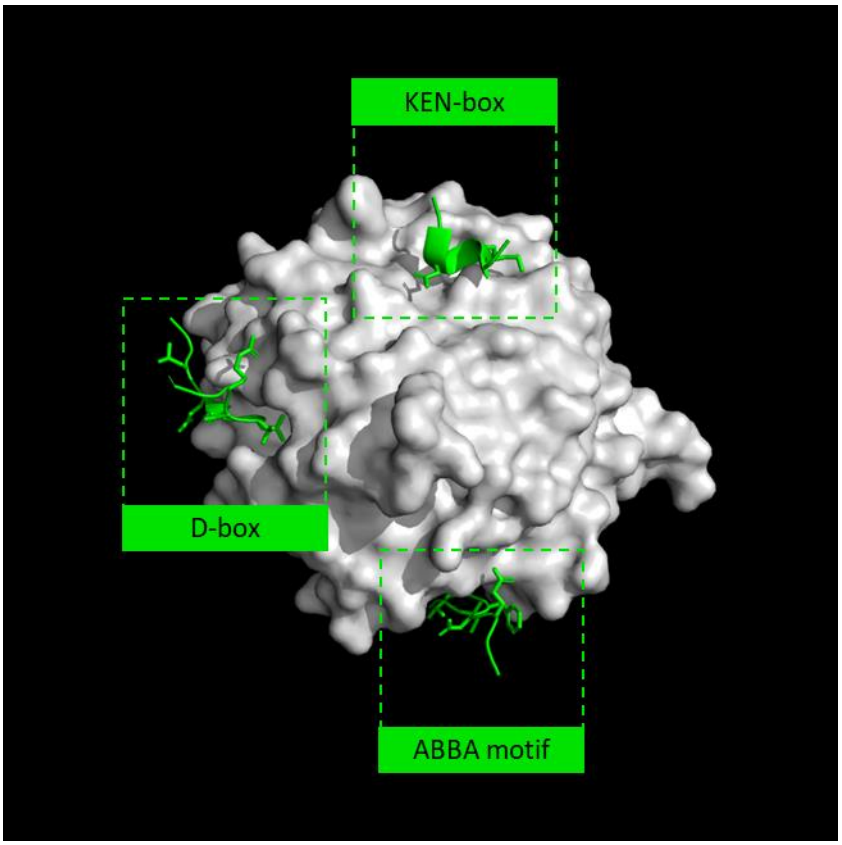

Figure 3.1. Three of the most well characterised Short Linear Motifs (SLiMs) engaging their respective binding sites on APC/C coactivator Cdc20

SLiMs on substrates engage the coactivator subunit of the APC/C to facilitate destruction or influence dynamics of destruction. This figure shows the binding sites of the KEN box, ABBA motif and D-box of BubR1 in-situ with Cdc20 from a cryo-EM structure of the anaphase-promoting complex/cyclosome bound to the Mitotic checkpoint complex (PDB: 6TLJ[116]). Cdc20 and BubR1 structures were isolated from the PDB model and colourised using PyMOL, solved by cryo-EM experiments from the Barford group. Motifs of BubR1 were identified and isolated using Table 3.1 alongside two residues either side. The exact sequences of the motifs have side chains included however the non-motif residues do not.

Canonical degrons are the most well understood APC/C recognition signals with the most defined being the Destruction-box motif or "D-Box" motif. Consisting of the consensus sequence RxxLx[D/E][Ø]xN[N/S], the D-box can be found in both APC/C^{Cdc20} and APC/C^{Cdh1} specific substrates[105]. The KEN-box is another canonical degron, with the consensus sequence KENxxxD/N and is specifically recognised by both APC/C coactivators, Cdc20 and

Cdh1. The KEN-box is often found in combination with the D-box in substrates which are targeted by both coactivators, an example being cyclin A2 (Figure 1.12, Figure 1.8) [104,109].

Generally, in mitosis cyclin proteins are bound to their respective kinases which in turn are also associated with a CKS subunit. These subunits are often referred to as cofactors or chaperones as they localise the substrate to the APC/C by utilising a phospho-peptide binding domain bind to hyperphosphorylated APC3[77,167]. After CKS association to APC3 and localisation of the substrate to the APC/C has been achieved, if capable, the D-box is able to engage the bipartite D-box binding site located between coactivator and APC10 (Figure 1.12). This subsequently results in the ubiquitination of substrates and their degradation via the proteasome. In the instance of cyclin A2, additional motif bindings allow for its destruction in a SAC-independent mechanism, namely the ABBA and KEN motifs, as discussed in Section 1.9.

Alongside the canonical degrons are non-canonical recognition motifs which differ from the consensus sequences of the well-established degrons, one of the most recently identified non-canonical motifs is a second D-box of cyclin A2, characterised by the Barford group, referred to as the D2-box [20]. This differs significantly from the consensus sequence of traditional D-boxes (Table 3.1) however it is the only motif in cyclin A2 which is sufficient for destruction in absence of all other currently known degrons in cyclin A2 and is thus presumed to be the principal D-box. Further evidence for this motif being a D-box and not another destruction motif is that it has been shown by cryo-EM to occupy the D-box binding pocket of Cdc20[20]. Other non-canonical motifs include the A-box of Aurora A Kinase and the CRY-box of Cdc20, both confer destruction abilities[113,168].

SLiM	Protein	Species	Sequence	Canonical?
D-box	Bub1B	Human	ssvpq^{224}**RSTLAEL**^{230}kskgk	Yes
		Mouse	psepq^{217}**RSSLAEL**^{223}ksrgk	Yes
		Rat	ssepq^{217}**RSTLAEL**^{223}ksrgk	Yes
		Frog	lsepq^{211}**RSSLADL**^{217}ksrgk	Yes
	Cyclin A2	Human	qqprt^{47}**RAALAVL**^{53}ksgnp (D1)	Yes
			Pktrr^{72}**VAPLKDL**^{78}pvnde (D2)	No
		Mouse	Lktrr^{63}**VAPLKDL**^{69}pinde (D2)	No
		Rat	Lktrr^{58}**VAPLKDL**^{64}pinde (D2)	No
		Frog	vpvgg^{26}**RTVLGVL**^{32}qenhr (D1)	Yes
	Cyclin B1	Human	pglrp^{42}**RTALGDI**^{48}gnkse	Yes
		Mouse	pglrp^{42}**RTALGDI**^{48}gnkvs	yes

		Rat	pllrs[41]**RTALGDI**[47]gnkvs	yes
		Frog	pglrp[36]**RTALGDI**[42]gnkae	Yes
	Securin	Human	lpkat[61]**RKALGTV**[67]nrate	Yes
		Mouse	vpkas[58]**RKALGTV**[64]nrvae	Yes
		Rat	lpkas[58]**RKALGTV**[64]nrvte	yes
		Frog	vskps[55]**RKALGNV**[61]nkqil	YES
	Shugoshin Like 1	Human	tqqsp[438]**HLSLKDI**[444]tnvsl	No
		Mouse	tqesp[428]**RCSLKDV**[434]tnilq	YES
		Rat	TQESP[428]**HRGLKDV**[434]TNSLR	No
KEN	Bub1B	Human	Ewels[26]**KEN**[26]vqplr	Yes
			Pmpra[304]**KEN**[306]elqag	Yes
		Mouse	ewels[19]**KEN**[21]iqplr	Yes
			pvpra[297]**KEN**[299]elqpg	Yes

		Rat	ewels[19]**KEN**[21]iqplr	Yes
			pvpra[297]**KEN**[299]elqpg	Yes
	Cyclin A2	Human	talqe [29]**DQEN**[32]INPEK	No
		Mouse	slhqe[23]**DQEN**[26]vnpek	No
	Securin	Human	liyvd[9]**KEN**[11]gepgt	Yes
		Mouse	Lifvd[9]**KDN**[11]eepgr	No
		Rat	lifvd[9]**KDN**[11]eepgs	No
		Frog	tvvfv[7]**DQEN**[11]gdvgs	No
	Shugoshin-like 1	Human	rmsky[310]**KEN** [312]ksenk	Yes
ABBA	Bub1B	Human	gpsvp[528]**FSIFDE**[533]fllse	Yes
			qnnsr[272]**ITVFDE**[277]nadea	No
			avlps[340]**FTPYVE**[345]etarq	No
	Cyclin A2	Human	skqpa[99]FTIHVD[104]eaeke	No

		Mouse	skqpa[91]FTIHVD[96]eaeet	No
		Rat	skqpa[82]FTIHVD [87]epdca	No

Table 3.1 - Instances of SLiMs and their conservation

SLiMs are found in all APC/C substrates which either provide the substrate with APC/C destruction capabilities or control their destruction in terms of rate and timing. This table shows a selection of SLiMs and their sequences in different substrates to show their conservation between species and the similarity between the SLiMs of other substrates. These sequences were determined using the UniProt Database[169] and literature search. Assessment of whether these motifs are canonical is based on: “RxxL” (D-box); “Fx[ILV][FY]x[DE” (ABBA motif); “[DNE]KENxxP” (KEN-box).

There exists a subset of motifs which do not provide the capability of destruction but instead influence the dynamics of destruction, one of these being the ABBA motif. The ABBA motif was identified by the Pines group in 2015 whom used a computational approach to identify SLiMs which consisted of compiling and aligning a list of mitosis specific human protein sequences; feeding these through the ‘SLiMPrints’ tool and isolating the search of motifs to disordered regions before applying a filtering protocol to exclude extracellular and transmembrane regions. The resulting output highlighted a highly conserved motif in A-type cyclins, separase, BubR1 and BUB1[102]. The ABBA motif itself is not a destruction signal as this motif does not confer destruction capabilities and removal of this motif does not impact the extent of substrate destruction. However, studies by the Pines and Barford groups have shown that the mutation of this motif in cyclin A2 does result in a lower rate of destruction compared to wildtype cyclin A2, specifically in SAC arrested cells expressing fluorescent versions of cyclin A2[20,102]. The Barford group took this further and validated this finding using *in-vitro* ubiquitination assays utilising recombinant proteins, which showed that the activity of the APC/C-MCC on ABBA mutant cyclin A2 was almost halved compared to wildtype cyclin A2. The data exploring the effect of an ABBA mutation in cyclin A2 in non-SAC arrested cells differ slightly between the two groups, however. The Pines lab found that the time to reach

the maximum rate of destruction of ABBA mutant cyclin A2 was longer compared to wildtype (while there was no significant different in the maximum rate of destruction itself), whereas the Barford group found the destruction profile of ABBA mutant cyclin A2 to be no different to wildtype. These inconsistencies could be due to the fact that these groups explored this in different cell types (HEK for the Barford group and HeLa for the Pines group), as differential expression of substrates could result in altered competition for substrates to the APC/C between these cell types. This also highlights the difficulty in measuring prometaphase destruction of proteins in mitotic cells as this is a rapid event and likely difficult to determine small differences in destruction timing. Curiously the Barford group did show a significant increase in ubiquitination activity by recombinant APC/C^{Cdc20} towards ABBA mutant cyclin A2 by nearly 50% compared to wildtype cyclin A2[20]. Why this group observed no change in destruction profiles of fluorescent ABBA mutant cyclin A2 in live cells but an increase in activity via a ubiquitination assay was not explained. This could be due to a rate-limiting step between ubiquitination of substrate and proteasomal destruction or a limitation to this particular experiment which does not reflect *in-vivo* conditions.

The addition of an ABBA motif to substrates lacking this, such as cyclin B1, enhances the rate of destruction in mitotic cells however this destruction does not occur any earlier than wildtype[102]. Prometaphase destruction of cyclin B1 cannot be achieved unless both a KEN and ABBA motif are included at appropriate distances[20]. Collectively, this data strongly suggests that the ABBA motif plays a role in enhancing the rate of destruction for substrates, specifically when being targeted by the APC/C-MCC in prometaphase, but does not confer the capability for SAC-independent destruction itself. One theory for how the ABBA motif confers increased destruction rate is that the ABBA motif simply increases the binding affinity of substrates to the APC/C, a theory which has significantly more merit when analysing how cyclin A2 avoids SAC induced APC/C inhibition.

Cyclin A2 is a substrate with a very high degree of processivity by the APC/C, likely owing to the importance of the destruction of this substrate in allowing stable kinetochore-microtubule attachments. To overcome the SAC inhibition of the APC/C and permit its

destruction in prometaphase, cyclin A2 utilises its high affinity ABBA motif to compete with that of BubR1 for $Cdc20^{MCC}$ binding. It also utilises its KEN box to compete with that of BubR1 for the KEN box binding site of $Cdc20^{APC/C}$ as well as its D2 box, binding to the D-box pocket of $Cdc20^{MCC}$. Together with this cassette of high affinity motifs, cyclin A2 competes for binding to the coactivators of the APC/C-MCC with BubR1 and spans both coactivator molecules, subsequently permitting its destruction in prometaphase (Figure 1.12). To summarise, no one motif permits SAC-independent destruction and removal of any singular motif severely impacts APC/C-MCC destruction capability, with the exception of D-box D1, whereby mutation of this did not significantly perturb APC/C-MCC destruction likely due to the fact that the D2 D-box is the primary D-box.

In 2019 our group discovered that cyclin B1 destruction in mouse oocyte MI initiates approximately -2-hours ahead of chromosome congression, in late prometaphase I while chromosomes were still aligning. We determined that while the D-box of cyclin B1 was sufficient to target this substrate to the full extent alone, without additional residues cyclin B1 could only be targeted approximately 1-hour prior to anaphase and initiation of destruction correlated with chromosome alignment. This suggested that an additional motif exists in cyclin B1 which could confer destruction in prometaphase I before full chromosome congression. Utilising a series of cyclin B1 truncation experiments, our group identified a novel motif located in the N-terminal helix, named the 'PM motif' (referring to its ability to permit ProMetaphase destruction). Interestingly, this motif is located on the binding interface to CDK1 whereby this motif becomes inaccessible when CDK1 is bound. This creates a degron masking mechanism in which the late prometaphase I destruction capability conferred by this motif only occurs to non CDK1 bound cyclin B1. Providing a method of distinguishing between and differentially targeting free or bound cyclin B1 which is unique to meiosis[160].

In mitosis CDK1 is in excess to cyclin B1 and is only targeted for destruction in metaphase after successful kinetochore microtubule attachments and chromosome alignment results in SAC satisfaction[161]. Important to note is that this process of attaching microtubules to

kinetochores, correcting erroneous attachments and aligning chromosomes in mitotic cells is very rapid and robust. In contrast to this, cyclin B1 in the mouse oocyte is in excess to CDK1 by approximately 6-fold and prometaphase I length is significantly extended for multiple reasons[160]. Firstly, it has been shown that bivalents in oocytes require on average three corrections of erroneous microtubule-kinetochore attachments before sufficient biorientation. This is a time consuming process[170]. Additionally, the large size of an oocyte, which is essential for post-fertilisation development, contributes to the longevity of bivalent alignment due to the length of time required to produce sufficient microtubules and locate kinetochores[53]. An effect of having a large nuclear-cytoplasmic volume ratio is thought to be a reduction in the stringency of the SAC owing to a dilution of nuclear anaphase inhibiting factors as well as factors produced by unattached kinetochores, namely the MCC. Ultimately this contributes to the finding that the meiotic SAC only induces a cell-cycle arrest in the presence of several unattached kinetochores as few unattached kinetochores do not produce sufficient signal to cause arrest [53]. Insufficient MCC signalling can result in 'meiotic slippage' whereby the APC/C targets anaphase substrates before sufficient alignment, often resulting in aneuploidy[171]. This explains why evolving to have an excess of cyclin B1 and a mechanism to target non-CDK1 bound cyclin B1 is so essential in the mouse oocyte. Firstly, an excess of cyclin B1 ensures maximal CDK1 activity to drive chromosome alignment to the fullest extent and by being able to differentially and preferentially target this excess pool of cyclin B1, the APC/C can be presented with a bait substrate in the instances of slippage but also prolong prometaphase I by preserving cyclin B1:CDK1 for an extended period of time. The differences between mitotic cells and oocytes also explains why this may not be observed in mitosis because generally there would not be a pool of free cyclin B1 in a mitotic cell and prometaphase would not need to be significantly extended.

The benefit of the PM motif could be likened to that of an ABBA motif as it is not itself is not a destruction motif as removal of the D-box of cyclin B1 results in complete stabilisation and the PM motif does not compensate for this, however its presence contributes to the destruction of this protein (specifically when not bound to CDK1) in prometaphase like the ABBA motif does in cyclin A2. This was further evidenced in nocodazole experiments by the

our group. Nocodazole prevents oocytes achieving metaphase and mutation of the PM motif of cyclin B1 largely resulted in stabilisation whereas when the PM motif was present, cyclin B1 could be targeted for destruction albeit perturbed. In high concentration nocodazole experiments, the PM motif could not confer destruction capabilities so it is unclear as to whether the PM motif actually permits destruction via the APC/C-MCC or whether it permits the destruction by a subset of non-MCC bound APC/C which could exist at this timepoint. Notably the PM motif bears no sequence similarity to the ABBA motif or any other currently established motifs. The PM motif does appear to promote cyclin B1 as more efficient substrate as well as conferring late prometaphase I destruction as our data shows that removal of the PM motif results in destruction 15% less extensive destruction. This is physiologically relevant. By targeting free cyclin B1 (using it's accessible PM motif) to a larger extent, the oocyte reduces the propensity for CDK1 reactivation upon cyclin B1 destruction. Additionally, cyclin B1 destruction should not be complete at the end of MI. Removal of all or most cyclin B1 between MI and MII would initiate a DNA synthesis step between these two divisions. Keeping a small amount of cyclin B1 and active CDK1 prevents this. Exactly how the PM motif facilitates free cyclin B1 destruction in late prometaphase I remains to be explored. This could be of particular challenge because this system appears to be unique to oocytes at this stage.

Identifying different interaction partners between cyclin B1 ± PM motif would provide significant insight into any protein-protein interactions facilitated by the motif itself. Standard protein-protein interaction techniques such as immunoprecipitations are difficult to conduct when exploring these interactions in cell types which are not in abundance, such as mouse oocytes due to low cell numbers and subsequent low protein amounts in lysates. Alongside the technical limitations, ethical considerations come into play also as acquiring the number of oocytes required for immunoprecipitations and Western blotting for example are possible however many numbers of mice will be required. Alongside these considerations, performing pull-downs using mitotic cells is unfeasible as the effects of early free cyclin B1 destruction has yet to be proven in these cell types. This highlights the need to explore an alternative way to analyse protein interactions and identify interacting partners in oocytes.

In this chapter I verify previous findings by our group which identify a function for a series of residues located in the N-terminal helix of cyclin B1 which permit prometaphase I destruction, as shown by an alanine-substituted mutant. I confirm the E3 ubiquitin ligase responsible for this destruction and explore a potential mechanism of how this motif could facilitate prometaphase destruction of cyclin B1. I also explore a potential live cell protein interaction assay to determine binding partners for the PM motif, as well as the role localisation plays, in destruction dynamics.

3.2 Results

3.2.1 A second destruction motif exists within the N-terminal Helix of cyclin B1 which permits early destruction

In 2019 data from our lab reported a motif in the N-terminal helix of cyclin B1 which acts to permit cyclin B1 destruction in late prometaphase I in mouse oocytes. I first set out to validate these previous findings in my own hands by generating and experimenting with cRNA encoding cyclin B1 mutants tagged C-terminally with a Venus fluorescent protein. Groups of GV stage oocytes were harvested and maintained in prophase I arrest by culture in IBMX supplemented media. Healthy oocytes were selected at random and microinjected with either cRNA encoding cyclin B1 with an unmodified PM motif (herein referred to as 'cyclin B1'), or cyclin B1 where residues 173-175 and 178-181 were mutated to alanines (DIYAYLRQL to AAAAYAAAA) to disrupt the PM motif (herein referred to as 'cyclin B1^{PM-A}'). Both forms of cyclin B1 also harboured a Y170A mutation to disrupt CDK1 binding. This is to ensure control, as without this mutation, expressed cyclin B1 protein is functional and capable of activating CDK1. A Y170A mutation allows us to determine the destruction dynamics of cyclin B1 ± PM motif without perturbing CDK1 activity.

Following confirmation of the expression of fluorescent cyclin B1 constructs (Figure 3.2A), oocytes were released from prophase I arrest via washing into non-IBMX supplemented media. Oocytes were then imaged every 10-minutes utilising a microscope fitted for epi-fluorescence to monitor them throughout MI maturation.

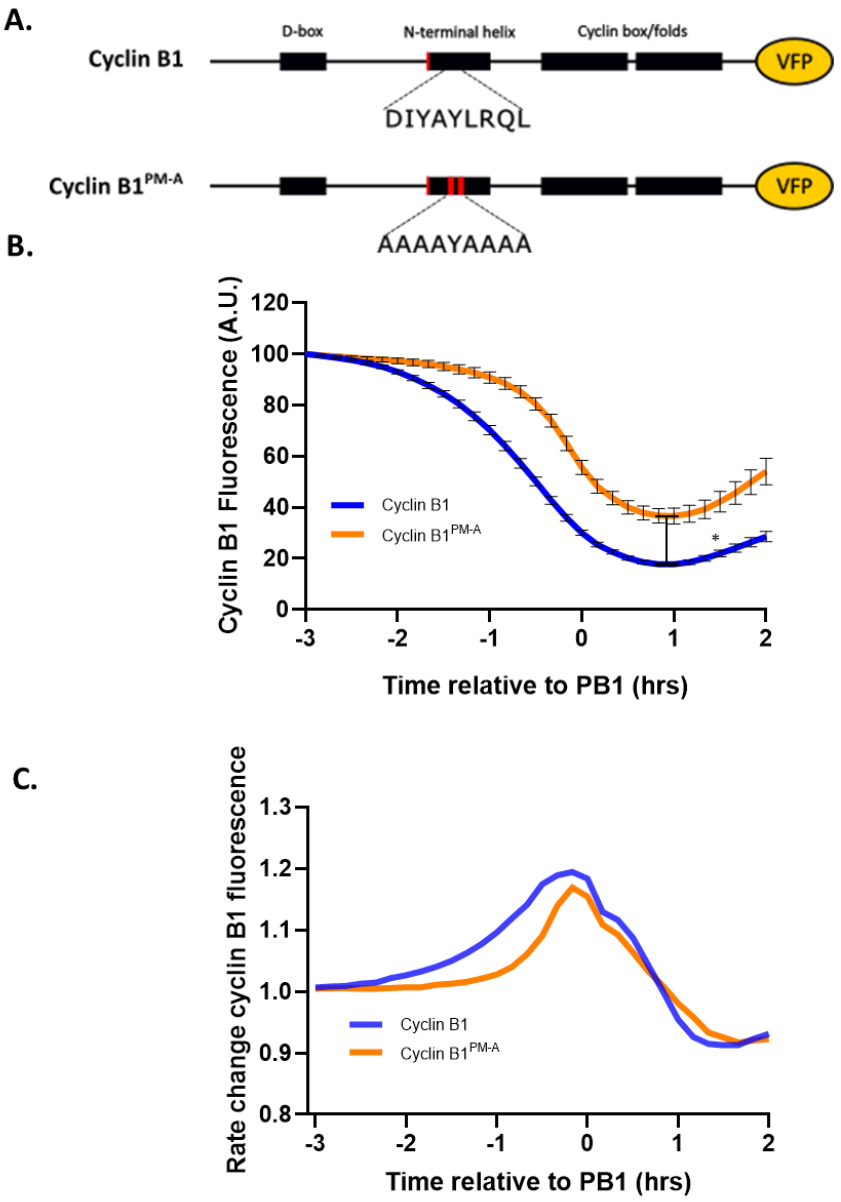

Figure 3.2. Cyclin B1 with an unmodified PM motif (cyclin B1) is destroyed earlier relative to polar body extrusion compared to Cyclin B1^{PM-A}.

A) Structure diagram describing the constructs used in these experiments highlighting the mutations used for each construct. Both constructs harbour Y170A mutation and the cyclin B1PM-A construct also contains alanine substitutions to PM motif (DIY,LRQL-A). B) Mean destruction profiles of venus-fluorescent protein tagged cyclin B1 (blue, n=84) and cyclin B1PM-A (orange, n=28) aligned to time of polar body extrusion (PB1). Minimum fluorescence values at -1 hour relative to PB1 was deemed to be normally distributed using the Kolmogorov-Smirnov test of normality, and calculated to be significant using an unpaired t test ($p<0.0001$). ii) Rate of destruction of cyclin B1 with (blue) and without (orange) a PM

motif. This was calculated using the formula Y=Mean Fluorescence at time x/Mean fluorescence at time x+1. Error Bars ± SEM.

When expressed in oocytes, fluorescent cyclin B1 the relative quantity and destruction dynamics of each different mutant per oocyte. This data was recorded and exported as a Microsoft Excel file for processing. A main aim of our data processing is to produce a destruction profile that represents the 'average' oocyte. This way we can reliably compare the destruction dynamics of different mutants. Naturally, starting fluorescence values vary between oocytes for both technical and biological reasons (it is not possible to precisely control the injection amount, and more importantly oocytes will differ in their capacity to translate message and fold proteins). Therefore, in order that each oocyte has the same value in our analysis, as a first stage of data processing, the fluorescence values of each oocyte are normalised such that the peak fluorescence intensity prior to destruction is 100%. As a second important data processing step, oocytes are not perfectly synchronous in their cell cycle, therefore data sets from individual oocytes are aligned to polar body extrusion as an indicator of anaphase. We wish to compare destruction profiles relative to anaphase and so this event gives us an excellent method (effectively synchronising traces). All subsequent live fluorescence data is processed in this way unless otherwise specified.

This data presentation reveals that cyclin B1 (with an unmodified PM motif, "cyclin B1") is targeted for destruction approximately -2 hours ahead of PB1 extrusion (Figure 3.2B). At this time point 10% of this cyclin B1 has been destroyed. This is in contrast to the cyclin B1 construct with a mutated PM motif (cyclin $B1^{PM\text{-}A}$) in which 10% of this protein is degraded 1-hour later. This is readily observable noting the divergence of lines -2 hours relative to PB1 extrusion. Additionally, approximately 50% of cyclin $B1^{PM\text{-}A}$ has been destroyed by the point of PB1 extrusion and by this time 70% of cyclin B1 has been destroyed. There is therefore a clear difference in the timing of destruction between the two constructs owing to the presence or absence of a PM motif.

In addition to timing of initiation of destruction, there are also differences in the final extent and the rate of destruction. Average cyclin B1 destruction is 18% more extensive cyclin B1^{PM-A}. However, while cyclin B1 destruction is more extensive with the motif present it is not faster, rather it occurs over a longer time period. This is evidenced in Figure 3.2C.

To determine whether this early destruction mediated by the PM motif is only dependent on the local PM motif itself and not also an additional region of cyclin B1 such as in the cyclin Box/folds, I produced short constructs which contain the 90 N-terminal amino acids (holding the D-box and surrounding lysine residues for ubiquitination) linked to the N-terminal helix only. Two constructs were generated with or without a mutated PM motif, these construct are termed N90-NTH and N90-NTH^{PM-A} respectfully (Figure 3.3A).

By expressing N90-NTH proteins with and without the PM motif in oocytes, we clearly see a difference in timing of the initiation of destruction, as well as rate and extent of destruction. These characteristics are comparable to their full-length counterparts (Figure 3.3B). When a PM motif is present and accessible in the N90-NTH construct, destruction initiates approximately 2-hours ahead of PB1 extrusion. N90-NTH levels reach a minimum of 21% over 3.5-hours. The destruction of this species is nearly identical to that of the full-length construct in terms of both timing and extent. When the PM motif is mutated in the N90-NTH^{PM-A} construct, destruction occurs later, closer to the -1hr time point relative to PB1 extrusion. In addition, the bulk of destruction occurs at the same time for the truncated and full-length PM-motif mutant construct. However, the N90-NTH^{PM-A} is not destroyed to the same extent as the full-length PM mutant product as the N90-NTH^{PM-A} is destroyed 10% less. Importantly though, this data shows that it is indeed the PM motif region only which determines the timing difference between these forms of cyclin B1 and not interactions/regions adjacent to this.

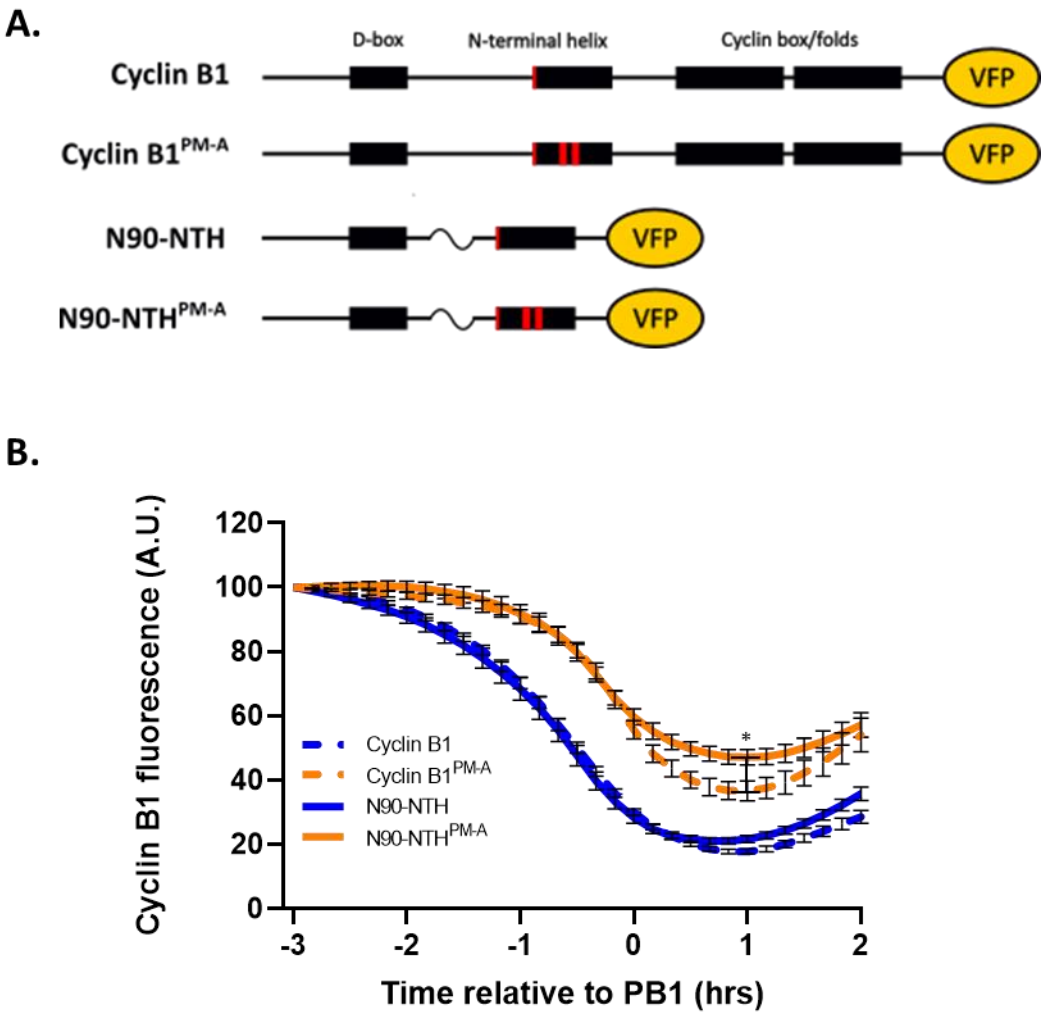

Figure 3.3. Truncating cyclin B1 to the first 90 N-terminal amino acids and its N-terminal helix is sufficient to retain destruction dynamics.

A) Structure diagram describing the constructs used in these experiments. Both forms of cyclin B1 harbour a Y170A mutation, with the cyclin B1PM-A harbouring a PM-motif-alanine substitution mutation. N90-NTH±PM motif is a construct comprising of the N-terminal 90 amino acids of cyclin B1 linked to the N-terminal helix of cyclin B1 using a short flexible linker. B) Quantification of destruction of N90-NTH (blue, solid, n=19) and N90-NTHPM-A (orange, solid, n=10) compared to controls cyclin B1 (blue, dashed, n=84) and cyclin B1PM-A (orange, dashed, n=28) relative to PB1 extrusion. Error Bars ± SEM.

While the cyclin B1 ± PM motif constructs are destroyed over different time periods to one another, it is likely that they are both targeted by the same destruction machinery (the APC/C) but in a different way. It is highly likely to be the APC/C^{Cdc20} responsible for this destruction because it is the predominant E3 ubiquitin ligase responsible for targeting cell cycle proteins at this timepoint. Cyclin B1 targeting depends on its D-box, a well-established APC/C interaction motif, giving further merit to this. It is known that the APC/C targets substrates in a temporal manner based on the differential presence of SLiMs on substrates.

Data here suggests a mechanism whereby the presence or absence of a PM motif allows the destruction machinery to discriminate between our fluorescent reporters. Further evidence that the APC/C is responsible for targeting cyclin B1 ± PM motif is that data from our lab shows that the SAC regulates the destruction of these constructs and the APC/C is strongly regulated by the SAC. Experiments in oocytes using nocodazole, a drug which maintains a constitutively active SAC, shows that cyclin B1 can be targeted with a reduced rate whereas cyclin $B1^{PM-A}$ is stabilised[160]. This shows that the SAC, which primarily exerts its function on the APC/C has a role in the regulation of both cyclin B1 constructs[160]. Additionally, an APC3 knockdown previously results in the complete stabilisation of cyclin B1. Therefore, destruction in either in the presence or absence of the PM motif is certainly regulated by the APC/C, but the mechanism of this discrimination is not known.

Curiously, data from our group shows that free cyclin B1 can still be targeted for destruction following a Cdc20 knockdown protocol[160]. Given it is expected that Cdc20 is the activator of the APC/C over the time period where cyclin B1 destruction initiates, this observation could be described as unusual. In addition, if the PM motif is a SLiM, this previous result is in conflict with our understanding of the way SLiMs operate (specifically by interacting with the APC/Cs co-activator). However, there are multiple reasons to explain this result. Firstly, Cdc20 knockdown is likely not complete. Second, there is precedent for the APC/C destroying a substrate independently of co-activator interaction such as Nek2A as described in Section 1.9. Finally, where Cdc20 is limited it is highly likely that Cdh1 replaces it's loss and could itself direct cyclin B1 destruction[172]. To address this I utilised the drug proTAME, a prodrug of

the drug TAME which mimics the IR tail of APC/C coactivators $Cdc20^{APC/C}$, $Cdc20^{MCC}$ and Cdh1, significantly preventing their binding to the APC/C[173,174]. By reducing instances of coactivators in APC/C complexes, I can this assess whether coactivator interaction to the APC/C is essential for all periods of cyclin B1 destruction, and confirm that the APC/C is the only E3 ubiquitin ligase responsible for free cyclin B1 destruction.

A series of proTAME dose response experiments determined that the minimum dose required to prevent polar body extrusion (indicating a loss of APC/C^{Cdc20} activity) in 100% of oocytes was 1.5 µM (Figure 3.4A). Following this GV stage oocytes were then treated as previously to express fluorescent cyclin B1. Once expression had been confirmed, oocytes were placed a heated stage on a microscope fitted for epifluorescence in media without IBMX supplementation to allow oocytes to resume MI. Images were taken every 10-minutes. 1.5-hours after all oocytes underwent GVBD, the media was replaced with fresh media supplemented with 1.5 µM proTAME. As a result of proTAME treatment, these oocytes did not undergo PB1 extrusion and thus individual oocyte destruction valued were aligned to GVBD. Strikingly cyclin B1 was completely stabilised after treatment with proTAME with relative abundance increasing to a maximum of 20% above their initial levels 10-hours after GVBD (Figure 3.4B). It is likely here that translation of cyclin B1 mRNA continues and the destruction of cyclin B1 has significantly diminished.

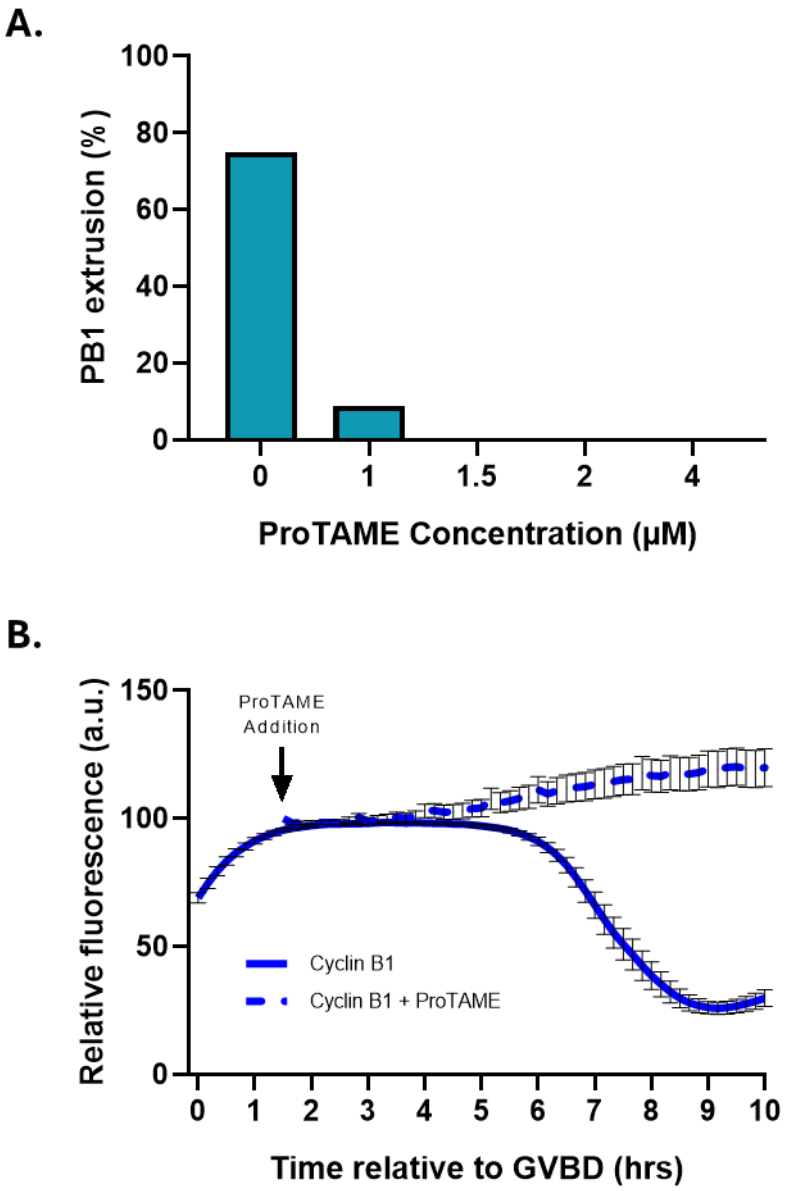

Figure 3.4. ProTAME causes a reduction in PB1 extrusion rates and stabilises cyclin B1.

A) Dose-response of oocytes incubated in varying concentrations of ProTAME (n=8;n=20;n=15;n=10;n=5;). B) Mean destruction profiles of cyclin B1 in oocytes treated with 1.5 µM proTAME, 1.5 hours after all oocytes underwent GVBD (blue, dashed, n=8). Alongside mean destruction profiles control oocytes expressing cyclin B1 having not undergone proTAME treatment (blue, solid, n=20). Destruction profiles were aligned to GVBD. Cyclin B1+ProTAME destruction traces initiate 1.5 hours post-GVBD as this was the timepoint in which oocytes were transferred to the imaging stage containing proTAME media.

3.2.2 Localising cyclin B1 to the membrane results in late destruction of free cyclin B1

Given that we know that the PM motif is not a degron, due to the fact that the PM motif doesn't confer destruction capabilities without a D-box, we must consider additional ways that SLiMs can influence the destruction dynamics of substrates[160]. An example of this is by localising proteins in such a way that they are brought closer to or partitioned away from the destruction machinery of the APC/C. This could include a competitive binding mode. For example, the ABBA motif does not itself direct destruction, but by outcompeting BubR1, promotes the positioning of cyclin A2 on the APC/C, enabling a specific D-box docking mechanism to accelerate destruction[20]. Yet alone and out of context the ABBA motif has no function.

Expressing fluorescent cyclin B1 constructs in the oocyte, we can see that cyclin B1 is expressed globally in the cytoplasm but also decorates the spindle at a low level which becomes slightly more obvious as chromosomes congress and the local fluorescence intensity increases (Figure 3.5B). In order learn more about PM motif interactions and to better understand how localisation impacts the destruction of cyclin B1, I designed, generated, and expressed in oocytes cyclin B1 constructs that readily localise to the cortex of the oocyte (Figure 3.5A). It was also hoped that these constructs would have a second substantial benefit in that they may be a useful tool in our aim to identify interacting partners of the PM motif. Specifically, previous experiments conducted in our lab have shown that tagging a protein to the cortex of the oocyte (specifically utilising a membrane localisation tag) can result in the co-localisation of interacting partners. This was validated specifically with a membrane localised cyclin B1, which strongly re-localised endogenous CDK1 to the cortex of the oocyte (determined by immunofluorescence). We hypothesised that membrane bound cyclin B1 with or without the PM motif might re-localise a different set of proteins as the PM motif likely promotes interaction with a binding partner that a PM mutant does not. An analysis of proteins which colocalise with membrane localised cyclin B1 (with a PM motif) that did not accumulate in the absence of a PM motif, could in theory contain any interacting degradation machinery important for prometaphase I destruction of

cyclin B1. Specifically, I would aim to fix oocytes expressing membrane localised cyclin B1 constructs at a time point whereby cyclin B1 degradation had initiated, but before the initiation of cyclin $B1^{PM\text{-}A}$, then following this incubate oocytes with antibodies to detect Cdc20, SAC components and APC/C subunits. Any membrane co-localisation would indicate an interaction.

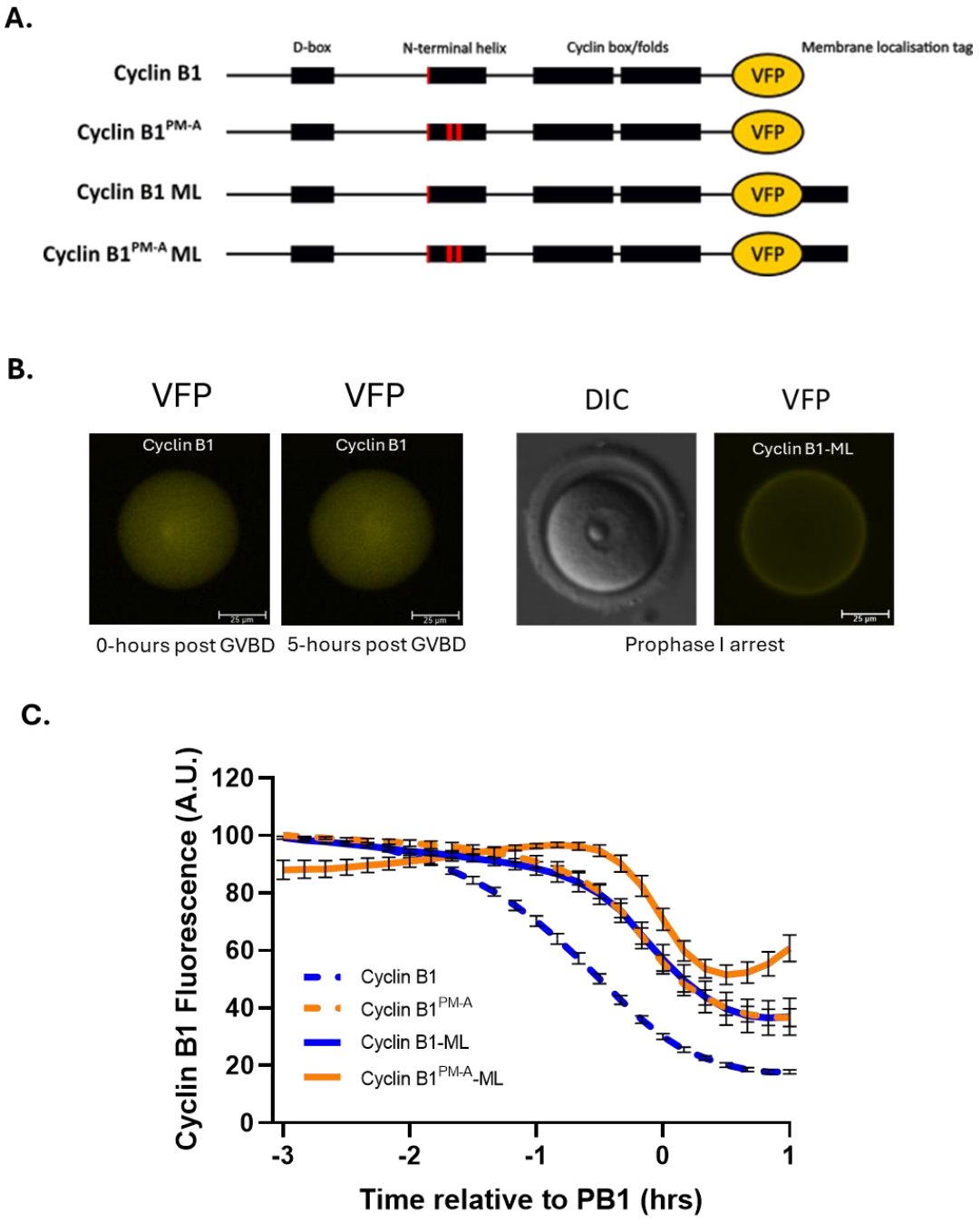

Figure 3.5. C-terminal membrane localisation tag brings cyclin B1 to the oocyte membrane and results in late destruction of cyclin B1

A) Structure diagram of cyclin B1 constructs used in these experiments. Cyclin B1 harbours a Y170A mutation. Cyclin B1PM-A harbours a Y170A mutation alongside an alanine substitution mutation of its PM-motif. Membrane localised (ML) constructs harbour a (KMSKDGKKKKKKSKTKCVIM) C-terminal to VFP (Cyclin B1-ML; Cyclin B1PM-A-ML). B) VFP

images of representative oocytes expressing cyclin B1 at the time of GVBD and 5-hours post GVBD (left) alongside DIC and VFP images of a representative oocyte expressing cyclin B1-ML C) Mean destruction profiles of oocytes expressing cyclin B1-ML (blue, solid, n=11) and cyclin B1PM-A-ML (orange, solid, n=15) aligned to polar body extrusion. Alongside mean destruction profiles of control oocytes expressing cyclin B1 (blue, dashed, n=84) and cyclin B1PM-A (orange, dashed, n=28). Error bars ± SEM. Scale bars=25 µm.

Given this, I followed a mutagenesis protocol to insert a polybasic prenylation domain originating from the KRAS protein (KMSKDGKKKKKKSKTKCVIM**)** onto the C-terminus of the Venus fluorescent protein linked to cyclin B1. The prenylation domain permits protein prenyltransferases associated with the endoplasmic reticulum membrane to add hydrophobic prenyl or isoprenoid groups via a thioester covalent linkage, specifically to the Cysteine of the CAAX motif. RAS-converting CAAX endopeptidase 1 then cleaves the terminal -AAX residues which is then followed by the capping of the C-terminal carboxyl with a methyl group by isoprenylcysteine carboxylmethyltransferase. The resulting protein contains a highly hydrophobic C-terminus which has a high propensity to associate with plasma membranes and is subsequently trafficked to the destination membrane[175].

This localisation tag was added to the C-terminus of the existing Venus fluorescent protein linked to cyclin B1 ± PM motif (herein cyclin B1-ML and cyclin B1^{PM-A}-ML, Figure 3.5A), with the aim of using this strategy as an assay to identify proteins that colocalise with cyclin B1 when the PM motif is present but not when the PM-motif is mutated.

Expressing cyclin B1 ± PM-A-ML in oocytes results in very clear localisation to the cell membrane as indicated by a cortical, fluorescent ring or halo, which forms due to the 3D curvature of the oocyte. This unique localisation is due to the membrane localisation tag, as the non-membrane localised constructs are expressed globally in the cytoplasm with slight decoration of the spindle, as discussed earlier (Figure 3.5B).

When analysing the destruction profiles of cyclin B1 ± PM motif-ML surprisingly, prometaphase cyclin B1 destruction is not permitted for either form of cyclin B1 (Figure

3.5C). Instead, even with a PM motif, destruction only really accelerates about 30-minutes prior to polar body extrusion, and interestingly now at the same time as the cyclin $B1^{PM-A}$ construct. This suggests two points. First that unfortunately utilising membrane localisation to identify interaction partners with the PM motif is not feasible, due to the removal of prometaphase I destruction capabilities. Second however, it does provide insight into the importance of the localisation of cyclin B1 for PM motif mediated destruction in late prometaphase I. Further this provides insight into the spatial regulation of cell cycle substrates by the APC/C and of the APC/C itself in oocytes. This is a current unknown in the literature. This observation suggests that proximity to the APC/C (which can be expected to be primarily surrounding chromosomes) is important for the timing destruction, and though this is not necessarily surprising, it further suggests that APC/C activity likely radiates outwards from this site, or at least a subpopulation of the APC/C in the correct mode for cyclin B1 prometaphase I destruction.

Surprisingly, the cyclin $B1^{PM-A}$-ML construct is targeted for destruction even later than its non-membrane localised counterpart. Destruction initiates for this construct approximately 20-minutes later. This suggests that there is still a clear difference in how the APC/C targets these substrates, dependent on the presence of a PM motif.

A further interesting feature is notable. Membrane tagged cyclin B1 constructs are not cleared from the oocyte to the same extent as their non-membrane targeted counterparts. The addition of a membrane localisation tag to reduced cyclin B1s destruction by 20%, and cyclin $B1^{PM-A}$ by 17%. There is also a clear difference in how well the APC/C targets these membrane localised constructs prior to intended destruction. Cyclin B1 protein is targeted for destruction at a low level prior to the acceleration of destruction (Figure 3.5C). By the 1-hour prior to PB1 extrusion, 21% of cyclin B1-ML has been destroyed compared to cyclin $B1^{PM-A}$-ML where translation exceeds destruction. This is further evidence that the PM motif may make cyclin B1 a more efficient target for the APC/C, perhaps by increasing binding affinity to the APC/C. One key observation is that timing and extent of destruction appear coupled. It appears that the earlier a substrate is targeted for destruction, the more

extensive the destruction is. This makes sense physiologically as APC/C activity and substrate targeting switches upon anaphase and a later destruction equates to less time to be able to destroy before APC/C inactivation.

Therefore, removal of cyclin B1 from its native location has profound implications for its timing of destruction. PM motif mediated prometaphase destruction of cyclin B1 is location dependent. This may also highlight the diffusible nature of the MCC. As discussed in section 1.8, the MCC is a diffusible inhibitor of the APC/C which is generated at kinetochores and diffuses outwards. Therefore, when the SAC is switched off and MCC generation ceases, the initial APC/C activity resumption likely occurs close to chromosomes and the last of the MCC produced continues to radiate outwards and continue to inhibit proximal APC/C complexes. These proximal APC/C complexes, located near the membrane in this instance, are uninhibited late compared to those closer to chromosomes resulting in cyclin B1 destruction later. Assuming cyclin B1 with an accessible PM motif is targeted by the APC/C-MCC (due to its ability to be targeted for destruction in prometaphase), the late destruction dynamics of cyclin B1-ML are curious given the above hypothesis. It could be possible that the membrane localisation has resulted in a steric hindrance of the PM motif, preventing its accessibility and resulting in its late destruction timing. Evidence for this could be that this cyclin B1-ML is targeted at the same time and extent as cyclin $B1^{PM\text{-}A}$. If however, cyclin B1 is not targeted by the APC/C-MCC but instead targeted by APC/C^{Cdc20}, the above hypothesis could have merit, and the differences in extent of destruction could be due to increased affinity for the APC/C brought about by the PM-motif.

Given that experiments tethering cyclin B1 to the membrane strongly suggests that localisation is a critical component of PM motif directed early APC/C targeting, I decided to complement these experiments by localising cyclin B1 constructs to the APC/C itself.

3.2.3 Targeting cyclin B1 to the APC/C using a CKS1 fusion results in earlier destruction of cyclin B1 and a co-localisation with TACC3 which requires the PM-motif

Significant literature has shown that APC/C substrates, specifically cyclins, are targeted to the APC/C using small, highly important regulatory subunits called CKS proteins[20,77]. In mitotic cells, prometaphase destruction of cyclin A2 is aided by interaction with CDK2 bound to CKS1. CKS1 contains an anion-binding pocket which is used to bind directly to a hyperphosphorylated APC3 allowing it to shuttle cyclin A2 to the APC/C for destruction. Studies have shown in mitotic cells that CKS1 is essential to mediate checkpoint-resistant degradation of cyclin A2[176,177].

As cyclin A2 is a substrate naturally targeted for destruction in prometaphase (while the SAC is still signalling) on account of CKS1 association and its cassette of APC/C binding motifs, I wanted to explore the impact of CKS1 association on the destruction timing of our cyclin B1 mutant constructs. In these experiments CKS1 would be used as a tool to directly localise each to the APC/C. By presenting these cyclin B1 constructs to the APC/C in this context, it was hoped this would provide yet greater insight into how the PM motif bestows preferential cyclin B1 destruction. Many outcomes were possible here and each could better our understanding. For example, if the PM-motif is involved in an APC/C localisation role, if we target our constructs to the APC/C using a CKS tag, this might bypass the need for a PM motif. In this case there might no change in destruction timing of cyclin B1, but now earlier destruction of cyclin $B1^{PM\text{-}A}$ if the CKS link gives the same advantage as the PM motif. In contrast, if the PM motif promotes substrate docking, perhaps by associating with a region on the APC/C itself, the differences in destruction timings would likely still exist. In that case while both substrates localise to the APC/C simultaneously, the PM motif would still give the advantage. Prior to these experiments Table 3.2 provides potential observations from as well as suggestions as to what that might mean for the identity of a potential mechanism.

Potential result	Description of observation in the data	Potential meaning
1. cyclin B1 ± PM motif-CKS1 constructs get destroyed at the same time as non CKS1 tagged cyclin B1 ± PM motif	Cyclin B1-CKS1 trace overlaps with Cyclin B1 trace. Cyclin B1^{PM-A}-CKS1 trace overlaps with cyclin B1^{PM-A} trace. There has been no change in destruction timing compared to non-CKS1 associated counterparts.	Localisation to the APC/C is not a determining factor in the PM-motifs ability to promote prometaphase I destruction of cyclin B1. The accessible PM motif of cyclin B1 is less likely to act in an interaction which delivers cyclin B1 to the APC/C ahead of CDK1 bound cyclin B1.
2. Cyclin B1^{PM-A}-CKS1 is destroyed at the same time as non-CKS1 tagged cyclin B1.	Cyclin B1^{PM-A}-CKS1 destruction trace overlaps with cyclin B1 trace. In other words, a CKS1 fusion of cyclin B1^{PM-A} has resulted in destruction in prometaphase I	Suggests a mechanism whereby an accessible PM motif targets cyclin B1 to the APC/C to permit prometaphase I destruction of cyclin B1. Here, CKS1 tagging has bypassed a potential role of the PM motif by directly linking cyclin B1^{PM-A} to the APC/C. This could indicate the PM motif has an intrinsic chaperone role or is used to facilitate binding to a chaperone protein (not necessarily CKS).
3. Both CSK1 tagged cyclin B1 mutants are destroyed earlier compared to non-CKS1	Destruction trace of cyclin B1-CKS1 occurs earlier relative to that of cyclin B1.	The timing with which cyclin B1 localises to the APC/C is a determining

tagged counterparts however a difference in destruction timing between the ±PM mutants remain	Destruction trace of cyclin B1^{PM-A}-CKS1 occurs earlier relative to cyclin B1 $^{PM-A}$. However, cyclin B1-CKS1 is still destroyed earlier compared to cyclin B1^{PM-A}-CKS1 and a difference in timing between these constructs still exists.	factor timing destruction targeting. However, the PM motif does not achieve its prometaphase I destruction effect only by delivering this substrate earlier because a difference in timing still remains.
4. CKS1 tagged cyclin B1 is destroyed later compared to non-CKS1 tagged cyclin B1 at a time more similar to cyclin B1^{PM-A}	Destruction trace of cyclin B1-CKS1 overlaps the destruction trace for cyclin B1^{PM-A}	Suggests that the association of cyclin B1 with a CKS1 protein is causing a steric hinderance or blocking accessibility to the PM-motif, inhibiting prometaphase I destruction.
5. CKS1 tagged cyclin B1 is destroyed earlier than cyclin B1	Cyclin B1-CKS1 destruction initiates earlier than cyclin B1	This would suggest an enhanced effect of early destruction brought about by CKS1 association potentially hinting at the PM motif acting like an ABBA motif

Table 3.2. Potential outcomes of linking cyclin B1±PM-motif with CKS1 and their potential meanings

I complemented the potential findings in Table 3.2 with examples of what these observations in the data (Figure 3.6).

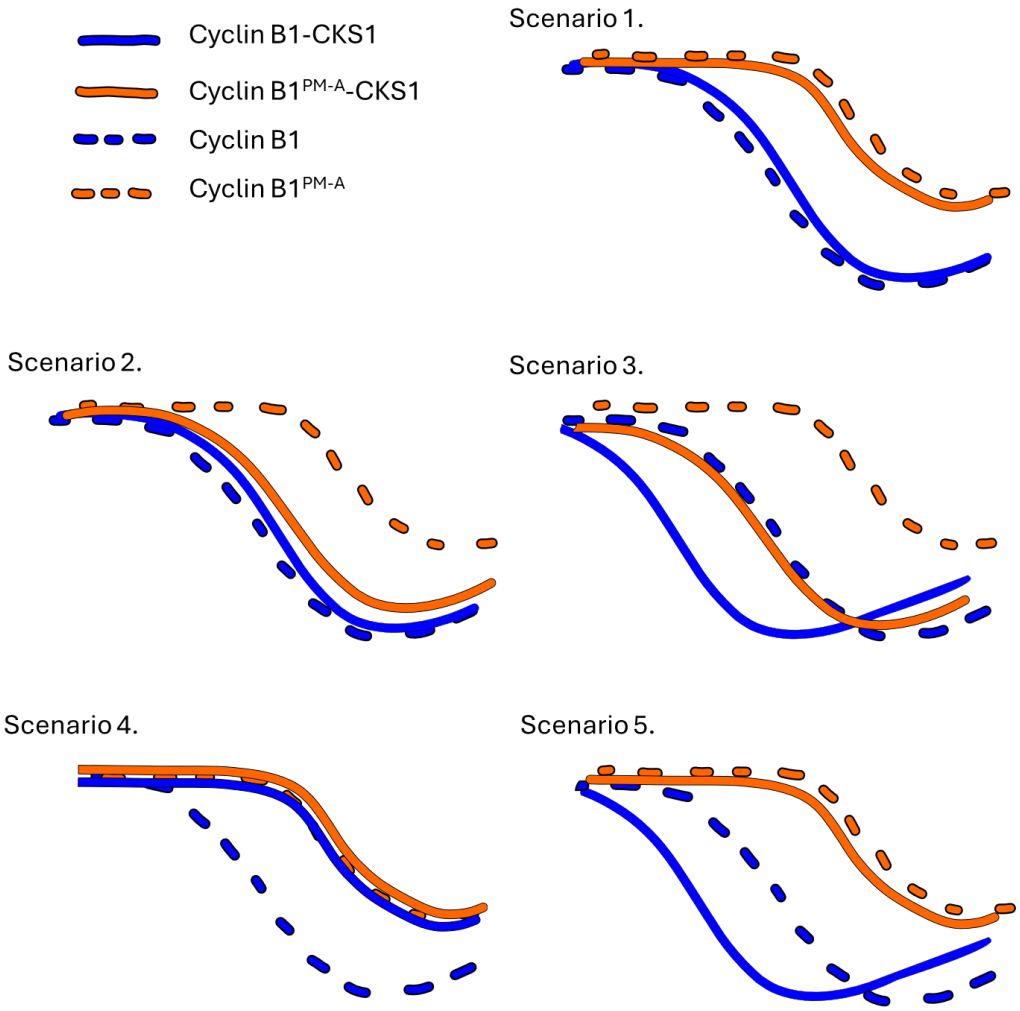

Figure 3.6. Scenarios of datasets corresponding to the experimental outcomes listed in Table 3.2

Linking CKS1 to cyclin B1 constructs was an exploratory line of experimentation with a number of potential outcomes, whereby destruction of the CKS1 linked constructs could be either shifted early, late or result in no change. This is a graphical representation of the potential experimental outcomes listed in Table 3-2.

I therefore inserted a CKS1 protein in between cyclin B1±PM-motif and the venus fluorescent protein utilising short flexible linkers (Figure 3.7A) and expressed these constructs in oocytes.

Excitingly, the destruction dynamics of cyclin B1 ± PM-A tagged with CKS1 (Figure 3.7B) revealed that localising either construct to the APC/C results in their earlier destruction compared to their non-CKS1 counterparts. This outcome was considered in Table 3.2, outcome 3. There is a 40-minute difference between cyclin B1 and cyclin B1-CKS1 reaching 10% destruction. And a 70-minute difference between cyclin $B1^{PM\text{-}A}$ and cyclin $B1^{PM\text{-}A}$-CKS1 in reaching 10% destruction. Interestingly, the destruction cyclin $B1^{PM\text{-}A}$-CKS1 protein occurs with very similar timings to cyclin B1 not linked to CKS1. This not only indicates that localising cyclin B1 to the APC/C results in earlier destruction, independent of the PM motif, but that the PM motif is still confers preferential targeting on top of this. Additionally, because of the now earlier destruction of the cyclin $B1^{PM\text{-}A}$ construct, association of a metaphase substrate with a CKS subunit results in destruction in prometaphase I.

The previous findings from the membrane localisation exploration shows that timing and extent of destruction for substrates are coupled, and these findings validate this. Specifically, the earlier destruction of cyclin $B1^{PM\text{-}A}$-CKS1, which occurs at the same time as cyclin B1, is also destroyed at the same extent. Notably the rate of destruction of the cyclin B1-CKS1 construct decreases as PB1 extrusion approaches in contrast to cyclin B1 which continues to be destroyed after PB1 extrusion. This is interesting as it suggests that the switch between APC/C targeting and cessation of targeting is not the determining factor for the extent of substrate destruction. It could be that substrate concentration has reduced to the point that local concentration of cyclin B1-CKS1 around the APC/C has reduced. However, considering we have localised this construct to the APC/C, this suggests that local concentration is also not the determining factor for extent of destruction. Instead, it seems likely that this is an effect of the oocyte regulating the amount of cyclin B1 destroyed, as destroying too much cyclin B1 would result in a DNA synthesis phase in between MI and MII.

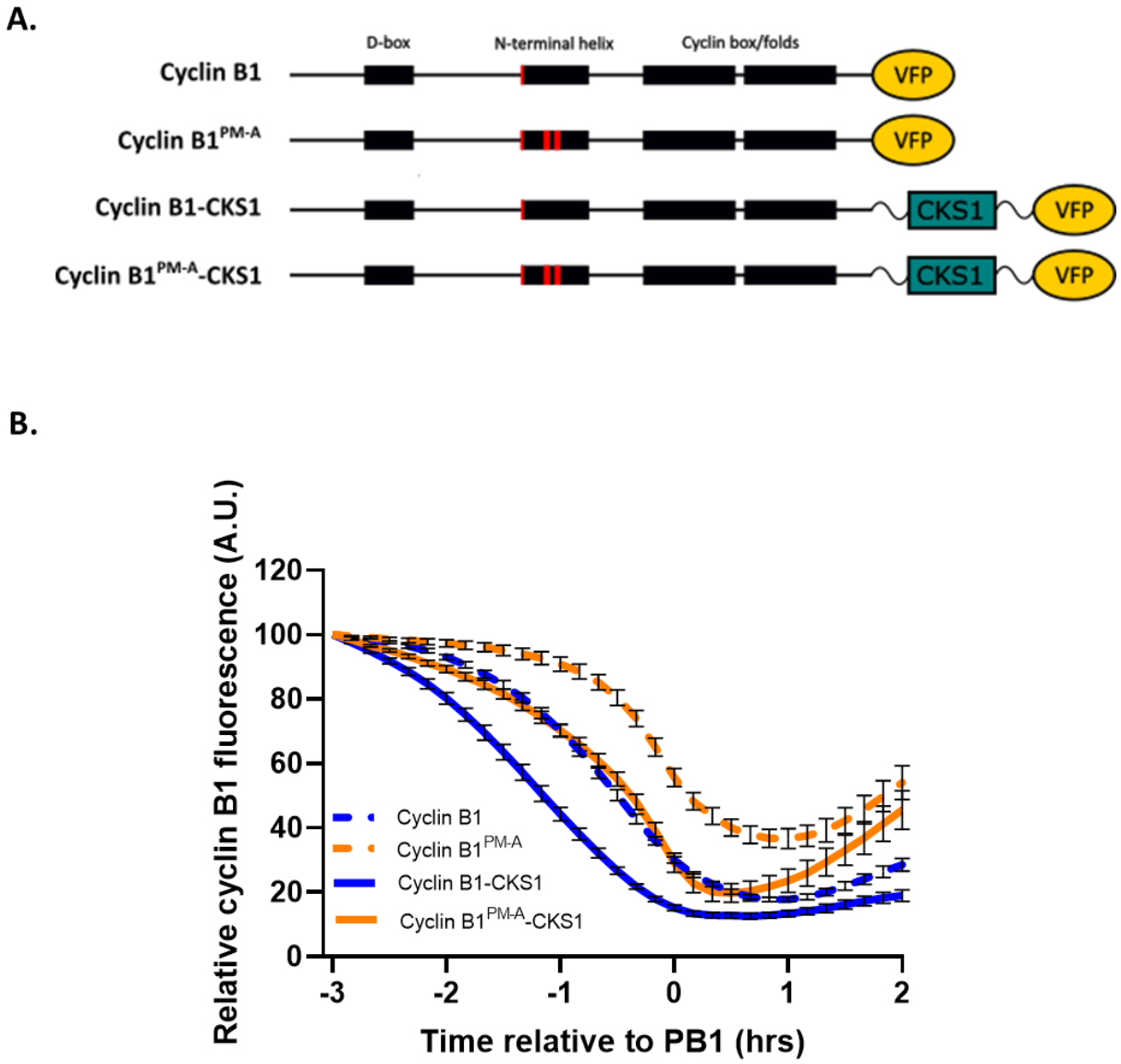

Figure 3.7. Linking a CKS1 protein C-terminal to cyclin B1 ± PM-motif results in earlier destruction for both constructs

A) Structure diagram describing the structures of cyclin B1 constructs used in these experiments. Cyclin B1 harbours a Y170A mutation and cyclin B1PM-A harbours a Y170A mutation alongside an alanine substitution mutation in the PM-motif. CKS1 linked constructs (cyclin B1-CKS1; cyclin B1PM-A-CKS1) are cyclin B1 constructs linked CKS1 on their C-terminus. B) Average destruction profiles of oocytes expressing cyclin B1-CKS1 (blue, solid, n=16), cyclin $B1^{PM-A}$-CKS1 (orange, solid, n=20). Alongside Mean destruction profiles cyclin B1 (blue, dashed, n=84), cyclin $B1^{PM-A}$ (orange, dashed, n=28) aligned to polar body extrusion. Error bars ± SEM.

Together, this data strongly suggest that localisation of cyclin B1 is a determining factor in the timing of cyclin B1 destruction. The finding that CKS1 tagged cyclin B1 with a mutated PM motif can be targeted for destruction at the same timepoint as cyclin B1, gives merit to the thought that the PM motif could facilitate early localisation to the APC/C as a mechanism for late prometaphase I destruction either directly, or indirectly by binding to an APC/C targeting chaperone protein. This is supported by the observation that driving cyclin B1 to the membrane (presumably away from the core of APC/C activity) results in later destruction; forcing these constructs away from their native localisation prevents PM motif mediated early destruction. However, this is not the only factor at play since even when delivered to the APC/C, a PM motif containing protein is still preferred.

Observing the destruction dynamics of CKS1 linked cyclin B1 constructs provides substantial insight as to how the PM-motif could be operating to permit prometaphase I destruction.

- Localisation to the APC/C is a strongly deciding factor for timing of destruction

- Localising to the APC/C using a CKS1 linkage results in earlier destruction of cyclin B1 (in late prometaphase I) even in the absence of a PM-motif. However, when a PM-motif is present, even earlier destruction occurs.

- Once in position at the APC/C cyclin B1 with a PM-motif is clearly the preferred target.

We were excited by these insights into APC/C processivity in oocytes. However, another most striking observation was captured by the experiments and explored further.

Cyclin B1-CKS1 protein, formed incredibly prominent localisation patterns in the majority of GV stage oocytes, most often surrounding the germinal vesicle or at the cortex of the oocyte (Figure 3.8A). The pattern with which cyclin B1-CKS1 localises varies significantly between oocytes. Some occur in thin strands of intense localisation surrounding the GV, others form small singular circular puncta, and some form multiple larger puncta. This is not dependent

on the amount of protein expressed, as even low expressing oocytes show puncta formation. By DIC imaging the oocytes presenting this patterning are indistinguishable from those do not, suggesting that it is not dependent on oocyte quality, size or GV number. Confocal imaging highlights the localisation of this construct alongside finer details of oocyte biology, whereby it is even more evident that this construct surrounds the GV at the boundary phase-separation between ooplasm and GV (Figure 3.8A, bottom right).

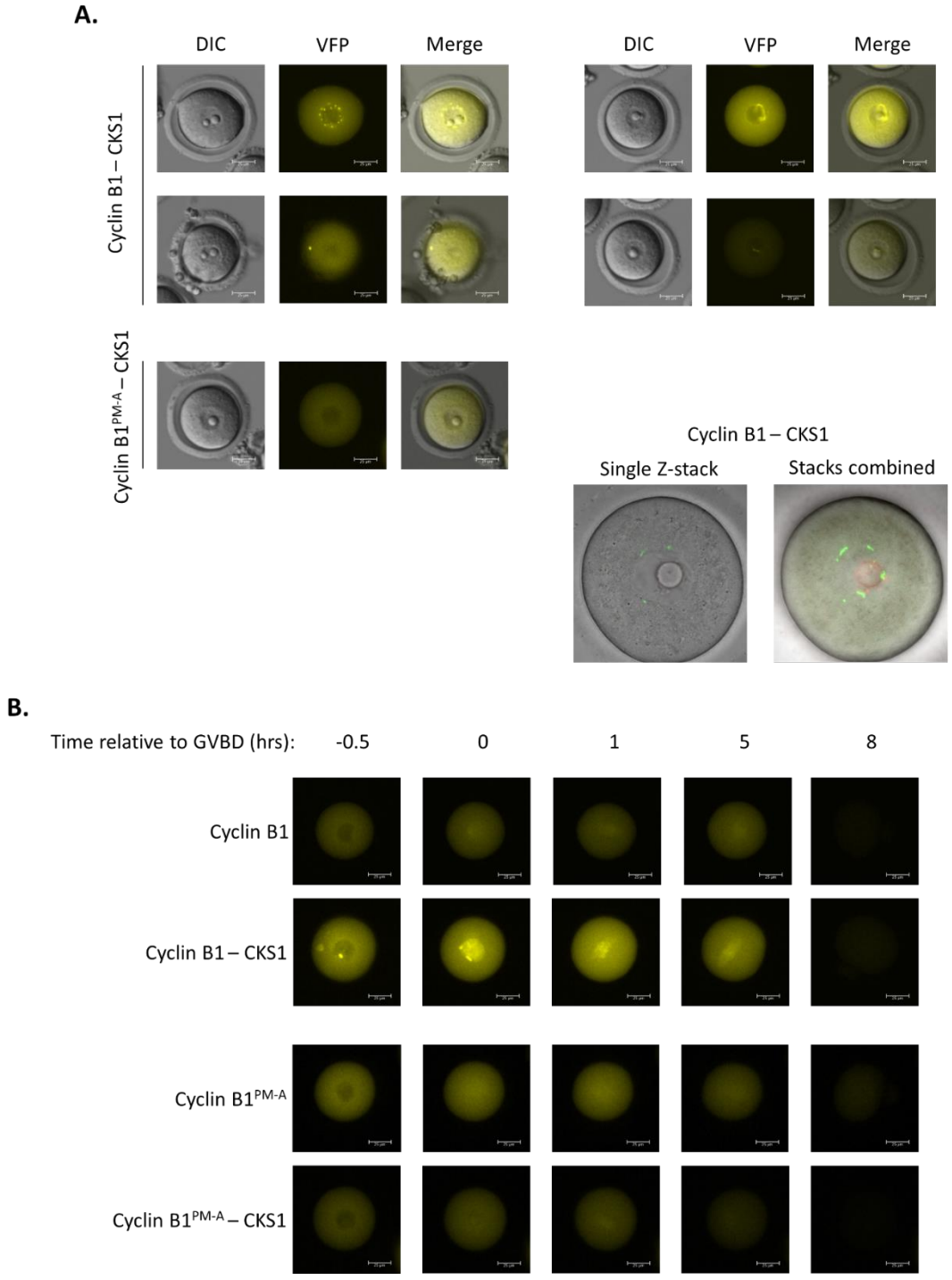

Figure 3.8. Cyclin B1-CKS1 presents with unique localisation patterns which does not occur for a PM-mutant cyclin B1-CKS1

A) Live cell imaging of oocytes arrested in prophase I using IBMX, expressing cyclin B1-CKS1 or cyclin B1PM-A-CKS1 as indicated, showing a range of localisation patterns as well as a

confocal image of an oocyte expressing cyclin B1-CKS1. B) Fluorescence live cell imaging of oocytes expressing cyclin B1 ± PM-A ± CKS1 showing varying localisation patterns in prophase through prometaphase and into meiosis II. These oocytes are representative of all other oocytes expressing these constructs with the exception of cyclin B1-CKS1 in prophase I which, presents with a range differing localisation patterns as seen in A. Scale bar = 25 μm.

Remarkably however, when the PM-motif is mutated to alanines in this CKS1 linked cyclin B1 (cyclin B1$^{PM\text{-}A}$-CKS1), no puncta formed in any oocyte regardless of expression extent or stage of meiosis. Puncta formation relies on the PM-motif.

Additionally, there are clear differences in the localisation of this construct throughout MI. Prior to GVBD, there is an apparent nuclear exclusion of non-CKS1 linked constructs (Figure 3.8B, -0.5hrs). This is expected on a physiological level as cyclin B1 is known to be exported out of the nucleus as to prevent premature CDK1 activation. As the oocyte undergoes GVBD the cyclin B1 constructs invade the nucleus resulting in an even localisation globally. As chromosomes congress in prometaphase, the cyclin B1 constructs begin to decorate the spindle. This has been observed by confocal microscopy, which revealed no differences in localisation between cyclin B1 and cyclin B1$^{PM\text{-}A\ 160}$. During GVBD, the nuclear invasion of the cyclin B1-CKS1 construct is dramatic and the pre-GVBD puncta appear to break down following GVBD (Figure 3.8B). There is a clear difference between the amount of cyclin B1-CKS1 that has flooded into the nucleus compared to the amount which is located in the cytoplasm, in contrast to the other proteins utilised (cyclin B1, cyclin B1$^{PM\text{-}A}$, cyclin B1$^{PM\text{-}A}$-CKS1). As the oocyte proceeds through prometaphase I, there is spindle localisation which is more intense than these other proteins.

I hypothesised that the interesting localisation pattern obtained by expressing cyclin B1-CKS1 (which has shown to be dependent on the PM motif) could be used to help identify potential interacting partners of the PM motif. In a method similar to that proposed for the membrane localisation experiments in section 3.2.2, oocytes could be fixed following expression of cyclin B1-CKS1 and co-localising proteins identified by immunofluorescence. Proteins which

co-localise with the interesting localisation patterns that present with cyclin B1-CKS1 could be potential interaction partners. I therefore performed a series of immunofluorescence experiments using GV stage oocytes expressing cyclin B1-CKS1.

Intriguingly, utilising immunofluorescence of fixed prophase I oocytes expressing cyclin B1-CKS1 was Transforming Acidic Coiled-coil Containing Protein 3 (TACC3), a component of microtubule organising centres (mTOCs) in oocytes [178]. In every oocyte tested, expressed cyclin B1-CKS1 in pronounced localisation patterns overlapped perfectly with TACC3 antibody localisation. This included instances where cyclin B1-CKS1 localised to the cortex of the oocyte instead of GV localisation (Figure 3.9A, rows 1-4). Notably, TACC3 can be found in locations where cyclin B1-CKS1 is not localised suggesting that cyclin B1-CKS1 is colocalising to TACC3 and not vice versa. (Figure 3.9A). In control oocytes not expressing cyclin B1-CKS1, TACC3 puncta are indistinguishable to those expressing cyclin B1-CKS1; thus this is the normal pattern of TACC3 localisation in the absence of exogenous cyclin B1 expression (Figure 3.9A, row 6).

One observation reported in literature is that the mTOC complex can be located at the cortex of the oocyte and migrate to the GV prior to the onset of GVBD[178]. Therefore, to further validate the finding that cyclin B1-CKS1 localises with the mTOC complex, I identified oocytes expressing cyclin B1-CKS1 with puncta at the cortex and used live imaging to follow movement over the course of GVBD (Figure 3.9B, white arrow). The intense puncta of cyclin B1-CKS1 (which was previously shown to co-localise with mTOC component TACC3 in every instance) begins to migrate to the GV approximately 20-minutes prior to GVBD. This provides further evidence that this construct is localising to the mTOC. As the oocyte prepares to initiate GVBD, key proteins essential for spindle formation position themselves at the GV, primed for their role in spindle formation[178]. Upon GVBD these regions of intense localisation appear to break up and strongly invade the GV which is to be expected from our understanding of mTOC behaviour initiating spindle production.

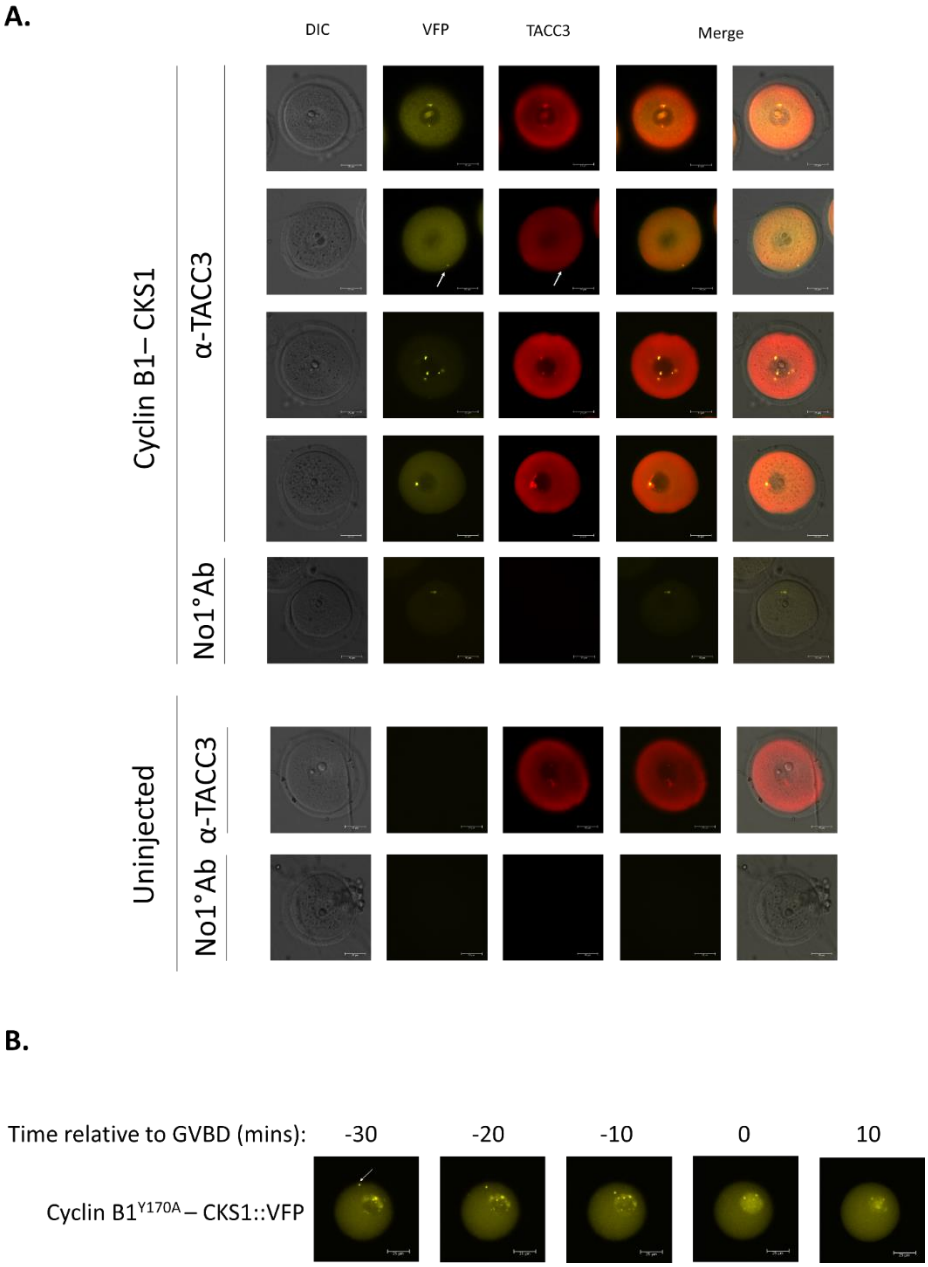

Figure 3.9. TACC3 colocalises with cyclin B1-CKS1 in a PM motif dependent manner and live cell imaging suggests that this construct colocalises with the mTOC complex

A) Immunofluorescence on prophase I oocytes expressing cyclin B1-CKS1 with varying localisation patterns, stained with an anti-TACC3 antibody to show co-localisation (Top, rows 1-4). A primary antibody-absent control is used to show co-localisation is not due to secondary antibody aggregation. Uninjected oocytes are also stained with anti-TACC3 to show that TACC3 localises in a similar manner to cyclin B1-CKS1 without this construct being expressed. B) Fluorescent live-cell imaging of an oocyte expressing cyclin B1-CKS1, specifically at the cortex of the oocyte, in the events leading up to and after GVBD. White

arrow indicates the cyclin B1-CKS1 foci which migrates. Scale bars = 25 µm. Arrows indicate puncta referred to in the text.

It must be kept in mind that the cyclin B1-CKS1 construct is purely synthetic (and to our knowledge not likely to occur in nature as CKS proteins are known bind to CDKs and not to cyclins directly). In these experiments CKS1 was used as a tool for localisation to the APC/C. However, this is an incredibly surprising finding. Why cyclin B1-CKS1 co-localises with mTOCs is unknown, and why this appears to be PM motif dependent is also unknown, but likely meaningful for our understanding of PM motif interactions. Investigating our proteins in different contexts begins to paint a picture of behaviour.

3.3 Discussion

SLiMs and their presence on cell cycle substrates are essential for highly regulated protein roles in mitosis and meiosis. The ability to correctly target cell cycle proteins for destruction in order, to put an end to their function, allows progression through distinct stages of cell division, and prevents the cell cycle slipping backwards. While many SLiMs themselves are well characterised, it is clear and accepted that there are more motifs to be identified, those able to influence the rate and timing of destruction such as the recently discovered ABBA and PM motifs[102,160].

The PM motif had previously been identified as a signal which permits the destruction of free cyclin B1 in prometaphase I of mouse oocyte meiosis, preserving cyclin B1-CDK1 activity until chromosomes are properly aligned[160]. The mechanism involves a strategy known as ‘degron masking’, whereby the association of a binding partner (in this instance CDK1) masks or restrict access to the motif. This action then permits discrimination between bound and unbound forms of the proteins. In mouse oocytes this is incredibly important. Cyclin B1 is in excess over CDK1 and thus exists in two forms, either bound or free[160]. The ability to target free cyclin B1 before bound cyclin B1 is critical for multiple reasons. First, due to the length of prometaphase I in oocyte meiosis, the APC/C has the propensity to slip or mistakenly target substrates prematurely[179]. The presence of free cyclin B1 both acts as a bait to “distract” the prematurely activated APC/C thus preserving cyclin B1:CDK1 activity. Additionally in this

instance, free cyclin B1 acts to replace the prematurely destroyed cyclin B1 to reactivate CDK1 and prolong prometaphase length. By preferentially targeting free cyclin B1 prior to CDK1-bound cyclin B1, the oocyte can also increase the rate of CDK1 inactivation, as a high amount of remaining cyclin B1 would simply result in the reactivation of CDK1 as cyclin B1 begins to be destroyed.

In this chapter, I have validated the finding that in mouse oocytes, the presence of an accessible PM motif in cyclin B1 is responsible for its destruction targeting in prometaphase I, reporting for free cyclin B1. Removal of this motif (as shown by an alanine-substitution mutant) results in later destruction, closer to the metaphase-anaphase transition (Figure 3.2). The prometaphase I targeting does not require other regions of the cyclin B1 protein, such as the cyclin box/folds. Truncating cyclin B1 to the first 90 N-terminal amino acids, which includes the D-box and lysine residues necessary for ubiquitination, as well as the N-terminal helix containing the PM motif, results in near identical destruction dynamics compared to full length constructs. However, when the PM-motif is mutated, destruction is incomplete. This suggests that the PM motif promotes cyclin B1 (full length or truncated) as a more efficient APC/C target as well as permits destruction earlier.

While it is clear that the accessibility of the PM motif allows for earlier destruction of cyclin B1, what is not clear is how this form of cyclin B1 is targeted for destruction and specifically how the PM motif facilitates this. Here I have shown that destruction of cyclin B1 with an accessible PM motif in oocyte meiosis I is APC/C-dependent using proTAME, and more specifically, dependent on APC/C activation by either Cdc20 or Cdh1 (Figure 3.4). Complete stabilisation of the cyclin B1 reporter after inhibition of APC/C coactivator interactions further indicate that the destruction of this form of cyclin B1 is solely orchestrated by the APC/C and not also by an alternative E3 ubiquitin ligase. Given the previously published finding that cyclin B1 can still be targeted (albeit inefficiently) following a Cdc20 knockdown protocol, the current data supports a hypothesis that Cdh1 can compensate for Cdc20 loss in meiosis I mouse oocytes[160].

To deduce how the PM motif is permitting prometaphase I destruction of cyclin B1, identification of any interaction partners is of upmost importance. Performing protein pulldown or interaction assays specifically in mouse oocytes is difficult. The amount of material required for a single co-immunoprecipitation pull-down followed by protein identification via Western blotting is substantial and questionable ethically. Finding alternative experiments to explore interactions would be a valuable contribution. I therefore explored experimental avenues which would use more reasonable oocyte numbers. To this end, I tested the possibility of using a membrane-localisation interaction assay in oocytes as an alternative. Here it was plausible that interacting proteins would co-localise to the membrane with the cyclin B1 reporter but be absent or reduced where cyclin B1 lacked a PM-motif. Any co-localising proteins subsequently identified by immunofluorescence screening would still require further validation, yet this would provide an excellent starting point.

Unfortunately, membrane targeted cyclin B1 with an accessible PM motif was not a destruction target in prometaphase, thus is not a tool able to help determine binding partners that facilitate destruction at that timepoint (Figure 3.5). This line of enquiry did however yield several important findings that expand our wider knowledge of cyclin B1 targeting and APC/C behaviour. Both membrane localised cyclin B1 constructs (±PM motif) were targeted for destruction late relative to PB1 extrusion. This suggests that prometaphase targeting of cyclin B1 is not permitted across all regions of the cell.

One possible explanation for location dependent differences in destruction timing of membrane localised cyclin B1 is that populations of APC/C able to carry out this role do not exist in this location, for instance if a particular subunit or post-translational modification is required. Another explanation could be that APC/C activity expands out from the spindle zone and simply does not reach this location until the metaphase to anaphase transition. Indeed, we know the SAC exerts its effect by producing a diffusible APC/C-inhibiting signal from kinetochores, the MCC, which radiates outwards towards the cortex. As MCCs diminish from kinetochores, a gradient would occur as pre-formed MCC is still migrating outwards.

Thus, APC/C at the cortex could be inhibited while APC/C closer to the spindle barrel is activated. Further merit is given to this model considering the fact that cyclin B1-CKS1, which is localised to the APC/C itself (evident by spindle localisation), is targeted for destruction very early (Figure 3.7). An interesting follow-up experiment would be to explore the destruction of membrane localised cyclin A2. If this MCC diffusing explanation for late cyclin B1-ML destruction is correct, we would likely see cyclin A2-ML destruction occurring at somewhat similar destruction dynamics to wildtype cyclin A2, as this is an APC/C-MCC target.

While localising cyclin B1 to the membrane in oocytes inhibited earlier targeting, the APC/C still handled substrates with and without a PM motif in a different way. These data show that cyclin B1$^{PM\text{-}A}$-ML is not turned over to the same extent as cyclin B1-ML, as indicated by its increasing abundance before destruction which is not seen when the PM motif is present (Figure 3.5). This suggests that localisation is not the only factor differentiating these two forms of cyclin. In support of this statement, while tagging cyclin B1±PM motif with a CKS1 fusion resulted in significantly earlier destruction of both proteins, cyclin B1 with a PM motif was still the preferred target (Figure 3.7).

The fact that cyclin B1$^{PM\text{-}A}$-CKS1 can be destroyed in prometaphase, largely rules out the possibility that the PM motif acts as a key to physically permit docking into the APC/C-MCC active site in prometaphase I. If it was the case that the PM-motif physically permits docking to the substrate recognition module, resulting in its destruction, cyclin B1$^{PM\text{-}A}$-CKS1 might be localised to the APC/C macromolecule (on account of binding to APC3), but still not a target until 1-hour before PB1 extrusion (due to disruption of the PM-motif). Additionally, the fact that cyclin B1-CKS1 is targeted for destruction even earlier than cyclin B1 suggests that the PM motif plays more of an enhancing role as opposed to a permitting role. By directing cyclin B1 more immediately to the APC/C, this further promotes even earlier destruction. This could be described in terms of stoichiometry between cyclin B1 and APC/C interaction factors. Assuming the PM motif does increase affinity for APC/C docking, cyclin B1$^{PM\text{-}A}$-CKS1 would contain one licensing factor (CKS1 subunit), and cyclin B1-CKS1 would contain two licencing factors (CKS1 subunit and the PM motif). Both promoting earlier destruction by

independent mechanisms, therefore the effect of CKS1 targeting and PM increased affinity is additive (Figure 3.10). This is backed up by the fact that the timing of destruction for cyclin B1 and cyclin B1^{PM-A}-CKS1, which occurs at the same time, appears to be roughly halfway between cyclin B1-CKS1 and cyclin B1^{PM-A}.

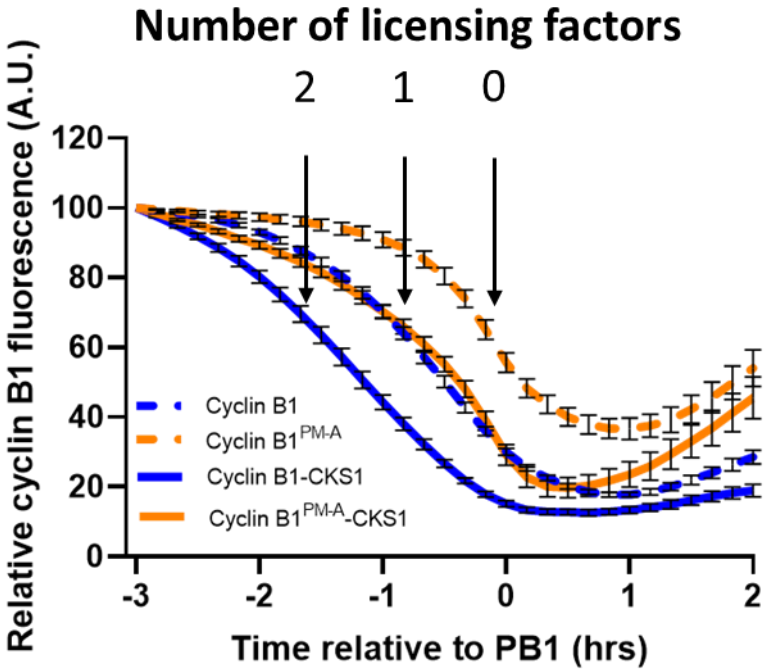

Figure 3.10. Proposed mechanism explaining the early destruction of cyclin B1 in terms of number of licensing factors.

The data from Figure 3.7 labelled with the number of licensing factors in the proposed mechanism of prometaphase I destruction. Here, assuming the PM motif and CKS1 both increase affinity or localisation to the APC/C (thus termed 'licensing factors') we can see an additive effect depending on the number of licensing factors. For example, a substrate with two licensing factors, the PM motif and CKS1, results in the earliest destruction (cyclin B1-CKS1). Removal of either PM motif or CKS1 fusion results in an intermediate timing of destruction (cyclin B1^{PM-A}-CKS1 and cyclin B1). Removal of both licensing factors results in the latest destruction (cyclin B1^{PM-A}-CKS1)

Very curiously CKS1-fusion of cyclin B1 with a PM motif resulted in significant localisation to MTOCs as indicated by TACC3 co-localisation, as well as pre-GVBD nuclear shuttling (Figure 3.9). Yet where the PM motif is mutated, I only ever observed a very slight increase in

localisation to the spindle apparatus, which was only visible in prometaphase (Figure 3.8) and vastly distinct from the prophase localisation patterns where the PM motif is present. This localisation pattern of cyclin B1-CKS1 in prophase I oocytes is both striking and unique. Experiments determine that this protein always colocalises with the mTOCs (as indicated by TACC3 immunofluorescence and complex migration). Why this occurs is unknown. However, the fact this does not occur when the PM motif is mutated indicates that the PM motif is essential for this localisation pattern. It is sensible to suggest that some cyclin B1 could associate with mTOCs in prophase I, primed for a localised increase of cyclin B1-CDK1 activity to induce GVBD and promote spindle assembly. If this is the case, this asks why we have not been able to detect endogenous cyclin B1 enrichment here. One possibility is that it is present, but in low abundance compared to a situation where excess cyclin B1 is forced to this region. A second possibility is that most endogenous cyclin B1 at this stage exists as bound-B1 with a masked PM-motif (free cyclin B1 increases after GVBD) which would not accumulate in the same way. This cyclin B1-CKS1 construct could have further uses in the wider oocyte research as a marker for mTOC localisation in live oocytes. This would avoid the need for fluorescence tagging (and likely overexpressing) mTOC components. It would be interesting to see whether this construct could be utilised to determine oocyte quality or an indicator of likelihood to complete meiosis by indicating the number or localisation of mTOCs.

A general trend through the results of this chapter is that the earlier a substrate is targeted for destruction, the greater the depth of destruction. Thus, timing of destruction and extent of destruction appear coupled. This makes physiological sense. Anaphase I, followed by polar body extrusion, results in a change in substrate targeting whereby destruction decreases significantly and translation of products prevails, preparing the oocyte to enter meiosis II. Initiating the destruction of some substrates earlier provides greater assurance that they will be removed most completely by anaphase, before APC/C activity reduces. This is perhaps evidence of an additional reason for preferential substrate targeting, to ensure that specific substrates (for example free cyclin B1) are depleted to a greater extent. In the case of oocytes, it is reasonable to suggest that removal of the majority of free cyclin B1 over CDK1-

bound cyclin B1 is essential to help with the fine balance of CDK1 activity that must remain between MI and MII; too much CDK1 activity and the cell will not complete MI, too little CDK1 activity and the oocyte will slip into S-phase, negating the goal of meiosis.

Following PB1 extrusion endogenous cyclin B1 levels increase as the oocyte enters MII. This is evident throughout our experiments as post PB1 extrusion, all constructs appear to increase in abundance. However, a trend can be observed across cyclin B1 mutants without a PM-motif (cyclin B1^{PM-A}, cyclin B1^{PM-A}-ML, cyclin B1^{PM-A}-CKS1) is that the rate of cyclin B1 recovery into MII is faster compared to when a PM motif is unmodified. This could be due to an increased efficiency in translation of PM-mutant constructs; or due to the PM motif providing greater affinity to any remaining active APC/C. This would support the current hypothesis that the PM motif increases the affinity of cyclin B1 to the APC/C. ProTAME treatment at the point of polar body extrusion could provide evidence for this as removal of APC/C activity may result in equal rates of cyclin B1 accumulation in MII. The greater accumulation of PM mutant constructs can be described as misregulation, as this is not the pattern of wild-type cyclin B1 accumulation.

Both membrane- and APC/C- localisation experiments provide substantial insight into the role of localisation in cyclin B1 targeting, and how the PM motif might influence destruction timing. First, the timing of destruction is dependent on localisation relative to the APC/C whereby substrates that are located (presumably) further away from the APC/C are destroyed later. While acute localisation results in earlier destruction. Second, the PM motif may provide cyclin B1 with increased affinity for the APC/C as evidenced by consistent earlier destruction in all PM motif containing (non-membrane localised) constructs as well as the low level turnover in the membrane localised cyclin B1 construct prior to intended destruction. Third, post PB1 extrusion increase in expression is lower for PM-motif containing constructs**.**

Chapter 4 - Exploration of a BubR1 competition hypothesis

4.1 Introduction

The consensus sequences of SLiMS are determined by collating the sequences of known motifs and analysing positional amino acid deviations as well as common characteristics of amino acids in each position. This means that motifs can differ (to an extent) in sequence while still binding to the same receptor site and produce a common effect upon binding[99]. This can be observed by comparing motifs, such as the D-box, of different substrates. Some motifs differ by only one amino acid, for example, cyclin B1 D-box (RTAL) and the cyclin A2 D1-box (RAAL), while others are quite different while still being classed as D-boxes (cyclin A2 D2-box VAPL). These sequences are functional D-boxes for these substrates even though they differ in sequence. It has been determined that these deviations in sequence are physiologically relevant in the context of targeting by the APC/C by altering binding affinities and contributing to the preferential targeting of substrates and inter-substrate competition for the same active site[99,105].

The prometaphase targeting of cyclin A2 is one example where motif sequence deviation has a huge impact on the processivity of a substrate. While the SAC is active, many APC/C complexes will be occupied by the MCC. Importantly though it is likely that not every APC/C will be in complex at all time points. BubR1 plays an incredibly important role in docking of the MCC as well as preventing the destruction of metaphase substrates. BubR1 does this by occupying motif binding sites on Cdc20, namely the KEN, D-box and ABBA motif sites, as well as preventing the formation of the bi-partite D-box receptor (Figure 1.10). However, in order to permit its destruction, cyclin A2 is capable of competing with BubR1 for binding to Cdc20 (Figure 1.12).

The binding affinity as well as dissociation rate determines the residence time of a substrate on the APC/C. The catalytic rate determines the processivity of substrates and to what extent

a substrate becomes ubiquitinated[180]. Groups have primarily utilised competition-based assays to determine which substrate motifs are more or less competitive than others. In these experiments, such as those conducted by Di Fiore et al., recombinant proteins, for example Cdc20, and biotin conjugated motif peptides are combined *in-vitro*[102]. Subsequently additional 'competition' peptides are introduced. Pulldowns with streptavidin beads and immunoblotting then report whether the second motifs was able to outcompete the first. This group used this technique to find that wildtype cyclin A2 was able to outcompete BubR1 for Cdc20 binding, and that mutating the ABBA motif this reversed the outcome. Interestingly, the ABBA motif peptides alone from either cyclin A2 or BubR1 were equally effective at outcompeting each other for Cdc20 in these experiments. This highlights the fact that the presence of multiple SLiMs on a substrate likely increases the affinity by a small increments, but the combined affinities of multiple SLiMs on one substrate (often referred to as a 'cassette') contributes to the overall effect.

Competition experiments have also been conducted *in-vivo* and highlight their potential as potent APC/C inhibitors such as in the work of Yamano et al. whereby metaphase arrest was caused by high concentrations of D-box fragments due to competition for the APC/C D-box receptor in fission yeast[102].

In the context of cyclin B1 and the PM motif, it is plausible that the PM motif is competing for binding to a site on a coactivator. Potentially with BubR1 for a region on Cdc20 to permit prometaphase destruction. There is extensive president for this with other motifs that promote prometaphase destruction, and we have identified a region of BubR1 that bares remarkable resemblance to the PM-motif of cyclin B1. This chapter explores a potential mechanism of prometaphase destruction of cyclin B1 by competing with BubR1 for a site on Cdc20.

In this chapter, I utilise a BubR1 morpholino to knockdown endogenous BubR1 in the oocyte and determine whether expressing replacing endogenous BubR1 with a BubR1 construct

lacking a potentially relevant region in PM motif processing, influences cyclin B1 destruction dynamics.

4.2 Results

4.2.1 Multiple sequence alignment reveals a PM-like motif in spindle assembly checkpoint protein BubR1

Observing instances of sequence similarity or homology for a peptide or protein is a strong indicator of conservation of function, particularly when it comes to protein interactions. Protein-protein interaction interfaces by nature will likely not vary significantly because there must be some conserved mechanism of interaction. Looking for sequence similarity to the PM motif in existing proteins would give an indication as to the function of the PM motif, potential binding partners, or similar binding interfaces.

A multiple sequence alignment of many proteins was performed for comparison with the PM motif region of cyclin B1. One instance of similarity was most exciting, the similarity of a region in BubR1 consisting of residues 137-145 (Figure 4.1A). The most conserved residues between these alignments are the conserved Aspartic Acid (D) in position 1; Tyrosine (Y) in positions 3 and 5 and Leucine (L) in position 6. The Isoleucine (I) in position 2 for the cyclin B1 PM motif differs to that of position 2 of the BubR1 region whereby the residue in this position is a Methionine (M). However, both Isoleucine and Methionine are hydrophobic residues suggesting that they are functionally conserved and the interchange between these two amino acids could be tolerated. I have herein referred to as this region as the “PM-like motif”.

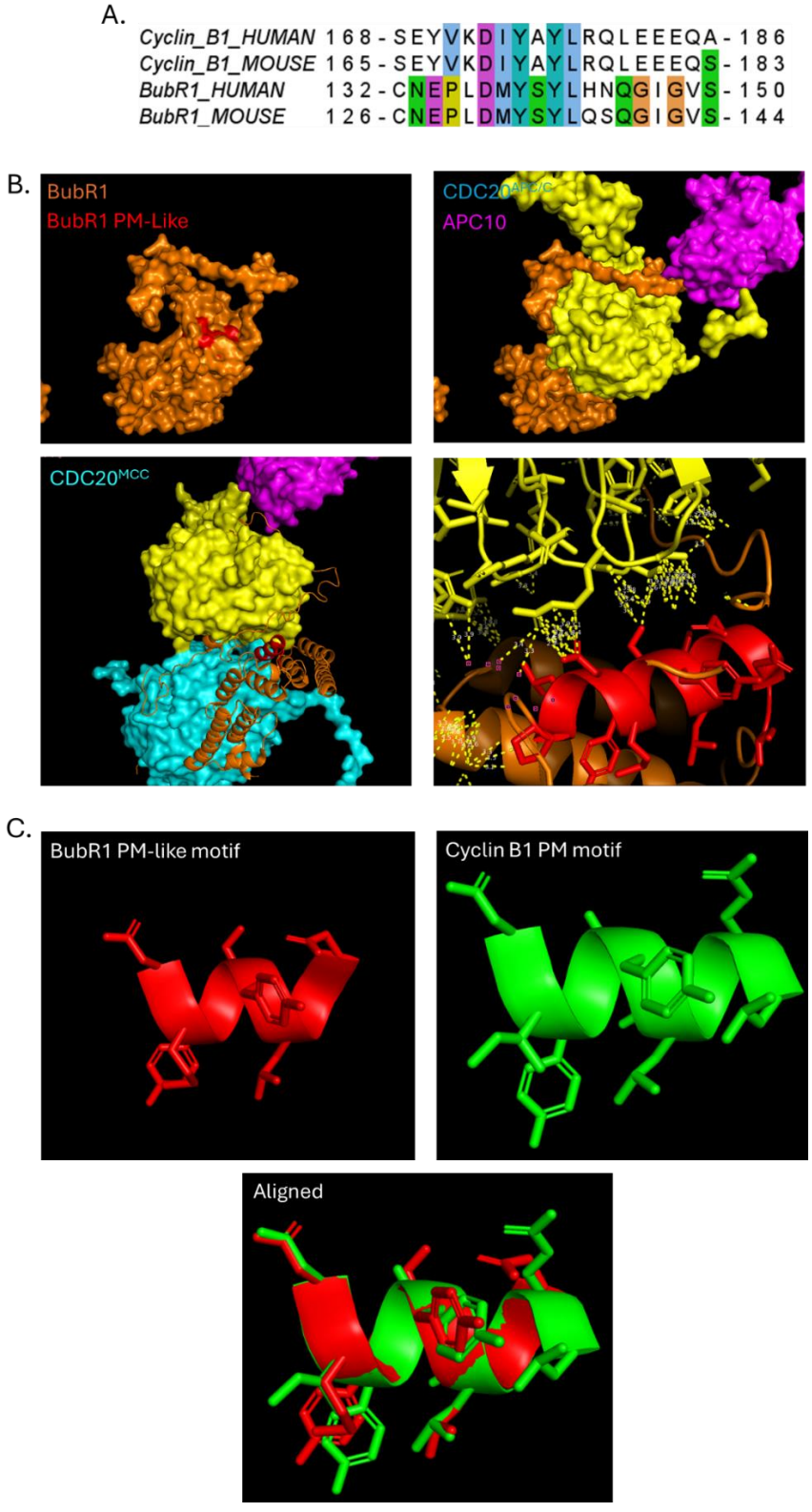

Figure 4.1. BubR1 harbours a region similar to the PM motif and makes contact with Cdc20$^{APC/C}$

A) Multiple sequence alignment of the human and mouse cyclin B1 PM motif and a region in the BubR1 TPR domain which appears to be similar including additional residues N- and C-terminal (utilising Jalview for alignment; coloured using the Clustal X colouring criteria). B) APC/C-MCC Cryo-EM structures solved by the Barford group and accessed using the ProteinDataBank (PDB:6TLJ[137]). Subunits have been isolated and shown in different graphical representations to show interactions and relative positioning using PyMOL. Subunits shown include BubR1 (orange with PM-like motif in red), $Cdc20^{APC/C}$ (yellow), APC10 (magenta), $Cdc20^{MCC}$ (cyan). The BubR1 PM-like motif is surface exposed (top left) and directed towards $Cdc20^{APC/C}$ (top right). The BubR1 PM-like motif forms a helix (bottom left, red) and makes contact with a number of $Cdc20^{APC/C}$ residues (bottom right). C) Structure of the BubR1 PM-like motif from the PDB:6TLJ[116] cryo-EM structure from the Barford group (red, left), alongside the PM motif of cyclin B1 (PDB:2JGZ[181] green). Additionally, a composite alignment of these two motifs utilising the 'align' feature on PyMOL (bottom centre).

Utilising cryo-EM data from David Barford's group and their previously solved structure of the APC/C bound to the MCC, we can visualise the secondary structure of this region of BubR1 as well as its location in relation to other APC/C or MCC subunits[137]. The PM-like motif of BubR1 forms a helix within its TPR domain, specifically the β–helix of TPR2. This region of BubR1 is surface exposed and excitingly appears to make contact with $Cdc20^{APC/C}$ (Figure 4.1B).

The region of $Cdc20^{APC/C}$ that the PM-like motif of BubR1 appears to contact is located between blades 2 and 3 of the WD40 domains, specifically a linear unstructured region linking the two blades. BubR1 D137 and S140 residue appear to make multiple contacts within 3Å of Cdc20 residues R285 and S266 respectively (Figure 4.1B, bottom right).

Alignment of the PM-like motif and the PM motif of cyclin B1 show a similarity in structure (Figure 4.1C). Both sequences form helical structures and the side chains mostly appear conserved. Note that this alignment method utilises the rigid structures and thus the angles of these side chains do not align perfectly. However, it is clear that the side chains are in similar relative positions.

As the PM-like motif of BubR1 shares sequence similarity to the PM motif of cyclin B1, I hypothesised that potentially they could be competing for the same region of Cdc20. Specifically $Cdc20^{APC/C}$, as determined by BubR1 PM-like motif position analysis (Figure 4.1). This is a valid line of enquiry as it has been well characterised that substrate motifs bind directly to Cdc20 to determine destruction dynamics. BubR1 has been well characterised to bind Cdc20 during an active SAC, specifically using its cassette of motifs to bind the ABBA, D-box and KEN box binding regions of Cdc20 to prevent substrates from binding to these regions during the period of chromosome alignment in prometaphase I (Figure 1.10). Cyclin A2 is an example of a substrate which is capable of displacing BubR1's contacts to Cdc20 utilising its cassette of ABBA, D-box and KEN motifs which are thought to compete due to enhanced affinity brought about by sequence differences (Figure 1.12). Therefore, it is sensible to suggest that similar to the other motifs, a PM motif binding site could exist on $Cdc20^{APC/C}$ to which BubR1 binds when the MCC is associated with the APC/C, but displaced when in competition with the PM motif of cyclin B1. This could permit free cyclin B1 binding to APC/C-MCC and prometaphase I destruction. This would explain how mutating the PM motif of cyclin B1 disrupts this earlier destruction (Figure 3.2). The precise mechanism PM motif directed destruction of cyclin B1 by the APC/C-MCC would need to be investigated further. In a mechanism more analogous to the prometaphase destruction of cyclin A2, PM motif binding to Cdc20 (displacing the PM-like motif of BubR1) could induce a conformational change in the MCC and the D-box of cyclin B1 occupies the D-box binding site of $Cdc20^{MCC}$ to permit destruction. Alternatively, PM motif binding to $Cdc20^{APC/C}$ could induce a change which resolves the bipartite D-box receptor to permit cyclin B1 destruction (Figure 4.2).

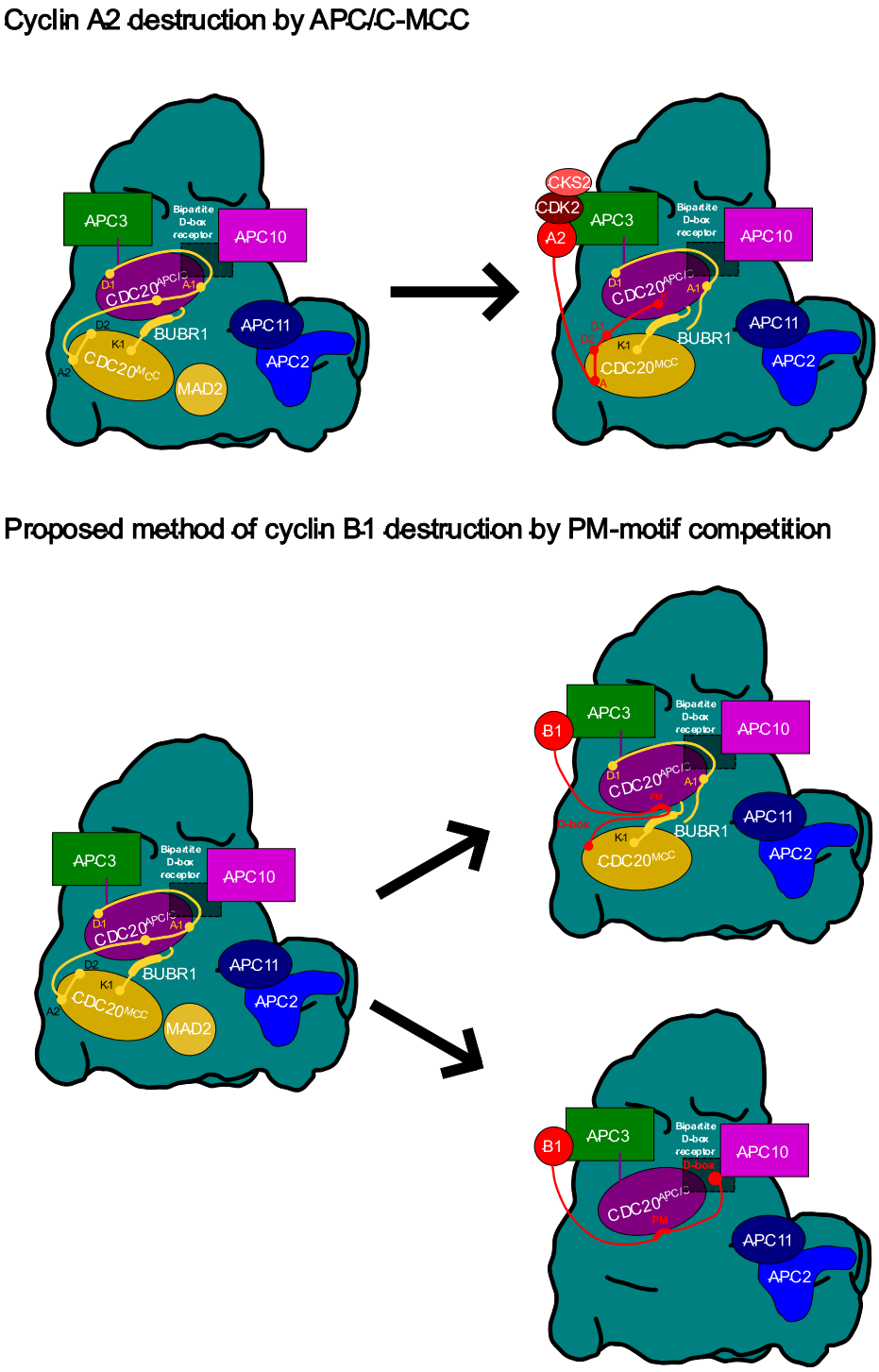

Figure 4.2. Proposed mechanism of cyclin B1 destruction by PM motif competition between the PM motif of cyclin B1 and the PM-like motif of BubR1

Cyclin A2 degradation by the APC/C-MCC relies on competitive binding between its ABBA, KEN and D-box motifs with those of BubR1. This results in these cyclin A2 motifs displacing

those of BubR1 and inducing a conformational change of the MCC which ultimately allows for cyclin A2 ubiquitination by the APC/C-MCC (top). BubR1 additionally contains a region of sequence and structure similarity to that of cyclin B1s PM motif. This is referred to as the PM-like motif of BubR1. In a proposed mechanism of destruction, cyclin B1, utilising its PM motif, could displace the PM-like motif of BubR1 to permit cyclin B1 destruction in prometaphase I. This could potentially induce a conformational change of the MCC, permitting cyclin B1 destruction (similar to the mechanism of cyclin A2 destruction). Alternatively, a mechanism could exist whereby the PM motif of cyclin B1 could compete with BubR1 and induce the removal of the MCC from the APC/C, freeing the bipartite D-box receptor for D-box mediated destruction. Graphical representations of the APC/C complexes are adapted from images by the Barford group[20].

4.2.2 A 20-hour knockdown of BubR1 in mouse oocytes presents as spindle abnormalities and a propensity to undergo GVBD in IBMX

To address this hypothesis and explore whether the PM-like motif of BubR1 is relevant to prometaphase I destruction of cyclin B1, I aimed to use a morpholino knockdown approach, to deplete endogenous BubR1 and replace it with exogenous BubR1 with a mutated PM-like motif sequence. Hypothetically, knocking down endogenous BubR1 and replacing it with PM-like motif mutant BubR1 will reduce the competition of cyclin B1s PM motif with the PM-like motif of BubR1 for Cdc20, potentially making it easier for the PM motif of cyclin B1 to find this position and to displace BubR1. This theoretically would allow earlier or more rapid prometaphase I destruction.

Morpholinos (MOs) are antisense oligonucleotides specific to endogenous mRNA sequences with altered backbone linkages to DNA and RNA which prevents their digestion by nucleases. MOs work by specific, complementary binding to endogenous mRNA to prevent translation[182]. This, together with the natural turnover of a protein reduces the intracellular levels of the target protein. This means that knockdown extent via MO is dependent on protein stability (which is different between proteins due to differing half-lives) and incubation time with the MO. MO sequences can be designed by analysing the mRNA nucleotide sequence of a protein target and identifying a ~25-base sequence near the 5’ end. Importantly, the MO must be designed to be the reverse complement of this sequence to be

able to bind endogenous mRNA. Conversely, MO sequences can be verified by determining the reverse complement of the MO sequence and performing a database search and alignment to identify the complementary mRNA. This is also useful in determining any potential off-target mRNA knockdowns which may occur due to sequence similarity.

The first step in this series of experiments is to design and validate a BubR1 knockdown protocol. Importantly, a knockdown phenotype must be noted, so that when exogenous BubR1 is introduced it can be determined whether this knockdown and rescue has been successful. By reversing the phenotype we confirm that the knockdown has not had off target effects, and that exogenous BubR1 is active and incorporate to replace endogenous BubR1 function.

After much trial and error, experiments began with GV stage oocytes injected with MO oligomer against endogenous BubR1 at a needle concentration of 1mM. Oocytes were injected, and following this incubated with IBMX for 20-hours before washing to release oocytes from prophase arrest. Oocytes were then monitored by time-lapse microscopy for GVBD and PB1 extrusion events. The first observation was that knocking down BubR1 in mouse oocytes increased the propensity for oocytes to resume meiosis spontaneously even while in IBMX inhibitor (Figure 4.3A). 27.8% of oocytes underwent GVBD in IBMX compared to 0% of controls. Surprisingly, following GVBD, there seemed to be little difference in the length of prometaphase I in BubR1 knockdown oocytes relative to non-injected controls whereby mean prometaphase I length for control oocytes was 8.9-hours and 9-hours for oocytes knocked down for BubR1 (GVBD to PBE timings are indicated by the gradient of the lines in Figure 4.3A). We had expected that this checkpoint perturbation would accelerate prometaphase due to a weaker ‘wait anaphase’ signal. Knockdown oocytes however did show reduced spindle organisation and, likely as a consequence of this, reduced chromosome alignment as visualised by immunofluorescence following fixation in late prometaphase (4.5-hours post GVBD Figure 4.3B).

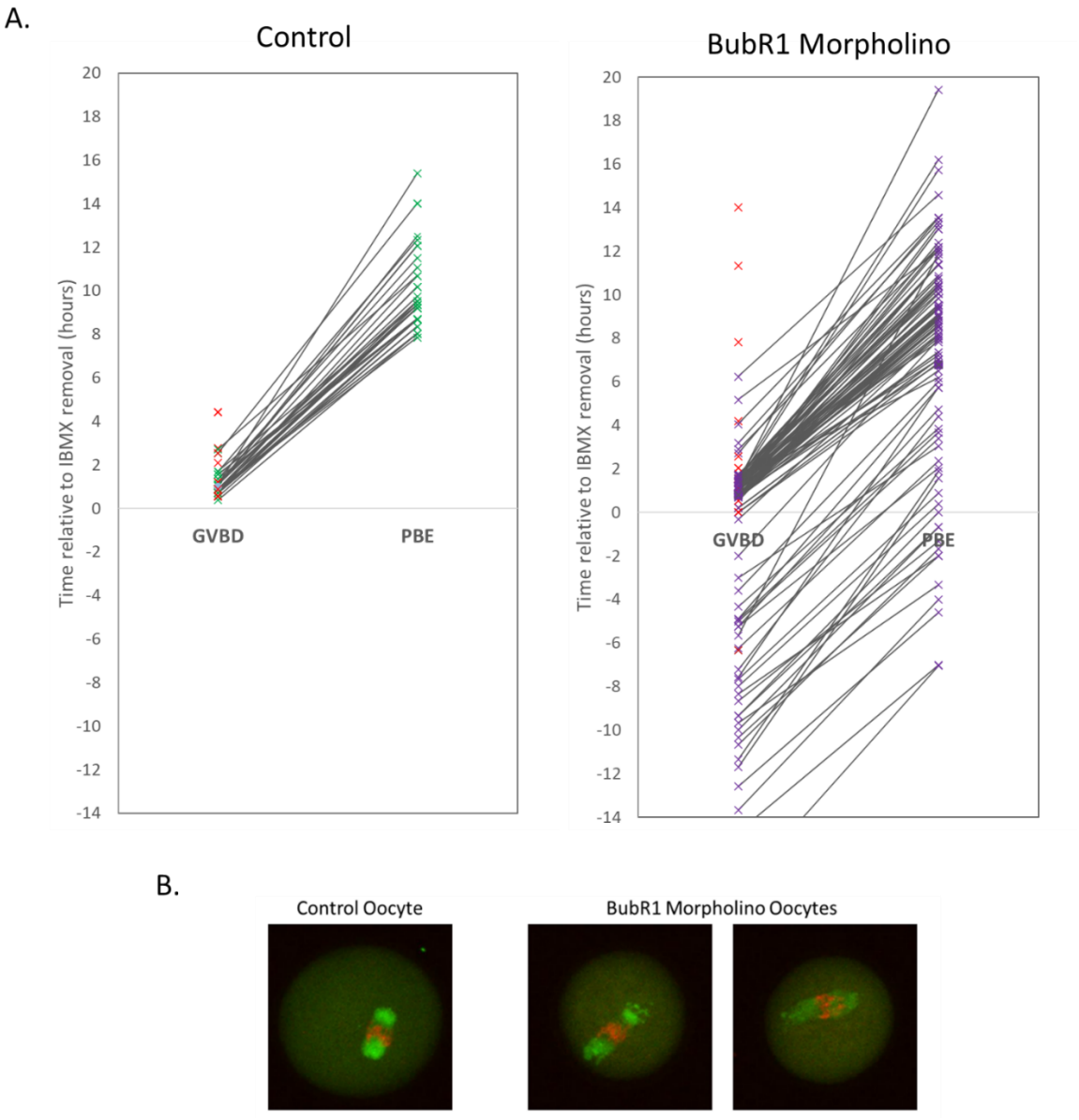

Figure 4.3. A 20-hour knockdown of BubR1 in oocytes increases the propensity to undergo GVBD in IBMX and results in disorganised spindles.

A)Graph to show the times at which individual oocytes undergo GVBD and PBE before (left) and after (right) a 20-hour BubR1 knockdown incubation period. Red crosses indicate oocytes which underwent GVBD but did not extrude polar bodies. The gradient between GVBD and PBE times indicates the length of time spent in prometaphase I. n=50 (left); n=115 (right). B) Immunofluorescence staining of oocytes fixed 4.5hours after GVBD without (left) and with (right) a 20-hour BubR1 knockdown incubation period, using a BubR1 antibody (green) and sirDNA (red).

Next, I sought to measure the impact of BubR1 knockdown on the destruction of cyclin B1. I therefore expressed fluorescent cyclin B1 ± PM-A constructs (Figure 4.4A) alongside the BubR1 morpholino oligomer and quantified destruction after 20-hours of incubation. For these experiments, I only measured destruction in oocytes that did not undergo GVBD in IBMX, and that produced polar bodies. It is only these oocytes that we can be sure have had both the full 20 hours of knockdown and also passed through a full prometaphase I.

Recording the destruction of the cyclin B1 reporter in oocytes knocked down for BubR1 revealed destruction traces with very similar dynamics to those of control oocytes (Figure 4.4B). Including that with or without BubR1 MO incubation, cyclin B1 was depleted to ~19% (Figure 4.4B). More surprisingly again, following BubR1 knockdown, cyclin $B1^{PM\text{-}A}$ was also destroyed at this earlier time point and to the same extent as the cyclin B1 construct under the same treatment.

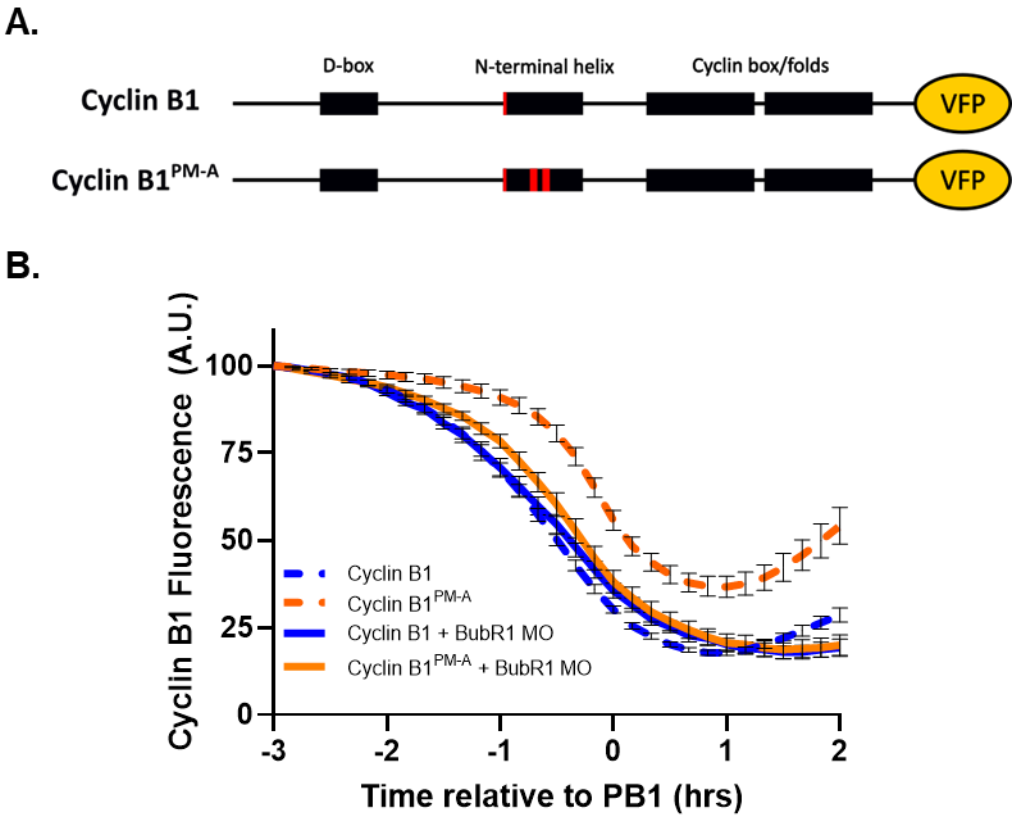

Figure 4.4. BubR1 knockdown results in earlier destruction for cyclin B1^{PM-A} and little difference in timing for cyclin B1

A) Structure diagram describing the cyclin B1 constructs used in this experiment. Cyclin B1 harbours a Y170A mutation and cyclin B1^{PM-A} harbours a Y170A mutation as well as an alanine substitution mutant in the PM motif. B) Mean destruction profiles oocytes having undergone a 20-hour BubR1 knockdown expressing cyclin B1 (blue, solid, n=17) or cyclin B1^{PM-A} (orange, solid, n=15). Alongside the mean destruction profiles of control oocytes expressing cyclin B1 (blue, dashed, n=84) or cyclin B1^{PM-A} (orange, dashed, n=28). Error bars ± SEM.

These results are somewhat unexpected. As discussed earlier, BubR1 is a major component of the SAC. It maintains MCC structure, prevents the formation of the APC/C bipartite D-box receptor, and blocks SLiM binding sites on Cdc20. One could expect that knocking down BubR1 would result in significantly early cyclin B1 destruction on account of improper MCC formation and accelerated APC/C activity (as well as possible premature anaphase). Yet, as

demonstrated, prometaphase lengths for BubR1 knockdown oocytes were not dissimilar to control oocytes. It could be that the extent of the knockdown was insufficient, and a longer incubation time was necessary. However, longer BubR1 morpholino incubations increase the incidence of spontaneous GVBD (in IBMX) significantly reducing n numbers. Furthermore, there is a severely disrupted spindle phenotype suggesting that knockdown has been effective.

After polar body extrusion in BubR1 knockdown oocytes, there is perturbed increase in cyclin B1 that ordinarily accompanies entry into MII and is observed in non-BubR1 knockdown oocytes expressing cyclin B1 constructs. This coupled with the similar destruction timings between oocytes with and without a PM-motif suggest significant dysregulation. The APC/C^{Cdc20} is no longer able to discriminate between cyclin B1 and cyclin $B1^{PM\text{-}A}$ constructs.

It is likely that in the absence of BubR1 many APC/C substrate interactions are perturbed. In this case many different substrates may be disrupted, and APC/C processivity/ordering rules no longer apply. To address, I replaced knocked down BubR1 with a BubR1 sequence with its PM-like motif disrupted. Importantly, the human BubR1 cRNA sequence used in this rescue experiment differs from that of endogenous mouse BubR1, therefore the BubR1 MO should not inhibit the translation of this exogenous BubR1. This BubR1 has intact ABBA, D-box and Ken-Box motifs, and so it is hoped this construct otherwise permits normal cell cycle progression, only disrupting the theoretical cyclin B1 PM motif interaction.

4.2.3 BubR1 knockdown oocytes injected with a mutant BubR1 construct partially rescued the phenotypes associated with knockdown

The PM-like motif of BubR1, was mutated from “DMYSYL” to “AAASYL” (Figure 4.5A). I hypothesize that mutation of the BubR1 PM-like motif would reduce its binding affinity for a binding site on $Cdc20^{APC/C}$ and allow for more efficient cyclin B1 binding to this site, permitting earlier or higher rate destruction of cyclin B1. In this model, BubR1 would likely

still bind to the MCC and act as a pseudosubstrate inhibitor to the APC/C but it is only the PM-like motif which is unbound to its potential binding site on $Cdc20^{APC/C}$.

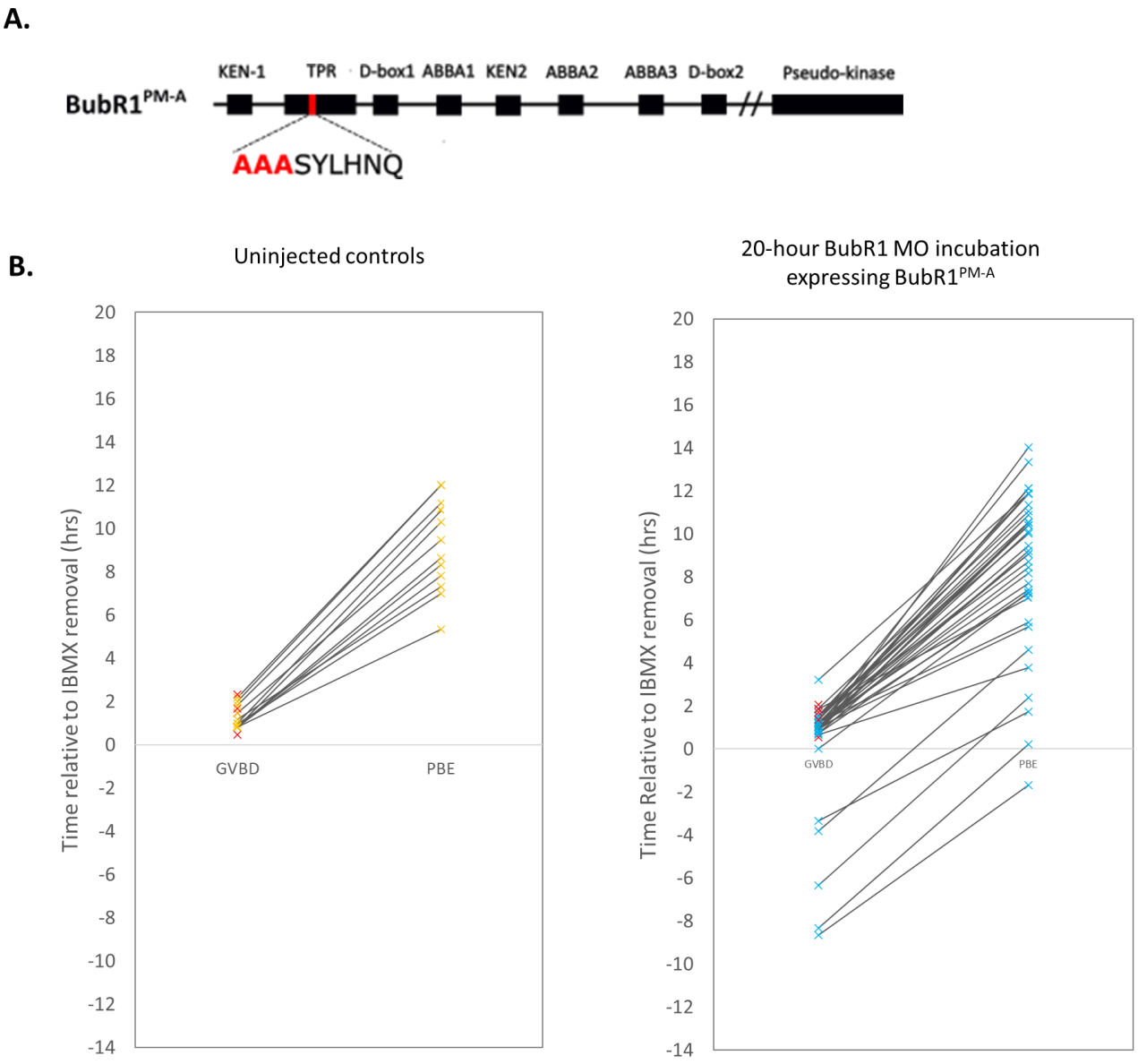

Figure 4.5. BubR1 MO oocytes expressing BubR1PM-A had a reduced propensity to undergo GVBD in IBMX.

A) Structure diagram describing the mutations made to the PM-like motif of BubR1. Residues 137-139 (DIY) were mutated to alanines. B) Graph to show the times at which individual oocytes undergo GVBD and PBE for uninjected control oocytes (left) and oocytes having undergone a 20-hour BubR1 knockdown incubation period while expressing $BubR1^{PM-A}$. Red

crosses indicate oocytes which underwent GVBD but did not extrude polar bodies. The gradient between GVBD and PBE times indicates the length of time spent in prometaphase I. Controls n=20; BubR1 MO+BubR1^{PM-A} n=45.

As a first attempt, I generated a C-terminally linked fluorescent BubR1 construct. However, this protein was unable to rescue any phenotype (data not shown). I therefore proceeded with a non-fluorescent BubR1 construct. This adds complexity to this line of experimentation, it is near impossible to quantify the amount of exogenous BubR1 injected in each oocyte. Determining the amount of exogenous BubR1 injected into the oocyte could be achieved by quantification of fixed oocytes using immunofluorescence or in cell extracts using Western blotting. However, there are limitations to this. Firstly, the extent of expression will vary between oocytes even with precise microinjection protocols, as it is difficult to inject the exact same amount of cRNA into each individual oocyte. Therefore, quantification methods which result in cell death would only be representative to those individual oocytes and not the ones which have cyclin B1 destruction monitored. Additionally, without a specific antibody for the PM-like motif mutation of BubR1, we would not be able to accurately determine how much BubR1^{PM-A} there is in any one oocyte as a commercial BubR1 antibody would reflect total BubR1 levels. For example, an oocyte with a successful knockdown and rescue may have the same amount of BubR1 which had an unsuccessful knockdown due to differing expression between oocytes. Second, the αBubR1 antibody used in the lab consistently produced no signal in Western blotting. While localisation of BubR1 could be determined by immunofluorescence, and a clear phenotype of knockdown observed (being perturbed substrate targeting by the APC/C in Figure 4.4, perturbed spindle organisation, and propensity to undergo GVBD in IBMX, as shown in Figure 4.3), quantification revealed no difference in BubR1 abundance. This could indicate that either the antibody signal was saturated (although unlikely due to extensive antibody validation) or BubR1 knockdown only needs to be subthreshold to induce an effect. Regardless of this however, a clear phenotype

of BubR1 MO incubation was determined and will be used as an indicator for a successful BubR1 rescue by the reversal of this phenotype.

Oocytes were injected with BubR1 MO alongside non-fluorescent BubR1^{PM-A} mutant construct (Figure 4.5A). These oocytes were incubated in IBMX for 20-hours on a heated stage fitted to a microscope which captured brightfield images every 10-minutes. After 20-hours oocytes were washed out of IBMX and left to resume into MI. Times of GVBD and PB1 extrusion were recorded (Figure 4.5B). 8% of the oocytes knocked down for BubR1 and injected with cRNA encoding BubR1^{PM-A} underwent GVBD in IBMX compared to 0% of control uninjected oocytes. Additionally average prometaphase for these knockdown oocytes expressing BubR1 was 8.28-hours compared to 7.89-hours for the uninjected controls.

To verify whether the regulated targeting of cyclin B1 destruction was restored following a BubR1 knockdown rescue, oocytes were subject to a 20-hour BubR1 MO incubation alongside injections of cRNA encoding fluorescent cyclin B1±PM motif, and non-fluorescent BubR1^{PM-A} (Figure 4.6A).

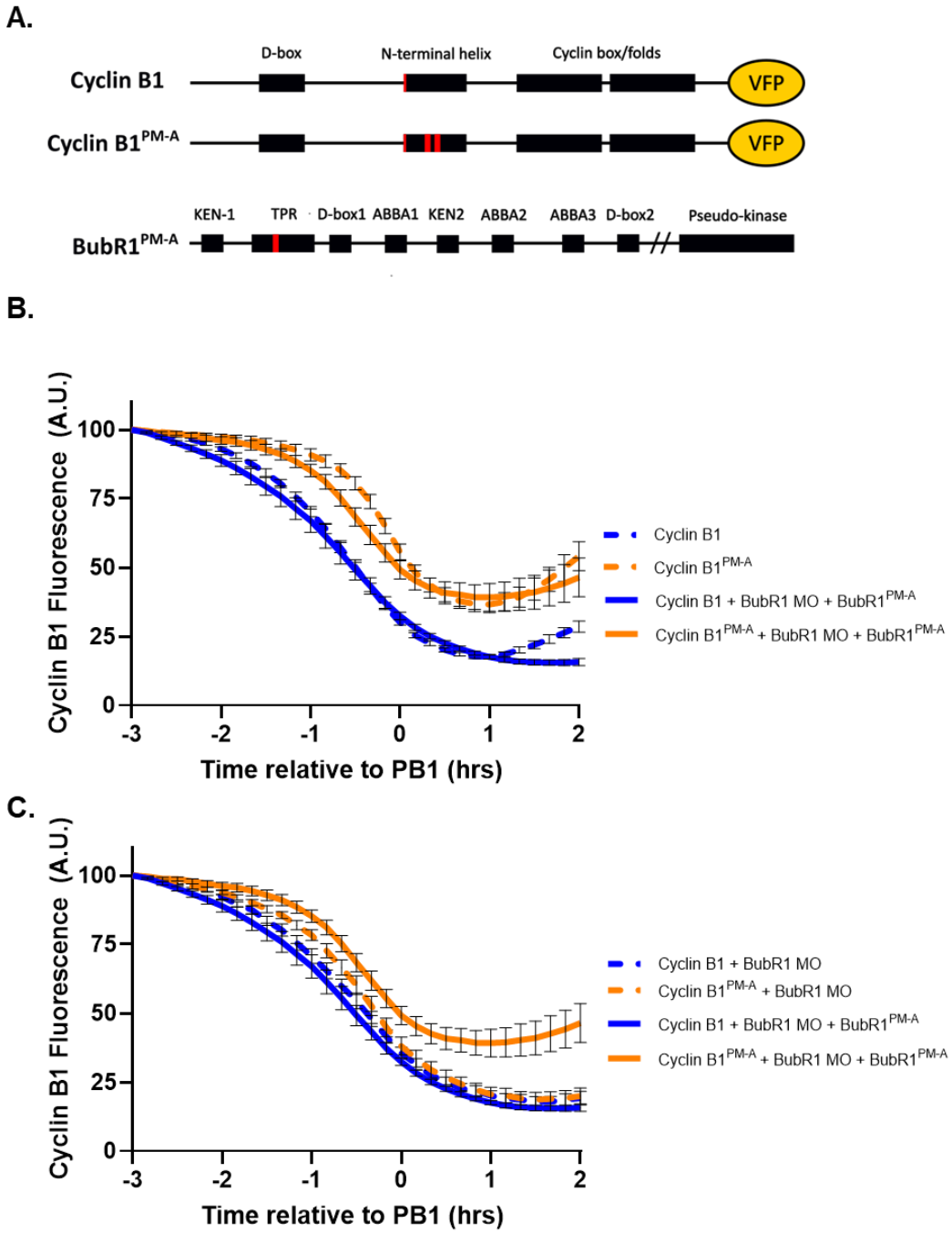

Figure 4.6. Expression of a BubR1 construct without a PM-like motif restores a BubR1 knockdown in terms of cyclin destruction

A) Structure diagram describing the cyclin B1 constructs used in this experiment. Cyclin B1 harbours a Y170A mutation and cyclin B1^{PM-A} harbours a Y170A mutation as well as an alanine substitution mutations in the PM motif. BubR1 has an alanine substitution mutations in its PM-like motif. B) Mean cyclin B1 destruction traces of oocytes having undergone a 20-hour BubR1 knockdown and expressing BubR1 with a PM-like motif mutation (BubR1^{PM-A}).

These oocytes expressed either Cyclin B1 (blue; solid; n=17) or cyclin B1^{PM-A} (orange; solid; n=12). Additionally mean destruction traces of control oocytes, not having undergone BubR1 knockdown and rescue, expressing cyclin B1 (dashed; blue; n=84) or cyclin B1^{PM-A} (orange; dashed; n=28). C. The Mean cyclin B1 destruction profiles in oocytes having undergone a 20-hour BubR1 knockdown with (solid) or without (rescue). All destruction profiles aligned to PB1 extrusion. Error bars ± SEM.

As demonstrated above, BubR1 knockdown resulted in earlier destruction of cyclin B1^{PM-A}, closer to that of cyclin B1 (with a PM motif) (Figure 4.4B). Interestingly, co-expressing the BubR1^{PM-A} mutant after a BubR1 knockdown resulted in cyclin B1^{PM-A} being destroyed once again over a later time period (Figure 4.6C). Indeed, this almost restores the destruction of cyclin B1^{PM-A} to that of cyclin B1^{PM-A} without BubR1 knockdown.

This demonstrates that expressing an exogenous BubR1^{PM-A} construct restores phenotypes associated with a BubR1 knockdown (both the premature GVBD and premature cyclin B1^{PM-A} destruction) and normal cell cycle protein regulation is mostly restored. This is interesting as it suggests that the PM-like motif of BubR1 is not essential for the functions of BubR1 assessed. However, the hypothesis that a BubR1 PM-A-like mutant could result in even earlier destruction of cyclin B1 was disproved. The loss of BubR1 without rescue did not result in earlier cyclin B1 destruction and replacing BubR1 with a BubR1 PM-like motif mutant resulted in 'normal' timings of both cyclin B1 contracts. It is still possible that the PM-motif of endogenous cyclin B1 can interact with the same region of Cdc20 that the PM-like-motif of BubR1 interacts with, but that this is not competitive binding. An unknown factor might time cyclin B1 destruction using only a population of APC/C complexes that are not BubR1 bound. Or cyclin B1's affinity for this Cdc20 site might be much higher than that of BubR1. In either of those cases, it could be imagined that the loss of BubR1 would not result in earlier cyclin B1 destruction.

This line of experimentation conducted so far is challenging. There could be multiple reasons as to why the BubR1 knockdown did not have the intended effect, which will be discussed in a later section. This ultimately means that this method of investigating competition between cyclin B1 and BubR1 was likely insufficient.

4.2.3 Replacing the PM motif of cyclin B1 with the PM motif of BubR1 perturbs early destruction

I decided to perform experiments in a more similar way to more conventional competition type assays as discussed in section 4.1, whereby motifs are swapped between substrates to determine whether destruction is more or less efficient. Ideally, inserting the PM motif of cyclin B1 into BubR1 would be the best way of doing this. The hypothesis surrounding this line of inquiry (relying on the cyclin B1 PM-motif outcompeting that of BubR1 in weaker checkpoint situations) suggests that the PM motif of cyclin B1 could have a higher binding affinity for Cdc20. However, having to knockdown BubR1 where many oocytes escape arrest, then express mutant BubR1 (at undetermined amounts) alongside cyclin B1 adds many variables and points at which the cell and cell cycle machinery are challenged. This makes it difficult to determine true phenotypes versus the effect of extended incubation periods. Additionally, knockdown experiments have not given expected results and fluorescent BubR1 is not functional. Control of these experiments becomes unsatisfactorily complex and would require significant mouse cull. Instead, I decided to take the opposite approach, to produce a cyclin B1 mutant whereby the PM motif is replaced with the PM-like motif of BubR1; (cyclin $B1^{BubR1\ PM\text{-}motif}$; Figure 4.7A). It is plausible that cyclin $B1^{BubR1\ PM\text{-}motif}$ protein would not be able to compete with BubR1 sufficiently (BubR1 has many points of contact with Cdc20) and this may restrict destruction to the late timepoint when the APC/C is free of MCC.

To this end, the PM motif of cyclin B1 was mutated to the PM motif of BubR1 (Figure 4.7A). Importantly, for technical reasons the control oocytes expressing a well established reporter protein in this line of experimentation failed and thus the following observation is based on

oocytes expressing this construct without an additional pool of oocytes expressing a reference construct imaged at the same time. This is less than ideal for numerous reasons. Without having measured the destruction profile of this construct at the same time as another already well-established protein, such as cyclin B1, and verifying that the well-established protein is targeted with expected destruction dynamics, we cannot accurately compare them. Therefore, the destruction trace for this construct should be treated with caution when making direct comparisons to other constructs. For this reason I have not graphed the destruction curve of this construct alongside cyclin B1 or cyclin $B1^{PM\text{-}A}$.

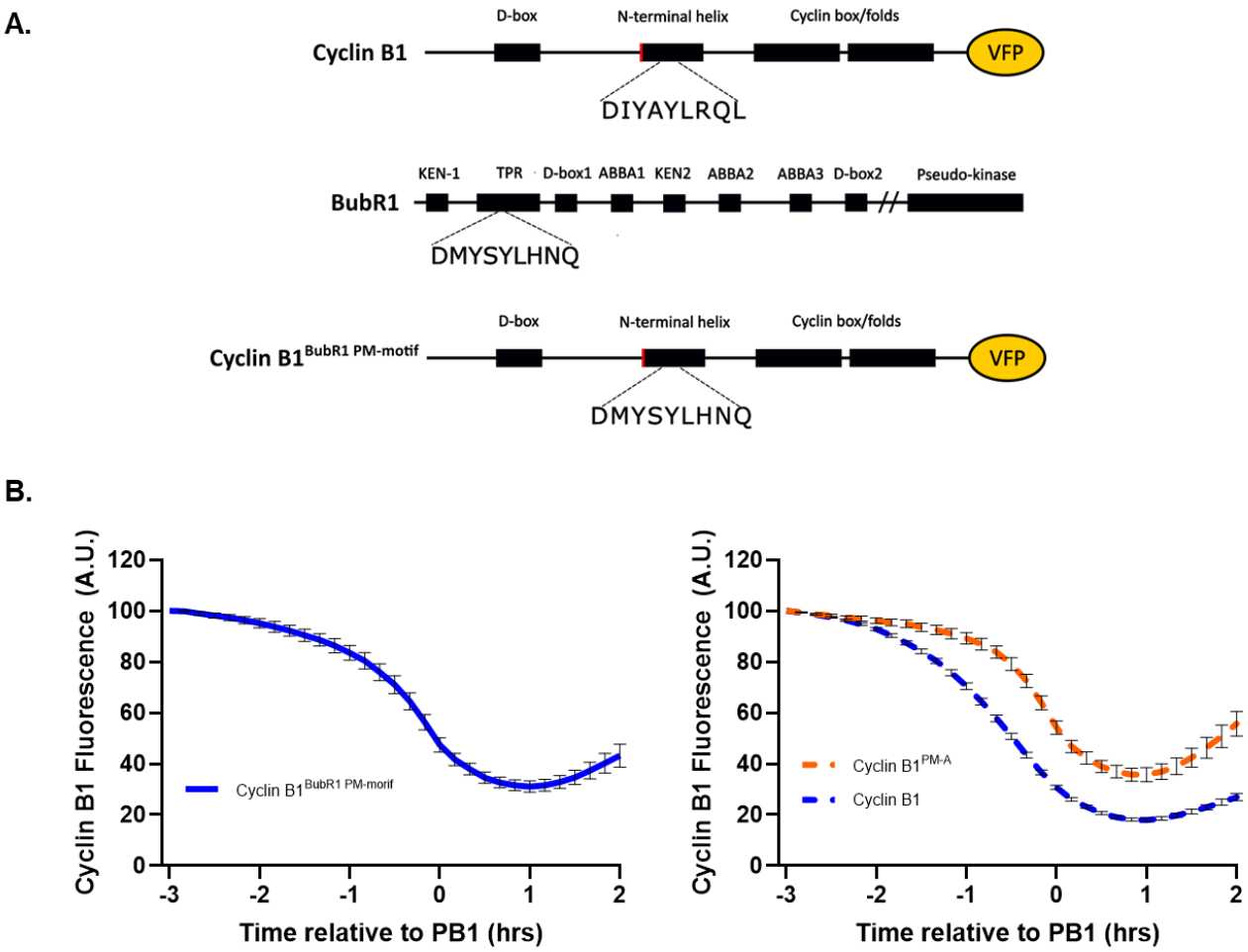

Figure 4.7. Replacing the PM-motif of cyclin B1 with the PM-like motif of BubR1 removes the ability of cyclin B1 to be targeted in prometaphase I.

A) Structure diagram describing the constructs used in these experiments whereby the PM motif of cyclin B1 was replaced with the BubR1 PM-like motif. B) Mean destruction profiles of oocytes expressing cyclin B1$^{BubR1\ PM\text{-}motif}$ (solid; blue; n=8) alongside the mean destruction profiles of oocytes expressing Cyclin B1 (dashed; blue; n=84), Cyclin B1$^{PM\text{-}A}$ (dashed; orange; n=28;) as a reference. Importantly, this observation is from experimentation whereby oocytes expressing a reference construct failed. Error bars ± SEM.

On injecting this cRNA into oocytes and quantifying expressed fluorescence over meiosis I, we now observe mean cyclin B1$^{BubR1\ PM\text{-}A}$ protein destruction initiating approximately -1.5-hours prior to PB1 extrusion whereby this point 10% has been destroyed. The extent of

destruction of cyclin B1$^{BubR1\ PM\text{-}A}$ is 69%. It is as if destruction initiates at an early time point (late prometaphase) but a low rate and less extensive. This supports the hypothesis that the PM-like motif of BubR1 could function as a PM motif however is significantly less efficient at binding compared to the PM-motif of cyclin B1.

4.3 Discussion

Competition between SLiMs is thought to be one of the major factors determining substrate targeting order for the APC/C, owing to their variable binding affinities, dissociation constants, and their abundance. It seems very likely that the mechanism of action of the PM motif of cyclin B1, in permitting its prometaphase timing of destruction, is one of a SLiM. Comparisons can be made with another APC/C prometaphase target, cyclin A2, which is able to compete with MCC components, specifically with BubR1, for binding to Cdc20. Indeed the only MCC component which makes contact with Cdc20$^{APC/C}$ is BubR1. Cyclin A2 utilises its cassette of ABBA, KEN and D-boxes to compete for the respective motif binding sites on Cdc20, displacing BubR1 to enable its ubiquitination. Therefore, it was sensible to suggest that the cyclin B1 SLiM, the PM-motif, also competes with BubR1 for a binding site on the coactivator, Cdc20. This hypothesis is strongly supported by the finding that BubR1 harbours a region with striking sequence and structural similarity to the PM motif, and that this site is a surface exposed and makes contact with Cdc20 (Figure 4.1).

Using live cell assays, I designed two ways to investigate whether this region of BubR1 is physiologically relevant in PM motif processivity. First, by replacing endogenous BubR1 with a mutant with the PM-like motif mutated (assessing if cyclin B1 would be able to outcompete this BubR1 mutant to a greater extent and present as an even earlier destruction target). Second, by replacing cyclin B1s PM-motif with the PM-like motif of BubR1. In this case to assess if this version of cyclin B1 was less able to compete with BubR1 for hypothetical Cdc20 binding, resulting in later destruction of this cyclin B1 mutant.

The BubR1 knockdown did not have the effect one would expect. It is reasonable to suggest that knocking down BubR1 would reduce either the effectiveness, or the amount of MCC

produced, and that this would result in a short prometaphase and premature anaphase. My results show no change in prometaphase length in BubR1 knockdown oocytes, as polar bodies are extruded at timepoints expected for controls. Instead, the primary phenotype associated with a BubR1 knockdown was an increase in the instances of GVBD in IBMX. In a 2009 paper, Homer et al. performed a knockdown of BubR1 in oocytes, also using a morpholino antisense oligomer[183]. They found that, similar to my data, a 24-hour BubR1 knockdown resulted in ~25% increase of GVBD in IBMX compared to control oocytes. In contrast however, they also report reduced the polar body extrusion rate; many oocytes arrested in meiosis I, which is not an outcome of my experiments. In a second example, similar BubR1 knockdown experiments were also conducted by Wei et al. again with a 24-hour knockdown[184]. In this case GVBD occurred early (in agreement with Homer et al. and my data), but like my data PB1 extrusion rates were not significantly different to control oocytes. However, Wei et al. report slightly earlier PB1 extrusion. The study by Homer et al. also examined spindle and DNA arrangements under a bubR1 knockdown and found that kinetochore-microtubule attachments were impaired and DNA was significantly more misaligned compared to control oocytes. This further validates that knockdown was successful in this line of experimentation. These differences are difficult to resolve but notably all three groups utilised different morpholino sequences, which may produce different extents of knockdowns.

Homer et al. suggested that the reason why BubR1 knockdown oocytes escape GV arrest in IBMX, is that BubR1 sustains Cdh1 levels in prophase I, in order to prevent unscheduled entry into meiosis[183]. Therefore, reducing BubR1 levels causes a reduction in APC/C-Cdh1 activity and likely allows cyclin B1 levels to gradually accumulate, activating CDK1, resulting in oocytes re-entering meiosis. The similarity of GV arrest escape across 3 groups gives confidence that my knockdown experiments are successfully knocking down BubR1. However, this phenotype makes it technically very difficult to increase the extent of the knockdown without further manipulations that are technically more difficult to control. The finding by Homer et al., that a BubR1 knockdown resulted in a lack of PB1 extrusion is surprising (inhibition of checkpoint activities more often promotes cell division). This is

explained by the following; the group report that securin levels were 2-fold higher in BubR1 knockdown oocytes compared to control oocytes. They suggest that this is owing to a reduction in APC/C^{Cdh1} mediated destruction of securin at earlier cell cycle time points as described above. This suggests that on completion of metaphase, the APC/C^{cdc20} was overwhelmed with an excess of securin and the oocyte was unable to complete anaphase. Indeed, by either expressing exogenous cdh1 in oocytes knocked down for BubR1, or using a securin knockdown, increased PB1 extrusion rates.

These experiments highlight how extremely interconnected cell cycle proteins are. Disrupting even one element in this system can result in unpredicted outcomes across many proteins, and indeed even altering levels slightly can result in substantially different outcomes.

My data shows that a 20-hour BubR1 knockdown incubation results in no change in the destruction dynamics of cyclin B1, yet the reporter for bound-cyclin B1 (cyclin $B1^{PM\text{-}A}$) is destroyed early. PB1 extrusion rates and prometaphase timings were like that of control oocytes. However, though prometaphase appears 'normal' in timing (albeit with severely disrupted spindle architecture), is it possible that we have 2 opposing factors that are abnormal in comparison to healthy oocytes. First, checkpoint inhibition/perturbation due to the loss of BubR1 that would act accelerate APC/C activity. Second, overloading of securin (as described by Homer et al.) that will occupy the APC/C for longer in metaphase. This could explain how cyclin $B1^{PM\text{-}A}$ appears to be targeted for destruction in prometaphase I (2 hours before anaphase). It is possible that biochemically prometaphase was shorter, while the metaphase – anaphase transition took much longer giving the overall effect of normal timing. Our current data cannot establish this. Further experiments are required here, reporting securin levels and the activity of other checkpoint proteins following BubR1 knockdown.

The expression of exogenous BubR1 can rescue phenotypes associated with BubR1 knockdown. Interestingly I found that a fluorescent BubR1 was unable to make the same rescue. This isn't entirely surprising, BubR1 is required to fit into the APC/C^{Cdc20} complex in an intricate way and the addition of a fluorescent tag could result in a steric hinderance,

preventing APC/C or MCC incorporation. Indeed, this has been reported elsewhere other MCC components such as Mad2, which is unable to be tagged C- or N-terminally with a fluorescent protein and still permit SAC signalling[185]. A non-fluorescent form of BubR1 could restore the knockdown phenotypes I observed even with a mutation in the PM-like motif.

Co-expression of BubR1$^{PM\text{-}A}$ alongside cyclin B1 ± PM motif after a BubR1 knockdown resulted in cyclin B1$^{PM\text{-}A}$ being targeted slightly earlier than cyclin B1$^{PM\text{-}A}$ without a BubR1 knockdown (Figure 4.6B). Specifically, there is a 30-minute time difference between these constructs reaching ~75% relative fluorescence. This is likely an effect of an incomplete phenotype reversal whereby exogenous BubR1 was not expressed to the extent of endogenous BubR1 prior to the knockdown. Therefore, the average destruction trace of cyclin B1$^{PM\text{-}A}$ occurs slightly earlier. In summary, this is perhaps a partial rescue, but nevertheless convincing.

Interestingly, replacing the PM motif of cyclin B1 with the PM-like motif of BubR1 did result in destruction initiating in late prometaphase I (10% destruction, -1.5 hours prior to PB1 extrusion). While we cannot make a direct comparison due to the limitations of this particular line of experimentation, cyclin B1$^{PM\text{-}A}$ reaches 10% destruction at -1-hour prior to polar body extrusion which likely marks the metaphase-anaphase transition. Of note however, destruction for this construct is not extensive. We would not want to overinterpret this result due to the limitations of this experiment not having a pool of oocytes co-cultured and expressing a reference construct. I predict that if a direct comparison could be made, this destruction would be an intermediate between cyclin B1 and cyclin B1$^{PM\text{-}A}$. If this is indeed a true reflection of the destruction of a cyclin B1$^{BubR1\ PM}$ construct, there could be a number of potential explanations. While both putative PM motifs (from cyclin B1 and BubR1) exist as helical structures (Figure 4.1C), without further structure analysis, it cannot be assumed that modifying the PM motif of cyclin B1 in this way maintains the secondary structure of this region. If the helical structure was modified or broken, we would expected a similar result to the original PM motif alanine substitution (destruction at the late time point), i.e. that the cyclin B1$^{BubR1\ PM\text{-}motif}$ construct is simply cyclin B1$^{PM\text{-}a}$. Alternatively, this

result could be explained by the following. Assuming that the PM motif of cyclin B1 has a higher binding affinity for Cdc20 compared to the PM-like motif of BubR1, by mutating the PM motif of cyclin B1 to be more like that of BubR1 would reduce its binding affinity and result in delayed destruction. The flanking residues of the PM motif may contribute to its binding affinity and by not changing these flanking residues, a slightly higher binding affinity could still be maintained. Therefore, we would observe more of a graded response whereby the potency of the PM motif has been reduced, but still sufficient to compete to some extent with BubR1s PM-like motif. More experimentation utilising this construct is required however this result is exciting, nonetheless.

The data from this line of experimentation is inconclusive with regard to understanding free cyclin B1 destruction yet provides insights into the function of BubR1 in mouse oocytes.

Chapter 5 - Feasibility of protein-protein interaction assays in mouse oocytes

5.1 Introduction

Previous chapters have shown that the PM motif of cyclin B1 facilitates its prometaphase I destruction. Accordingly, mutating this motif to alanine residues restricts cyclin B1 destruction to the metaphase-anaphase transition. Exactly how the PM motif facilitates this early destruction has yet to been elucidated. There are however, a number of educated predictions that can be made. For example:

- Cdc20 is the coactivator of the APC/C at the time at which cyclin B1 is destroyed in prometaphase I. This is evidenced in the literature. Furthermore experiments that deplete Cdc20 report that cyclin B1 destruction is perturbed[160].
- APC/C complexes are likely to be bound to the MCC. This is because chromosomes have not fully congressed at the timepoint at which cyclin B1 destruction targeting initiates. Thus, the SAC is likely signalling and MCC complexes are being generated for APC/C association. Furthermore, previous published data form our lab demonstrates that oocytes bathed in nocodazole (to constitutively activate the SAC), still destroy cyclin B1 (albeit reduced in rate). Cyclin $B1^{PM\text{-}A}$ is stabilised in the same context[160].

It is possible that a chaperone protein may promote free cyclin B1 destruction. Abundant mitotic literature shows that cyclin proteins associate with the APC/C utilising a CKS protein chaperone to bind to a phosphorylated APC3[20,186]. In this case it is thought that cyclin B1 must also be CDK1 bound, as the CKS subunit binds to CDK1, but it is plausible that a currently unidentified player also exists to guide free cyclin B1 to the APC/C. However, these model scenarios lack experimental data in oocytes, and there are other sensible possibilities which could be responsible for or contribute to prometaphase I destruction of cyclin B1.

The APC/C is highly dynamic, likely capable of existing in different modes at any one time on account of its many regulation mechanisms (Figure 1.11). For example, while Cdc20 is the primary coactivator at the time point at which cyclin B1 is targeted for destruction, a subset

of APC/C could reasonably be Cdh1 bound. Similarly, even while the SAC is active, there likely exists a subpopulation of APC/C not bound by MCC (even is this is simply just to do with MCC turnover or a refractory period between MCC associations), which could in theory be responsible for targeting cyclin B1 in prometaphase I. Furthermore, while nocodazole "strengthens" the SAC, it is still difficult to determine whether all APC/Cs are bound by MCCs in this situation. Treatment of oocytes with higher concentrations of nocodazole reduces the extent of the destruction of PM motif containing cyclin B1 constructs, demonstrating that this is a graded, rather than all or nothing response[160]. An explanation for this could be increasing MCC coverage of APC/C complexes as the concentration of nocodazole increases. The results of Cdc20 knockdown experiments are also complicated[160]. This significantly reduces APC/C activity and inhibits SliM binding, highly likely resulting in a large backlog of substrates for any remaining active APC/C that has lost much ability to differentiate between substrates at this point. These experiments tell us something, but they are not to be overinterpreted. Cell cycle perturbations have many knock-on effects and it is difficult to isolate and test individual mechanisms/interactions.

Ideally, this project would benefit enormously from experiments that could determine the interactome of cyclin B1 in mouse oocytes at prometaphase I. This would allow us to determine which proteins are associated with cyclin B1 when the PM motif is present, whether that be directly with the motif itself, or indirectly, alongside whether these interactions occur when the PM motif is not present. This line of experimentation could also tell us many things about the APC/C mode that targets this form of cyclin B1. Such as, is the MCC present? Which coactivator is present? Is a chaperone required for cyclin B1s association at this time point? Does cyclin B1 take advantage of the APC/C actively targeting another substrate? In this latter example, I am referring to a hypothetical scenario whereby as APC/C-MCC is targeting Cyclin A2, cyclin B1 could associate with the APC/C using its PM motif while the MCC is out of its 'inhibitory' positioning in the APC/C. This could be described as an opportunistic mechanism of cyclin B1 association to the APC/C. The ability to answer these questions would provide profound insight into the meiotic APC/C as well as cyclin B1 destruction in the mouse oocyte.

Traditional methods of determining protein-protein interactions include co-immunoprecipitations. In this procedure, antibodies (specific to a protein of interest), are combined with whole cell lysates resulting in an association between antibody and protein target. In the correct experimental conditions, the protein of interest remains associated with any interaction partners. Antibody-binding beads are then added to immobilise the antibody-protein complexes, this is then followed by a series of wash steps to separate the immobilised antibody-protein complexes from non-interacting proteins. The protein of interest, bound to interaction partners, can then be eluted and identified directly by procedures such as Western blotting (if candidates are suspected), or by mass spectrometry. Interaction partners must then be verified *in-vivo,* and truncation/mutagenesis experiments may determine which domains and regions are key in interactions.

Substantial literature dissecting which form of the APC/C targets specific substrates has included the IP procedure in mitotic cell lines. For instance, Di Fiore et al. utilised stable, inducible HeLa cell lines expressing cyclin A2 linked to a flag epitope[102]. Cells were then synchronised in mitosis using a thymidine and nocodazole protocol to arrest cells in prometaphase. A pull down of cyclin A2 using a flag antibody, followed by Western blotting, showed that in this setting cyclin A2 constructs bound to Cdc20. Importantly, removing the extended D-box motif of cyclin A prevented this interaction. The group also immunoprecipitated Cdc20 and added GST fusion proteins to determine that excess cyclin A2 displaced BubR1 from Cdc20. These experiments provided the foundation behind the mechanism of cyclin A2 targeting by the APC/C-MCC and highlights the power of these experiments.

Many groups have also benefited from the demonstration that APC/C and MCC components can be expressed recombinantly and assemble spontaneously *in-vitro* with surprising ease. The addition then of recombinant substrates and ubiquitin allows researchers to perform *in-vitro* ubiquitination assays and determine the effect of knockouts and mutations of APC/C subunits. Zhang et al. utilised this technique to determine the effects of cyclin A2 degron mutations on its ubiquitination by both the APC/C^{Cdc20} and $APC/C^{MCC\ 20}$. They subsequently

produced a table of the different degron mutations (single or multiple) to collate this processivity information. Key take homes from this are that the D2 degron was the only single mutation that resulted in a significant reduction of cyclin A2 by APC/C^{Cdc20}, and that the ABBA and KEN motifs are important in APC/C^{MCC} mediated destruction of cyclin A2. These *in-vitro* experiments have been highly valuable, important contribution to the field. They must be caveated however, that interactions are never in isolation and lack the context of a complex cellular environment.

Performing traditional protein-protein interaction experiments in mouse oocytes is particularly challenging. Firstly, lysates generally require a lot of protein, especially if immobilising endogenous proteins. But even if one was to use recombinant proteins as immunoprecipitation "bait", whole cell lysates are required to incubate with any bait protein. As our mechanism of interest operates in mouse oocytes, a substantial number would be required to perform these experiments. This raises both ethical and practical concerns. These types of experiments are also not ideal for transient interactions, which is the nature of enzyme-substrate targeting.

BioID (proximity-dependent biotin identification) presents itself as a potential method to explore protein-protein interactions in mouse oocytes (though to our knowledge they have not been attempted in this cell type in this context)[187]**.** This procedure utilises a mutant of the Escherichia coli biotin ligase BirA, which specifically binds and biotinylates the biotin carboxyl carrier protein subunit of acetyl-coA carboxylase. The result is the formation of an amide bond between a biotin molecule and a specific lysine residue on a protein surface[188]. The BioID technique mutant is a $BirA^{R118G}$ (herein referred to as BioID), which removes its specificity and allows it to behave as a promiscuous biotin ligase for proteins in proximity. In this case proximity is thought to include proteins that have come within 10 nm of the BioID molecule *in-vivo*. These proteins are biotinylated and can be isolated via pull-down using avadin or streptavidin-based systems for subsequent identification. Proteins of interest can be fused to a BioID protein and therefore any interaction partners will be biotinylated and can be identified[187,188].

This technique is incredibly useful for detecting weak interactions or proteins with low expression levels. Also, with the ability to supplement biotin as and when necessary, the proximity ligation of protein interaction partners can be regulated temporally. The types of biotinylated proteins include, direct interactions; indirect interactions or proximal proteins that do not interact[187]. The latter scenario adds complexity to these experiments as isolating true interactions from false positives is essential. Fortunately, a significant amount of literature exists surrounding the APC/C and cyclin B1 so in our mechanism of interest, isolating many false positives may not be difficult. We also have excellent assays to determine the potential of positive results, namely where the disruption of any potential interaction shifts the destruction timing of cyclin B1 in mouse oocytes.

Since it's conception, the BioID technique has been adapted over the years. Some significant advancements include:

- The use of the BioID protein in a protein fragment complementation assay. Schopp et al. discovered that the BioID protein can be split into two fragments (N-BioID; C-BioID). These fragments are associated with FKBP or FRB proteins which only interact in the presence of rapamycin. Therefore, expressing both split-BioID constructs alongside treatment with rapamycin, results in the fusion of the FKBP/FRB components and the formation of a full-length BioID construct[189]. This is particularly useful in verifying the interactions between two known proteins of interest.
- Development of alternative biotinylation enzymes with more desirable properties such as BioID2. BioID2 is a smaller promiscuous biotin ligase developed by Kim et al from A. aeolicus. Producing a smaller biotin ligase alleviates issues whereby the larger BioID enzyme occasionally prevents efficient targeting. This smaller enzyme also required less biotin supplementation than BioID. This same group also demonstrated the ability to sample a variable proximity range using different sized flexible linkers[190].
- A major disadvantage of the two biotin ligase enzymes mentioned above is that their biotinylation rate is slow, taking a number of hours for efficient biotinylation. To address this, Cho et al. produced TurboID, overcoming the slow labelling kinetics of

the previous enzymes. By performing a yeast display-based directed evolution of the BirA^{R118S} mutant, TurboID (and its smaller counterpart miniTurbo) are capable of labelling in as little as 10 minutes, in a range of temperatures, and more efficiently and without the need of exogenous biotin[191].

Proximity biotinylation assays, especially utilising TurboID, give us great potential to explore protein-protein interactions in the mouse oocyte. This technique gives the opportunity to tag the entire interactome of cyclin B1 reporters in the oocyte, without relying on immunoprecipitations which require large amounts of material. These assays are also well suited to weaker and transient interactions. I propose that proximity biotinylation will allow us to explore the interactome of cyclin B1 in oocytes in native context. Compared to traditional IP protocols, our assays would be enhanced by the biotin-streptavadin interaction, one of the strongest interactions in nature, giving confidence in efficient pull-down[192]. The rapid nature of TurboID also offers the opportunity to more confidently explore the interactome of cyclin B1 at a specific time points in meiosis.

5.2 Results

5.2.1 C-terminally linked TurboID yields the greatest potential for use in a biotin proximity ligation assay

As a first step I decided to test both new generation biotin proximity ligation enzymes, to determine which would be best suited to fuse with cyclin B1 reporters for use in live mouse oocytes. By fusing different biotin ligase enzymes to fluorescent tagged cyclin B1±PM motif constructs, it was hoped that I could highlight proteins that were in proximity where the PM motif is present, but reduced or absent in outputs without a PM motif. Therefore, I needed to be sure that both cyclin B1 reporters behaved as previously when fused to a ligase enzyme. Namely that the cyclin B1 reporter is targeted for destruction in prometaphase I, and the cyclin B1^{PM-A} mutant reporter is destroyed later, at the metaphase-anaphase transition.

To this end, I obtained a BioID2 plasmid as a gift from Leinhard Schmitz (pTet-on-Puro-Myc-BirA) as well as a C- and N- split Turbo-ID plasmids from Prof. Alice Tings' lab (Addgene plasmids #153005 and #153004 respectively[191]). A PCR and Gibson assembly protocol isolated N-TurboID and C-TurboID fragments, which I combined to produce a full length TurboID construct. This was inserted N-terminally to cyclin B1-VFP in a vector which allows for *in-vitro* transcription and subsequent microinjection into mouse oocytes. Similarly, the BioID2 enzyme was inserted N-terminally into cyclin B1 plasmids. I chose to insert the biotinylation enzymes N-terminal to cyclin B1 because of the presence of a convenient BglII site upstream of the cyclin B1 gene. I also produced fluorescent constructs of the biotyinalation enzymes only (not cyclin B1 linked) as a control to rule out that the biotinylation enzymes themselves would influence destruction dynamics.

After verifying that these constructs were fluorescent, I proceeded to quantify their destruction over the course of meiosis I.

cRNA of the aforementioned N-terminally linked BioID2 constructs (Figure 5.1A) were injected into mouse oocytes and quantified over time. The BioID2-VFP control showed a clear linear increase in abundance over time suggesting that the enzyme itself is not targeted for destruction at any point and is continuously translated. In contrast cyclin B1 containing BioID2-fused proteins show clear differences in destruction dynamics, influenced by the presence or absence of the PM motif. However, substrate dynamics are being perturbed by the presence of the N-terminal BioID2 tag.

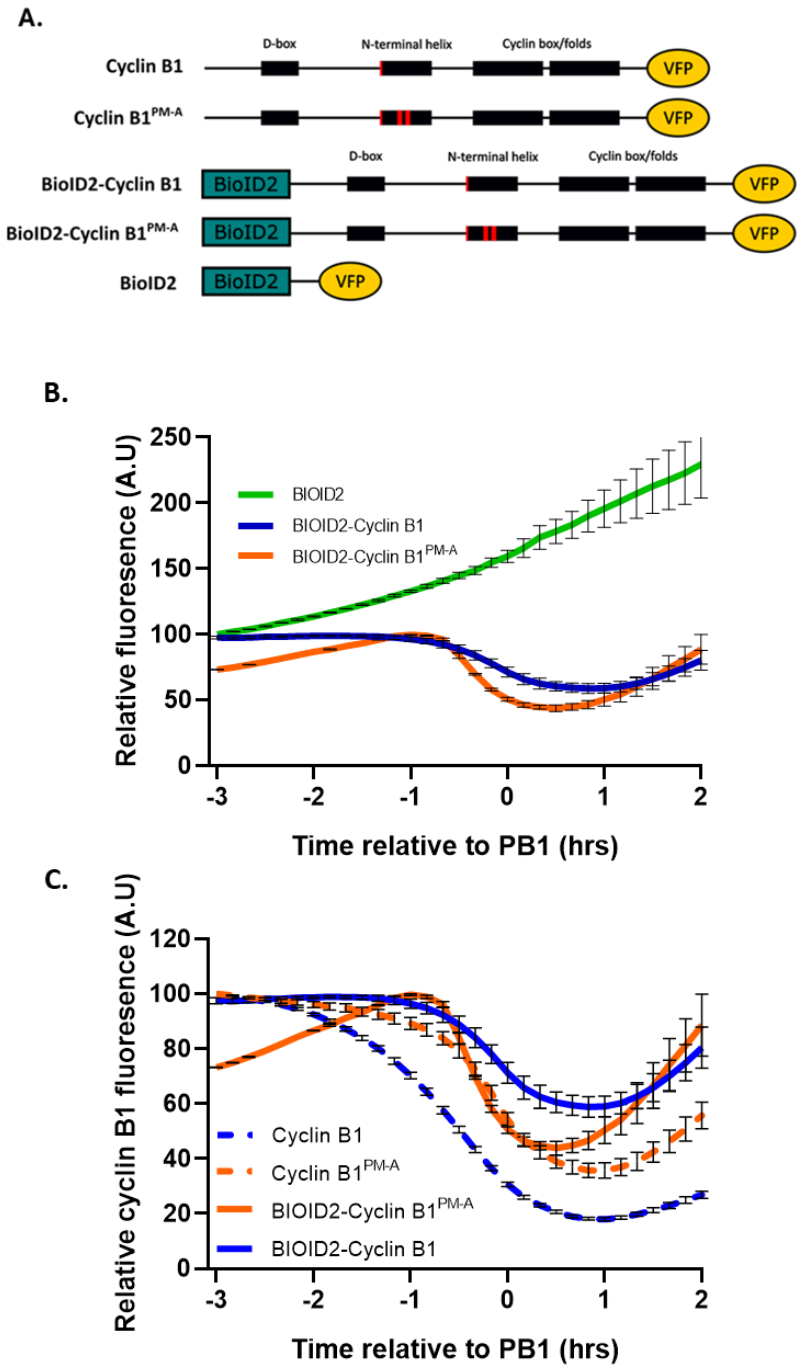

Figure 5.1. Destruction dynamics of BioID2 linked cyclin B1 constructs

A) Structure diagram describing the constructs used in these experiments. Cyclin B1 harbours a Y170a mutation and cyclin B1^{PM-A} harbours alanine substitution mutations in the PM-motif. BioID2 was linked N-terminal to cyclin B1 constructs or VFP. B) Average destruction profiles of BioID2 (green; n=3), BioID2-Cyclin B1 (orange, n=5), BioID2-Cyclin B1^{PM-A} (blue, n=3), relative to PB1 extrusion. C) Average destruction profiles of BioID2-Cyclin B1 (orange,

n=5), BioID2-Cyclin B1^{PM-A} (blue, n=3) alongside cyclin B1 (dashed blue, n=84), and cyclin B1^{PM-A} (dashed orange, n=28). Error bars ± SEM.

BioID2-cyclin B1 protein destruction initiates approximately 30-minutes ahead of PB1 extrusion (reaching a minimum abundance of 60% 1-hour post PB1 extrusion). The BioID2-cyclin B1^{PM-A} increases in abundance until approximately 30-minutes ahead of PB1 extrusion, then is targeted for destruction extraordinarily rapidly to reach a minimum of 44% around 30-minutes post PB1 extrusion.

Comparing the destruction of the BioID2 linked cyclin B1 reporters with non-BioID2 linked reporters reveal that both BioID2 linked reporters are targeted at the late timepoint most similar to cyclin B1^{PM-A}. Interestingly, in BioID2 proteins, the PM motif again seems to influence the rate of cyclin B1 accumulation and destruction, with more rapid kinetics. Removal of a PM motif has potentially generated a more efficient APC/C target. In contrast, the presence of a PM motif in the BioID2-Cyclin B1 construct seems to make it a less efficient target as the rate and extent of destruction is low. Importantly however, the periods of destruction are later regardless of the presence of a PM-motif and therefore N-terminally tagged BioID2 tagged cyclin B1 reporters are not suitable to address our aims.

As a next step I measured the destruction dynamics of a N-terminally linked TurboID cyclin B1 construct (Figure 5.2A).

Measuring the destruction of a fluorescent TurboID control construct indicates the possibility of a short and shallow period of destruction. This was unexpected, but limited to a period approximately 10-minutes before PB1 extrusion and only accounting for ~2% loss over the course of 20-minutes (Figure 5.2B).

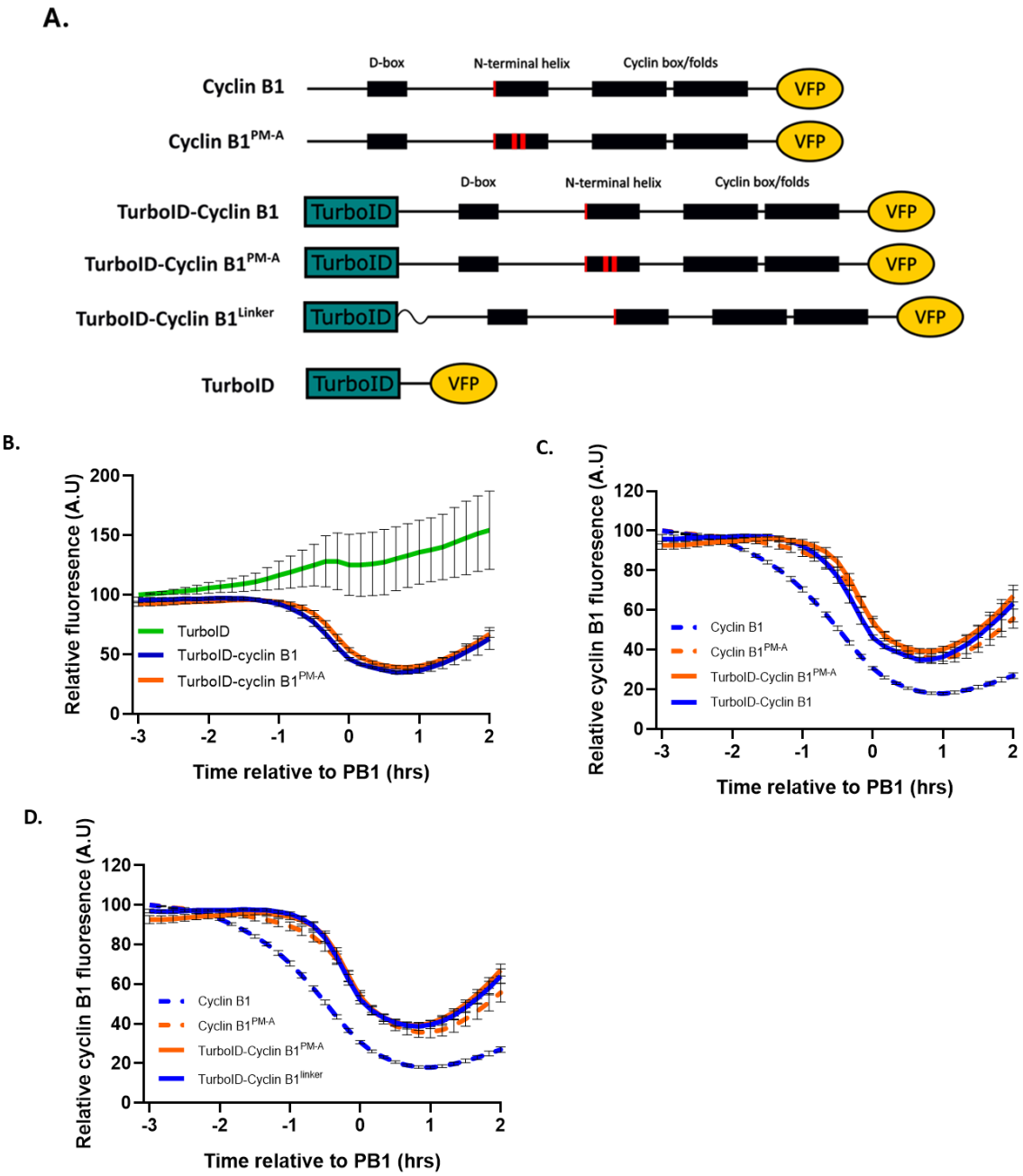

Figure 5.2. TurboID linked N-terminally to cyclin B1 reporters results in destruction at the late timepoint.

A) Structure diagram describing the constructs used in these experiments. Cyclin B1 harbours a Y170A mutation and cyclin B1^{PM-A} harbours alanine substitution mutations of the PM-motif. TurboID was linked to the N-terminus of cyclin B1 constructs or VFP. B) Mean destruction profiles of TurboID-VFP (green, n=4), TurboID-cyclin B1 (blue, n=6), TurboID-cyclin B1^{PM-A} (orange, n=30) relative to PB1 extrusion. C) The same average destruction profiles of

alongside cyclin B1 (dashed blue, n=84), cyclin B1^{PM-A} (dashed orange, n=28) relative to PB1 extrusion. D) Average destruction profiles of TurboID-cyclin B1^{Linker} (blue, n=20), TurboID-cyclin B1^{PM-A} (orange, n=30), cyclin B1 (dashed blue, n=84), cyclin B1^{PM-A} (dashed orange, n=28) relative to PB1 extrusion.

Unfortunately, similarly to the BioID2 experiments, the APC/C was not able to discriminate between N-terminally linked TurboID-Cyclin B1 constructs with and without a PM motif. Both were destroyed with nearly identical timings, targeted from ~40 minutes ahead of PB1 extrusion and to a minimum of 39%. When comparing these profiles to non TurboID-linked cyclin B1 reporters, the timing and extent of destruction is nearly identical to that of Cyclin B1^{PM-A}. The PM interaction driving earlier targeting is not able to operate in this context (Figure 5.2C).

Due to the result that adding either an N-terminal BioID2 or TurboID sequence to cyclin B1 delays the destruction of cyclin B1, I proposed that this tag causes clear steric hinderance of the PM motif interaction mechanism. To address this and persevere with this line of investigation I added a flexible 10 amino acid linker between TurboID and cyclin B1, hypothesizing that this would alleviate masking and reduce steric hinderance (Figure 5.2A).

The addition of a flexible linker between TurboID and cyclin B1 did not result in earlier destruction of cyclin B1, suggesting that either the PM-motif is still under a steric hinderance, or the addition of an enzyme itself makes it more difficult for the APC/C to target this form of cyclin B1 (Figure 5.2C). Indeed, if cyclin B1 is being targeted in prometaphase I by the APC/C-MCC, it could be expected that a significantly larger substrate would be more difficult to target. At this time point the APC/C is occupied by a large MCC subunit and thus it is plausible that there would be a restriction in the size of the substrate which could be targeted.

I decided to continue efforts to generate tools for this line of investigation with only TurboID. The extent of TurboID linked cyclin B1 destruction is closer to that of non-biotinylating

construct. In addition, BIOID2 experiments would likely require a longer biotinylation time, meaning that it would be less effective tagging transient interactions compared to TurboID. I next explored C-terminal tagging, predicting that greater distance from the N-terminal helix would reduce steric hinderance of PM-motif interactions (Figure 5.3A). The aim was that this construct would restore the prometaphase I destruction of cyclin B1.

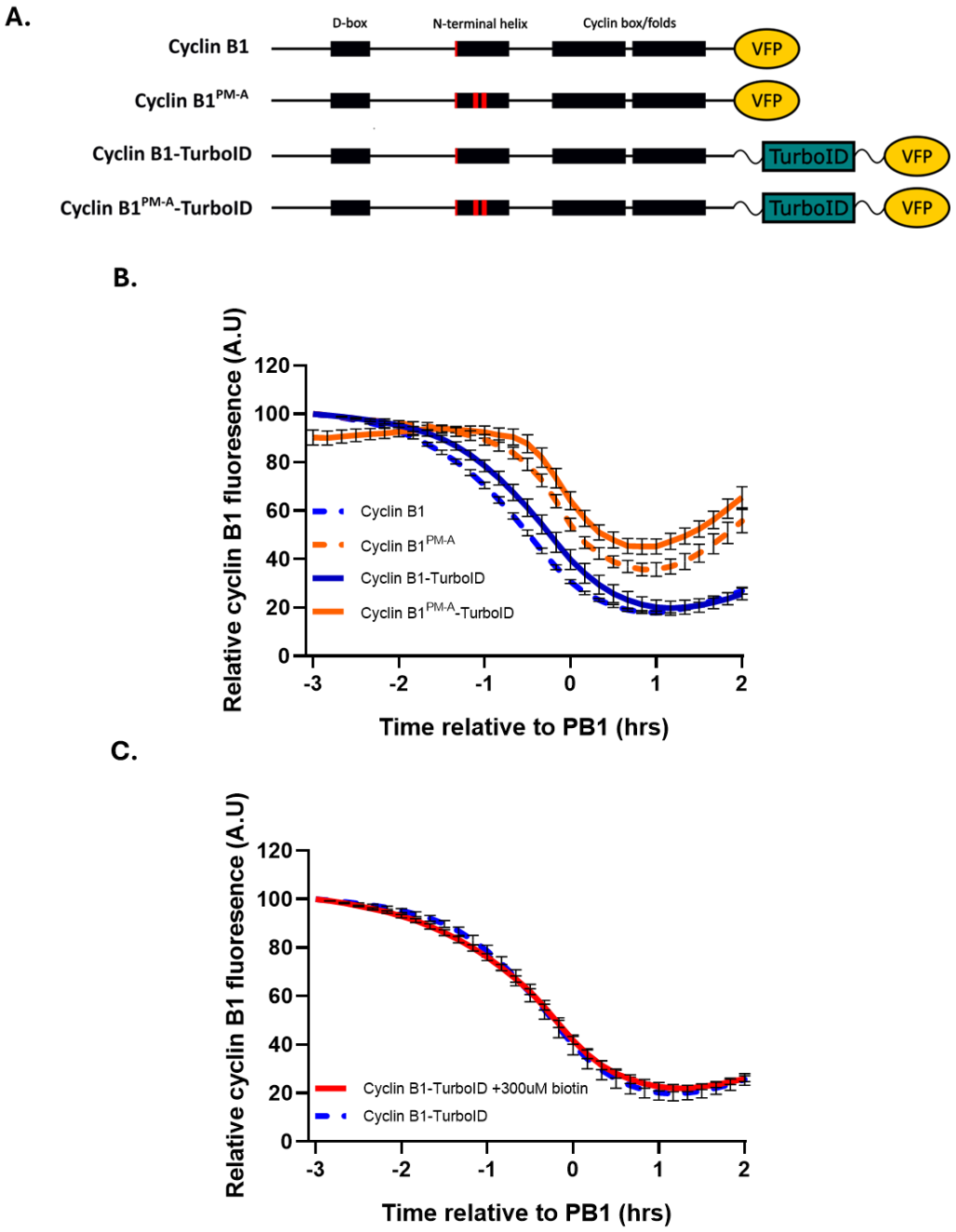

Figure 5.3 - TurboID linked C-terminally to cyclin B1 restores its prometaphase I destruction timing.

A) Structure diagram describing the constructs used in these experiments. B) Average destruction profiles of cyclin B1-TurboID (blue, n=15), cyclin B1PM-A-TurboID (orange, n=18) alongside cyclin B1 (dashed blue, n=84), cyclin B1PM-A-TurboID (dashed orange, n=28) relative to PB1 extrusion. C) Average destruction profile of cyclin B1-TurboID in 300 µM biotin

supplemented media (red, n=16) alongside the average destruction profiles of cyclin B1-TurboID (dashed blue, n=18) for reference. Error bars ± SEM.

Fortunately, the APC/C is able to discriminate between expressed cyclin B1 protein linked C-terminally to TurboID and that of a PM motif mutant. The Cyclin B1-TurboID protein is targeted for destruction at a timepoint similar to that of cyclin B1 (albeit slightly delayed). The cyclin B1-TurboID construct exceeds 10% destruction 20-minutes after the non-tagged construct. Additionally the rate and extent of destruction between cyclin B1-TurboID and cyclin B1 are similar. Importantly however, there is a clear difference between cyclin B1-TurboID and cyclin $B1^{PM\text{-}A}$-TurboID, whereby for latter destruction does not initiate until ~20 minutes ahead of PB1 extrusion, compared to 1 hour for cyclin $B1^{PM\text{-}A}$ (Figure 5.3B).

This result is promising and suggests that a C-terminally linked cyclin B1-TurboID construct can be used to identify the interactome of the PM motif of cyclin B1. Specifically, by comparing the interactome of cyclin B1 and cyclin $B1^{PM\text{-}A}$, given that the cyclin B1-TurboID construct is a target for destruction from late prometaphase I and the cyclin $B1^{PM\text{-}A}$-TurboID construct is targeted through the metaphase-anaphase transition.

In order to use these constructs effectively in a biotinylation assay, there are several additional points of validation. A first validation is to determine whether biotin supplementation of oocyte culture media will influence the destruction dynamics of cyclin B1-TurboID. It is plausible that a biotinylating enzyme, which will be actively ligating biotin to substrates, could limit PM motif interactions, or make it a less efficient target for the APC/C. To address this, I quantified the destruction of cyclin B1-TurboID in the presence of high biotin concentration (300 µM). Measuring the destruction of cyclin B1-TurboID with and without biotin supplementation indicates no change in destruction targeting (Figure 5.3). This shows that the oocyte retains original APC/C destruction dynamics in the presence of biotin, and an active TurboID enzyme does not impair destruction of cyclin B1.

Given that fluorescent cyclin B1±PM motif linked C-terminally to TurboID retained a clear difference in destruction dynamics, and that biotin supplementation had no impact on destruction, I next tested whether intracellular biotinylation was indeed taking place.

Populations of oocytes were injected to express cyclin B1±TurboID in non-biotin supplemented media or media supplemented with 100 µM biotin. Oocytes were fixed in late prometaphase I, and probed with a streptavidin fluorophore to determine the extent of global biotinylation in each population (Figure 5.4A).

Where both TurboID and biotin supplementation are present, there is a clear increase in intracellular biotinylation, suggesting that the TurboID sequence is directing biotinylation and biotin supplementation increases the extent of this intracellular biotinylation. Where either the TurboID sequence or media supplementation are absent, signal is substantially reduced. Interestingly the streptavidin fluorophore tends to accumulate in the centre of the oocyte at the liquid-like spindle domain (regardless of whether TurboID or biotin are present, Figure 5.4A). This could either be representative a high abundance of intracellular endogenous biotinylated proteins, or an effect of the probe binding non-specifically.

I quantified the VFP and streptavidin signals, which represents cyclin B1 and biotin abundance respectfully, and averaged the intensities between groups before normalising them to the control -TurboID -Biotin group (Figure 5.4B). Here we can see that when either biotin, TurboID or both are removed from the experiment, intracellular biotinylation signals are near identical. However, when 100 µM biotin is supplemented into the media there is a clear increase in intracellular biotinylation. Together this data suggests that the biotinylation ability of the cyclin B1-TurboID construct is present, and that biotin supplementation dramatically increases the activity of this enzyme.

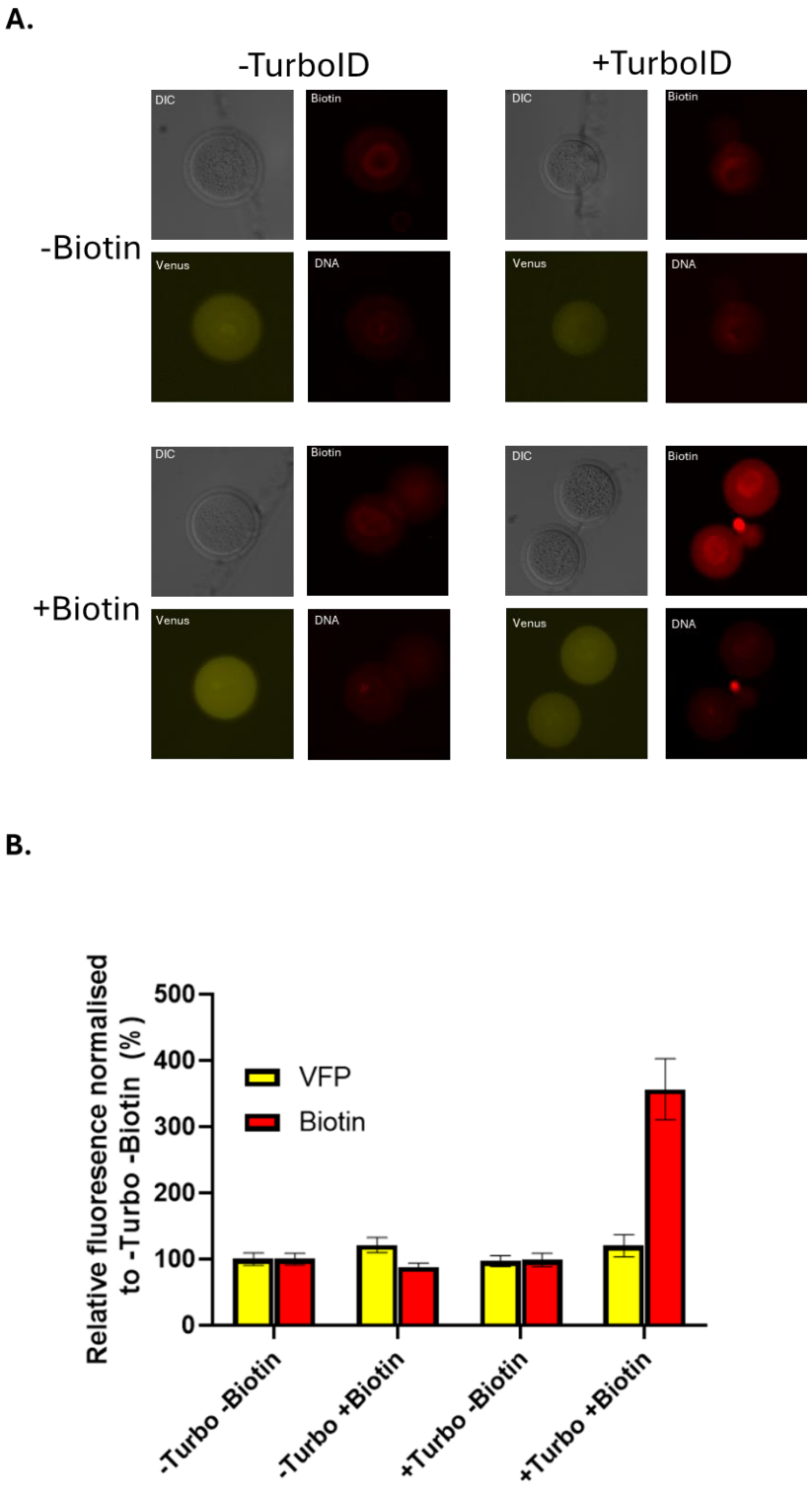

Figure 5.4. TurboID expression and biotin supplementation increases the extent of intracellular biotinylation in the oocyte

A)Fluorescence images of representative oocytes expressing cyclin B1±TurboID ±100 µM Biotin supplementation. Expressing oocytes were cultured for 4.5-hours post-GVBD before being fixed and stained with a streptavidin conjugated fluorophore. B) Average quantifications of fixed oocytes expressing cyclin B1-TurboID (VFP) and stained with a streptavidin fluorophore (biotin). -Turbo-Biotin (n=3); -Turbo+Biotin (n=4); +Turbo-Biotin(n=7); +Turbo+Biotin (n=5); Error bars ± SEM.

As a further step in protocol development I conduct a time course experiment with differing incubation times in media supplemented with 100 µM biotin (Figure 5.5). The results of these experiments are in agreement with the literature, TurboID takes approximately 15-minutes to begin biotinylating proteins and the extent of biotinylation increases with time up until 1-hour where biotinylation rates is stabilised[191]. This stabilisation could be a result of maximum biotinylation of cyclin B1 interaction partners. Ultimately this suggests that 1-hour biotin incubation would be sufficient for cyclin B1-TurboID to biotinylate the vast majority of interaction partners.

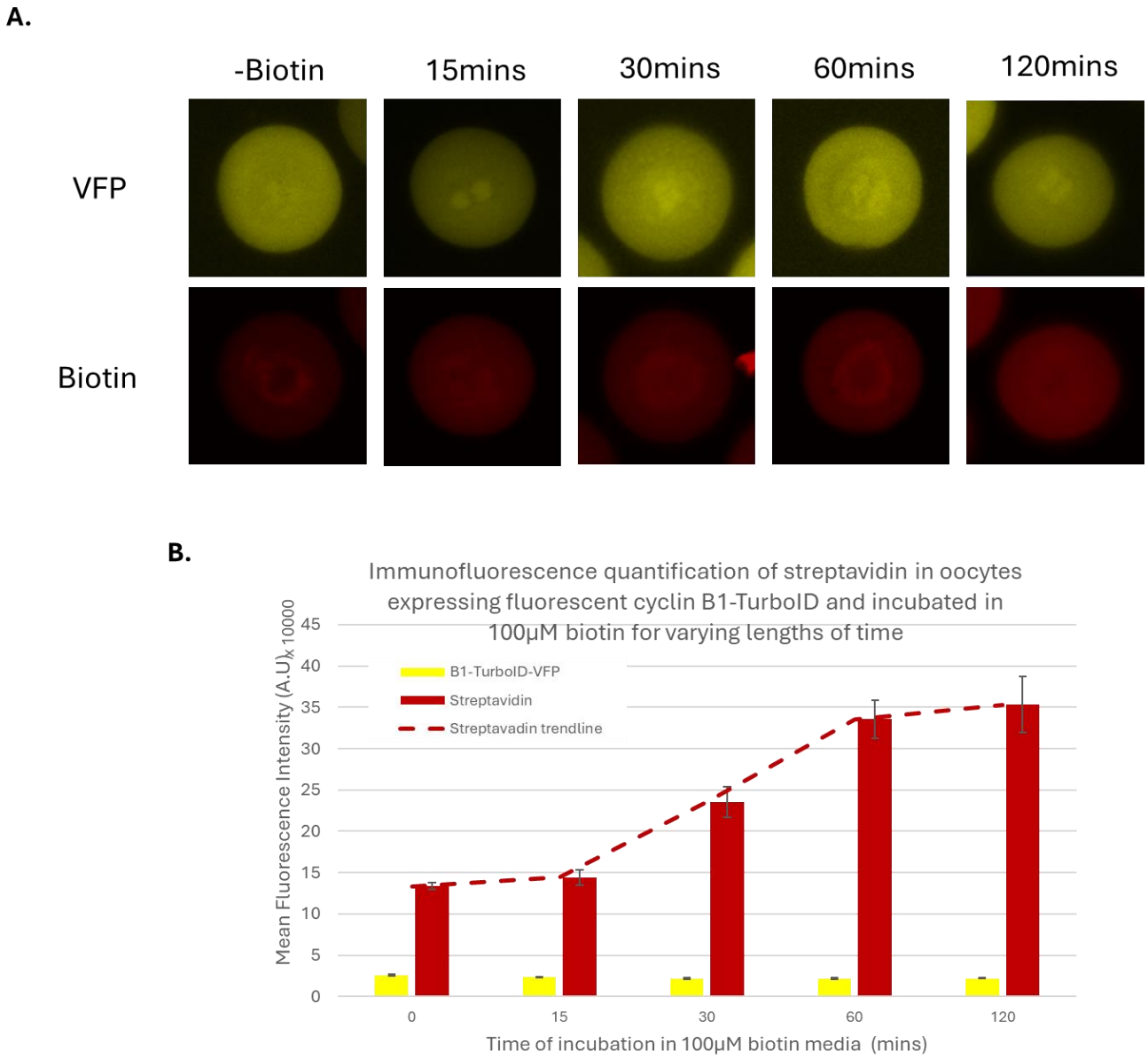

Figure 5.5. Intracellular biotinylation increases over time after expressing cyclin B1-TurboID and cultured in biotin supplemented media

A) Fluorescence images of representative oocytes expressing cyclin B1±TurboID ±100 µM Biotin supplementation for varying lengths of time. Expressing oocytes were cultured until 4.5-hours post-GVBD before being fixed and stained with a streptavidin conjugated fluorophore. Oocytes cultured in biotin containing media were moved into pools of biotin containing media at the indicated timepoints prior to fixation. B) Average quantifications of VFP and streptavidin in oocytes expressing cyclin B1-TurboID and incubated in biotin supplemented media for the indicated lengths of time before being fixed and stained with a streptavidin conjugated fluorophore.

Taken together, this data shows that Cyclin B1±PM-motif linked C-terminally to TurboID retained a difference in destruction timing, with cyclin B1-TurboID still being targeted in prometaphase I. Alongside this, the presence of TurboID and 1-hour of 100 µM biotin supplementation results in an increase in intracellular biotinylation in the oocyte.

Following these findings, I began to build up a stocks of oocyte lysates which were either uninjected, injected with cyclin B1-TurboID or injected with or cyclin $B1^{PM\text{-}A}$-TurboID. In each case oocytes were collected at 5.5-hours post GVBD following incubation in 100 µM biotin supplemented media for 1-hour. Timings were designed to capture a period of time where cyclin B1-TurboID destruction has initiated, but the cyclin $B1^{PM\text{-}A}$-TurboID substrate is stable. The aim is that the TurboID will biotinylate the cyclin B1 interactome, and that we can compare this with proteins proximal to cyclin $B1^{PM\text{-}A}$ (Figure 5.6).

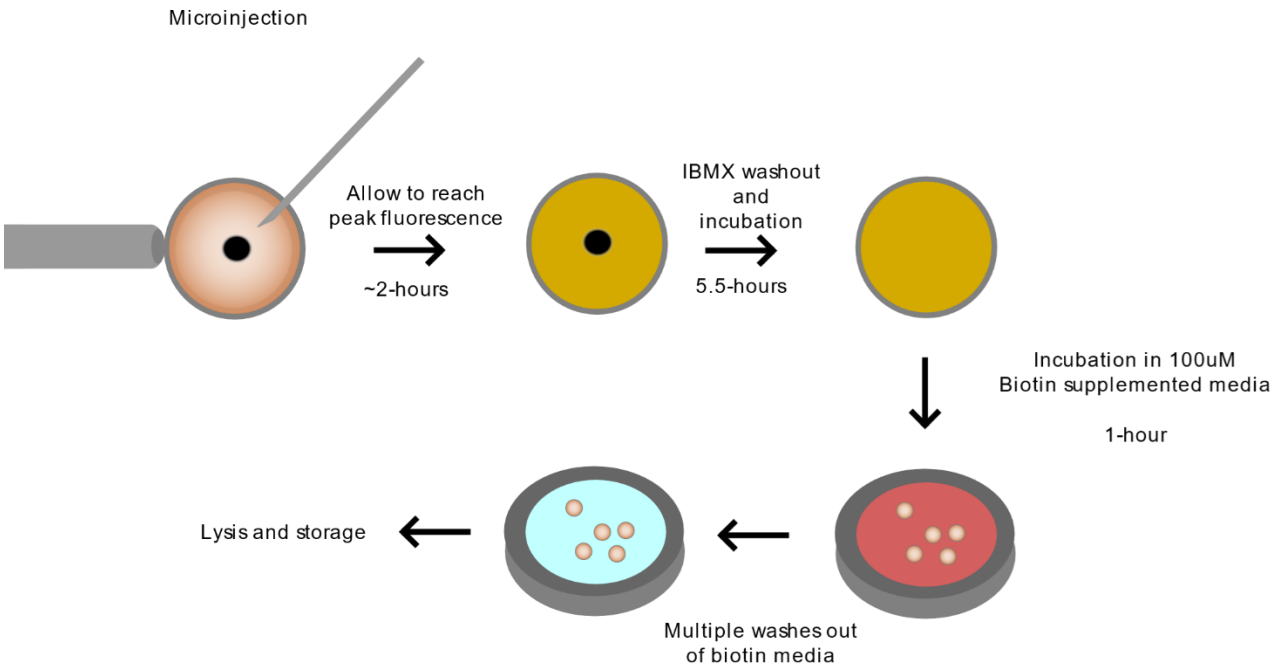

Figure 5.6. Experimental workflow of a biotin proximity ligation experiment in oocytes for subsequent pulldown and identification of interaction partners

Experimental workflow conducted to create a whole-cell oocyte lysate bank containing the lysates of oocytes expressing cyclin B1±PM motif-TurboID (or uninjected controls) incubated in biotin supplemented media at the timepoint in which cyclin B1 constructs are targeted for destruction.

As an additional control, prior to lysis, samples from each batch of oocytes were imaged to confirm expression, and destruction initiation of the cyclin B1-TurboID during biotin incubations. Oocytes were then extensively washed out of biotin containing media with additional washes in PBS prior to lysis. Oocytes were snap-frozen in liquid nitrogen for future use. I have accumulated lysates of 300 oocytes for each group (900 oocytes total) with the aim of performing a pull-down of biotinylated proteins using streptavidin beads. This will be a 3-replicate experiment, 100 oocytes per treatment per replicate. Proteins eluted from beads will be identified by mass spectrometry.

There have been several disappointing frustrations with the company we have been corresponding with over many months to analyse these samples. These are incredibly precious samples and I have not yet been confident to commit them to a protocol. However, we do now believe we have a solution and are in contact with another proteomics facility.

5.3 Discussion

Determining the interaction partners of cyclin B1 that permit PM motif dependent prometaphase I destruction is key in determining the mechanism of destruction. Unfortunately, substantial challenges limit options for protein-protein interaction experiments in oocytes. Predominantly, the number of cells that can be collected, practically and ethically. Traditional experiments such as immunoprecipitations are in conflict with principals of the 3Rs (Replacement, Reduction, Refinement), a framework which aims at performing more humane animal research by looking for alternatives to using animal models, or by reducing the number of animals used in research[193]. Therefore, I decided to explore alternatives to those methodologies that require up to milligrams of protein per treatment group per replicate.

In this chapter I tested the feasibility of performing a biotin proximity ligation assay in oocytes with the aim of revealing the interactome of cyclin B1. By determining interaction partners of both cyclin B1 and cyclin $B1^{PM-A}$, I could identify any differences between protein data sets. Specifically, proteins that interact with cyclin B1 with a PM motif but are absent or reduced where the PM motif is absent and can be predicted to contribute to the destruction of cyclin B1 in prometaphase I. This would be a substantial leap forward in in understanding the destruction of cyclin B1, and potentially determine whether cyclin B1 is targeted by the APC/C-MCC in prometaphase I or by a subpopulation of non-MCC bound APC/C.

The ability to perform a biotin proximity ligation experiment in this system would rely on the ability of the enzyme linked fluorescent cyclin B1±PM motif constructs to retain their differences in destruction timing, and for the enzyme linked cyclin B1 construct to be targeted in prometaphase I. I explored two different biotinylation enzymes, BioID2 and

TurboID. Even though TurboID would be the preferred biotinylation enzyme due to its short ligation time (~15-minutes), I deemed that it would be useful to increase options if BioID2 is also suitable.

Through 2 rounds of experimentation my data suggests that N-terminal BioID2-tagged cyclin B1 is not a suitable tool. Both cyclin B1 and cyclin $B1^{PM-A}$ BIOID2-tagged proteins were targeted for destruction from the late timepoint only, close to the metaphase-anaphase transition. In addition, BioID2-cyclin B1 destruction was incomplete, suggesting that the presence of BioID2 both prevents prometaphase I destruction of cyclin B1 and a poor APC/C substrate in metaphase. Interestingly when the PM motif is mutated in the BioID2-cyclin $B1^{PM-A}$ construct, destruction is more extensive (Figure 5.1). Together this suggests that the BioID2 enzyme causes a steric hinderance to the PM motif. It is possible that when the PM-motif is present, BioID2 is positioned in such a way that makes it more difficult to targeted by the APC/C.

Cyclin B1 constructs linked N-terminally to TurboID were also unsuitable for proximity ligation assay to determine the interactome of cyclin B1. Again, both proteins were targeted for destruction later in the cell cycle, more akin to cyclin $B1^{PM-A}$. However, unlike the BioID2 linked proteins, TurboID linked protein were diminished to the expected extent by anaphase. This is interesting, data suggests that N-terminally linking proteins to cyclin B1 prevents prometaphase I destruction, (possibly due PM motif obstruction), but additionally, different proteins linked N-terminally have different impacts on a separate aspect of destruction dynamics – the depth of destruction. This could potentially be due to the different sizes of these proteins. BioID2 is 26.6 kDa compared to TurboID at 35 kDA[194,195].

Fortunately, C-terminally linking TurboID to cyclin B1 restored prometaphase I destruction capabilities, and the extent of destruction was nearly identical to that of the non-TurboID linked counterparts. While this construct was targeted for destruction slightly later than the non-TurboID linked, this timepoint is still be before chromosome congression, and a time difference between cyclin B1-TurboID and cyclin $B1^{PM-A}$-TurboID remains. Importantly,

incubating oocytes expressing cyclin B1-TurboID with high concentrations of biotin, did not prevent its prometaphase I destruction (Figure 5.3). Oocytes in these experiments extruded polar bodies at the expected timepoint, suggesting they are healthy in biotin supplemented media.

Immunofluorescence shows that the addition of TurboID to cyclin B1 and a 100 µM biotin supplement causes an increase in intracellular biotinylated proteins (Figure 5.4). This was an important experiment, it was essential to determine that TurboID is active in oocytes to biotinylate proteins in proximity to cyclin B1. This was also a good indication that TurboID in oocytes significantly benefits from biotin supplementation. Endogenous biotin was insufficient to provide strong signal. The biotin supplementation is also likely a benefit to the oocyte as TurboID in this system would quickly deplete the oocyte of endogenous biotin. Indeed, Tsuji et al. have shown that severe biotin deficiency inhibits normal meiosis function causing improper chromosome condensation[196]. One important control for this experiment is that the amount of cyclin B1-TurboID expressed in oocytes is similar across all oocytes. This is technically very challenging to achieve, microinjecting an identical amount of cRNA into individual oocytes is difficult, and even then oocytes have their own inherent differences in translation and protein folding rates. To achieve consistency in data, oocytes overexpressing or under expressing cyclin B1 were removed from populations lysed for data collection.

A clear positive correlation exists between the extent of intracellular biotinylation and the length of time incubating in biotin supplemented media. I determined that 1-hour of 100 µM biotin supplementation to be optimal for oocytes expressing cyclin B1±PM-A-TurboID (Figure 5.5). My result suggests that this length and concentration of biotin will likely provide the greatest number of potential interacting proteins in pulled-down experiments but also with a large amount of non-specific biotinylation and noise. However, I reasoned that since these experiments are being carried out in oocytes, and cell number is the most substantial limiting factor, that it is best to err on the side of caution. A greater amount of biotinylated protein would provide the best chance of deducing the interactome of these cyclin B1 constructs. Here I would benefit from extensive literature in mitosis advising how to distinguish between

noise and non-specific biotinylations. Importantly, if this technique was unable to allow us to determine any difference in interaction partners between the two forms of cyclin B1, this would also be significantly informative in regards interactome of all cyclin B1 in mouse oocytes. Additionally, the success of this method in this context would still be a great achievement and proof of experimental principle.

After confirming the ability of TurboID to biotinylate substrates in the presence of biotin supplemented media, I began the process of accumulating oocyte lysates for a future mass spectroscopy experiment (Figure 5.6). Whole cell lysate aliquots containing 300 uninjected controls, 300 cyclin B1-TurboID expressing oocytes and 300 cyclin $B1^{PM\text{-}A}$-TurboID expressing oocytes are currently stored at -80°C. Alongside this I also banked 100 uninjected control oocytes and 100 cyclin B1-TurboID oocytes for use in preliminary testing of the protocol and to verify the mass-spectrometry facility that we intend to use has the capacity to process these samples.

This experiment was incredibly technically difficult and time consuming. Oocytes for lysates were microinjected, released, treated and lysed over the course of one day, with many sessions required to build up the number of lysed oocytes. Potentially, I could have microinjected oocytes and kept them in prophase I arrest overnight for release, treatment and lysis the following day. It would have been significantly easier to perform the experiment in this way. However I deemed it important to have the oocytes as healthy as possible for these lysates. My experience suggests that extended periods of *ex-vivo* oocyte culture (from BubR1 MO investigations) decreases the quality of oocytes and reduces rates of PB1 extrusion. This is less problematic in experiments where meiosis I is monitored throughout, oocytes which do not undergo PB1 extrusion can be excluded in the resulting dataset and we have a measure of oocyte health. However, in this experiment, oocytes are lysed before PB1 extrusion occurs, and thus unhealthy oocytes are less distinguishable from healthy oocytes. Conducting this experiment in one day reduces this impact and increases the reliability of data. To mitigate further, only oocytes achieving a very strict grade of visual quality were used in these experiments.

To complement these experiments, I have purchased recombinant proteins of His-tagged N90-NTH±PM-motif for follow-up pulldown experiments with both mitotic and/or meiotic cell lysates. By His-tagged N90-NTH±PM motif validation experiments I have revealed that the destruction dynamics of these proteins are not perturbed by His-tagging (data not shown). This will provide further verification of any interaction partners identified by mass-spectrometry following completion of biotin proximity ligation assays, as well as observing any similarities in mitotic cells.

We had identified a facility to perform mass-spectrometry on the oocyte lysates banked in this line of experimentation however we ultimately lost confidence in the ability of this facility to handle these precious samples and therefore could not commit. As a risk mitigation measure, we sent multiple samples of uninjected oocyte lysates to gauge the accuracy of the mass-spectrometry equipment at this facility. These samples however were either not processed correctly by them or lost. Since beginning these investigations Newcastle University Protein and Proteome Analysis (NUPPA) facility has obtained highly advanced new instrumentation which we are confident will be better suited to our needs.

Chapter 6 - Processivity of destruction boxes in meiosis I oocytes

6.1 Introduction

The Destruction Box (D-box) motif was the first to be discovered by Glotzer et al. in 1991 who used sea urchin extracts to determine that cyclin proteins are degraded by the ubiquitin proteasome pathway[95]. Since this finding, D-boxes have been identified in the vast majority of APC/C substrates. Defined by a nine-residue linear sequence of amino acids, the consensus sequence of a D-box is RxxLx[D/E][Ø]xN[N/S] where x represents any amino acid and Ø refers to leucine, isoleucine or valine[105]. The D-box is of upmost importance for targeting by the APC/C, just the presence of this sequence alone, alongside adequately spaces lysine residues, is enough for APC/C interaction. Indeed Tian et al. showed that a 24 residue peptide of cyclin B1s D-box sequence was enough to bind to the APC/C with sufficient potency to prevent the ubiquitination of other substrates *in-vitro*[101]. The D-box is incredibly important in the destruction of APC/C targets. Countless papers have shown that complete removal of this motif, or even the mutation of the conserved residues in positions 1, 4 and 9 are enough to prevent substrate destruction in most cases[95,104]. This is also a transposable signal, capable of transforming a non-APC/C substrate into an APC/C substrate[197,198].

Since the discovery of the D-box, many other motifs have been identified that influence the efficiency and temporal regulation of substrate ubiquitination. The KEN box is another SLiM which fits the definition of a degron as it confers destruction capabilities of substrates which lack a D-box such as Cdc20[104,109]. Defined by the consensus sequence [DNE]KENxxP, the KEN box is often found in substrates also containing a D-box. However the two can also be found mutually exclusive and sometimes in multiple copies[105]. The ABBA motif is a SLiM not considered to be a degron as it is not essential for degradation but does influence temporal regulation of substrate targeting as discussed throughout this thesis. Thus far recognition sites for the ABBA motif have been identified in human Cdc20 and S. cerevisiae Cdh1. Yet interestingly human Cdh1 lacks the conserved residues required for ABBA motif binding[102].

The mechanism of action of the APC/C involves introducing a substrate into close proximity with E2 ubiquitin ligases to prime polyubiquitination. The initiation of ubiquitin chain formation begins with monoubiquitination by UbcH10 brought about by a change in coactivator conformation, induced by D-box binding[130,199]. This conformational change involves the catalytic module, composed of APC11 and APC2 shifting to form a UbcH10 binding site. Binding of the UbcH10 E2 ubiquitin ligase primes the complex for ubiquitination of substrate lysine residues[122]. Binding of a second E2 ubiquitin ligase called Ube2S allows for the extension of this monoubiquitination on Lys11 producing K11 and K48 ubiquitin chains. Dissociation of the now ubiquitin-linked substrate allows for its destruction via the proteasome[131,200].

Recent cryo-EM structural data has provided the field with unprecedented insight into the structure of the APC/C complex in different contexts, importantly displaying how substrate motifs interact with coactivators[20,114,122,152]. Cdh1 and Cdc20 share significant structural similarity through conservation, consisting of seven WD40 β-propellor domains which provide the motif recognition capabilities[101]. The highly conserved D-box residues in positions 1 and 4 bind acidic and hydrophobic pockets respectively between blades 1 and 7 of the coactivator. Hydrophilic residues in the C-terminus of the motif, specifically in positions 8 to 10, interact with APC10 on a highly conserved hydrophilic surface which gives the D-box a description of being “bi-partite” thought to be composed of two distinct parts (Figure 6.1). This hydrophilic surface on APC10 is composed of the 80s and 140s loops which are positioned facing the APC/C coactivator[114,201,202]. Various mutagenesis experiments in which key residues on these loops are mutated to alanine, impairs D-box-dependent substrate recognition. The 80s loop, specifically the side chain of Glu87, has also been shown to be positioned to more N-terminal D-box residues between P2, 5 and 7, which Alfieri et al suggests could explain the propensity for basic amino acids at these positions.[105]

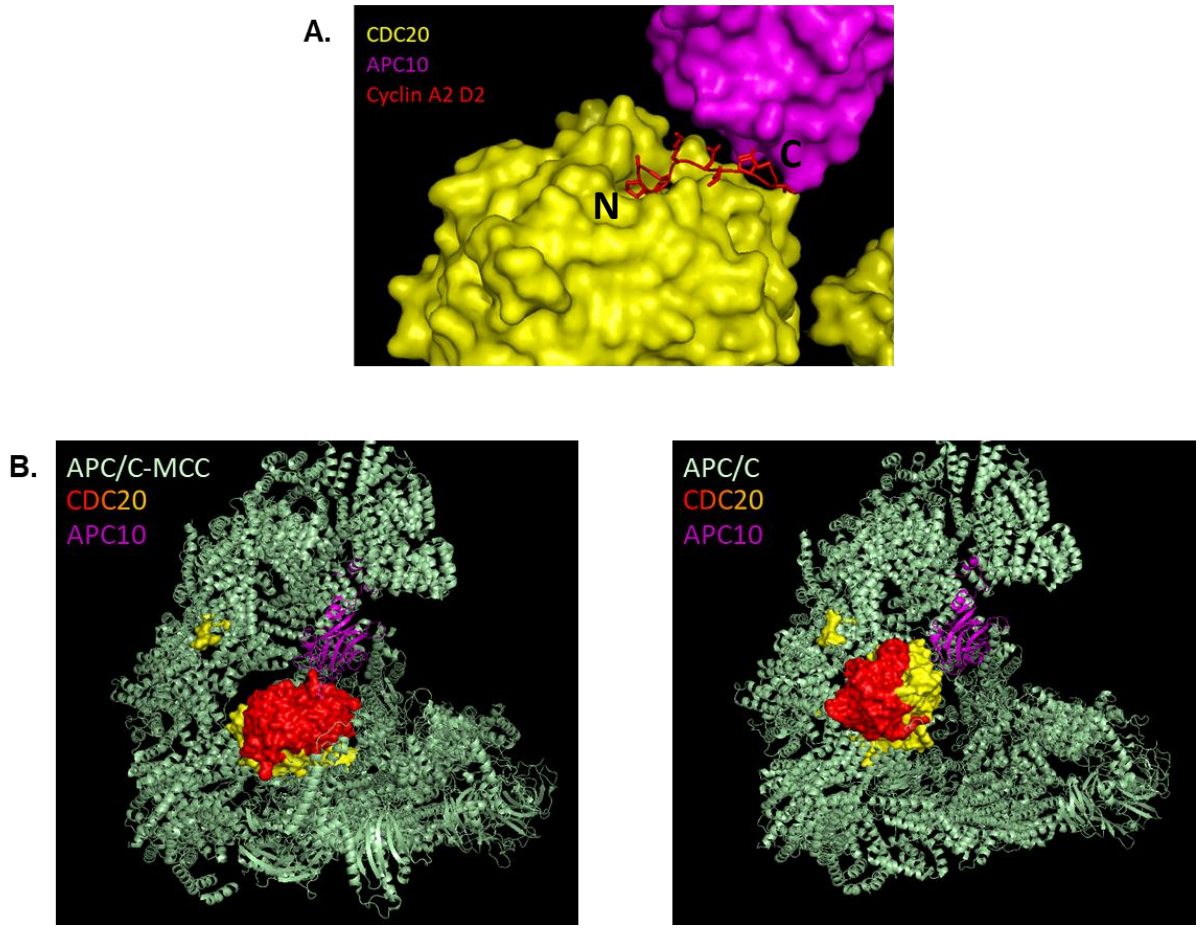

Figure 6.1. Binding of a D-box to the bipartite D-box receptor and the change of positioning of APC/C coactivator Cdc20 upon MCC binding.

(A) Cryo-EM structure of the Cyclin A2 D2-box motif associating with $Cdc20^{APC/C}$ solved by David Barford's group (PDB:6Q6H[20]). This structure was adapted to isolate bipartite D-box receptor composed of Cdc20 (yellow, surface) and APC10 (magenta, surface) bound to Cyclin A2 D2-box substrate (red, cartoon with N- and C-termini indicated by 'N' and 'C' respectfully). (B) Cryo-EM structures of the APC/C without (left, PDB:5G04[115]) and with (right, PDB:6TLJ[116]) the MCC present. The bipartite D-box receptor components APC10 (magenta, cartoon) and Cdc20 (red and yellow, surface) are highlighted. Cdc20 residues between A248 to F420 were coloured red and the remaining residues coloured yellow using PyMOL to better visualise the rotation and movement in 3D space of Cdc20, especially the D-box binding region of Cdc20 relative to APC10 upon MCC binding.

While APC10 binding appears to be common in substrates harbouring a D-box, it seems to not be required in all instances such as when the MCC is incorporated into the complex. This is most clearly observed in cryo-EM images published by the Barford group[152]. Binding of the MCC complex to the APC/C induces a 90° rotation and ~40° tilt of the existing Cdc20 molecule (now referred to as the $Cdc20^{APC/C}$) which positions the D-box binding pocket away from APC10. Subsequently disrupting the formation of the bipartite D-box receptor (Figure 6.1B). While the bipartite D-box receptor is disrupted, Cyclin A2-CDK2-CKS2 is still able to be targeted for destruction in prometaphase in a D-box dependent mechanism (Figure 1.12). The Barford group showed that mutation of the hydrophobic residues in the $Cdc20^{MCC}$ D-box binding pocket significantly reduced ubiquitination of cyclin A2 *in-vitro*, indicating that the D2-box of cyclin A2 binds to the D-box binding site of $Cdc20^{MCC}$ [20]. This site is very distant to APC10 in terms of positioning. This would strongly suggest that APC10 binding is not required for D-box mediated substrate destruction by the APC/C for all substrates. Important to note is that experimentation performing mutations to binding sites on either $Cdc20^{MCC}$ or $Cdc20^{APC/C}$ is only feasible using recombinant proteins *in-vitro,* whereby mutant Cdc20s can be incorporated into either APC/C or MCC separately, then combined. The destruction of cyclin A2 by APC/C-MCC requires the binding of KEN and/or ABBA motifs, which may also play a role in anchoring the D-box into this site. Deletion of either KEN or ABBA results in a less extensive ubiquitination by the APC/C^{MCC} and removal of both prevents it entirely[20]. Therefore, the D-box recognition sites of coactivators are functional irrespective of positioning relative to APC10 in certain configurations however, the exact requirements of this is unclear and literature lacks other substrate examples.

Given that the timing of free cyclin B1 destruction occurs in late prometaphase I (previous chapters), while the spindle assembly checkpoint is still signalling, it could be assumed that over this period, the APC/C responsible for the ubiquitination of free cyclin B1 is the APC/C-MCC. Findings in this thesis may indicate that non-MCC bound APC/C could be responsible for prometaphase I targeting of cyclin B1 however more thorough experimentation is required. Significant literature has shown that APC/C-MCC can target various substrates (such as Cyclin A2 as described earlier), but that APC/C-MCC substrates critically require the

presence of additional motifs to facilitate destruction by this mode of APC/C. To date, no ABBA motif has been found in cyclin B1 meaning that destruction via the APC/C^{MCC} cannot be explained. It could be that the PM motif, which facilitates prometaphase I destruction of free cyclin B1, acts as a de facto ABBA motif, however the amino acid sequence of the PM motif does not fit the consensus sequence of known ABBA motifs and ABBA motifs are not known to be helical. Alternatively, another site in cyclin B1 could act as an ABBA motif, however *in-silico* tools designed to detect instances of ABBA motifs, such as the "APC/C degron prediction tool" developed by the Davey and Morgan labs do not identify any in cyclin B1.

Collin et al. published the finding that the SAC is not an 'all or nothing' signal; in fact it acts as a rheostat with the signal diminishing as chromosomes begin to align[27]. Indeed, by nature, the APC/C^{MCC} is in a constant state of assembly and disassembly which allows for the efficient signalling of the spindle assembly checkpoint and its rapid shut down. This suggests that at any one time after the initiation of chromosome alignment, the APC/C exists in a mixed population in the cell – either bound to or not bound to the MCC. This could therefore also suggest that free cyclin B1 might be being targeted by a prometaphase sub-population of non-MCC bound APC/C.

Based on this hypothesis that in late prometaphase I it is likely that two populations of APC/C exist, on account of the diminishing SAC signal due to an amount of chromosome alignment, I asked the question how we can distinguish which form of the APC/C is responsible for free cyclin B1 destruction. This would be an important finding in the context of how the PM motif of cyclin B1 facilitates prometaphase I destruction, specifically whether the APC/C or APC/C-MCC is responsible for PM motif mediated cyclin B1 destruction.

I took two approaches to explore this. First, I aimed to determine whether the prometaphase I destruction of cyclin B1 in mouse oocytes could still be achieved after knockdown of APC10. This ideally would give an insight to whether the formation of the bipartite D-box receptor between Cdc20 and APC10 is required for the targeting of cyclin B1, or whether cyclin B1 at this time point accesses the D-box receptor independently of APC10 as appears to be the

case for prometaphase I targeting of cyclin A2. Second, I explored the substrates themselves and mutated the C-terminal hydrophilic residues of their D-boxes (referred to as the "extended D-box"), known to interact with APC10 as described earlier. This now tests more directly if the destruction of these substrates can still occur without any APC10 binding. An outcome here indicates whether a substrate can engage a D-box binding site irrespective of APC10, and specifically in the case of cyclin B1, address whether the PM motif can engage a D-box binding site located away from APC10, as would be the case if targeted APC/C-MCC.

6.2 Results

6.2.1 Extensive APC10 depletion using morpholino in oocytes requires a minimum of 48-hours incubation and results in Prophase I arrest

To determine whether the MCC is present in the population of APC/C targeting cyclin B1 in prometaphase I, I decided that the APC/C subunit APC10 would be a viable subject for investigation. APC10 is located in catalytic subcomplex of the APC/C and forms a bipartite D-box receptor alongside a coactivator (Cdh1 in prophase and early prometaphase, and Cdc20 in late prometaphase/anaphase). When the MCC is not associated with the APC/C, the coactivator is positioned in a way in which its D-box recognising WD40 domain faces an interaction site of APC10, forming the bipartite D-box receptor which is required for substrate D-box binding in this mode. MCC binding to the APC/C induces a positional change of $Cdc20^{APC/C}$ which positions the D-box recognition residues away from APC10, disrupting the formation of the bipartite D-box receptor. It is important to note that the D-box recognition sites of coactivators are functional irrespective of APC10 positioning (Figure 6.1)[137]. For instance, the prometaphase destruction of cyclin A2-CDK2-CKS2 by the APC/C^{MCC} is mediated by binding of the D2 motif onto the D-box recognition site of $Cdc20^{MCC}$, requiring the binding of non-canonical motifs on both $Cdc20^{APC/C}$ and $Cdc20^{MCC}$ [20]. Therefore, if a substrate was able to be destroyed by the APC/C^{MCC}, such as cyclin A2, in theory binding to the bipartite D-box receptor would not be necessary. However, if a substrate can only be targeted by the APC/C once the MCC has dissociated, bipartite D-box receptor binding would

be required. I therefore decided to target the bipartite D-box receptor to determine whether it is used to target free cyclin B1.

To test this, a pool of oocytes was injected with an APC10 MO antisense oligomer at a needle concentration of 1 mM to knock down APC10 gene expression. The reverse complement of the APC10 MO sequence submitted to BLASTn, a nucleotide sequence database to confirm no off-target knockdowns would occur. Oocytes knocked down for APC10 were also injected with cRNA encoding fluorescent reporters cyclin B1 ± PM motif and imaged over time. Morpholinos work by specific complementary binding to endogenous mRNA to prevent translation. This, together with the natural turnover of a protein reduces the intracellular levels of the target protein. This means that knockdown extent via morpholino is dependent on incubation time.

Initial experiments suggested an APC10 knockdown phenotype whereby oocyte release from prophase I arrest upon IBMX washout is perturbed. I quantified the number of oocytes arrested in prophase I subjected varying lengths of APC10 knockdown. At 24-hours 87% of oocytes knocked down for APC10 were able to undergo GVBD after two hours compared to 100% of uninjected controls (13% failure). But by 48 hours of APC10 morpholino incubation, I found that 20% of oocytes underwent GVBD compared to 50% of controls (50% failure) (Figure 6.2A). This suggests that incubating oocytes *ex-vivo* for an extended period of time decreases the propensity to release from prophase I arrest, and similarly a decreasing level of intracellular APC10 also results in an inability to release from prophase I arrest after 2-hours. In oocytes with a more extensive knockdown such as a 42-hour incubation time period, those oocytes that were able to undergo GVBD, present with a dynamic 'blebbing' appearance across the entire cell circumference. Blebbing begins anywhere from 4-11-hours post GVBD and lasts approximately 3 hours (Figure 6.2B). Curiously this period would be where we would expect an oocyte to be preparing to extrude a first polar body. However no clear polar body forms in the majority of these oocytes. This phenotype is often observed where the structure of the spindle is severly perturbed or where anaphase is attempted but the spindle has failed to migrate. In these situations the cortext of the oocyte still softens in

preparation for extrusion however is unable to complete. I strongly suggest that this is the case in this context.

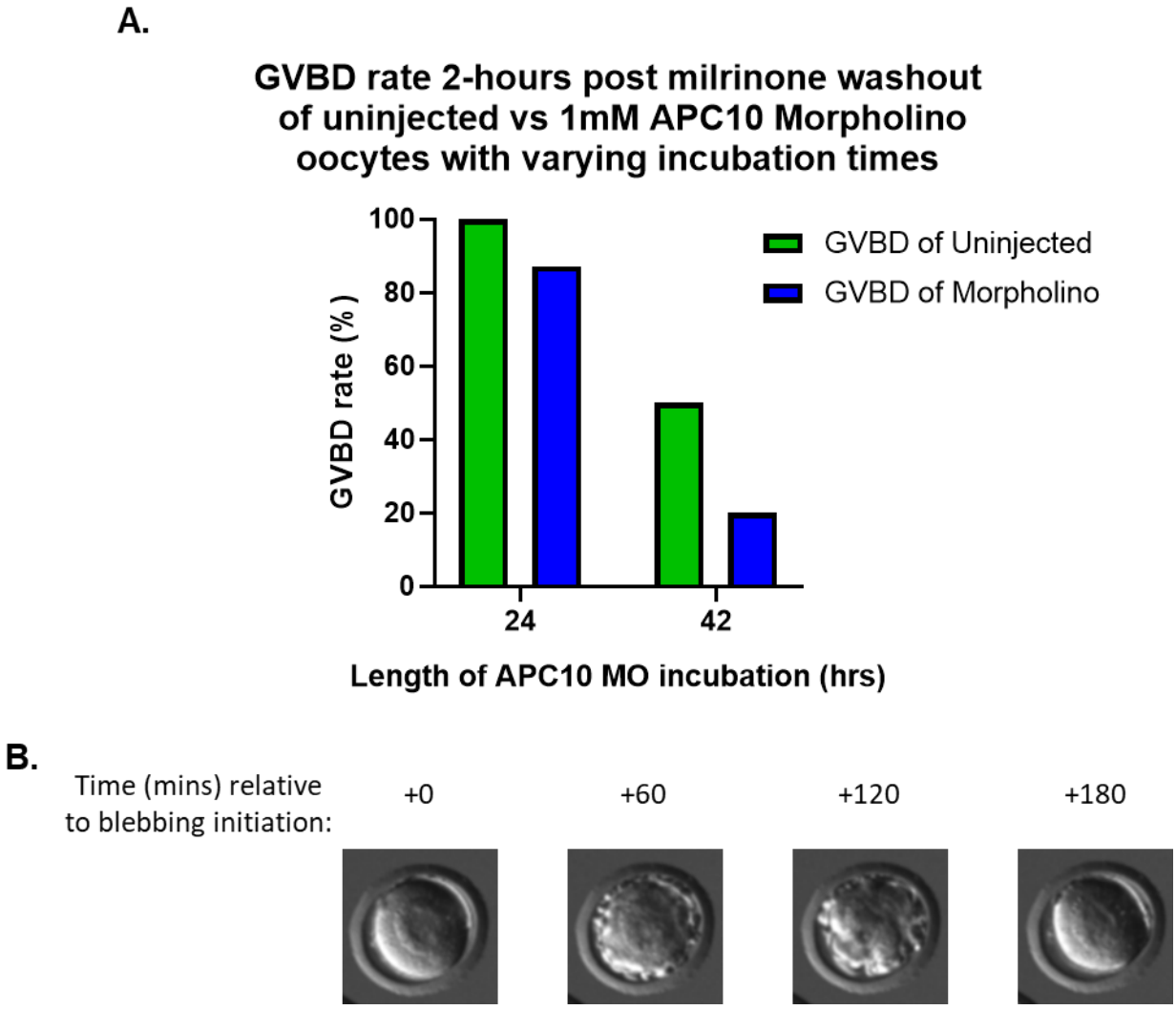

Figure 6.2. Phenotypes associated with APC10 knockdown via morpholino oligomer.

A)Graph showing the GVBD rate in oocytes injected with APC10 morpholino oligomer at a needle concentration of 1mM or uninjected and incubated for 24-hours (Uninjected n=14; MO n=31) and 42-hours (Uninjected n=6; MO n=10). (B) Images taken in DIC of oocytes every hour undergoing a 'blebbing' process at the time at which they would be expected to undergo PB1.

These data suggests that oocytes with more extensive APC10 knockdowns, are not useful to explore cyclin B1 destruction. They are unable to progress through meiosis I, perhaps given that they lack a functional bipartite D-box receptor. Indeed, this is a strong phenotype of APC10 knockdown however but without GVBD and meiotic resumption, destruction of cyclin B1 constructs cannot be determined. Shorter morpholino incubation times would result in a less extensive APC10 knockdown, however would yield more data due to the higher GVBD rate and give an indication as to the effect of reduced bipartite D-box receptor sites on the effects of cyclin B1 destruction.

Curiously, on measuring the destruction of cyclin B1 reporters (±PM-motif) after a 24-hour APC10 MO incubation, the difference in the destruction targeting timing between the two reporters was no longer apparent. Both are targeted at the same time relative to polar body extrusion and to a similar extent (Figure 6.3). Compared to non APC10 knockdown controls, this timing is closer to that of the bound cyclin B1 construct.

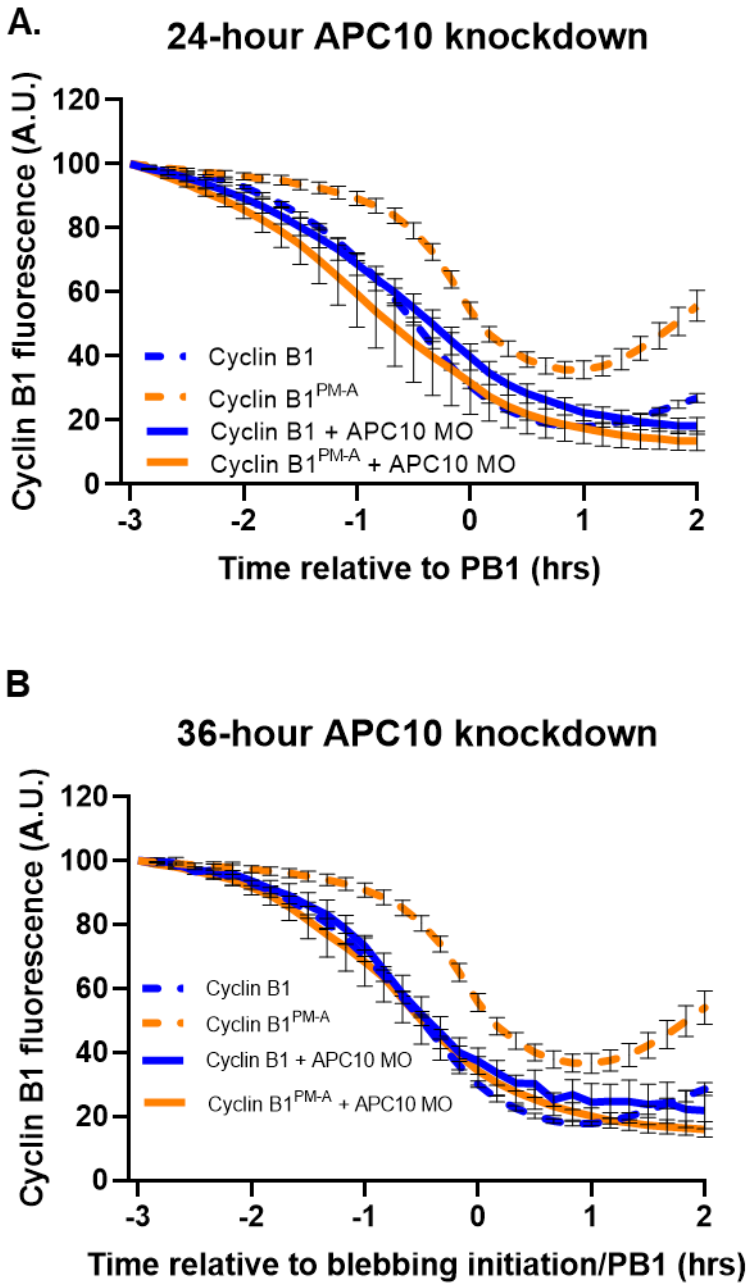

Figure 6.3. Destruction profiles of reporters for free or bound cyclin B1 after APC10 morpholino incubation.

Average destruction profiles of cyclin B1 (blue) and cyclin B1PM-A (orange) control oocytes (dashed) or injected with APC10 morpholino antisense oligomer at a needle concentration of 1mM (MO, solid) for (A) 24-hours (Cyclin B1+APC10 MO n=14; Cyclin $B1^{PM-A}$+APC10 MO n=8) (C) 36-hours (Cyclin B1+APC10 MO n=6; Cyclin B1PM-A+APC10 MO n=8). Error Bars ± SEM.

A more extensive knockdown incubation period of 36-hours resulted in oocytes presenting with significant 'blebbing', as discussed earlier (Figure 6.2). Blebbing mostly results in no polar-bodies being produced, however when a polar-body is produced, the exact point of extrusion is near impossible to be determine with any degree of confidence, thus destruction traces could not be aligned to anaphase accurately. Instead, I decided to align destruction profiles in these oocytes to the initiation of blebbing, reasoning that this is the first time point at which the oocyte attempts a PB1 extrusion. This resulted in very little difference between destruction of cyclin B1 and cyclin $B1^{PM\text{-}A}$ in terms of both rate and timing (Figure 6.3). Compared to average cyclin B1 without APC10 knockdown, the knockdown treated oocytes destroy both constructs at a time similar to cyclin B1 with an accessible PM motif. It is important to note though, that without a precise timing of PB1 in APC10 knockdown oocytes, destruction timing comparisons will also not be entirely reliable. Regardless of APC10 morpholino incubation length, in oocytes capable of undergoing GVBD, both cyclin B1 reporters were able to be destroyed extensively suggesting that the bipartite D-box receptor is still available in a significant pool of APC/C complexes.

Quantification of APC10 in oocytes incubated with APC10 morpholino was unsuccessful, no signal was detected by Western blotting in control oocytes, and immunofluorescence using an APC10 antibody showed significant zona staining and is currently unreliable (data not shown).

Ultimately, an APC10 knockdown of all time points resulted in the removal of the time difference between the two constructs (Figure 6.3). This suggests that the substrate recognition and differentiation capabilities of the APC/C are being altered and significant substrate targeting dysregulation is occurring. It appears that knocking down APC10 still permits substrate destruction, perhaps by reconfiguring into a different mode which still targets substrates, but without the finesse of highly ordered processivity. This highlights the dynamic nature of the APC/C. A caveat with this line of experimentation here is that we do not know the extent of the knockdown.

6.2.2 Literature and structural data suggest that D-box residues in positions 8-10 could be used to determine which form of APC/C is responsible for targeting a substrate

Interestingly, APC10 knockdown did not prevent the destruction of cyclin B1 reporters, thus an alternative method of determining the effects of disrupting access to the bipartite D-box receptor was required. I therefore decided to look at the D-boxes of substrates themselves. Chang et al. used cryoEM of APC/C^{Cdh1} bound to a HSL1 D-box substrate and identified that this D-box localised to the bipartite D-box receptor formed between Cdh1 and APC10[114]. They determined that residues in positions 1-7 of the D-box (RxxLxx(V/I/L)) engaged the D-box binding region of the WD40 domain on the coactivator, whereas extended D-box residues (C-terminal hydrophilic residues in positions 8-10) of the D-box contact APC10 on a polar surface of its 140s loop. This can also be observed when analysing the cryo-EM structure of a HSL1 substrate binding to the bipartite D-box receptor of APC/C^{Cdc20} (Figure 6.4A). Mutating residues on either the 140s loop of APC10 or those in position 8-10 of the D-box prevented ubiquitination of this substrate in the Chang et al. study. While this study was conducted on APC/C^{Cdh1}, considering extreme conservation between coactivators, it is highly likely that a similar result would be obtained with APC/C^{Cdc20} (Figure 6.4B). Indeed, analysing the cryo-EM structures solved by the Barford group whereby coactivators have been aligned using pyMOL of APC/C-Cdc20 and APC/C-Cdh1 structures shows that the positioning of APC10 in 3-dimentional space only deviates by 5Å and the interfaces remain the same (Figure 6.4B). In addition, by aligning the D-boxes of various APC/C substrates relative to D-box position 1, we can observe a largely hydrophilic stretch of amino acids (Figure 6.4C) suggesting that C-terminal D-box binding to APC10 is conserved.

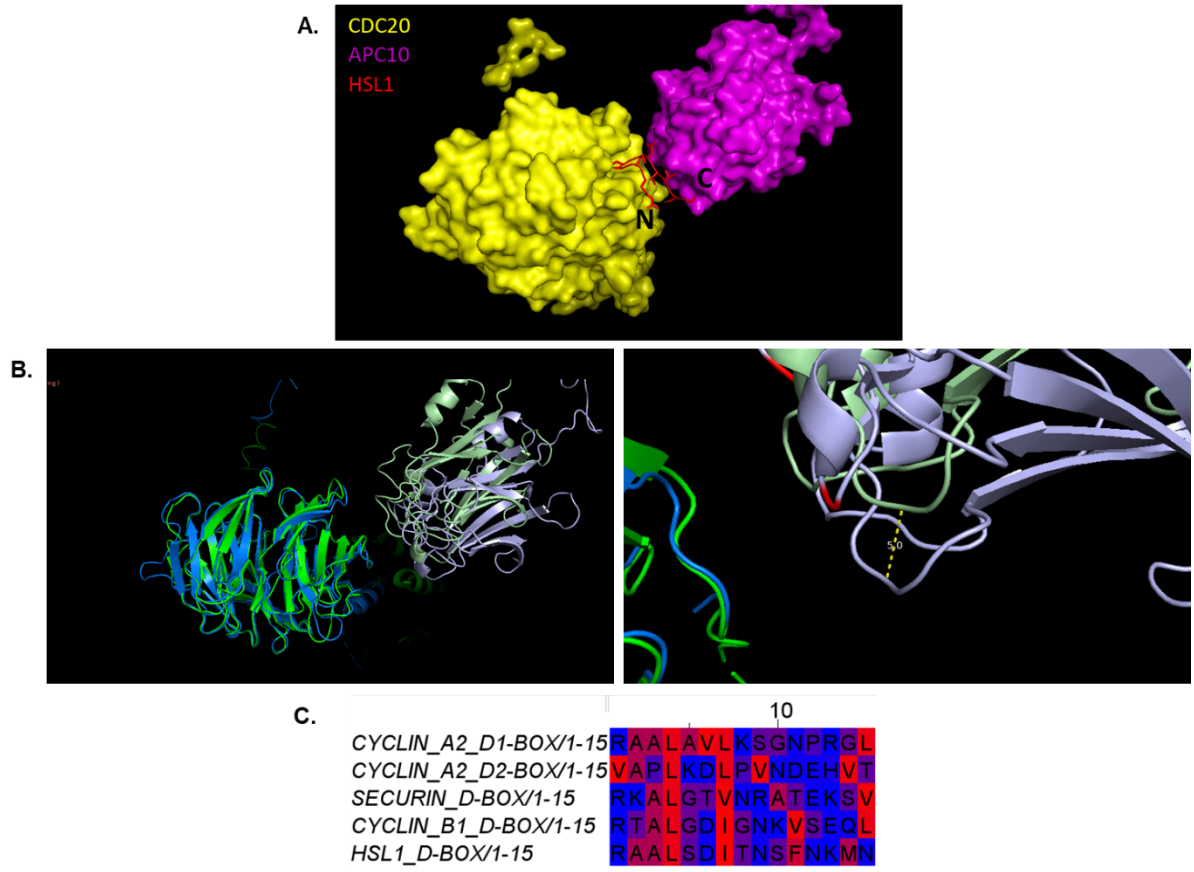

Figure 6.4. Cryo-EM images of the bipartite D-box receptor.

(A) Cryo-EM image from the Barford group of non-MCC bound APC/C^{Cdc20} showing Cdc20 (yellow, surface) and APC10 (magenta, surface) forming the bipartite D-box receptor, bound to HSL1 D-box substrate (red, cartoon) with the N- and C-termini indicated (PDB:5G04[115]). B) Cryo-EM structures of APC/C^{Cdh1} (blue shades; Cdh1 blue; APC10; metallic blue; PDB:8PKP[115]) as well as APC/C^{Cdc20} and APC10 (green shades; Cdc20 green; APC10 pale green). These subunit chains were isolated and aligned at coactivators to produce a composite image showing the structural conservation and the positioning of APC10 respective to each other (left) and the distance in angstrom, calculated using PyMOL, between GLY58 of the two APC10 structures indicating positional deviation between the two structures (right). (C) Alignment of D-boxes for various substrates coloured by hydrophobicity using JalView (Red=hydrophobic; Blue=hydrophilic, numbering relative to D-box position 1)

These findings suggest that mutating D-box C-terminal hydrophilic residues in positions 8-10 (herein referred to as the 'extended D-box') could be used to determine which D-box receptor is being used to target a substrate, and thereby which form of APC/C is destroying it. For instance, for substrates that are capable of being targeted by the APC/C^{MCC}, we should not see a dramatic difference in destruction following mutation of the extended D-box. These mutations would likely prevent D-box binding to APC10 (and thus the bipartite D-box receptor), but this binding is not required for destruction by the APC/C^{MCC}, as the bipartite D-box receptor is not formed in this context. Importantly, these mutations do not affect the coactivator binding residues of a D-box, those in positions 1-7, thus prometaphase substrates should still be targeted by the APC/C^{MCC}. Alternatively, for substrates that require MCC disassociation and bipartite D-box formation, their destruction should be inhibited by the loss of their extended D-box positions. APC10 binding would be required for destruction by the APC/C in this mode. The model for this line of experimentation is outlined in Figure 6.5.

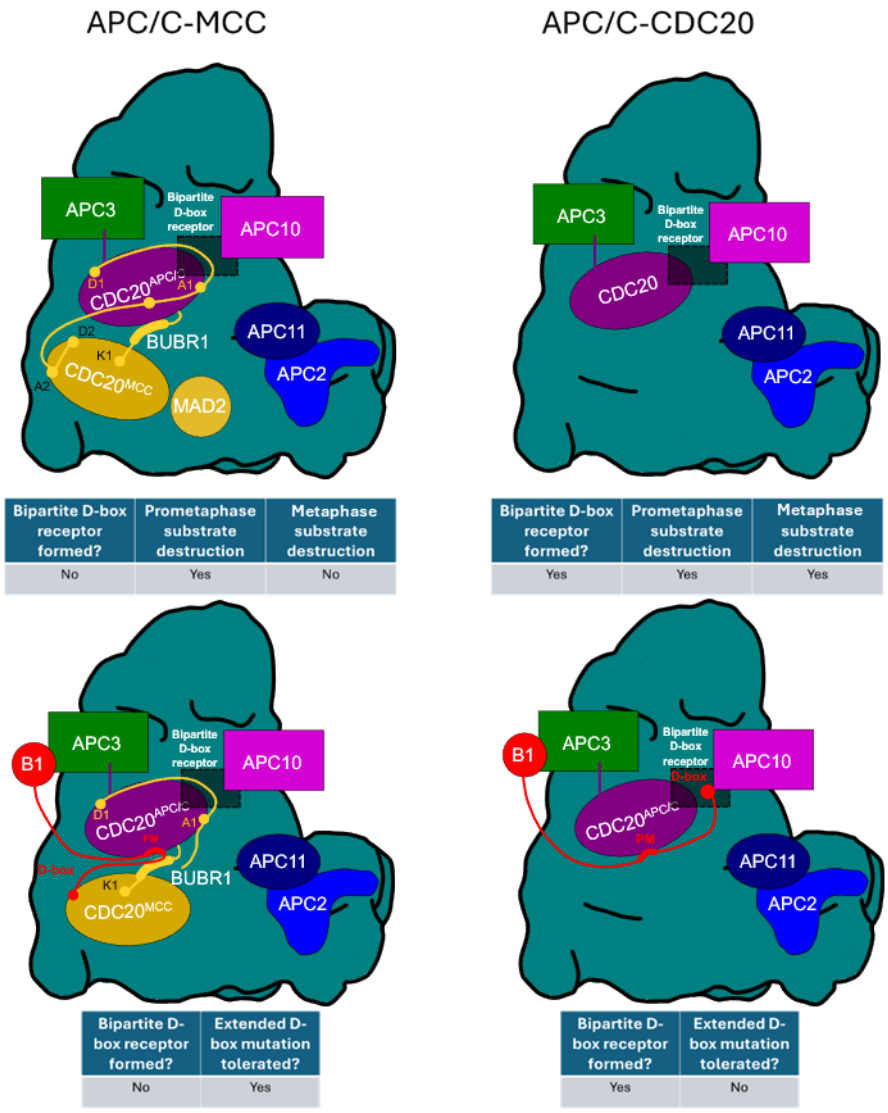

Figure 6.5. Model describing the rationale behind mutation of extended D-boxes to deduce which mode the APC/C is in to target cyclin B1 in prometaphase I

Structures of the APC/C complexes in this figure are adapted graphical representations by the Barford group. In prometaphase, the APC/C is bound to the MCC in a mode whereby the bipartite D-box receptor (comprised of Cdc20 and APC10) is not formed. The APC/C in this mode can target prometaphase substrates such as Cyclin A2. Importantly, it cannot target Metaphase substrates as these substrates require binding to the bipartite D-box receptor and lack the additional motifs required to permit destruction by APC/C-MCC. Therefore, extended D-box binding to APC10 is not required for substrate targeting in this mode (top left). In Metaphase, disassociation of MCC from the APC/C resolves the bipartite D-box receptor. All D-box containing substrates can be targeted by the APC/C in this mode. APC10 binding is therefore likely required for D-boxes to associate with the bipartite D-box receptor (top right). Further evidence is required to determine which mode the APC/C is in to target

cyclin B1 in prometaphase I. If cyclin B1 is being targeted by APC/C-MCC, a extended D-box mutation is likely tolerated as the APC10 binding (as part of the bipartite D-box receptor) is likely not required (bottom left). If cyclin B1 is targeted by a fraction of APC/C not bound to the MCC in late prometaphase, then this will be via binding to the bipartite D-box receptor and an extended D-box mutation will likely not be tolerated.

6.2.3 Securin and cyclin A2 does not require the presence of C-terminal hydrophilic residues for destruction

I decided to explore the destruction of securin harbouring alanine substitution mutations of residues in the extended D-box. Previously published data from our lab shows that similar to cyclin B1, securin is primarily a metaphase substrate. However because of the presence of a novel FxxF motif, it can also be targeted early in prometaphase I of mouse oocyte meiosis[156]. In this system, the FxxF-A fluorescent construct report bound securin protein dynamics, while the un-mutated version reports free securin destruction. Interestingly, the FxxF motif fits the consensus sequence of an ABBA motif. Whether this is indeed an ABBA motif, able to bind the ABBA motif binding site of APC/C coactivators, is yet to be determined. This means securin is a very interesting subject with which to test extended D-box mutations. By abolishing metaphase destruction by APC/C^{Cdc20} using extended D-box mutations, while retaining an FxxF motif, this could indicate whether or not the FxxF motif permits destruction via the APC/C^{MCC}. Destruction in this context would be strong evidence for the FxxF identifying as an ABBA motif. This would also provide additional reassurance that this line of experimentation is a valid way of distinguishing between different modes of APC/C targeting for cyclin B1 constructs. Securin only contains one D-box and thus residues in the extended D-box were mutated to alanines in constructs with and without a mutated FxxF motif.

Microinjection of cRNA encoding fluorescent securin containing mutations in its extended D-box (herein referred to as 'securin$^{short\ D\text{-}box}$' , Figure 6.6A) results in the expression of a protein that is still targeted for destruction from 6.5 hours post-GVBD (Figure 6.6B). Note that in this experiment, relative to other substrates that I have tested, there is greater variation between oocytes in the extent to which they destroy securin$^{short\ D\text{-}box}$. Figure 6-5 shows the average

trace. However, some oocytes show very little evidence of destruction, while others destroy to a much greater extent. This could be an indication of the variation of APC/C modes in these oocytes, some harbouring more APC/C^{MCC} complexes that can target short D-boxes, and others with reduced checkpoint activity that have greater numbers of APC/C-Cdc20, but which would be less able to handle this mutated substrate. It is also important to highlight that with reduced capacity to destroy securin (and fully released separase), polar body extrusion fails in many of these oocytes. For this reason, these data are aligned to GVBD as the most certain cell cycle landmark. However, most overwhelmingly, securin is still destroyed with a 'short D-box', while excitingly, co-mutating the FxxF motif alongside a short D-box (securin$^{\text{short D-box, FxxF-A}}$) completely stabilises this protein.

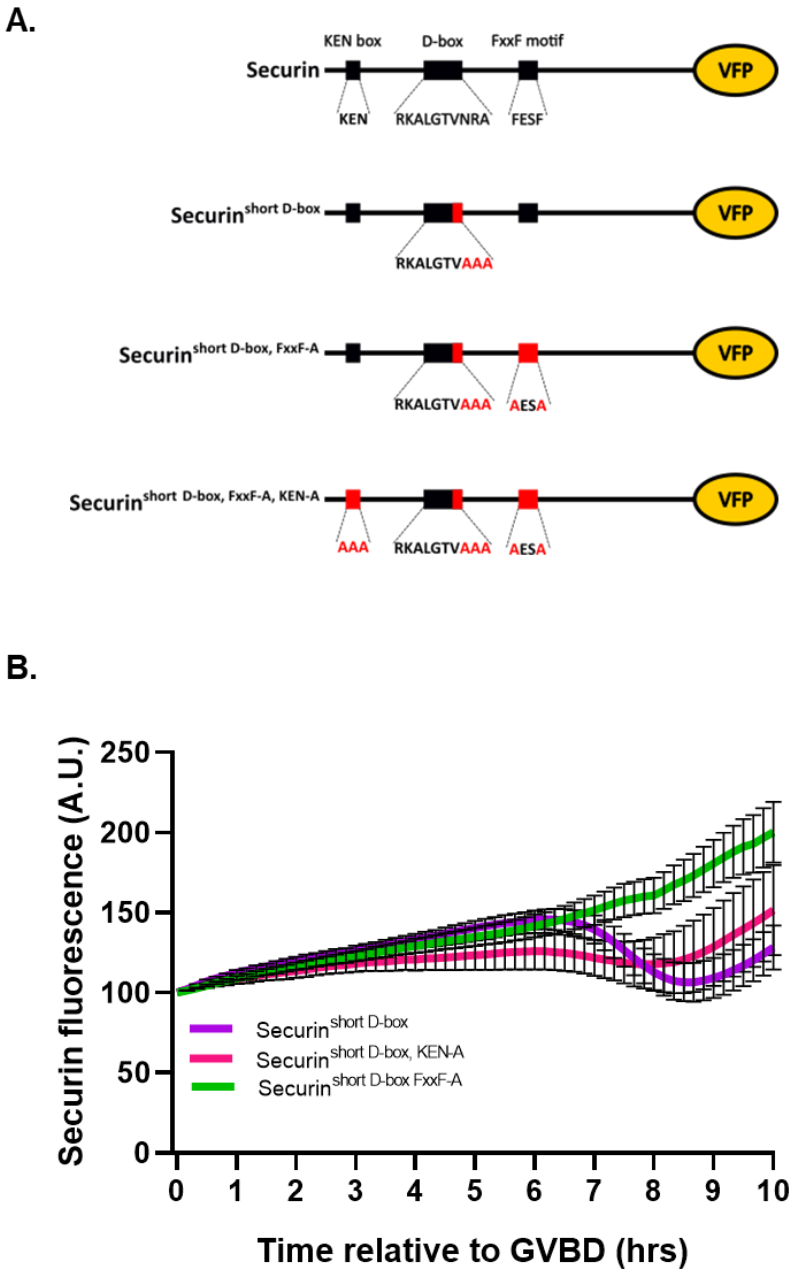

Figure 6.6. Mutating C-terminal hydrophilic D-box residues in positions 8-10 (the extended D-box) of securin still permits its destruction however this requires non-canonical motifs.

A)Structure diagram describing the constructs used in these experiments highlighting the mutations used for each construct. B) Average destruction profiles of securin$^{\text{short D-box}}$ (purple, n=25), securin$^{\text{short D-box, KEN-A}}$ (red, n=6) and securin$^{\text{short D-box, FxxF-A}}$ (green, n=11). Traces are aligned to GVBD and normalised to the fluorescence at GVBD as oocytes did not extrude polar bodies.

Furthermore, co-mutating the KEN motif of securin$^{\text{short D-box}}$ (securin$^{\text{short D-box, KEN-A}}$) partially stabilises securin but not to the same extent as securin$^{\text{short D-box, FxxF-A}}$ (Figure 6.6B). These results are highly characteristic of ABBA motif behaviour.

Cyclin A2 is a substrate that is targeted for destruction in prometaphase and harbours two D-boxes as well as ABBA and KEN motifs. This is a more complicated substrate to test in this system neither D-box entirely fits the consensus sequence for a D-box, especially the D2-box which is classified as non-canonical[20]. However, as it is a prometaphase substrate and has been proven by numerous studies to be targeted by the APC/C^{MCC} it was important to test the effects of mutations in its extended D-boxes to validate this line of enquiry[20,157]. To this end, the extended D-box residues of both D-boxes in cyclin A2 were mutated to alanines and this protein was expressed in oocytes following microinjection of mRNA (Figure 6.7A).

Fluorescent wildtype Cyclin A2 (Cyclin A2) and cyclin A2 with extended D-box mutations on both D-boxes (cyclin A2$^{\text{short D-box}}$) was steadily destroyed from 1.5-hours post GVBD. Destruction then continued to an expected time point of PB extrusion. For cyclin A2 the rate of this destruction dropped off approximately 8-hours post-GVBD whereby destruction ceased. For cyclin A2$^{\text{short D-box}}$ the rate of destruction reduced at an earlier time point, approximately 7-hours post GVBD. The destruction traces between these two proteins deviates after 6-hours and cyclin A2 WT is destroyed more extensively that cyclin A2 P8-10-A (Figure 6.7B). This is interesting as it suggests that in late prometaphase, cyclin A2$^{\text{short D-box}}$ becomes a worse substrate for the APC/C however destruction in early prometaphase is identical to that of cyclin A2. This could highlight that as the SAC begins to diminish and APC/C begins to become increasingly disassociated with the MCC, substrates with a short D-box (mutations in its extended D-box) become worse targets. This may be evident that the extended D-box mutations are preventing association with the bipartite D-box receptor as predicted.

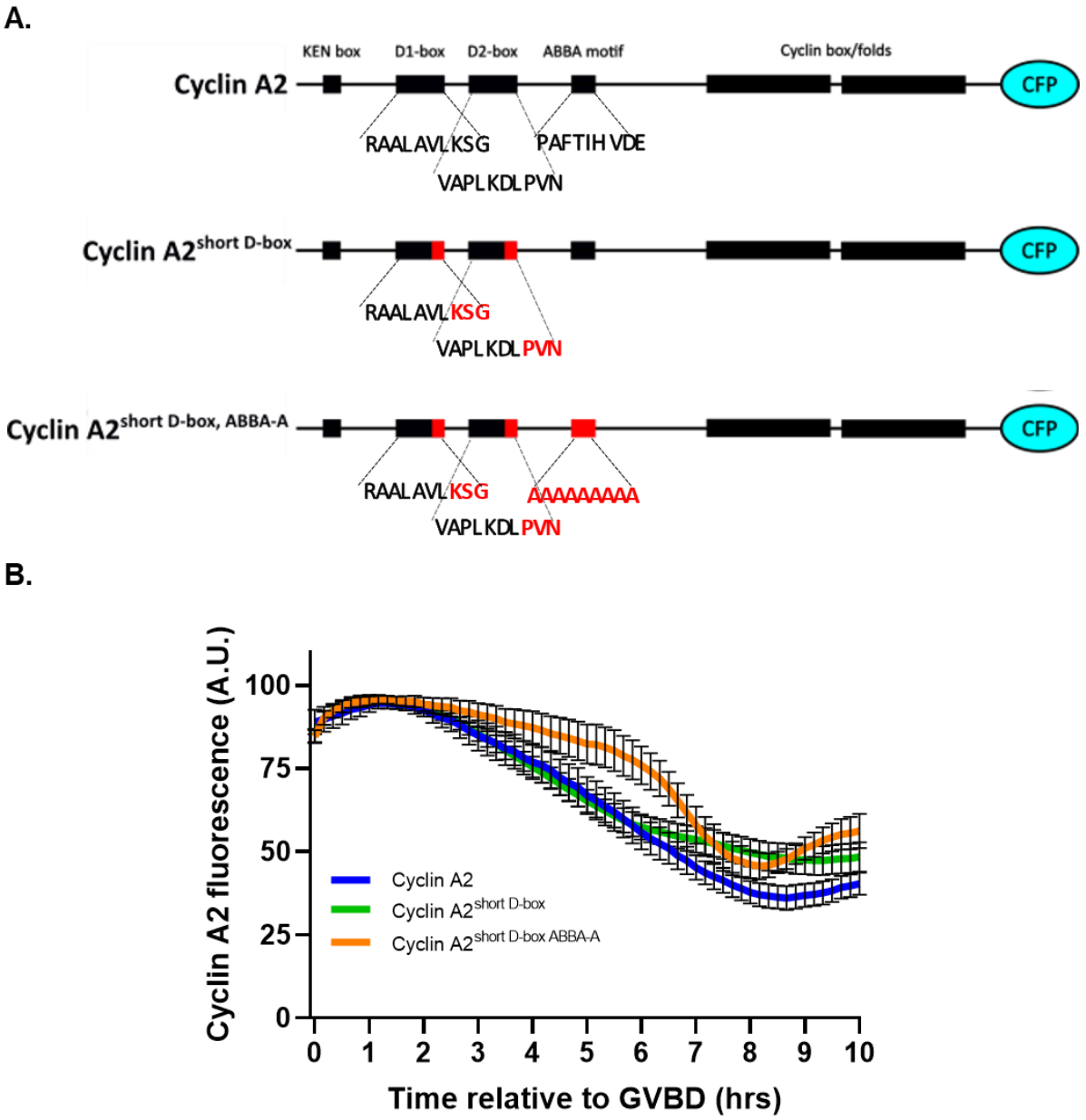

Figure 6.7. Mutations of C-terminal hydrophilic D-box residues had little impact on cyclin A2 destruction and co-mutating the ABBA motif reduced prometaphase destruction.

(A) Structure diagram describing the constructs used in these experiments highlighting the mutations used for each construct. (B) Average cyclin A2 (blue, n=15), Cyclin A2$^{\text{short D-box}}$ (n=9), Cyclin A2$^{\text{short D-box,ABBA-A}}$ (green, n=13) destruction profiles. Traces are aligned to GVBD and normalised to the fluorescence at GVBD as oocytes did not extrude polar bodies.

Co-mutating the ABBA motif alongside the extended D-box (Cyclin A2$^{\text{short D-box, ABBA-A}}$) resulted in a reduced rate of destruction through prometaphase compared to the protein with an ABBA motif present. However, from approximately 6-hours post-GVBD there is a marked increase the rate of destruction until PB1 extrusion would be expected in unperturbed oocytes (Figure 6.7B). This is interesting as it is clear that an ABBA motif is important in prometaphase I targeting of cyclin A2, in agreement with literature. Interestingly, the Barford group published findings utilising an *in-vitro* ubiquitination assay that mutation of an ABBA motif actually increases ubiquitination specifically by APC/C$^{\text{Cdc20}}$.

Note that in all instances, no polar bodies were extruded by cyclin A2 expressing oocytes, likely due to cyclin A2 overexpression and associated elevated CDK activity overwhelming the APC/C with additional substrates. I suggest in this context anaphase stalls.

6.2.4 Destruction of reporters for free or bound cyclin B1 does require C-terminal hydrophilic residues

Although securin and cyclin A2 are targets for destruction with mutations in their extended D-boxes, there is some contrast in the way that both are targeted by the APC/C (Figure 6.6B, Figure 6.7B). For instance, securin absolutely requires its FxxF motif for destruction when harbouring a mutation in its extended D-box residues, whereas cyclin A2 is still able to be targetted with an ABBA mutation. The extent of securin$^{\text{short D-box}}$ destruction is much shallower compared to the expected destruction profile for securin WT, which we have seen to be very extensive[156]. Cyclin A2$^{\text{short D-box}}$ destruction however is very similar to cyclin A2 WT.

I next wanted to test whether mutations in the extended D-box of cyclin B1 perturbed its destruction. I microinjected cDNA encoding fluorescent cyclin B1 ± PM-motif with alanine substitutions in the extended D-box to generate cyclin B1$^{\text{Short D-box, ±PM-A}}$, and measured the fluorescence of expressed protein over the duration of MI (Figure 6.8A). The effect of this mutation was very clear. Levels of cyclin B1$^{\text{short D-box}}$ protein do not decrease (Figure 6.8B).

When co-mutating the PM motif alongside the extended D-box residues in the cyclin B1$^{\text{Short D-box, PM-A}}$ construct, protein levels were still relatively stable, but there appears to be an increased rate of turn over compared to cyclin B1$^{\text{short D-box}}$ protein. 24% loss from post-GVBD peak. This destruction takes place gradually over 7-hours. It is important to note however that while the average destruction seems to be more extensive for cyclin B1$^{\text{short D-box, PM-A}}$, quantifying the fluorescence change in individual oocytes suggests that the destruction is no more extensive than some of the traces of cyclin B1$^{\text{short D-box}}$ and the destruction of cyclin B1$^{\text{short D-box, PM-A}}$ may seem more extensive due to lower n-numbers.

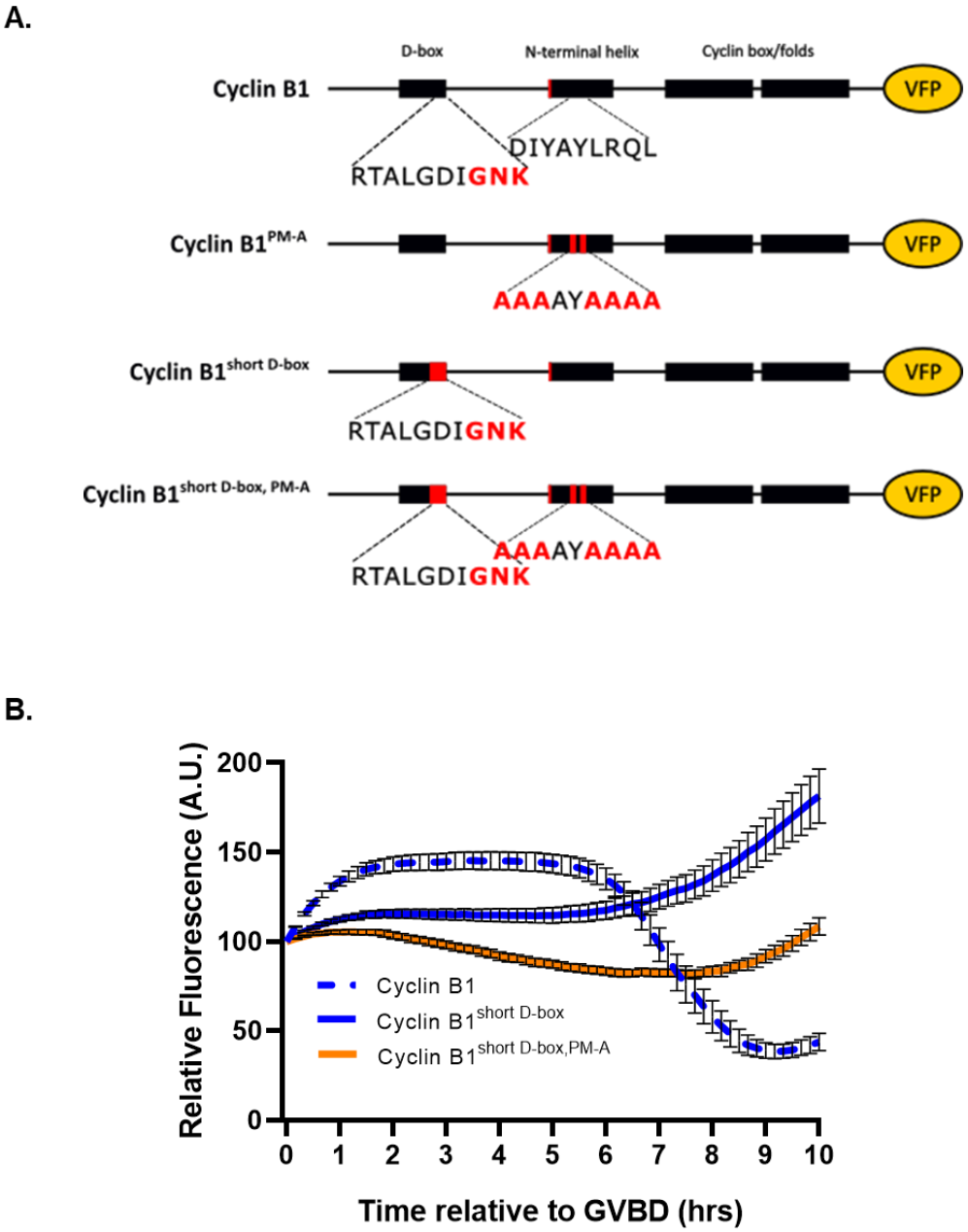

Figure 6.8. Efficient cyclin B1 destruction requires the extended D-box irrespective of PM motif presence.

A) Structure diagram describing the constructs used in these experiments highlighting the mutations used for each construct. B) Average cyclin B1$^{\text{short D-box}}$ (blue, n=24) and cyclin B1$^{\text{short D-box, PM-A}}$ (orange, n=11) destruction profiles alongside average destruction profile for cyclin B1 (dashed, blue; n=25). Traces are aligned to GVBD and normalised to the fluorescence at GVBD.

The expression of cyclin B1$^{short\ D\text{-}box}$ is in complete contrast to the regular length D-box cyclin B1 control, where on average destruction initiates 6-hours post GVBD and is reduced by on average 74% from peak abundance (Figure 6.8B).

6.2.5 D-boxes are dynamic and certain substrates can tolerate residues in their extended D-box

As previous observations have shown that securin$^{short\ D\text{-}box}$ is an APC/C destruction target, I wanted to determine how late this destruction is respective to other substrates. To address this, I injected cRNA encoding cerulean fluorescent protein tagged securin$^{short\ D\text{-}box}$ as well as Venus fluorescent protein cyclin B1 (Figure 6.9A). This allowed me to quantify the abundance of both proteins and measure the destruction of each, respective to each other in single oocytes.

When expressed at the same time as securin$^{short\ D\text{-}box}$, we can see that cyclin B1 reaches a peak at 1.5-hours post GVBD and remains largely stable (translation rates match destruction rates), until active destruction initiates (Figure 6.9B). This accelerated destruction occurs at approximately 6-hours post GVBD and continues until a minimum of 19.1% at 9-hours post GVBD on average. This is the exact same profile of cyclin B1 destruction noted in control oocytes not co-expressing a securin mutant as seen in other figures. In contrast securin$^{short\ D\text{-}box}$ destruction is delayed by the presence of co-expressed cyclin B1. Destruction initiates at ~7.5-hours post-GVBD, more than an hour later than the destruction of securin$^{short\ D\text{-}box}$ when not co-expressed with cyclin B1. As the length of prometaphase between oocytes does vary, aligning traces to GVBD and using averages may not give an accurate indication as to how constructs are degraded relative to each other. However here, when analysing the destruction curves for both substrates in the same oocyte, we can see that consistently, securin$^{short\ D\text{-}box}$ is targeted over an hour later than cyclin B1 (Figure 6.9C).

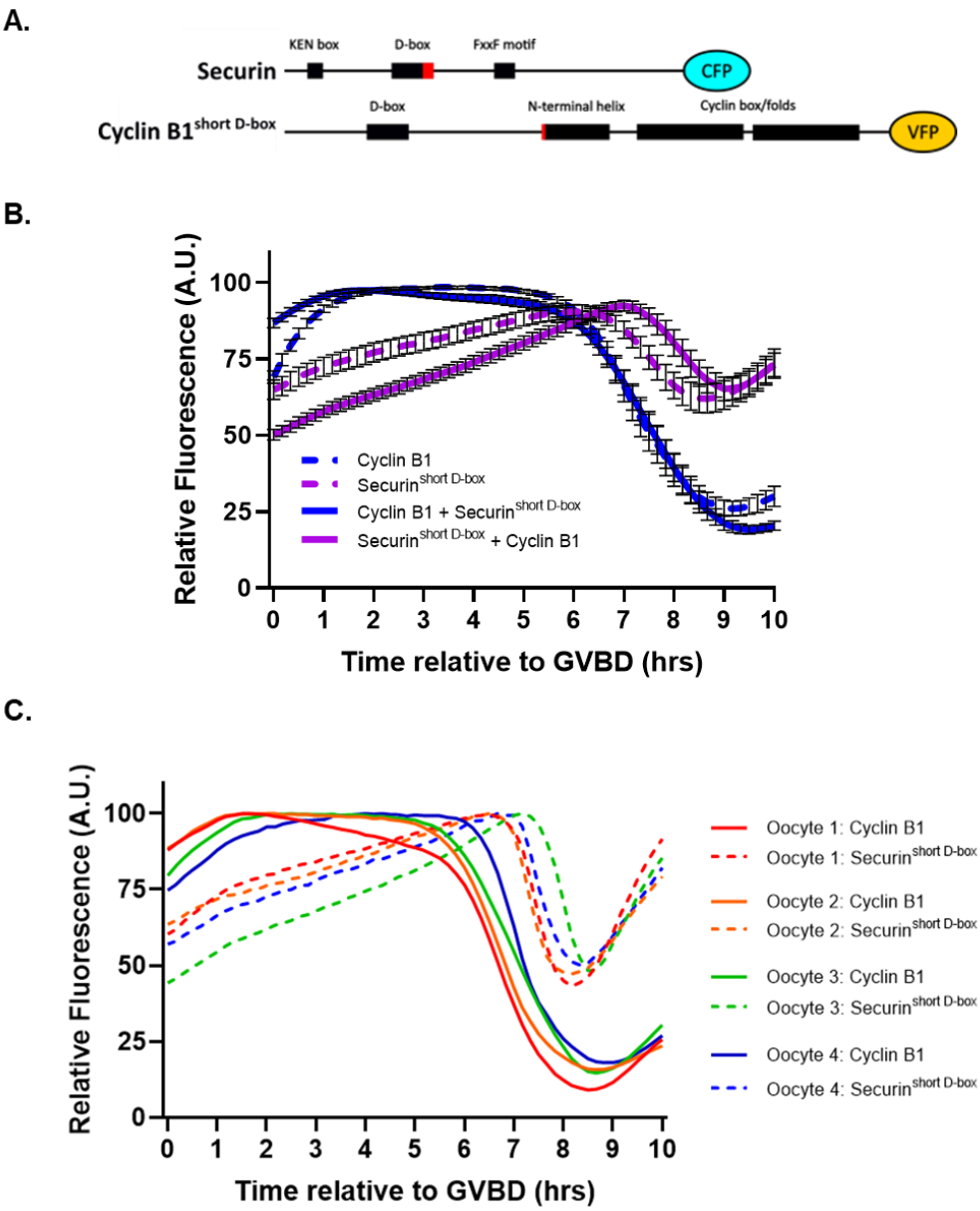

Figure 6.9. Securin P8-10-A destruction occurs late in respect to free cyclin B1.

A) Structure diagram describing the constructs used in these experiments highlighting the mutations used for each construct. Cyclin B1$^{short\ D\text{-}box}$ harbours an alanine substitution mutation in its extended D-box B) Average destruction profiles of securin$^{short\ D\text{-}box}$ (dashed, magenta, n=25) and cyclin B1 (dashed, blue, n=20) alongside the average destruction profiles when co-expressed together in individual oocytes (Securin$^{short\ D\text{-}box}$ is Cerulean fluorescent protein linked; Cyclin B1 is venus fluorescent protein linked; n=21) aligned at GVBD. Error bars ± SEM. C) Destruction profiles of cyclin B1 (VFP-linked; solid traces) and securin$^{short\ D\text{-}box}$ (CFP-linked; dashed traces) when co-expressed together in individual oocytes. Each

individual colour refers to a single oocyte, these traces representative of the experiment as a whole.

It was predicted that a mutation of extended D-box residues (resulting in a short D-box) should prevent binding to the bipartite D-box receptor, which in theory becomes available in late prometaphase/metaphase. Yet, in conflict with this, destruction of securin with a short D-box occurs very late, likely when the SAC is largely satisfied. I therefore decided to try and test whether or not this construct can be targeted by the bipartite D-box receptor using an alternative method, by treating oocytes expressing fluorescent securin constructs using the drug reversine. Reversine is an inhibitor of MPS1 which rapidly induces the onset of anaphase[203]. I hypothesised that reversine would rapidly switch off the SAC and with the natural turnover of MCC complexes would result in a large proportion of APC/C^{Cdc20} complexes prematurely. If securin$^{short\ D\text{-}box}$ can be targeted after reversine treatment, then this species likely can be targeted by the bipartite D-box receptor.

Oocytes expressing different forms of securin (wildtype, short D-box, short D-box,FxxF-A) were left for two-hours to allow for sufficient translation of these constructs and washed out of IBMX to induce GVBD (Figure 6.10A). Three hours post release, 100 nM reversine was added to media and carefully mixed. Upon addition of reversine, 100% of securin WT injected oocytes extrude polar bodies within 3.67-hours indicating reversine treatment was effective. However, only 20% of securin$^{short\ D\text{-}box}$ injected oocytes and 0% of securin$^{short\ D\text{-}box,\ FxxF\text{-}A}$ expressing oocytes extruded within the same time period. This is likely due to impaired release of separase activity given that either mutation has a dramatic effect on securin destruction targeting (Figure 6.10B). Securin WT levels drop 20-minutes after treatment with reversine, ~90% of this protein is lost in ~2 hours. However, in response to reversine, securin$^{short\ D\text{-}box}$ protein destruction initiates later, 50-minutes after drug addition and only half of the protein is destroyed over the following 2.5-hours. Co-mutating the FxxF motif alongside D-box residues in positions 8-10 (securin$^{short\ D\text{-}box,\ FxxF\text{-}A}$) almost completely stabilises the protein.

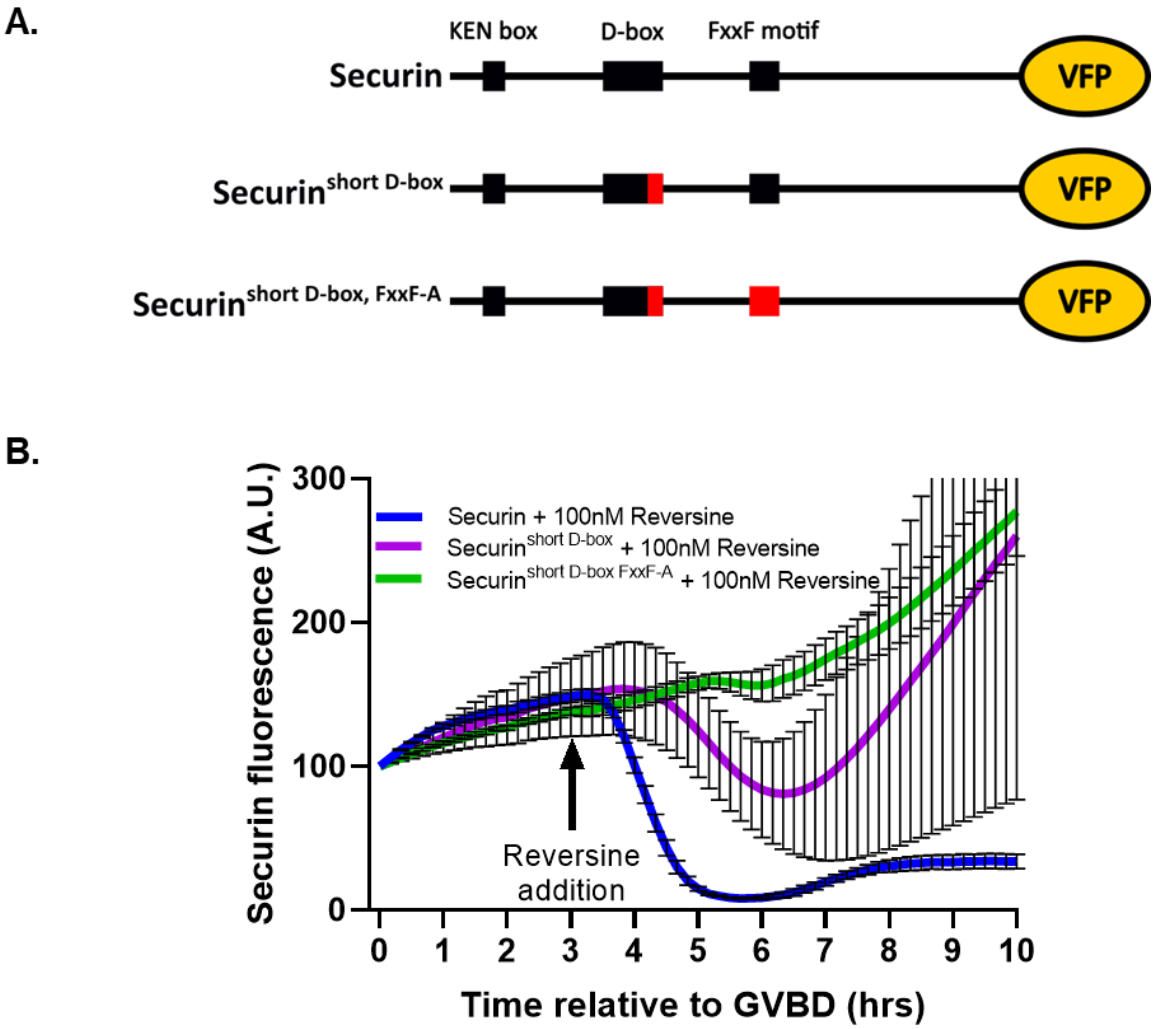

Figure 6.10. Treatment with reversine results in extended securin$^{short\ D\text{-}box}$ destruction and no additional destruction of securin$^{FxxF\text{-}A}$.

A) Structure diagram describing the constructs used in these experiments highlighting the mutations used for each construct. Average securin WT (blue, n=5), securin$^{short\ D\text{-}box}$ (magenta, n=9) and securin$^{short\ D\text{-}box}$, FxxF-A (green, n=7) destruction profiles aligned to GVBD. 100 nM reversine was supplemented into the media 3-hours post-GVBD. Error bars ± SEM.

6.3 Discussion

The Anaphase Promoting Complex/Cyclosome is dynamic and complex, especially during the period of chromosome alignment where constant flux of MCC association and disassociation both prevents premature anaphase but also allows for rapid APC/C activation. Importantly the APC/C is catalytically active towards prometaphase substrates regardless of MCC incorporation, however this is dependent on the presence of multiple SLiMs such as D-boxes, ABBA and KEN boxes. While free cyclin B1 is targeted by the APC/C in prometaphase, a time point in which one can expect the MCC would be incorporated into the APC/C, destruction is not as early as better characterised prometaphase substrates such as cyclin A2**.** In fact, the destruction of free cyclin B1 occurs in late prometaphase I when SAC signalling has likely begun to diminish. These points suggest that more experimental evidence is required to confirm whether the APC/C is MCC bound or not when targeting free cyclin B1. This information would give a better understanding of PM motif processivity. Preventing the formation of the bipartite D-box receptor, observing whether or not free cyclin B1 can be targeted for destruction in this context, seemed a sensible method to determine more definitively whether free cyclin B1 destruction requires MCC dissociation.

Knocking down endogenous APC10 in oocytes using a morpholino and measuring the destruction of free and bound cyclin B1 reporters was not informative (Figure 6.2). An expected phenotype of a sufficient APC10 knockdown was that oocytes would arrest in prometaphase I due to the inability to destroy many substrates, predominantly cyclin B1-bound to CDK1 and securin-bound to Separase. At the same time cyclin A2 should still be destroyed due to well established KEN and ABBA motif mediated destruction pathways that do not require the bipartite D-box receptor. A proportion of cyclin A2 will still be targeted by non-MCC bound APC/C and thus higher than usual cyclin A2 levels would also likely contribute to prometaphase I arrest. Nevertheless the principle behind the experiment was that we might still be able to detect prometaphase destruction dynamics even if oocytes did not progress beyond this. However there were several substantial practical challenges associated with these experiments, and how the APC/C reforms in the absence of a 10^{th} subunit is unknown.

I found that increasing the duration of APC10 morpholino incubation periods resulted in oocytes failing to release from prophase I arrest (Figure 6.2). In APC10 morpholino incubations of 24-hours, few oocytes were stuck in prophase I arrest suggesting that knockdown was not as extensive in these oocytes. But above the 24-hour incubation time, APC10 knocked down oocytes increasingly presented with a prophase I arrest phenotype, unable to resume meiosis I. I propose that this is because the bipartite D-box receptor (which also forms between Cdh1 as a coactivator and APC10 - the primary coactivator of the APC/C during prophase arrest) is perturbed and insufficient destruction of APC/C^{Cdh1} substrates is likely resulting in an inability to permit progression from prophase arrest.

Because extensive APC10 knockdown in oocytes caused a prophase I arrest phenotype, measuring the destruction of substrates in prometaphase was not possible in these cells. I was however able to measure the destruction of cyclin B1 ± PM motif in oocytes with a shorter APC10 knockdown incubation. These oocytes presented with 'blebbing', and I observed cyclin $B1^{PM-A}$ destruction to be like that of oocytes expressing cyclin B1 (Figure 6.3). Interestingly however, APC10 MO treatment did result in dysregulated destruction, since the timing difference ordinarily observed between these cyclin b1 constructs was now markedly diminished. This suggests that an APC10 knockdown dysregulates the ability of the APC/C to differentiate between certain substrates and thus the temporal control of substrate targeting is perturbed. This could be due to an APC10 knockdown resulting in a reconfiguration of the APC/C into a mode which is still functional to facilitate the ubiquitination of substrates, however is unable to differentiate between them.

The fact that substrates are still able to be targeted for destruction during an APC10 knockdown suggests that the knockdown is not extensive enough, and perhaps only the oocytes that do not undergo GVBD have sufficient knockdown. A next step in regards to this method of bipartite D-box receptor exploration could be to artificially induce GVBD either by drug or by overexpressing a substrate such as cyclin A2, however this would impact cyclin B1 destruction by altering the cell cycle or overloading the APC/C respectively. An alternative would be to use a more rapid method of knockdown such as the Trim-Away approach which

uses an antibody based system to deplete proteins[204]. This would allow for IBMX washout to induce GVBD in oocytes and quickly remove APC10 without relying on its natural turnover which my data suggests takes more than 48-hours. Still though, we are left with a system that likely perturbs the destruction of many substrates, and it is likely that increased competition could result in unpredictable APC/C activity.

Altering cell cycle substrates themselves to force destruction by either APC/C complex is a far better method to explore how substrates are targeted as this should not affect the processivity of other substrates or have off-target effects. The use of nocodazole or reversine to force the APC/C into the SAC inhibited or satisfied configurations respectively could have been a viable method however this would affect the processivity of all APC/C substrates as well as having various off-target effects such as an impact on cell cycle timing. Previous data from our group have shown that cyclin B1, with an accessible PM-motif, can be targeted by the APC/C in nocodazole however further experimental evidence that it is indeed the APC/C^{MCC} complex which allows for PM motif mediated cyclin B1 targeting is required[160].

Instead, I turned to the D-boxes themselves. Structural data information based on cryo-EM data from the Barford group suggests that the D-boxes of substrates themselves could be useful indicators as to which APC/C form they are most likely targets of. Currently, the only structural data on the RCSB Protein Data Bank which involves a substrate being targeted by the bipartite D-box receptor is the D-box peptide HSL1 (PDB:5G04) and cyclin A2 (PDB:6Q6G; 6QGH)[20,115]. Their results are clear though. N-terminal residues of a D-box interact with coactivator Cdc20, specifically a highly conserved arginine in P1 and leucine in P4, while C-terminal hydrophilic D-box residues in P8-10 (the extended D-box) interact with APC10 (Figure 6.4). Chang et al. used a ubiquitination assay to show that a HSL1 D-box peptide required these extended D-box residues to be ubiquitinated by APC/C^{Cdh1} [122]. This experiment was not attempted using APC/C^{Cdc20}, but a significant amount of literature suggests this mechanism is the same for both coactivators. I have utilised the aforementioned cryo-EM structures, isolating structures of Cdc20-APC10 as well as Cdh1-APC10 and aligned them using PyMOL to show the similarities in their positioning within the

APC/C and highlight their conservation. This suggests that the bipartite D-box receptor comprising of either form of coactivator will likely require the extended D-boxes of substrates for destruction (Figure 6.4B). Therefore, extended D-box residues could be predicted to prevent bipartite D-box receptor binding. Importantly, prometaphase substrates harbouring such mutations should still be targeted for destruction by APC/C-MCC, as the presence of multiple SLiMs permit Cdc20 D-box receptor binding while the MCC is present and this site is positioned away from APC10. This could be a cleaner method of APC/C mode identification as it does not require the use of drugs, knockdowns or modifications to the APC/C itself.

With a short D-box, securin is targeted for destruction albeit not extensively and late in the cell cycle. This destruction requires the FxxF motif as well as the KEN motif (Figure 6.6). Interestingly, the APC/C seems to be unable to maintain levels of securin$^{\text{short D-box}}$, especially in prometaphase, because levels of this construct steadily increase constantly until the point of destruction. Taken together these results suggest that a mutation in the extended D-box, comprised of alanine substitution mutations in C-terminal hydrophilic D-box residues, makes this construct a significantly worse substrate for the APC/C and, contradictory to the initial hypothesis, a shorter D-box in securin actually prevents prometaphase destruction as levels increase in prometaphase as translation exceeds destruction. These points are further emphasised in experiments where treatment with reversine, which prevents MCC formation, increased the extent of securin$^{\text{short D-box}}$ destruction (Figure 6.10) as well as the data in Figure 6.9 which shows that securin$^{\text{short D-box}}$ is targeted an hour later than free cyclin B1.

Even after treatment with reversine, the FxxF motif is absolutely required for the destruction of securin$^{\text{short D-box}}$ (Figure 6.10). This is interesting because destruction by non-MCC bound APC/C (which should be occurring after reversine treatment) should not require non-degron motifs as only D-boxes are required. There are instances where these SLiMs play a role in destruction by the bipartite D-box receptor, for example Barford et al. used cryo-EM to find that cyclin A2 has two different binding modes to APC/C$^{\text{Cdc20}}$, both of which can use KEN and/or ABBA motifs[20]. Interestingly, the use of these motifs are not essential for destruction as removing both of them had no effect on APC/C$^{\text{Cdc20}}$ mediated destruction. I predict that

binding of the FxxF and KEN motifs, to Cdc20, allow the D-box of securin$^{short\ D\text{-}box}$ to bind to the bipartite D-box receptor in a way where C-terminal hydrophilic residues more downstream than positions 8-10, likely 11-13 which are also hydrophilic (Figure 6.4C) permit APC10 binding. Binding in this way would likely be less efficient, accounting for the reduced destruction dynamics, but also explain how it can engage the bipartite D-box receptor in a way which may require additional SLiMs. This theory does not suggest why securin$^{short\ D\text{-}box}$ is unable to be targeted in prometaphase (Figure 6.6).

Cyclin A2 is also able to be destroyed with extended D-box mutations and co-mutating the ABBA motif also results in destruction (Figure 6.7). A number observations can be made from this dataset. Mutating both extended D-boxes of cyclin A2 only slightly reduces destruction extent compared to wildtype, and only towards the end of the experiment which is evident by the mean destruction traces diverging 6-hours post-GVBD. This timepoint also coincides with an increase in destruction extent for the cyclin A2$^{short\ D\text{-}box,\ ABBA\text{-}A}$ mutant which together suggests a shift in the mechanism of APC/C targeting potentially marking a prometaphase-metaphase transition and APC/C mode switching (APC/C^{MCC} to APC/C^{Cdc20}). If this is the case, then it is likely that an ABBA mutation has perturbed destruction by APC/C^{MCC}, resulting in this lesser destruction in prometaphase which could be expected. From 6-hours post-GVBD onwards, cyclin A2$^{short\ D\text{-}box}$ destruction begins to plateu whereas cyclin A2 continues destruction. This suggests that targeting of cyclin A2$^{short\ D\text{-}box}$ by APC/C^{Cdc20} is perturbed, in agreement with the hypothesis that mutation in the extended D-box could prevent bipartite D-box receptor binding. In contrast to the decline of cyclin A2$^{short\ D\text{-}box}$ destruction at 6-hours post GVBD, cyclin A2$^{short\ D\text{-}box,ABBA\text{-}A}$ is able to be targeted for destruction at this point, and rapidly. This suggests that a binding mode exists whereby cyclin A2$^{short\ D\text{-}box}$ is able to engage the bipartite D-box receptor when an ABBA motif is present but not when an ABBA motif is absent.

In contrast to securin$^{short\ D\text{-}box}$ and cyclin A2 $^{short\ D\text{-}box}$, cyclin B1$^{short\ D\text{-}box}$ is stabilised, regardless of PM motif presence (Figure 6.8). This adds further weight to the aforementioned suggestion, that a potential method of targeting securin$^{short\ D\text{-}box}$ using alternative SLiMs (such

as the KEN and ABBA-like FxxF motif) permits binding D-box receptor binding in a different manner. Cyclin B1 does not contain either a KEN or an ABBA-like and is therefore restricted. The PM motif appears not to permit cyclin B1 destruction in the same way the FxxF motif allows for securin destruction in this system. A follow-up experiment to test this hypothesis would be to insert an FxxF motif into the N-terminus of cyclin B1$^{\text{short D-box}}$ at a similar position relative to the D-box of securin to see if this rescues cyclin B1$^{\text{short D-box}}$ destruction. The alignment of substrate D-boxes (Figure 6.4C) show that the substrates which do tolerate short D-box mutations (cyclin A2 and securin) have extended uninterrupted sections of C-terminal hydrophilic amino acids which could suggest that more downstream residues could be used for APC10 binding as described earlier. Contrary to this, cyclin B1, which cannot tolerate short D-box mutations, has a hydrophobic valine in position 11. This could indicate that this D-box is much more restricted in the way in which it can bind to APC10 and downstream hydrophilic residues are unable to compensate for mutations in the extended D-box, resulting in stabilisation. Mutating the valine in position 11 of the cyclin B1 D-box to a hydrophilic amino acid such as asparagine could allow for less restriction in terms of APC10 binding and allow for it's destruction.

This chapter has highlighted that differentiating the mode of APC/C responsible for substrate targeting is difficult in oocytes. APC/C subunit knockdown seems to require extensive lengths of time and has significant impacts on the cell cycle which makes this line of experimentation difficult. Mutating residues which were thought to be able to distinguish between the bipartite D-box receptor mode of targeting versus a prometaphase mode of targeting yielded contradictory results. Therefore, to better answer the question of 'what form is the APC/C in to target free cyclin B1 using the PM motif" a few further techniques could be used. Firstly, an indication as to precisely when the spindle assembly checkpoint begins to diminish would be useful. A potential 'SAC sensor' could be produced whereby a split-GFP type system could be used to produce a signal upon MCC binding which then reduces as MCC disassociates, while not producing a signal when not bound. This could be achieved by tagging APC/C and MCC components which have been shown to tolerate fluorescent protein fusions, with half fluorophores which produce a signal in proximity. Potential candidates for this could be the

APC/C core component APC8 and MCC component MAD2. This would allow us to determine the extent of APC/C inhibition when the initiation of free cyclin B1 destruction occurs. Another method of study would be to find a way to mutate the D-box binding site of either the $Cdc20^{MCC}$ or $Cdc20^{APC/C}$ to see which D-box is responsible for free cyclin B1 destruction. Unfortunately, there seems to be no way to accurately differentiate the two coactivators with strong controls.

Chapter 7 – Discussion

The data throughout this thesis provides insight into APC/C substrate targeting in mouse oocyte meiosis I, as well as insight into the roles of some other cell cycle proteins. The APC/C is clearly a highly dynamic complex, with strong substrate ordering capabilities. However, even where APC/C subunits or activators are knocked down, while substrate ordering may be dysregulated, this is tolerated and the complex still directs destruction. Indeed, even when substrates have mutations in extended D-box residues, known to be important for targeting by the canonical bipartite D-box receptor, the APC/C still finds a way to tag them for ubiquitylation. This highlights that the APC/C is determined to target substrates, precisely if possible, but regardless if not. This was beautifully summed up in the title of an important 2006 review by Jan-Michael Peters 'The anaphase-promoting complex/cyclosome: a machine designed to destroy'[205].

That there are so many routes to destruction, and that even a perturbed system will attempt a work around, highlights the absolutely essential role of this complex. However this, and the studies contained within my thesis also highlights the difficulties of exploring protein behaviours cell cycle proteins regulation. This is difficult in all cell types, and perhaps especially in oocytes. These cell cycle proteins are highly interconnected. Simple protein knockdowns or expression of substrates can have dramatic adverse effects. One example of this is the knockdown of BubR1 in Section 4.2, which from our understanding of checkpoint activity, would almost certainly be expected to result in a premature anaphase and shorter prometaphase. Instead, as suggested by Homer et al., a BubR1 knockdown results in low Cdh1 levels in prophase, resulting in an increase in securin, preventing a premature anaphase. This level of interdependence between cell cycle proteins will not be restricted to BubR1, but the vast majority. Careful considerations must also be made when studying of cell cycle proteins by expressing exogenous forms in live cells. Primarily how adverse effects arising from overexpression can be reduced. In this thesis, I utilised a Y170A mutation in fluorescent cyclin B1 in all cyclin B1 constructs to prevent CDK1 binding and minimise any changes in CDK1 activity, attempting to separate cell cycle driving activity from our aim to

report destruction timings. There is however always a careful balance between preventing off-target effects while still accurately representing endogenous proteins.

There are also many difficulties associated with conducting experiments in live mammalian oocytes. Primarily because of the number of healthy, mature oocytes that we may collect both practically and ethically. Then beyond this the technical demands manipulating and microinjecting oocytes, often coupled with long culture or time-lapse imaging periods. The use of this cell type limits us in the range of experimentation we can conduct. Experimentation in mitotic cell lines can involve the production of cells stably expressing fluorescent reporters, avoiding the difficulty of microinjection and low n numbers. Additionally, the ability to obtain high amounts of cell lysates for immunoprecipitation experiments in mitotic cell lines for example provides great insight into protein-protein interactions which simply isn't feasible in oocytes. While experimentation in this cell type is challenging, oocytes are nevertheless an incredibly useful model with which to explore cell cycle regulation in prometaphase. The prometaphase I stage of mouse oocyte meiosis lasts approximately 8-12 hours, compared to mitotic prometaphase length which completes in a matter of minutes. This provides a significant amount of time to monitor chromosome alignment and the control of proteins involved. Additionally, microinjection allows for expression of proteins in live oocytes at consistent levels, and this is truly a single cell technique. Each cell can be handled individually and oocytes are highly synchronous.

An assay used throughout this thesis is to monitor the timing and extent of APC/C substrate destruction in live oocytes, comparing differences between cyclin B1 and a PM-mutant cyclin B1 proteins. Destruction was recorded in various in contexts, designed to understand how targeting is governed I employed protein knockdowns, protein fusions, and other mutations to test how dynamics deviate between cyclin B1 and cyclin $B1^{PM\text{-}A}$. This is a robust assay and there is still much more to learn by this method.

7.1 What role does the PM-motif play in cyclin B1 destruction?

This thesis initially set out to validate previous findings that a region located in the N-terminal helix of cyclin B1, named the PM motif, permits destruction in oocytes in prometaphase I. Throughout this thesis, I utilise an alanine-substitution mutation of the PM motif which validates this finding and confirms that this motif, and not another region of cyclin B1 permits destruction at this time.

Because of the ability of the PM motif to permit destruction in a different way, in terms of both timing and extent, this motif fits the definition of a SLiM. Importantly, the PM motif does not permit any destruction capabilities alone, as only perturbation of the D-box (specifically the extended D-box) results in stabilisation. This not only confirms that the PM motif is a SLiM, but also verifies that it cannot be defined as a degron. Importantly, my data highlights that PM-motif mediated destruction and the non-PM-motif mediated destruction of cyclin B1 are through distinct mechanisms. This is of course shown by the fact that they are destroyed at different times but also that performing the same modifications to these constructs (thus the only difference being the presence or absence of a PM motif) can result in vastly different dynamics. For instance the N-terminal fusion of a BIOID2 protein results in very rapid destruction of the BIOID2-cyclin B1^{PM-A} construct but less extensive destruction of BIOID2-cyclin B1.

Substrate SLiMs are known to bind to the coactivator of the APC/C to either permit (in which case they can be referred to as a degron) or enhance destruction dynamics. Enhancement of destruction dynamics can be by more than one action, for example by localisation or by increased affinity, or related to this, by outcompeting another protein for binding. My data shows that when using proTAME, a competitive inhibitor for both APC/C coactivators (Cdc20 and Cdh1), cyclin B1 is completely stabilised. Interestingly, data from our group previously showed that a truncated cyclin B1, with a PM motif present, is still a destruction target following an extensive Cdc20 knockdown protocol (though notably destruction is perturbed)[160]. In comparison, a cyclin B1 truncation lacking the N-terminal helix (and therefore the PM motif) is stabilised. It is possible that in the event of Cdc20 knockdown,

Cdh1 instead takes its place as the APC/C coactivator at this timepoint. Taken together, this may suggest that the PM motif can allow for (or enhance) the destruction of cyclin B1 by APC/C-Cdh1 activity as well as APC/C-Cdc20. More thorough investigation would be required to validate this, and this would be technically very difficult. Cdc20 and Cdh1 seem to have the propensity to replace one another if reduced (as is their natural cyclical action), and co-knockdown will cause complete cell cycle arrest.

Considering that the PM motif is a SLiM, we can use precedent in the literature to suggest how the PM motif may be permitting its role, following the 'rules' of other SLiMs. This must be caveated by noting that the vast majority of literature in this field is conducted using recombinant proteins or studies in mitotic cell lines and thus these motifs may play different roles in meiosis. However, it is highly likely that mechanisms are transferable between mitosis and meiosis. It is well established that SLiMs promote protein-protein interactions. This does likely indicate that the PM motif is binding to a partner site within the oocytes proteome in prometaphase. Furthermore, this is a site that cyclin b1 without a PM motif will likely have a reduced or no affinity for. Second, we know that SLiMs on APC/C substrates specifically permit association with an APC/C coactivator to regulate destruction. Therefore, it is highly likely that the PM motif is permitting destruction of cyclin B1 in prometaphase by association with the APC/C, and specifically with the coactivator. While the investigations around the PM-like motif of BubR1 in this thesis did not yield any conclusive insight into whether a PM motif binding site exists on Cdc20, the PM-like motif of BubR1 does bear striking resemblance to the PM-motif terms of structure, and sequence. Additionally, this Cdc20 interaction hypothesis is aided by the fact that the PM-like motif of BubR1 is surface exposed and appears to make contact with Cdc20.

I have shown that localisation plays an incredibly important role in PM motif mediated prometaphase I targeting of cyclin B1. Tagging cyclin B1 to the cell membrane completely prevented any prometaphase I targeting. And utilising a CKS1-fusion, predicted to localise cyclin B1 to the APC/C, resulted in very early destruction. Interestingly, a CKS1-fusion of a cyclin B1 construct lacking the PM motif (cyclin $B1^{PM\text{-}A}$-CKS1) is targeted for destruction in

prometaphase at the exact timing of a non-CKS1 fused cyclin B1 with a PM motif. This may suggest that the PM motif harbours localisation roles either directly or indirectly via association with a chaperone protein, potentially even CKS. Strikingly, as the construct harbouring both CKS1 and PM-motif is destroyed very early. This could suggest that these 'localisation' factors are additive. Alternatively, the CKS1 protein might be providing direction, while the PM motif is increasing affinity or docking via particular binding mode which permits destruction (which itself could be described as a method of finely tuned localisation). Though in this latter suggestion, it is curious then that cyclin $B1^{PM\text{-}A}$-CKS1 destruction takes place so perfectly in time with a more wild-type cyclin B1. If the PM motif does exert its effect due to a localisation role, then why do we not see significant differences in localisation between cyclin B1 and cyclin $B1^{PM\text{-}A}$, even with confocal microscopy?[160] It could be that PM directed localisation represents such a minor, but very dynamic population that is constantly being replaced as it is ubiquitylated and destroyed. This could be referred to as a "plug hole" effect whereby destruction of cyclin B1 using its PM motif occurs near the alignment barrel but is near immediately replaced by other cyclin B1 proteins in the cytoplasm. This would be difficult to detect by our method. Or that APC/C expression is widespread across the spindle zone in oocytes and cyclin B1 destruction occurs all across the cytoplasm.

7.2 Which form of APC/C is targeting free cyclin B1?

Nearly every experiment in this thesis aimed to answer this question in one way or another. From protein-protein interaction assays such as membrane-incorporation colocalization analysis (chapter 3) and biotin proximity ligation assays (chapter 5) to MCC component knockdown (chapter 4) and bipartite D-box receptor disruption (chapter 6). Indeed, answering this question is a significant undertaking and there is a huge complexity brought about by the profound interconnections between cell cycle regulation, substrate targeting and APC/C activity.

In answer to this question, I propose that a fraction of non-MCC bound APC/C is responsible for targeting cyclin B1 in prometaphase I. This is based on current understandings regarding

of how cyclin A2 is targeted for destruction in prometaphase. As discussed throughout this thesis, cyclin A2 is targeted by the APC/C-MCC in prometaphase on account of its multiple SLiMs which compete with BubR1 for coactivator binding, inducing a conformational change to the MCC and permitting the ubiquitination of cyclin A2. Many studies have shown that the presence of multiple SLiMS are essential for this, likely for increasing binding affinity so that cyclin A2 APC/C interactions are favoured over the BubR1 pseudosubstrate inhibitor[20,157]. Remarkably however, cyclin B1^{PM-A}-CKS1 is targeted for destruction in prometaphase I with nearly identical timings to that of cyclin B1. The cyclin B1^{PM-A}-CKS1 construct is thought to now only contain a D-box motif and thus will have likely have too low a binding affinity to displace BubR1 for destruction via APC/C-MCC binding. If a D-box alone was sufficient to displace BubR1 for coactivator binding, nearly all APC/C substrates would be targeted by the APC/C-MCC in prometaphase, however they are clearly not. Importantly, CKS1 is not a SLiM, and while it is known to enhance localisation of substrates to the APC/C, it is not predicted to bind Cdc20 and be responsible for BubR1 displacement. The fact that cyclin B1^{PM-A}-CKS1 can be targeted in prometaphase I suggests it is being targeted by non-MCC bound APC/C (it only has a D-Box), but it is now favoured over non-CKS bound, as it is effectively in the right place at the right time to take advantage of any available MCC free APC/C.

This may be evidenced by published data from our group where oocytes incubated in 100 nM nocodozole supplemented media destroy some free-cyclin B1(albeit perturbed)[160]. Cyclin B1^{PM-A} on the other hand was completely stabilised. As nocodozole is known to induce a constitutively active SAC, it is predicted that high concentrations of MCC are produced upon treatment. Therefore, one would expect that this cyclin B1 destruction is mediated by APC/C-MCC. Importantly however, this data showed that cyclin B1 destruction was inhibited by higher concentrations of nocodozole, in an apparent dose-dependent stabilisation. This could suggest that at lower concentrations of nocodozole, cyclin B1 utilising its PM motif, is still able to occupy reduced numbers of non-MCC bound APC/C as they will still become available due to the constant turnover of MCC complexes. At higher concentrations all APC/C complexes are more likely to be completely saturated with MCC, resulting in stabilisation. Further experimentation combining multiple techniques used in this thesis could be used to

investigate this further. First, utilising a membrane localised cyclin A2 construct to determine whether APC/C-MCC mediated targeting can occur at the cortex. If this substrate can be targeted for destruction in prometaphase, then this is another strong indication that APC/C-MCC is not responsible for PM motif prometaphase destruction of cyclin B1 as I did not observe membrane localised cyclin B1 destruction in prometaphase. Second, determining the destruction profile of a cyclin A2$^{\text{short D-box,ABBA-A}}$-CKS1 construct. In my data, cyclin A2$^{\text{short D-box,ABBA-A}}$ had reduced destruction in prometaphase compared to cyclin A2 WT, but more rapid destruction in late prometaphase, suggesting this is a worse target for APC/C^{MCC} but still an efficient target for APC/C^{Cdc20}. Localising cyclin A2$^{\text{short D-box, ABBA-A}}$ to the APC/C using a CKS1 fusion may result in this more rapid period of destruction occurring earlier, again hinting at the capacity to be targeted for destruction by APC/C^{Cdc20} in prometaphase.

There is precedence for a subpopulation of non-MCC bound APC/C existing during an active SAC in oocytes. Firstly, detection and correction of erroneous kinetochore-microtubule attachments is a slow process in oocytes therefore the activity of the SAC can start to diminish before proper alignment. Second, there is evidence that mad2 localisation at kinetochores declines before chromosomes are bioriented suggesting that the SAC begins to diminish before the metaphase-anaphase transition[206]. This also ultimately highlights the need for an excess of free cyclin B1 in the oocyte during the period of chromosome alignment. By acting as a "bait" substrate for any non-MCC bound APC/C, free cyclin B1 destruction aids in to prevent premature targeting of metaphase substrates by APC/C^{Cdc20}.

7.3 What is responsible for the precise timing of initiation of cyclin B1 targeting?

This above hypothesis, that APC/C^{Cdc20} is targeting cyclin B1 for destruction in prometaphase I prompts the question as to how this uninhibited form of APC/C exists at this timepoint. Significant or unbridled APC/C^{Cdc20} activity would induce anaphase. Additionally, why does prometaphase I targeting occur at such a specific timepoint? There must be a physiological explanation as to why destruction initiates so consistently at a very similar timepoint in most oocytes. This is suggestive of an event that switches on prometaphase targeting of cyclin b1.

I propose that the initiation of cyclin B1 targeting in prometaphase I reflects the point by which the MCC has diminished to such an extent that cyclin B1 is able to bind to APC/C-Cdc20 utilising its PM motif opportunistically. As discussed throughout, Collin et al. describe SAC signalling as a rheostat as opposed to an on-off signal, on account of lessening MCC production chromosome alignment progresses[27]. Therefore, early in prometaphase vast numbers of MCCs are produced on account of severely misaligned chromosomes, and there is simply too much MCC coverage for cyclin B1 to access MCC-free APC/C complexes. As prometaphase progresses and MCC production begins to slow and diminish, I hypothesise that cyclin B1 is able to bind to APC/C^{Cdc20} before new MCC associations. Importantly, binding at this stage is now dependent on the increased binding affinity of cyclin B1 brought about by the PM motif, either by a localisation dependent role or an increase in binding affinity. When the PM motif is not present, it is possible that cyclin B1 either has reduced access to the APC/C or reduced affinity and thereby cannot compete with the speed of MCC complex associations. Even though reduced in abundance at this time point their production is still active. This theory could explain why initial destruction of cyclin B1 occurs somewhat slowly at the very early stages of destruction, but then increase as prometaphase I continues. As MCC and cyclin B1 are both looking to occupy the APC/C, the tide is turned in favour of cyclin B1 as MCC production diminishes. Indeed, when the SAC is silenced, the APC/C is capable of very rapid substrate targeting, as is seen in numerous constructs such as BIOID2-Cyclin B1^{PM-A}. A model of the balance of cyclin B1-MCC APC/C occupancy is displayed in Figure 7.1.

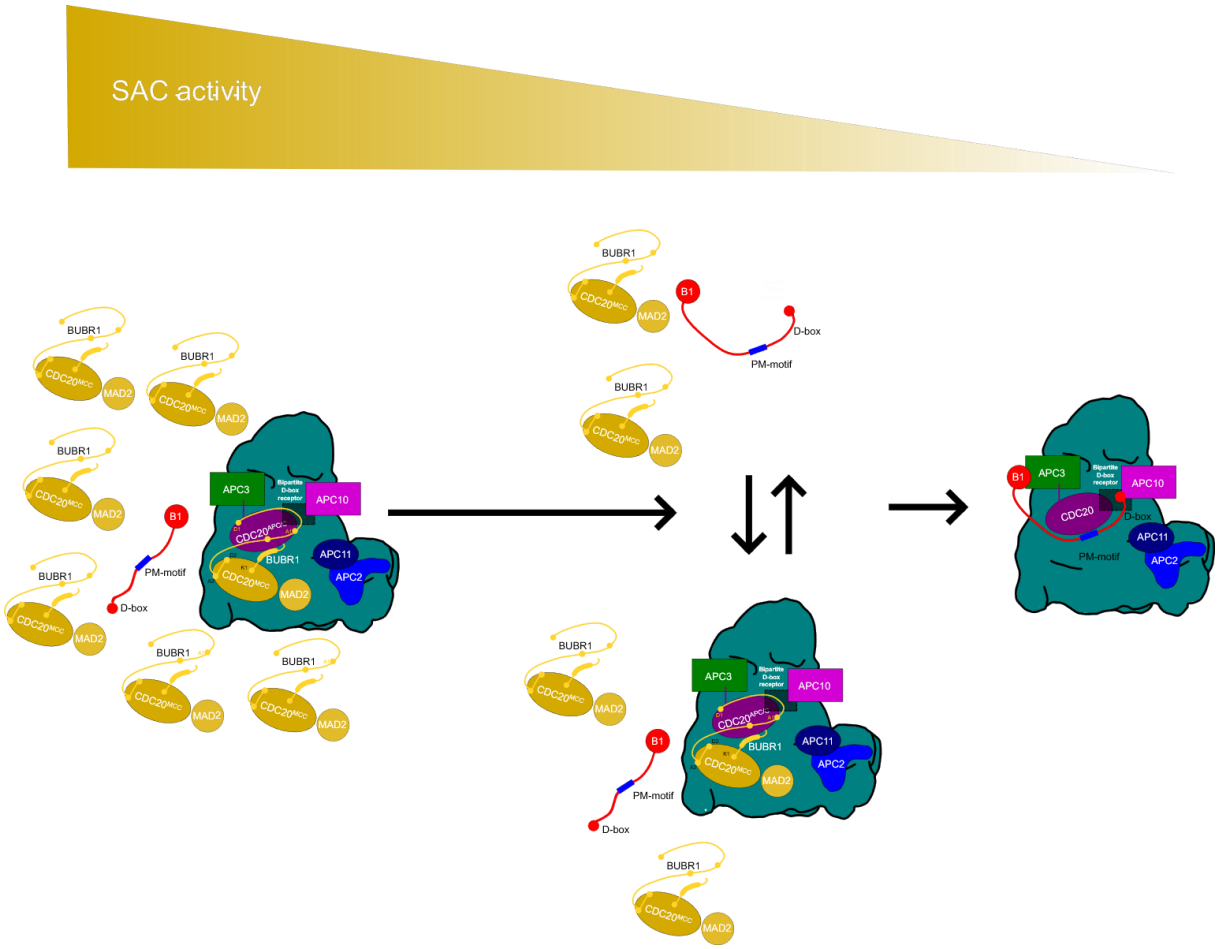

Figure 7.1. Model of cyclin B1 destruction whereby the PM motif permits cyclin B1 to associate with APC/C in between MCC associations

Early in prometaphase SAC activity is high and substantial numbers of MCC complexes are being produced on account of severely misaligned chromosomes. The MCC has a high affinity for the APC/C and is in extreme abundance. Cyclin B1 has no access to the APC/C substrate recognition module. As prometaphase progresses, MCC complex numbers decline, the MCC is less of a competitor to cyclin B1 for position on the APC/C. Thus, using its PM motif, for preferential access, cyclin B1 is targeted for destruction. Constant flux between APC/C association with cyclin B1 or MCC both maintains prometaphase and accounts for the slowly increasing extent of destruction of cyclin B1. Cyclin $B1^{PM-A}$, without a PM-motif, does not have sufficient binding affinity to outcompete the MCC at this stage or is not preferentially localised to this form of the APC/C. Importantly, as MCC still exists, many MCC complexes are still binding the APC/C, preventing the destruction of other substrates. When the MCC is near completely diminished, the APC/C is free to target all substrates, including cyclin $B1^{PM-A}$.

So why are other substrates not destroyed on account of diminishing MCC at this timepoint if the amount of uninhibited APC/C^{Cdc20} is increasing? One explanation for this could be that, given free cyclin B1 is in excess in the mouse oocyte at this point, and the PM motif may be localising cyclin B1 to the APC/C^{Cdc20}, it outcompetes most other substrates for APC/C^{Cdc20} access. A second explanation could be that increased binding affinity brought about by the PM motif. Indeed, the PM motif is a SLiM and is highly likely to contribute to the binding affinity of cyclin B1.

Evidence for either situation is provided by experiments expressing cyclin B1 alongside securin$^{shortD\text{-}box}$. Expression of both proteins together resulted in destruction of securin$^{short\ D\text{-}box}$ approximately half an hour later than securin$^{short\ D\text{-}box}$ expressed alone. While in the same context cyclin B1 destruction was unperturbed by the presence of additional securin. Cyclin B1 is the preferred substrate, and its presence delayed the destruction of another substrate. If this is the case, then it would be expected that eventually overexpression of cyclin B1 would result in prometaphase I arrest. This is indeed the case when expression of cyclin B1 is too high in mouse oocytes, however it is important not to draw too many conclusions from this, overloading APC/C could be have many off-target effects.

The late destruction timing of membrane localised cyclin B1 fits this model. The membrane localisation tag essentially fixes cyclin B1 to one position in the oocyte. Therefore, it is unable to migrate to the APC/C during prometaphase and access the APC/C during the flux of MCC associations and disassociations. Here these constructs are forced to await APC/C^{Cdc20} radiating outwards from the spindle zone and reach the cortex. Interestingly the PM motif still has an impact in this context as destruction differences between these constructs still exist. Again, likely reflecting the increased binding affinity brought about by PM motif presence (Figure 7.2).

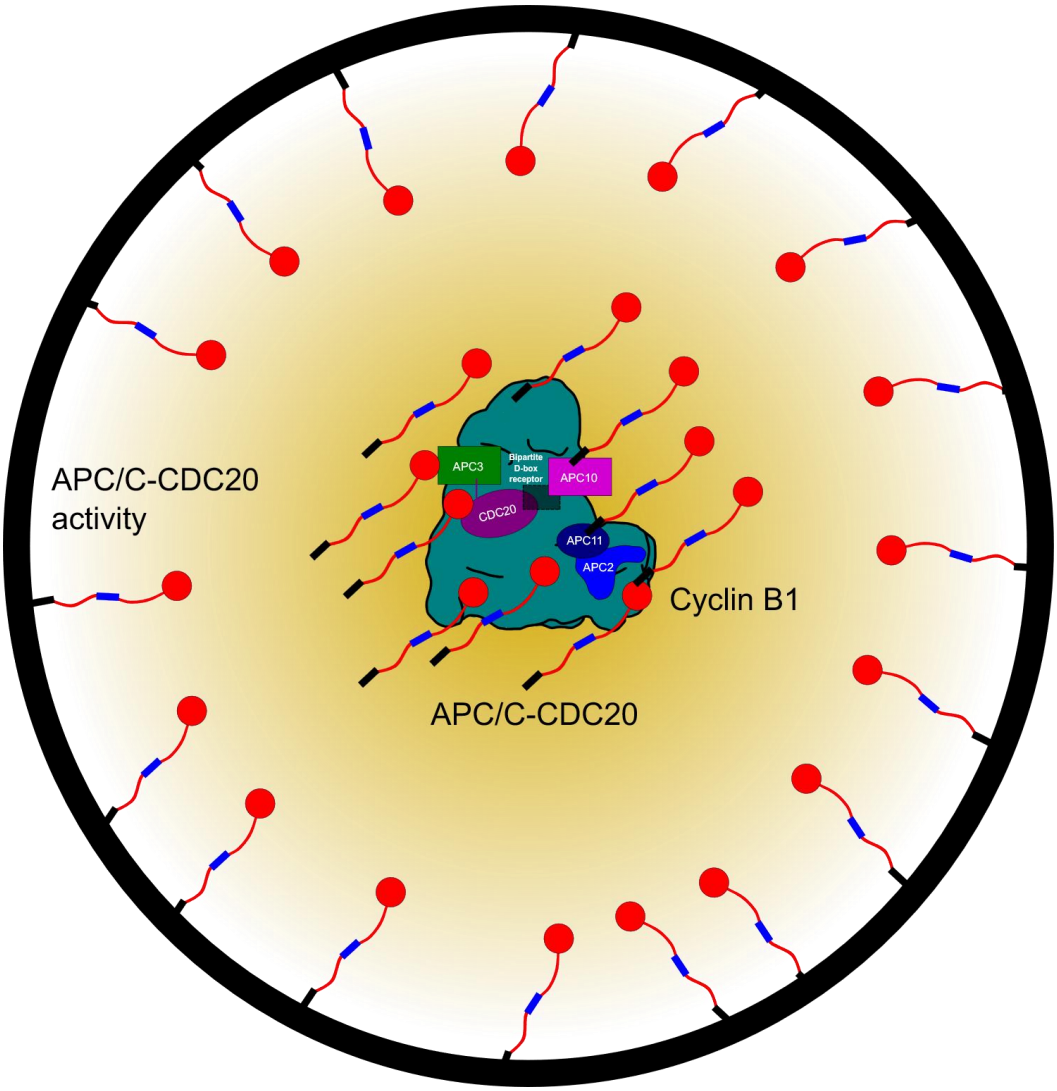

Figure 7.2. Model describing how APC/C-Cdc20 activity radiating outwards from the spindle results in membrane localised cyclin B1 destruction at a late time point.

In this model, non-membrane localised cyclin B1 (red; PM-motif in blue) is able to localise and associate with APC/C-Cdc20 in between fluctuations of MCC association and disassociations. After the SAC diminishes, APC/C activity radiates outwards from the spindle zone. Membrane localised cyclin B1 constructs are fixed in place and forced to await APC/C activity migrating outwards towards the cortex resulting in destruction in a late timepoint.

Potentially alongside the model whereby cyclin B1 is able to associate with APC/C in between MCC association and disassociation, cyclin B1 may bind to an increasing amount of non-MCC incorporated Cdc20 (as opposed to the APC/C) using its PM motif, which could be predicted to exist as the SAC begins to diminish in late prometaphase (Figure 7.3). This “free Cdc20” could originate from MCC complexes which are being turned over or are present as APC/C coactivators primed for association. This could in theory permit the incorporation of cyclin B1 into the APC/C as the coactivator binds. Again, membrane localisation would prevent this binding to Cdc20 on account of the inability to migrate to free Cdc20 and a CKS1-fusion would likely localise cyclin B1 to regions of high Cdc20 concentration (across the spindle zone) resulting in very early destruction. This could also explain the observation that a bubR1 knockdown results in early destruction of cyclin $B1^{PM\text{-}A}$. Here, we have reduced competition for Cdc20, allowing even the lower affinity cyclin $B1^{PM\text{-}A}$ construct to bind Cdc20 early and be destroyed. If this hypothesis is correct in regards to bubR1 knockdown effects, other APC/C substrates will also be destroyed early. There may be evidence of this, as discussed in Section 4.3, Homer et al. reports that in oocytes with reduced levels of BubR1, Cdh1 is turned over by the APC/C^{Cdc20} as at a much greater rate[183]. Therefore, other substrates could be being targeted in during this knockdown and it would be interesting to explore the destruction of later APC/C substrates in this context (for example shugoshin-2).

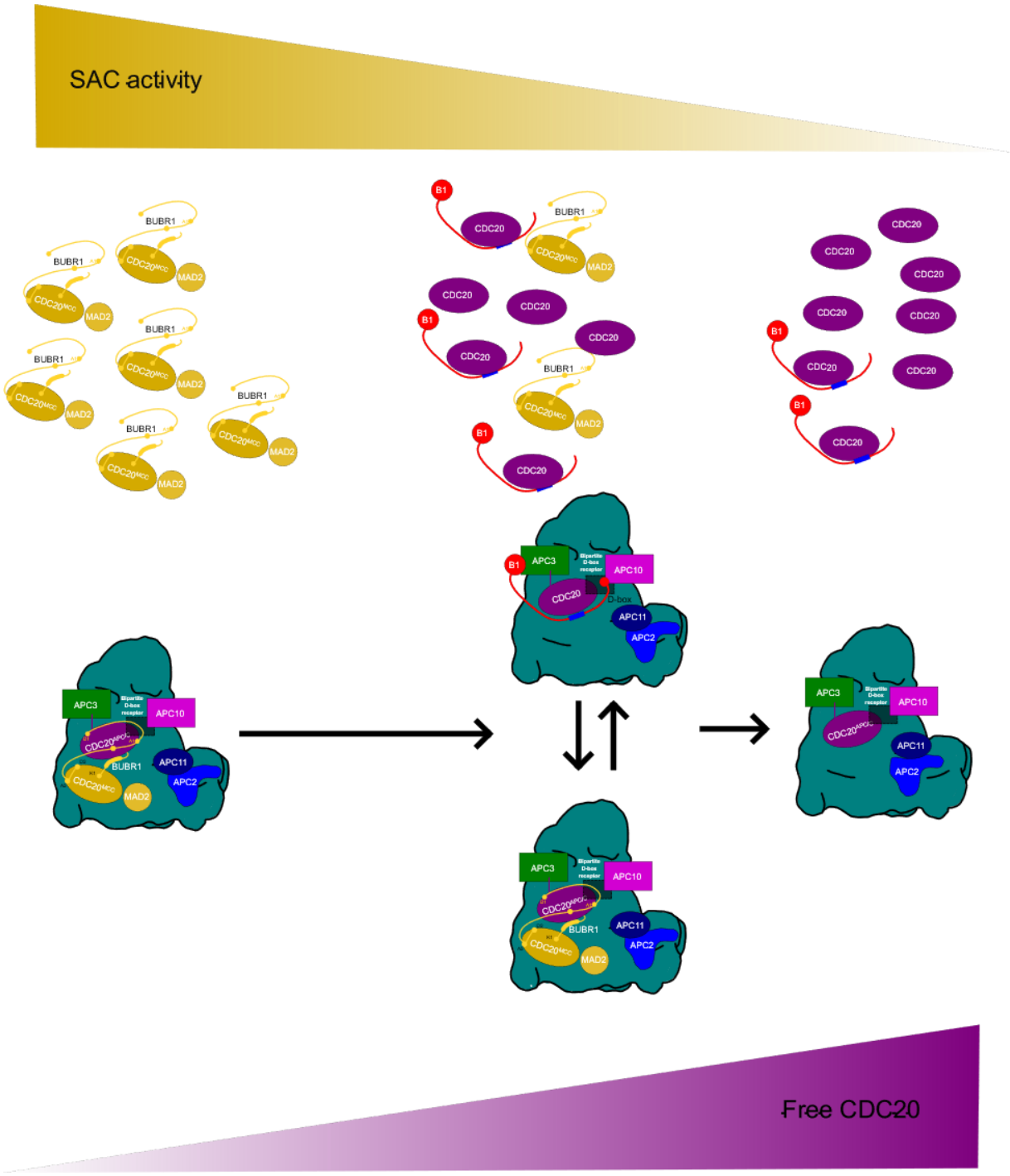

Figure 7.3. Cdc20 centric model of cyclin B1 destruction over the course of meiosis I

Due to severe chromosome misalignment early in prometaphase, the activity of the SAC is strong, resulting in a high amount of MCC complexes in the cell, primed to associate with APC/C-Cdc20 and prevent the destruction of substrates such as cyclin B1. As the SAC diminishes over the course of MI, the ratio between MCC and non-MCC associated Cdc20 increases. Due to the potential higher affinity for Cdc20 that the PM motif provides cyclin B1,

cyclin B1 is able to bind to free Cdc20 which is then incorporated into the APC/C complex to permit its prometaphase I destruction. Cyclin $B1^{PM-A}$, without a PM motif, is unable to compete with BubR1 for Cdc20 binding due to a lower affinity. As prometaphase continues to progress, the MCC is no longer produced and the APC/C is free to target all substrates at this point.

These hypotheses satisfy the literatures current understanding that cyclin B1 cannot be targeted by the APC/C-MCC, while still providing an explanation for prometaphase I targeting of cyclin B1 in mouse oocytes. This mechanism would be difficult to determine in mitosis. Free cyclin B1 is a rare species as CDK1 is found in excess in mitotic cell lines[161]. Additionally, the period over which dual populations of APC/C-MCC and APC/C-Cdc20 exist would be very rapid compared to this period of time in meiosis.

It was reasonable to assume from previous data that the PM motif may allow targeting by the APC/C-MCC. Destruction occurs during the chromosome alignment stage when the SAC is active, and some substrates are known to be destroyed in this context (for example cyclin A2). However, this suggestion has thus far been difficult to explore, and my data contradicts this. One way to better understand whether this is the case would be the regular use of cyclin A2 as an additional control in these experiments, as a substrate shown extensively to be targeted by APC/C-MCC. However, due to the difficult nature of these experiments, inclusion of this control would add to the complexity of this line of experimentation.

7.4 What do CKS1 fusion constructs tell us about PM motif processivity?

Through my studies I utilised various protein fusion experiments to deduce more information regarding how cyclin B1 constructs are targeted by the APC/C. One of the more interesting lines of experiments was that of CKS1-linked constructs. CKS1 fusion was used as a mechanism to localise cyclin B1± PM motif to the APC/C to see if destruction could be permitted. CKS proteins are known to bind to phosphorylated APC3 to localise substrates to

the APC/C[177]. These chaperones have been shown to bind to CDK proteins and to our knowledge not cyclin proteins themselves. Fusing CKS1 to cyclin B1 is likely an unnatural construct but provides a unique opportunity learn about a protein by placing it in new context. CKS1 association resulted in very early cyclin B1 destruction where the PM motif was present (cyclin B1-CKS1), and early destruction when the PM motif was not present (cyclin $B1^{PM\text{-}A}$-CKS1 – now destroyed with timings more similar to cyclin B1). Assuming a CKS1 fusion is localising each protein mutant to APC3, a few hypotheses can be drawn from this.

Firstly, I suggest that the cyclin B1-CKS1 constructs will likely dock to the APC/C and await a point in which they can be destroyed, assuming a CKS1 fusion is working in the intended way. The timing of destruction for cyclin B1, even while docked to the APC/C is highly dependent on the PM motif. This is an incredibly interesting observation as it provides further evidence that PM motif dependent prometaphase I destruction is not exclusively due to a difference in localisation. Additionally, as discussed earlier, the prometaphase I destruction of cyclin $B1^{PM\text{-}A}$-CKS1 suggests that this destruction is mediated by APC/C^{Cdc20} and not APC/C^{MCC} because a D-box alone will likely not be able to compete with BubR1 for Cdc20 binding. Therefore, I propose that in this instance, PM-motif or CKS1-fusion, localises cyclin B1 constructs to the APC/C^{MCC} and these proteins must wait for MCC disassociation to be destroyed. We know that MCC is rapidly turned over in a mechanism which allows for the efficient monitoring of kinetochore-microtubule attachments. Thus, CKS1-fused cyclin B1 constructs could be associated with the APC/C-MCC but the PM-motif allows a rapid binding to the non-MCC bound APC/C during the refractory period between MCC switching. Without a PM motif, the binding affinity is not high enough to permit binding in this short time period (Figure 7.4).

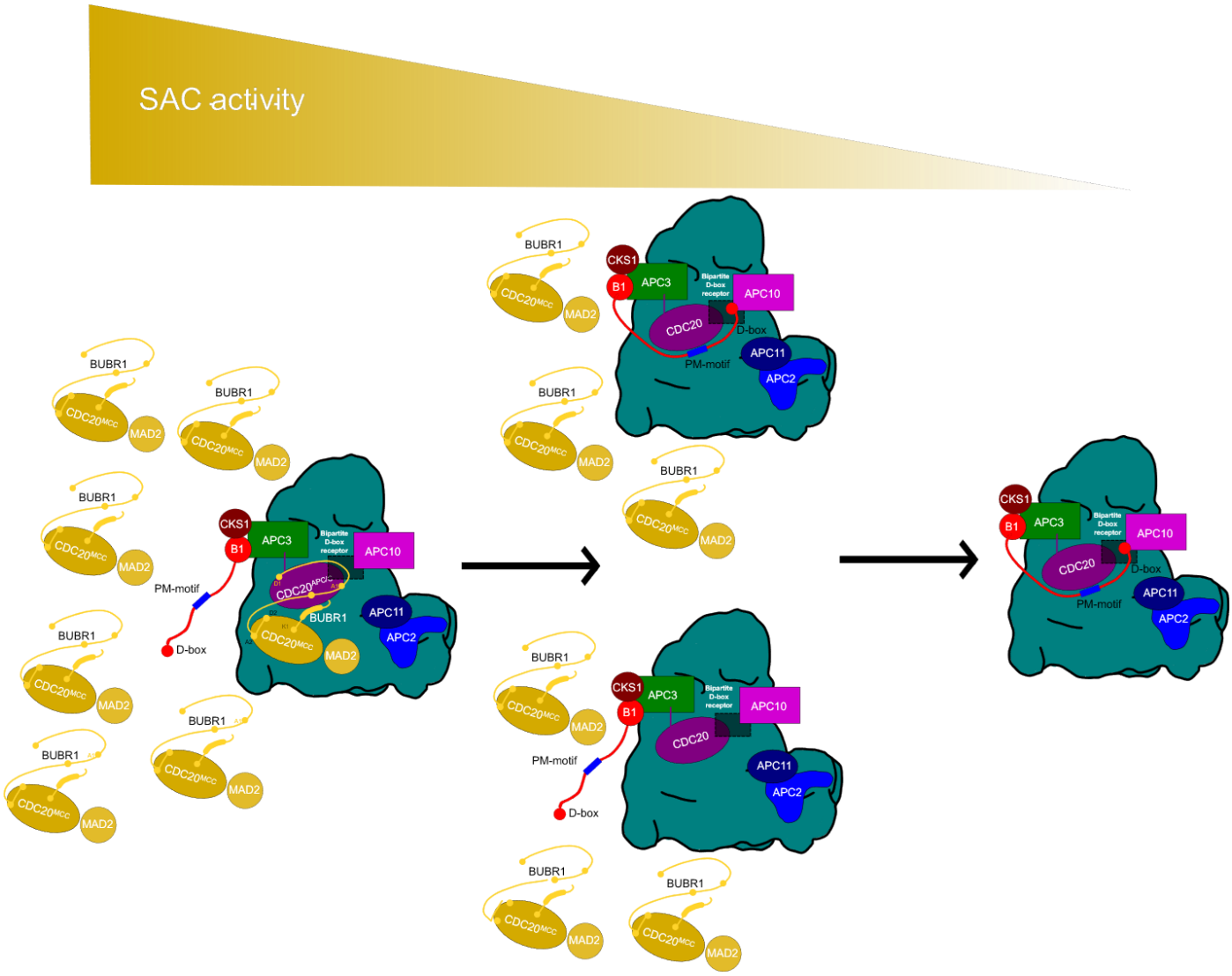

Figure 7.4 - Model of cyclin B1-CKS1 destruction dynamics.

CKS1 proteins dock substrates to phosphorylated APC3. Early in prometaphase, the amount of MCC in the cell his high due to misaligned chromosomes. Even docked to the APC/C, cyclin B1 constructs cannot associate with the APC/C due to the rapid MCC association with the APC/C at this timepoint due to the abundance of complexes. As MCCs diminish, CKS1-cyclin B1 with its PM motif is able to be targeted for destruction. Without a PM-motif, CKS1-cyclin $B1^{PM\text{-}A}$ has reduced binding affinity, but does have advantage over non CKS1 cyclin B1-PM-A in that it is highly concentrate in a preferential location. Still CKS1 fused Cyclin $B1^{PM\text{-}A}$must await further SAC decline to be targeted, but not to the same extent as a non-CKS1 protein. When the SAC is nearly completely diminished, the majority of APC/C is free to target other substrates.

It would be interesting to follow the destruction dynamics of CKS1 fused cyclin B1 during a nocodazole treatment. Ultimately, to determine whether cyclin $B1^{PM-A}$-CKS1 is a target for destruction in a dose dependent manner. Cyclin $B1^{PM-A}$ is not destroyed in low dose nocodozole, however localising this form of cyclin $B1^{PM-A}$-CKS1 to the APC/C may still offer an advantage[160].

A striking observation in this line of experimentation is the unique localisation pattern of the cyclin B1-CKS1 construct. I strongly suggest that this form of cyclin B1 is localising to mTOCs, as indicated by consistent co-localisation with TACC3 and the observation that often, puncta migrates from the oocyte cortex to the GV prior to GVBD. This could be further proof that the APC/C-localisation capabilities of CKS1 fusion is indeed working; The APC/C is known to localise to centrosomes and the spindle in mitosis[207]. Why this does not occur for the PM mutant cyclin B1 is unknown. What is clear however is that this localisation is dependent on the PM motif. If the PM motif is contributing to the binding affinity of cyclinB1 for APC/C binding, the addition of a CKS1 fusion boosting localisation, has had a dramatic effect.

7.4 Future direction of this project

In order to determine how the PM motif is mediating cyclin B1 destruction in prometaphase I of oocyte meiosis, a full characterisation of the interactome of cyclin B1 and cyclin $B1^{PM-A}$ would be a substantial step forward. Indeed, multiple lines of experimentation in this thesis set out to achieve this. I have performed preliminary experiments to show the feasibility of utilising biotin proximity ligation assays in mouse oocytes to determine the interactome of cyclin B1. I have taken this further to produce a bank of lysates for future mass-spec analysis and identification of different interaction partners of cyclin B1 and specifically the PM motif. Work is currently underway to have these samples analysed and we are eager to see these results.

I have also designed and outsourced the production of recombinant proteins of mutant cyclin B1 peptides; N90-NTH±PM motif constructs with purification tags. I have also conducted the necessary controls to confirm that these tags to not impair destruction timing differences in oocytes. This would allow our group to perform pulldown experiments to determine the interactome of the PM motif in an alternative way to biotin proximity ligation. Ultimately this would provide further validation of the findings of a successful biotin proximity ligation assay. These recombinant proteins can be used with mitotic lysates first, to explore the roles of PM motif cyclin B1 destruction in mitosis and will be informative for meiosis before committing to oocyte lysates.

In my opinion, further exploration in this project requires the regular use of substrates which are known to be targeted in prometaphase, such as cyclin A2. This would allow us to better compare the destruction of substrates between APC/C and APC/C^{MCC}. Additionally, alternative routes of protein knockdown need to be used to have more potent effects than morpholino knockdowns which are both time consuming and difficult to quantify. The TRIM-AWAY approach developed by the Schuh group appears to be a potential solution to this and should become routine in mammalian oocyte research groups[204]. This has the advantage of rapid knockdown (~10-20 minutes) reducing the need of long MO incubations and gives the advantage of allowing oocytes to resume meiosis I without knocking down these proteins at GV stage.

Full characterisation of the localisation of cell cycle proteins at different stages of meiosis would provide profound insight as to the regulation of these proteins over meiosis I. This project would benefit from such knowledge, for example analysing the colocalization of various cyclin B1 constructs with APC/C subunits, or the extent of MCC coverage over the oocyte. Some of this was attempted but we expect we need to move into higher resolution (even single molecule) microscopy. Another project in our lab underway is performing significant immunofluorescence antibody validation in oocytes to explore expression profiles, and determine differences between healthy and less competent healthy oocytes.

Additionally, this project is determining the feasibility of Imaging Mass Cytometry to improve throughput protein expression studies and provide wider context of protein networks.

PM motif mediated destruction of cyclin B1 is clearly an important regulatory pathway for controlling the levels of cyclin B1 in mouse oocyte meiosis. Considering the well documented observations that cyclin B1 is overexpressed in many cancers such as breast and cervical, the PM-motif mediated cyclin B1 destruction mechanism may have onco-preventative roles. Or, this mechanism may be perturbed, increasing the likelihood of cancers occurring. An ongoing project in our lab has set out to determine whether this mechanism of cyclin B1 destruction occurs in cancer cells and yielded several interesting observations thus far.

7.5 Final remarks

Considering the prevalence of miscarriages and fertility decline with age in humans, alongside the fact that couples are increasingly waiting until later in life to conceive, the need to investigate the mechanisms responsible for these high rates will only increase with time. In addition, infertility is not just a human health concern, but one that threatens food security and our ability to protect endangered mammals. Understanding the mechanisms behind aneuploidy prevention is a significant step forward in our understanding of cell cycle regulation and how healthy oocytes are made.

This thesis highlights the need for more cell cycle research in this unique cell type. The literature surrounding cell cycle regulation, APC/C processivity and substrate targeting is incredibly mitosis centric. Mitotic regulation occurs in all other cell types except gametes and has profound roles in cancers. However, exploring how cell cycle proteins are differentially regulated or targeted between mitosis and meiosis, viewing behaviours in different contexts, contributes to our overall understanding of cell division and its regulation as a whole.

Exploring cell cycle proteins in oocytes is incredibly difficult, an experimental ideal would be that we have huge amounts of protein from a large number of model organisms. But this is unsustainable and unethical. I have verified the feasibility of biotin proximity ligation in

oocytes, and to our understanding are the first group to do this in this context. If this method does indeed work, this could become a more routine method of exploring protein-protein interactions in oocytes.

In this thesis, I have provided further mechanistic insight into the regulation of cyclin B1 in mouse oocyte meiosis which not only increases our understanding of cell cycle regulation as a whole, but also aneuploidy prevention mechanisms in this unique cell type.

Appendix I: Abbreviations

APC/C	Anaphase Promoting Complex/Cyclosome
CFP	Cerulean Fluorescent Protein
GVBD	Germinal Vesicle Breakdown
IBMX	3-isobutyl-1-methyl xanthine
MCC	Mitotic Checkpoint Complex
MI	Meiosis I
MII	Meiosis II
MO	Morpholino
MTOC	Microtubule Organising Centre
NTH	N-Terminal Helix
PB1	First Polar Body
VFP	Venus Fluorescent Protein
WT	wildtype

Appendix II: List of cRNA constructs and resulting protein sequences

Cyclin B1

Y170A mutation is highlighted in yellow.

MALRVTRNSKINAENKAKINMAGAKRVPTAPAATSKPGLRPRTALGDIGNKVSEQLQAKMPMKKEAKPS
ATGKVIDKKLPKPLEKVPMLVPVPVSEPVPEPEPEPEPEPVKEEKLSPEPILVDTASPSPMETSGCAPAEEDL
CQAFSDVILAVNDVDAEDGADPNLCSEAVKDIYAYLRQLEEEQAVRPKYLLGREVTGNMRAILIDWLVQV
QMKFRLLQETMYMTVSIIDRFMQNNCVPKKMLQLVGVTAMFIASKYEEMYPPEIGDFAFVTDNTYTKH
QIRQMEMKILRALNFGLGRPLPLHFLRRASKIGEVDVEQHTLAKYLMELTMLDYDMVHFPPSQIAAGAFC
LALKILDNGEWTPTLQHYLSYTEESLLPVMQHLAKNVVMVNQGLTKHMTVKNKYATSKHAKISTLPQLNS
ALVQDLAKAVAKV

Cyclin B1$^{PM\text{-}A}$

Y170A and PM motif mutations are highlighted in yellow.

MALRVTRNSKINAENKAKINMAGAKRVPTAPAATSKPGLRPRTALGDIGNKVSEQLQAKMPMKKEAKPS
ATGKVIDKKLPKPLEKVPMLVPVPVSEPVPEPEPEPEPEPVKEEKLSPEPILVDTASPSPMETSGCAPAEEDL
CQAFSDVILAVNDVDAEDGADPNLCSEAVKAAAAYAAAAEEEQAVRPKYLLGREVTGNMRAILIDWLVQV
QMKFRLLQETMYMTVSIIDRFMQNNCVPKKMLQLVGVTAMFIASKYEEMYPPEIGDFAFVTDNTYTKH
QIRQMEMKILRALNFGLGRPLPLHFLRRASKIGEVDVEQHTLAKYLMELTMLDYDMVHFPPSQIAAGAFC
LALKILDNGEWTPTLQHYLSYTEESLLPVMQHLAKNVVMVNQGLTKHMTVKNKYATSKHAKISTLPQLNS
ALVQDLAKAVAKV

N90-NTH

Derived from cyclin B1. First N-terminal 90 amino acids linked to the N-terminal helix residues (164-196) by a short flexible linked. Linker is highlighted in blue and Y170A mutation is highlighted in yellow.

MALRVTRNSKINAENKAKINMAGAKRVPTAPAATSKPGLRPRTALGDIGNKVSEQLQAKMPMKKEAKPS
ATGKVIDKKLPKPLEKVPMLVTGSTGSPNLCSEAVKDIYAYLRQLEEEQAVRPKYLLGRE

N90-NTH^{PM-A}

Derived from cyclin B1. First N-terminal 90 amino acids linked to the N-terminal helix residues (164-196) by a short flexible linked. Linker is highlighted in blue and Y170A and PM motif mutations are highlighted in yellow.

MALRVTRNSKINAENKAKINMAGAKRVPTAPAATSKPGLRPRTALGDIGNKVSEQLQAKMPMKKEAKPS
ATGKVIDKKLPKPLEKVPMLVTGSTGSPNLCSEAVKAAAAYAAAAEEEQAVRPKYLLGRE

Membrane localised Venus Fluorescent Protein linked constructs

Cyclin B1 constructs used in membrane localisation experiments were tagged to a modified Venus Fluorescent Protein with a C-terminal polybasic prenylation domain tag. This sequence is for the Venus Fluorescent Protein with polybasic prenylation (membrane localisation) tag highlighted in yellow.

VSKGEELFTGVVPILVELDGDVNGHKFSVSGEGEGDATYGKLTLKLICTTGKLPVPWPTLVTTLGYGLQCFAR
YPDHMKQHDFFKSAMPEGYVQERTIFYKDDGNYKTRAEVKFEGDTLVNRIELKGIDFKEDGNILGHKLEYN
YNSHNVYITADKQKNGIKANFKIRHNIEDGGVQLADHYQQNTPIGDGPVLLPDNHYLSYQSALSKDPNEK
RDHMVLLEFVTAAGITLGMDELYKKMSKDGKKKKKKSKTKCVIM

Cyclin B1-CKS1

Cyclin B1 Y170A mutation is highlighted in yellow. Flexible linker to CKS1 is highlighted in blue. CKS1 is highlighted in green

MALRVTRNSKINAENKAKINMAGAKRVPTAPAATSKPGLRPRTALGDIGNKVSEQLQAKMPMKKEAKPS
ATGKVIDKKLPKPLEKVPMLVPVPVSEPVPEPEPEPEPEPVKEEKLSPEPILVDTASPSPMETSGCAPAEEDL
CQAFSDVILAVNDVDAEDGADPNLCSEAVKDIYAYLRQLEEEQAVRPKYLLGREVTGNMRAILIDWLVQV
QMKFRLLQETMYMTVSIIDRFMQNNCVPKKMLQLVGVTAMFIASKYEEMYPPEIGDFAFVTDNTYTKH
QIRQMEMKILRALNFGLGRPLPLHFLRRASKIGEVDVEQHTLAKYLMELTMLDYDMVHFPPSQIAAGAFC
LALKILDNGEWTPTLQHYLSYTEESLLPVMQHLAKNVVMVNQGLTKHMTVKNKYATSKHAKISTLPQLNS
ALVQDLAKAVAKVTGSTGSTGSTGSTGSTGSMSHKQIYYSDKYDDEEFEYRHVMLPKDIAKLVPKTHLMSE
SEWRNLGVQQSQGWVHYMIHEPEPHILLFRRPLPKKPK

Cyclin B1$^{PM\text{-}A}$-CKS1

Cyclin B1 Y170A and PM-motif mutations are highlighted in yellow. Flexible linker to CKS1 is highlighted in blue. CKS1 is highlighted in green

MALRVTRNSKINAENKAKINMAGAKRVPTAPAATSKPGLRPRTALGDIGNKVSEQLQAKMPMKKEAKPS
ATGKVIDKKLPKPLEKVPMLVPVPVSEPVPEPEPEPEPEPVKEEKLSPEPILVDTASPSPMETSGCAPAEEDL
CQAFSDVILAVNDVDAEDGADPNLCSEAVKAAAAYAAAAEEEQAVRPKYLLGREVTGNMRAILIDWLVQV
QMKFRLLQETMYMTVSIIDRFMQNNCVPKKMLQLVGVTAMFIASKYEEMYPPEIGDFAFVTDNTYTKH
QIRQMEMKILRALNFGLGRPLPLHFLRRASKIGEVDVEQHTLAKYLMELTMLDYDMVHFPPSQIAAGAFC
LALKILDNGEWTPTLQHYLSYTEESLLPVMQHLAKNVVMVNQGLTKHMTVKNKYATSKHAKISTLPQLNS
ALVQDLAKAVAKVTGSTGSTGSTGSTGSTGSMSHKQIYYSDKYDDEEFEYRHVMLPKDIAKLVPKTHLMSE
SEWRNLGVQQSQGWVHYMIHEPEPHILLFRRPLPKKPKK

BubR1^{PM-A}

Mutation in the PM-like motif is highlighted in yellow.

MAAVKKEGGALSEAMSLEGDEWELSKENVQPLRQGRIMSTLQGALAQESACNNTLQQQKRAFEYEIRFY
TGNDPLDVWDRYISWTEQNYPQGGKESNMSTLLERAVEALQGEKRYYSDPRFLNLWLKLGRLCNEPLAA
ASYLHNQGIGVSLAQFYISWAEEYEARENFRKADAIFQEGIQQKAEPLERLQSQHRQFQARVSRQTLLALE
KEEEEEVFESSVPQRSTLAELKSKGKKTARAPIIRVGGALKAPSQNRGLQNPFPQQMQNNSRITVFDENAD
EASTAELSKPTVQPWIAPPMPRAKENELQAGPWNTGRSLEHRPRGNTASLIAVPAVLPSFTPYVEETARQP
VMTPCKIEPSINHILSTRKPGKEEGDPLQRVQSHQQASEEKKEKMMYCKEKIYAGVGEFSFEEIRAEVFRKK
LKEQREAELLTSAEKRAEMQKQIEEMEKKLKEIQTTQQERTGDQQEETMPTKETTKLQIASESQKIPGMTL
SSSVCQVNCCARETSLAENIWQEQPHSKGPSVPFSIFDEFLLSEKKNKSPPADPPRVLAQRRPLAVLKTSESI
TSNEDVSPDVCDEFTGIEPLSEDAIITGFRNVTICPNPEDTCDFARAARFVSTPFHEIMSLKDLPSDPERLLPE
EDLDVKTSEDQQTACGTIYSQTLSIKKLSPIIEDSREATHSSGFSGSSASVASTSSIKCLQIPEKLELTNETSENP
TQSPWCSQYRRQLLKSLPELSASAELCIEDRPMPKLEIEKEIELGNEDYCIKREYLICEDYKLFWVAPRNSAEL
TVIKVSSQPVPWDFYINLKLKERLNEDFDHFCSCYQYQDGCIVWHQYINCFTLQDLLQHSEYITHEITVLIIY
NLLTIVEMLHKAEIVHGDLSPRCLILRNRIHDPYDCNKNNQALKIVDFSYSVDLRVQLDVFTLSGFRTVQILE
GQKILANCSSPYQVDLFGIADLAHLLLFKEHLQVFWDGSFWKLSQNISELKDGELWNKFFVRILNANDEAT
VSVLGELAAEMNGVFDTTFQSHLNKALWKVGKLTSPGALLFQ

Cyclin B1$^{BubR1\ PM-motif}$

Mutation of Y170A is highlighted in yellow and the PM motif mutation to the PM-like motif of BubR1 is highlighted in blue

MALRVTRNSKINAENKAKINMAGAKRVPTAPAATSKPGLRPRTALGDIGNKVSEQLQAKMPMKKEAKPS
ATGKVIDKKLPKPLEKVPMLVPVPVSEPVPEPEPEPEPEPVKEEKLSPEPILVDTASPSPMETSGCAPAEEDL
CQAFSDVILAVNDVDAEDGADPNLCSEAVKDMYSYLHNQEEEQAVRPKYLLGREVTGNMRAILIDWLVQ
VQMKFRLLQETMYMTVSIIDRFMQNNCVPKKMLQLVGVTAMFIASKYEEMYPPEIGDFAFVTDNTYTKH
QIRQMEMKILRALNFGLGRPLPLHFLRRASKIGEVDVEQHTLAKYLMELTMLDYDMVHFPPSQIAAGAFC

LALKILDNGEWTPTLQHYLSYTEESLLPVMQHLAKNVVMVNQGLTKHMTVKNKYATSKHAKISTLPQLNS
ALVQDLAKAVAKV

BioID2

MFKNLIWLKEVDSTQERLKEWNVSYGTALVADRQTKGRGGLGRKWLSQEGGLYFSFLLNPKEFENLLQLP
LVLGLSVSEALEEITEIPFSLKWPNDVYFQEKKVSGVLCELSKDKLIVGIGINVNQREIPEEIKDRATTLYEITGK
DWDRKEVLLKVLKRISENLKKFKEKSFKEFKGKIESKMLYLGEEVKLLGEGKITGKLVGLSEKGGALILTEEGIK
EILSGEFSLRRSLERPPLCWISAEFHHTGLVDPSSVPSLSLNR

BIOID2 cyclin B1

BIOID2 linked to the N-terminus of cyclin B1 using the short linker native to the MDL9 plasmid vector. BIOID2 is highlighted in blue. Short linker is highlighted in green. Cyclin B1 is unhighlighted with the Y170A mutation highlighted in yellow.

MFKNLIWLKEVDSTQERLKEWNVSYGTALVADRQTKGRGGLGRKWLSQEGGLYFSFLLNPKEFENLLQLP
LVLGLSVSEALEEITEIPFSLKWPNDVYFQEKKVSGVLCELSKDKLIVGIGINVNQREIPEEIKDRATTLYEITGK
DWDRKEVLLKVLKRISENLKKFKEKSFKEFKGKIESKMLYLGEEVKLLGEGKITGKLVGLSEKGGALILTEEGIK
EILSGEFSLRRSLERPPLCWISAEFHHTGLVDPSSVPSLSLNREFSVDMALRVTRNSKINAENKAKINMAGA
KRVPTAPAATSKPGLRPRTALGDIGNKVSEQLQAKMPMKKEAKPSATGKVIDKKLPKPLEKVPMLVPVPVS
EPVPEPEPEPEPEPVKEEKLSPEPILVDTASPSPMETSGCAPAEEDLCQAFSDVILAVNDVDAEDGADPNLC
SEAVKDIYAYLRQLEEEQAVRPKYLLGREVTGNMRAILIDWLVQVQMKFRLLQETMYMTVSIIDRFMQNN
CVPKKMLQLVGVTAMFIASKYEEMYPPEIGDFAFVTDNTYTKHQIRQMEMKILRALNFGLGRPLPLHFLR
RASKIGEVDVEQHTLAKYLMELTMLDYDMVHFPPSQIAAGAFCLALKILDNGEWTPTLQHYLSYTEESLLP
VMQHLAKNVVMVNQGLTKHMTVKNKYATSKHAKISTLPQLNSALVQDLAKAVAKV

Bioid2 cyclin B1^{PM-A}

BIOID2 linked to the N-terminus of cyclin B1 using the short linker native to the MDL9 plasmid vector. BIOID2 is highlighted in blue. Short linker is highlighted in green. Cyclin B1 is unhighlighted with the Y170A and PM motif mutations highlighted in yellow.

MFKNLIWLKEVDSTQERLKEWNVSYGTALVADRQTKGRGGLGRKWLSQEGGLYFSFLLNPKEFENLLQLP
LVLGLSVSEALEEITEIPFSLKWPNDVYFQEKKVSGVLCELSKDKLIVGIGINVNQREIPEEIKDRATTLYEITGK
DWDRKEVLLKVLKRISENLKKFKEKSFKEFKGKIESKMLYLGEEVKLLGEGKITGKLVGLSEKGGALILTEEGIK
EILSGEFSLRRSLERPPLCWISAEFHHTGLVDPSSVPSLSLNREFSVDMALRVTRNSKINAENKAKINMAGA
KRVPTAPAATSKPGLRPRTALGDIGNKVSEQLQAKMPMKKEAKPSATGKVIDKKLPKPLEKVPMLVPVPVS
EPVPEPEPEPEPEPVKEEKLSPEPILVDTASPSPMETSGCAPAEEDLCQAFSDVILAVNDVDAEDGADPNLC
SEAVKAAAAYAAAAEEEQAVRPKYLLGREVTGNMRAILIDWLVQVQMKFRLLQETMYMTVSIIDRFMQN
NCVPKKMLQLVGVTAMFIASKYEEMYPPEIGDFAFVTDNTYTKHQIRQMEMKILRALNFGLGRPLPLHFL
RRASKIGEVDVEQHTLAKYLMELTMLDYDMVHFPPSQIAAGAFCLALKILDNGEWTPTLQHYLSYTEESLL
PVMQHLAKNVVMVNQGLTKHMTVKNKYATSKHAKISTLPQLNSALVQDLAKAVAKV

TurboID

MKDNTVPLKLIALLANGEFHSGEQLGETLGMSRAAINKHIQTLRDWGVDVFTVPGKGYSLPEPIPLLNAK
QILGQLDGGSVAVLPVVDSTNQYLLDRIGELKSGDACIAEYQQAGRGSRGRKWFSPFGANLYLSMFWRLK
RGPAAIGLGPVIGIVMAEALRKLGADKVRVKWPNDLYLQDRKLAGILVELAGITGDAAQIVIGAGINVAMR
RVEESVVNQGWITLQEAGINLDRNTLAATLIRELRAALELFEQEGLAPYLPRWEKLDNFINRPVKLIIGDKEI
FGISRGIDKQGALLLEQDGVIKPWMGGEISLRSAEK

TurboID-cyclin B1

TurboID sequence is highlighted in blue. Short linker native to the MDL9 plasmid vector is highlighted in green. Cyclin B1 is unhighlighted with the Y170A mutation highlighted in yellow.

MKDNTVPLKLIALLANGEFHSGEQLGETLGMSRAAINKHIQTLRDWGVDVFTVPGKGYSLPEPIPLLNAK
QILGQLDGGSVAVLPVVDSTNQYLLDRIGELKSGDACIAEYQQAGRGSRGRKWFSPFGANLYLSMFWRLK
RGPAAIGLGPVIGIVMAEALRKLGADKVRVKWPNDLYLQDRKLAGILVELAGITGDAAQIVIGAGINVAMR
RVEESVVNQGWITLQEAGINLDRNTLAATLIRELRAALELFEQEGLAPYLPRWEKLDNFINRPVKLIIGDKEI
FGISRGIDKQGALLLEQDGVIKPWMGGEISLRSAEKEFSVDMALRVTRNSKINAENKAKINMAGAKRVPT
APAATSKPGLRPRTALGDIGNKVSEQLQAKMPMKKEAKPSATGKVIDKKLPKPLEKVPMLVPVPVSEPVPE
PEPEPEPEPVKEEKLSPEPILVDTASPSPMETSGCAPAEEDLCQAFSDVILAVNDVDAEDGADPNLCSEAVK
DIYAYLRQLEEEQAVRPKYLLGREVTGNMRAILIDWLVQVQMKFRLLQETMYMTVSIIDRFMQNNCVPKK
MLQLVGVTAMFIASKYEEMYPPEIGDFAFVTDNTYTKHQIRQMEMKILRALNFGLGRPLPLHFLRRASKIG
EVDVEQHTLAKYLMELTMLDYDMVHFPPSQIAAGAFCLALKILDNGEWTPTLQHYLSYTEESLLPVMQHL
AKNVVMVNQGLTKHMTVKNKYATSKHAKISTLPQLNSALVQDLAKAVAKV

Turbo-cyclin B1^{PM-A}

Cyclin B1^{PM-A} linked to TurboID on its N-terminus. TurboID sequence is highlighted in blue. Short linker native to the MDL9 plasmid vector is highlighted in green. Cyclin B1 is unhighlighted with the Y170A and PM-A mutations highlighted in yellow.

MKDNTVPLKLIALLANGEFHSGEQLGETLGMSRAAINKHIQTLRDWGVDVFTVPGKGYSLPEPIPLLNAK
QILGQLDGGSVAVLPVVDSTNQYLLDRIGELKSGDACIAEYQQAGRGSRGRKWFSPFGANLYLSMFWRLK
RGPAAIGLGPVIGIVMAEALRKLGADKVRVKWPNDLYLQDRKLAGILVELAGITGDAAQIVIGAGINVAMR
RVEESVVNQGWITLQEAGINLDRNTLAATLIRELRAALELFEQEGLAPYLPRWEKLDNFINRPVKLIIGDKEI
FGISRGIDKQGALLLEQDGVIKPWMGGEISLRSAEKEFSVDMALRVTRNSKINAENKAKINMAGAKRVPT
APAATSKPGLRPRTALGDIGNKVSEQLQAKMPMKKEAKPSATGKVIDKKLPKPLEKVPMLVPVPVSEPVPE
PEPEPEPEPVKEEKLSPEPILVDTASPSPMETSGCAPAEEDLCQAFSDVILAVNDVDAEDGADPNLCSEAVK
AAAAYAAAAEEEQAVRPKYLLGREVTGNMRAILIDWLVQVQMKFRLLQETMYMTVSIIDRFMQNNCVP
KKMLQLVGVTAMFIASKYEEMYPPEIGDFAFVTDNTYTKHQIRQMEMKILRALNFGLGRPLPLHFLRRASK
IGEVDVEQHTLAKYLMELTMLDYDMVHFPPSQIAAGAFCLALKILDNGEWTPTLQHYLSYTEESLLPVMQ
HLAKNVVMVNQGLTKHMTVKNKYATSKHAKISTLPQLNSALVQDLAKAVAKV

TurboID-cyclin B1^{linker}

Cyclin B1 linked to TurboID on its N-terminus using a long flexible linker. Linker is highlighted in green. Y170A mutation is highlighted in yellow.

MKDNTVPLKLIALLANGEFHSGEQLGETLGMSRAAINKHIQTLRDWGVDVFTVPGKGYSLPEPIPLLNAK
QILGQLDGGSVAVLPVVDSTNQYLLDRIGELKSGDACIAEYQQAGRGSRGRKWFSPFGANLYLSMFWRLK
RGPAAIGLGPVIGIVMAEALRKLGADKVRVKWPNDLYLQDRKLAGILVELAGITGDAAQIVIGAGINVAMR
RVEESVVNQGWITLQEAGINLDRNTLAATLIRELRAALELFEQEGLAPYLPRWEKLDNFINRPVKLIIGDKEI
FGISRGIDKQGALLLEQDGVIKPWMGGEISLRSAEKEFSVDGGSGGSGGGSMALRVTRNSKINAENKAKI
NMAGAKRVPTAPAATSKPGLRPRTALGDIGNKVSEQLQAKMPMKKEAKPSATGKVIDKKLPKPLEKVPML
VPVPVSEPVPEPEPEPEPEPVKEEKLSPEPILVDTASPSPMETSGCAPAEEDLCQAFSDVILAVNDVDAEDG
ADPNLCSEAVKDIYAYLRQLEEEQAVRPKYLLGREVTGNMRAILIDWLVQVQMKFRLLQETMYMTVSIIDR
FMQNNCVPKKMLQLVGVTAMFIASKYEEMYPPEIGDFAFVTDNTYTKHQIRQMEMKILRALNFGLGRPL
PLHFLRRASKIGEVDVEQHTLAKYLMELTMLDYDMVHFPPSQIAAGAFCLALKILDNGEWTPTLQHYLSYT
EESLLPVMQHLAKNVVMVNQGLTKHMTVKNKYATSKHAKISTLPQLNSALVQDLAKAVAKV

Cyclin B1-TurboID

Cyclin B1 linked to TurboID on its C-terminus. Mutation of Y170A is highlighted in yellow. Short flexible linkers linking cyclin B1 to TurboID and TurboID to Venus fluorescent protein are highlighted in green.

MALRVTRNSKINAENKAKINMAGAKRVPTAPAATSKPGLRPRTALGDIGNKVSEQLQAKMPMKKEAKPS
ATGKVIDKKLPKPLEKVPMLVPVPVSEPVPEPEPEPEPEPVKEEKLSPEPILVDTASPSPMETSGCAPAEEDL
CQAFSDVILAVNDVDAEDGADPNLCSEAVKDIYAYLRQLEEEQAVRPKYLLGREVTGNMRAILIDWLVQV
QMKFRLLQETMYMTVSIIDRFMQNNCVPKKMLQLVGVTAMFIASKYEEMYPPEIGDFAFVTDNTYTKH
QIRQMEMKILRALNFGLGRPLPLHFLRRASKIGEVDVEQHTLAKYLMELTMLDYDMVHFPPSQIAAGAFC
LALKILDNGEWTPTLQHYLSYTEESLLPVMQHLAKNVVMVNQGLTKHMTVKNKYATSKHAKISTLPQLNS
ALVQDLAKAVAKVGGSGGSGGGSMKDNTVPLKLIALLANGEFHSGEQLGETLGMSRAAINKHIQTLRDW
GVDVFTVPGKGYSLPEPIPLLNAKQILGQLDGGSVAVLPVVDSTNQYLLDRIGELKSGDACIAEYQQAGRGS
RGRKWFSPFGANLYLSMFWRLKRGPAAIGLGPVIGIVMAEALRKLGADKVRVKWPNDLYLQDRKLAGILV
ELAGITGDAAQIVIGAGINVAMRRVEESVVNQGWITLQEAGINLDRNTLAATLIRELRAALELFEQEGLAPY
LPRWEKLDNFINRPVKLIIGDKEIFGISRGIDKQGALLLEQDGVIKPWMGGEISLRSAEKGGSGGSGGGS

Cyclin B1^{PM-A}-TurboID

Cyclin B1^{PM-A} linked to TurboID on its C-terminus. Mutation of Y170A and PM motif is highlighted in yellow. Short flexible linkers linking cyclin B1 to TurboID and TurboID to Venus fluorescent protein are highlighted in green.

MALRVTRNSKINAENKAKINMAGAKRVPTAPAATSKPGLRPRTALGDIGNKVSEQLQAKMPMKKEAKPS
ATGKVIDKKLPKPLEKVPMLVPVPVSEPVPEPEPEPEPEPVKEEKLSPEPILVDTASPSPMETSGCAPAEEDL
CQAFSDVILAVNDVDAEDGADPNLCSEAVKAAAAYAAAAEEEQAVRPKYLLGREVTGNMRAILIDWLVQV
QMKFRLLQETMYMTVSIIDRFMQNNCVPKKMLQLVGVTAMFIASKYEEMYPPEIGDFAFVTDNTYTKH
QIRQMEMKILRALNFGLGRPLPLHFLRRASKIGEVDVEQHTLAKYLMELTMLDYDMVHFPPSQIAAGAFC
LALKILDNGEWTPTLQHYLSYTEESLLPVMQHLAKNVVMVNQGLTKHMTVKNKYATSKHAKISTLPQLNS
ALVQDLAKAVAKVGGSGGSGGGSMKDNTVPLKLIALLANGEFHSGEQLGETLGMSRAAINKHIQTLRDW
GVDVFTVPGKGYSLPEPIPLLNAKQILGQLDGGSVAVLPVVDSTNQYLLDRIGELKSGDACIAEYQQAGRGS

RGRKWFSPFGANLYLSMFWRLKRGPAAIGLGPVIGIVMAEALRKLGADKVRVKWPNDLYLQDRKLAGILV
ELAGITGDAAQIVIGAGINVAMRRVEESVVNQGWITLQEAGINLDRNTLAATLIRELRAALELFEQEGLAPY
LPRWEKLDNFINRPVKLIIGDKEIFGISRGIDKQGALLLEQDGVIKPWMGGEISLRSAEKGGSGGSGGGS

Securin

MATLIYVDKENGEPGTRVVAKDGLKLGSGPSIKALDGRSQVSTPRFGKTFDAPPALPKATRKALGTVNRAT
EKSVKTKGPLKQKQPSFSAKKMTEKTVKAKSSVPASDDAYPEIEKFFPFNPLDFESFDLPEEHQIAHLPLSGV
PLMILDEERELEKLFQLGPPSPVKMPSPPWESNLLQSPSSILSTLDVELPPVCCDIDI

Securin[short D-box]

Mutation of the extended D-box residues in positions 8-10 are highlighted in Yellow

MATLIYVDKENGEPGTRVVAKDGLKLGSGPSIKALDGRSQVSTPRFGKTFDAPPALPKATRKALGTVAAAT
EKSVKTKGPLKQKQPSFSAKKMTEKTVKAKSSVPASDDAYPEIEKFFPFNPLDFESFDLPEEHQIAHLPLSGV
PLMILDEERELEKLFQLGPPSPVKMPSPPWESNLLQSPSSILSTLDVELPPVCCDIDI

Securin[short D-box, FxxF-A]

Mutation of the extended D-box residues in positions 8-10 are highlighted in yellow.
Mutations of the FxxF motif are highlighted in blue.

MATLIYVDKENGEPGTRVVAKDGLKLGSGPSIKALDGRSQVSTPRFGKTFDAPPALPKATRKALGTVAAAT
EKSVKTKGPLKQKQPSFSAKKMTEKTVKAKSSVPASDDAYPEIEKFFPFNPLDAESADLPEEHQIAHLPLSGV
PLMILDEERELEKLFQLGPPSPVKMPSPPWESNLLQSPSSILSTLDVELPPVCCDIDI

Securin[short D-box, FxxF-A, KEN-A]

Mutation of the KEN motif is highlighted in green. Mutation of the extended D-box residues in positions 8-10 are highlighted in yellow. Mutations of the FxxF motif are highlighted in blue.

MATLIYVDAAAGEPGTRVVAKDGLKLGSGPSIKALDGRSQVSTPRFGKTFDAPPALPKATRKALGTVAAAT
EKSVKTKGPLKQKQPSFSAKKMTEKTVKAKSSVPASDDAYPEIEKFFPFNPLDAESADLPEEHQIAHLPLSGV
PLMILDEERELEKLFQLGPPSPVKMPSPPWESNLLQSPSSILSTLDVELPPVCCDIDI

Cyclin A2

MLGNSAPGPATREAGSALLALQQTALQEDQENINPEKAAPVQQPRTRAALAVLKSGNPRGLAQQQRPKT
RRVAPLKDLPVNDEHVTVPPWKANSKQPAFTIHVDEAEKEAQKKPAESQKIEREDALAFNSAISLPGPRKP
LVPLDYPMDGSFESPHTMDMSIILEDEKPVSVNEVPDYHEDIHTYLREMEVKCKPKVGYMKKQPDITNSM
RAILVDWLVEVGEEYKLQNETLHLAVNYIDRFLSSMSVLRGKLQLVGTAAMLLASKFEEIYPPEVAEFVYITD
DTYTKKQVLRMEHLVLKVLTFDLAAPTVNQFLTQYFLHQQPANCKVESLAMFLGELSLIDADPYLKYLPSVI
AGAAFHLALYTVTGQSWPESLIRKTGYTLESLKPCLMDLHQTYLKAPQHAQQSIREKYKNSKYHGVSLLNP
PETLNL

Cyclin A2$^{\text{short D-box}}$

Mutations of the extended D1-box residues in positions 8-10 are highlighted in yellow. Mutations of the extended D2-box residues in positions 8-10 are highlighted in blue.

MLGNSAPGPATREAGSALLALQQTALQEDQENINPEKAAPVQQPRTRAALAVLAAANPRGLAQQQRPK
TRRVAPLKDLAAADEHVTVPPWKANSKQPAFTIHVDEAEKEAQKKPAESQKIEREDALAFNSAISLPGPRK
PLVPLDYPMDGSFESPHTMDMSIILEDEKPVSVNEVPDYHEDIHTYLREMEVKCKPKVGYMKKQPDITNS
MRAILVDWLVEVGEEYKLQNETLHLAVNYIDRFLSSMSVLRGKLQLVGTAAMLLASKFEEIYPPEVAEFVYIT
DDTYTKKQVLRMEHLVLKVLTFDLAAPTVNQFLTQYFLHQQPANCKVESLAMFLGELSLIDADPYLKYLPSV

IAGAAFHLALYTVTGQSWPESLIRKTGYTLESLKPCLMDLHQTYLKAPQHAQQSIREKYKNSKYHGVSLLNP
PETLNL

Cyclin A2[short D-box, ABBA-A]

Mutations of the extended D1-box residues in positions 8-10 are highlighted in yellow.
Mutations of the extended D2-box residues in positions 8-10 are highlighted in blue.
Mutations of the ABBA motif are highlighted in green.

MLGNSAPGPATREAGSALLALQQTALQEDQENINPEKAAPVQQPRTRAALAVLAAANPRGLAQQQRPK
TRRVAPLKDLAAADEHVTVPPWKANSKQAAAAAAAAAAEKEAQKKPAESQKIEREDALAFNSAISLPGPR
KPLVPLDYPMDGSFESPHTMDMSIILEDEKPVSVNEVPDYHEDIHTYLREMEVKCKPKVGYMKKQPDITN
SMRAILVDWLVEVGEEYKLQNETLHLAVNYIDRFLSSMSVLRGKLQLVGTAAMLLASKFEEIYPPEVAEFVYI
TDDTYTKKQVLRMEHLVLKVLTFDLAAPTVNQFLTQYFLHQQPANCKVESLAMFLGELSLIDADPYLKYLPS
VIAGAAFHLALYTVTGQSWPESLIRKTGYTLESLKPCLMDLHQTYLKAPQHAQQSIREKYKNSKYHGVSLLN
PPETLNL

Cyclin B1[short D-box]

Y170A mutation is highlighted in yellow. Extended D-box residues in positions 8-10 mutations are highlighted in blue.

MALRVTRNSKINAENKAKINMAGAKRVPTAPAATSKPGLRPRTALGDIAAAVSEQLQAKMPMKKEAKPS
ATGKVIDKKLPKPLEKVPMLVPVPVSEPVPEPEPEPEPEPVKEEKLSPEPILVDTASPSPMETSGCAPAEEDL
CQAFSDVILAVNDVDAEDGADPNLCSEAVKDIYAYLRQLEEEQAVRPKYLLGREVTGNMRAILIDWLVQV
QMKFRLLQETMYMTVSIIDRFMQNNCVPKKMLQLVGVTAMFIASKYEEMYPPEIGDFAFVTDNTYTKH
QIRQMEMKILRALNFGLGRPLPLHFLRRASKIGEVDVEQHTLAKYLMELTMLDYDMVHFPPSQIAAGAFC
LALKILDNGEWTPTLQHYLSYTEESLLPVMQHLAKNVVMVNQGLTKHMTVKNKYATSKHAKISTLPQLNS
ALVQDLAKAVAKV

Cyclin B1 **short D-box, PM-A**

Y170A and PM motif mutations are highlighted in yellow. Extended D-box residues in positions 8-10 mutations are highlighted in blue.

MALRVTRNSKINAENKAKINMAGAKRVPTAPAATSKPGLRPRTALGDIAAAVSEQLQAKMPMKKEAKPS
ATGKVIDKKLPKPLEKVPMLVPVPVSEPVPEPEPEPEPEPVKEEKLSPEPILVDTASPSPMETSGCAPAEEDL
CQAFSDVILAVNDVDAEDGADPNLCSEAVKAAAAYAAAAEEEQAVRPKYLLGREVTGNMRAILIDWLVQV
QMKFRLLQETMYMTVSIIDRFMQNNCVPKKMLQLVGVTAMFIASKYEEMYPPEIGDFAFVTDNTYTKH
QIRQMEMKILRALNFGLGRPLPLHFLRRASKIGEVDVEQHTLAKYLMELTMLDYDMVHFPPSQIAAGAFC
LALKILDNGEWTPTLQHYLSYTEESLLPVMQHLAKNVVMVNQGLTKHMTVKNKYATSKHAKISTLPQLNS
ALVQDLAKAVAKV

Appendix III: References

1. Virant-Klun, I. Postnatal oogenesis in humans: a review of recent findings. *Stem Cells Cloning Adv. Appl.* 49 (2015) doi:10.2147/SCCAA.S32650.

2. Imaimatsu, K., Uchida, A., Hiramatsu, R. & Kanai, Y. Gonadal Sex Differentiation and Ovarian Organogenesis along the Cortical–Medullary Axis in Mammals. *Int. J. Mol. Sci.* **23**, 13373 (2022).

3. Bolcun-Filas, E. & Handel, M. A. Meiosis: the chromosomal foundation of reproduction. *Biol. Reprod.* **99**, 112–126 (2018).

4. Shibuya, H. & Watanabe, Y. The meiosis-specific modification of mammalian telomeres. *Cell Cycle* **13**, 2024–2028 (2014).

5. Paigen, K. & Petkov, P. M. PRDM9 and Its Role in Genetic Recombination. *Trends Genet.* **34**, 291–300 (2018).

6. MacLennan, M., Crichton, J. H., Playfoot, C. J. & Adams, I. R. Oocyte development, meiosis and aneuploidy. *Semin. Cell Dev. Biol.* **45**, 68–76 (2015).

7. Brooker, R. J. *Genetics: Analysis & Principles*. (McGraw-Hill Higher Education, Boston, Mass., 2009).

8. Carabatsos, M. J., Sellitto, C., Goodenough, D. A. & Albertini, D. F. Oocyte–Granulosa Cell Heterologous Gap Junctions Are Required for the Coordination of Nuclear and Cytoplasmic Meiotic Competence. *Dev. Biol.* **226**, 167–179 (2000).

9. Alam, M. H. & Miyano, T. Interaction between growing oocytes and granulosa cells in vitro. *Reprod. Med. Biol.* **19**, 13–23 (2020).

10. Pirino, G., Wescott, M. P. & Donovan, P. J. Protein kinase A regulates resumption of meiosis by phosphorylation of Cdc25B in mammalian oocytes. *Cell Cycle* **8**, 665–670 (2009).

11. Kaur, S. & Kurokawa, M. Regulation of Oocyte Apoptosis: A View from Gene Knockout Mice. *Int. J. Mol. Sci.* **24**, 1345 (2023).

12. Esencan, E., Kallen, A., Zhang, M. & Seli, E. Translational activation of maternally derived mRNAs in oocytes and early embryos and the role of embryonic poly(A) binding protein (EPAB). *Biol. Reprod.* **100**, 1147–1157 (2019).

13. Abuetabh, Y. *et al.* DNA damage response revisited: the p53 family and its regulators provide endless cancer therapy opportunities. *Exp. Mol. Med.* **54**, 1658–1669 (2022).

14. Pei, Z., Deng, K., Xu, C. & Zhang, S. The molecular regulatory mechanisms of meiotic arrest and resumption in Oocyte development and maturation. *Reprod. Biol. Endocrinol.* **21**, 90 (2023).

15. Adhikari, D. *et al.* Cdk1, but not Cdk2, is the sole Cdk that is essential and sufficient to drive resumption of meiosis in mouse oocytes. *Hum. Mol. Genet.* **21**, 2476–2484 (2012).

16. Cairo, G. & Lacefield, S. Establishing correct kinetochore-microtubule attachments in mitosis and meiosis. *Essays Biochem.* **64**, 277–287 (2020).

17. Sudakin, V., Chan, G. K. T. & Yen, T. J. Checkpoint inhibition of the APC/C in HeLa cells is mediated by a complex of BUBR1, BUB3, CDC20, and MAD2. *J. Cell Biol.* **154**, 925–936 (2001).

18. Rieder, C. L., Schultz, A., Cole, R. & Sluder, G. Anaphase onset in vertebrate somatic cells is controlled by a checkpoint that monitors sister kinetochore attachment to the spindle. *J. Cell Biol.* **127**, 1301–1310 (1994).

19. Sudakin, V. *et al.* The cyclosome, a large complex containing cyclin-selective ubiquitin ligase activity, targets cyclins for destruction at the end of mitosis. *Mol. Biol. Cell* **6**, 185–197 (1995).

20. Zhang, S., Tischer, T. & Barford, D. Cyclin A2 degradation during the spindle assembly checkpoint requires multiple binding modes to the APC/C. *Nat. Commun.* **10**, 3863 (2019).

21. Kirschner, M. Beyond self-assembly: From microtubules to morphogenesis. *Cell* **45**, 329–342 (1986).

22. Ault, J. G. & Rieder, C. L. Chromosome mal-orientation and reorientation during mitosis. *Cell Motil.* **22**, 155–159 (1992).

23. Schuh, M. & Ellenberg, J. Self-Organization of MTOCs Replaces Centrosome Function during Acentrosomal Spindle Assembly in Live Mouse Oocytes. *Cell* **130**, 484–498 (2007).

24. Wang, Z.-W., Zhang, G.-L., Schatten, H., Carroll, J. & Sun, Q.-Y. Cytoplasmic Determination of Meiotic Spindle Size Revealed by a Unique Inter-Species Germinal Vesicle Transfer Model. *Sci. Rep.* **6**, 19827 (2016).

25. Lampson, M. A. & Cheeseman, I. M. Sensing centromere tension: Aurora B and the regulation of kinetochore function. *Trends Cell Biol.* **21**, 133–140 (2011).

26. Balboula, A. Z. & Schindler, K. Selective Disruption of Aurora C Kinase Reveals Distinct Functions from Aurora B Kinase during Meiosis in Mouse Oocytes. *PLoS Genet.* **10**, e1004194 (2014).

27. Collin, P., Nashchekina, O., Walker, R. & Pines, J. The spindle assembly checkpoint works like a rheostat rather than a toggle switch. *Nat. Cell Biol.* **15**, 1378–1385 (2013).

28. Zou, H., McGarry, T. J., Bernal, T. & Kirschner, M. W. Identification of a Vertebrate Sister-Chromatid Separation Inhibitor Involved in Transformation and Tumorigenesis. *Science* **285**, 418–422 (1999).

29. Kudo, N. R. *et al.* Resolution of Chiasmata in Oocytes Requires Separase-Mediated Proteolysis. *Cell* **126**, 135–146 (2006).

30. Lei, W.-L., Qian, W.-P. & Sun, Q.-Y. Critical Functions of PP2A-Like Protein Phosphotases in Regulating Meiotic Progression. *Front. Cell Dev. Biol.* **9**, 638559 (2021).

31. Kim, J. *et al.* Meikin is a conserved regulator of meiosis-I-specific kinetochore function. *Nature* **517**, 466–471 (2015).

32. Mihajlović, A. I. & FitzHarris, G. Segregating Chromosomes in the Mammalian Oocyte. *Curr. Biol.* **28**, R895–R907 (2018).

33. Terret, M. E. *et al.* DOC1R: a MAP kinase substrate that control microtubule organization of metaphase II mouse oocytes. *Development* **130**, 5169–5177 (2003).

34. Zhang, Q.-H. *et al.* Cyclin A2 modulates kinetochore–microtubule attachment in meiosis II. *J. Cell Biol.* **216**, 3133–3143 (2017).

35. Dumont, J. *et al.* A centriole- and RanGTP-independent spindle assembly pathway in meiosis I of vertebrate oocytes. *J. Cell Biol.* **176**, 295–305 (2007).

36. Lee, J. *et al.* Unified mode of centromeric protection by shugoshin in mammalian oocytes and somatic cells. *Nat. Cell Biol.* **10**, 42–52 (2008).

37. Wetherall, B., Bulmer, D., Sarginson, A., Thomas, C. & Madgwick, S. SGO2 does not play an essential role in separase inhibition during meiosis I in mouse oocytes. *PLOS Biol.* **23**, e3003131 (2025).

38. Masui, Y. & Markert, C. L. Cytoplasmic control of nuclear behavior during meiotic maturation of frog oocytes. *J. Exp. Zool.* **177**, 129–145 (1971).

39. Madgwick, S., Hansen, D. V., Levasseur, M., Jackson, P. K. & Jones, K. T. Mouse Emi2 is required to enter meiosis II by reestablishing cyclin B1 during interkinesis. *J. Cell Biol.* **174**, 791–801 (2006).

40. Herbert, M., Wolstenholme, J., Murdoch, A. P. & Butler, T. J. Mitotic activity during preimplantation development of human embryos. *Reproduction* **103**, 209–214 (1995).

41. Currie, C. E. *et al.* The first mitotic division of human embryos is highly error prone. *Nat. Commun.* **13**, 6755 (2022).

42. Clift, D. & Schuh, M. Restarting life: fertilization and the transition from meiosis to mitosis. *Nat. Rev. Mol. Cell Biol.* **14**, 549–562 (2013).

43. Hassold, T. & Hunt, P. To err (meiotically) is human: the genesis of human aneuploidy. *Nat. Rev. Genet.* **2**, 280–291 (2001).

44. Chiang, T., Schultz, R. M. & Lampson, M. A. Meiotic Origins of Maternal Age-Related Aneuploidy1. *Biol. Reprod.* **86**, (2012).

45. Habbema, J. D. F., Eijkemans, M. J. C., Leridon, H. & Te Velde, E. R. Realizing a desired family size: when should couples start? *Hum. Reprod.* **30**, 2215–2221 (2015).

46. Delbaere, I., Verbiest, S. & Tydén, T. Knowledge about the impact of age on fertility: a brief review. *Ups. J. Med. Sci.* **125**, 167–174 (2020).

47. Chiang, T., Duncan, F. E., Schindler, K., Schultz, R. M. & Lampson, M. A. Evidence that Weakened Centromere Cohesion Is a Leading Cause of Age-Related Aneuploidy in Oocytes. *Curr. Biol.* **20**, 1522–1528 (2010).

48. Nabti, I., Grimes, R., Sarna, H., Marangos, P. & Carroll, J. Maternal age-dependent APC/C-mediated decrease in securin causes premature sister chromatid separation in meiosis II. *Nat. Commun.* **8**, 15346 (2017).

49. Cheng, J.-M. & Liu, Y.-X. Age-Related Loss of Cohesion: Causes and Effects. *Int. J. Mol. Sci.* **18**, 1578 (2017).

50. Lister, L. M. *et al.* Age-Related Meiotic Segregation Errors in Mammalian Oocytes Are Preceded by Depletion of Cohesin and Sgo2. *Curr. Biol.* **20**, 1511–1521 (2010).

51. Keefe, D. L., Marquard, K. & Liu, L. The telomere theory of reproductive senescence in women. *Curr. Opin. Obstet. Gynecol.* **18**, 280–285 (2006).

52. Heasley, L. R., Markus, S. M. & DeLuca, J. G. "Wait anaphase" signals are not confined to the mitotic spindle. *Mol. Biol. Cell* **28**, 1186–1194 (2017).

53. Kyogoku, H. & Kitajima, T. S. The large cytoplasmic volume of oocyte. *J. Reprod. Dev.* **69**, 1–9 (2023).

54. Yoshida, S., Kaido, M. & Kitajima, T. S. Inherent Instability of Correct Kinetochore-Microtubule Attachments during Meiosis I in Oocytes. *Dev. Cell* **33**, 589–602 (2015).

55. Gao, L. *et al.* The Error-Prone Kinetochore-Microtubule Attachments During Meiosis I in Vitrified Oocytes. *Front. Cell Dev. Biol.* **8**, 621 (2020).

56. Dong, J. *et al.* Ectopic expression of human TUBB8 leads to increased aneuploidy in mouse oocytes. *Cell Discov.* **9**, 105 (2023).

57. Ruiz, E. J., Vilar, M. & Nebreda, A. R. A Two-Step Inactivation Mechanism of Myt1 Ensures CDK1/Cyclin B Activation and Meiosis I Entry. *Curr. Biol.* **20**, 717–723 (2010).

58. Fung, T. K., Ma, H. T. & Poon, R. Y. C. Specialized Roles of the Two Mitotic Cyclins in Somatic Cells: Cyclin A as an Activator of M Phase–promoting Factor. *Mol. Biol. Cell* **18**, 1861–1873 (2007).

59. Hagting, A., Jackman, M., Simpson, K. & Pines, J. Translocation of cyclin B1 to the nucleus at prophase requires a phosphorylation-dependent nuclear import signal. *Curr. Biol.* **9**, 680–689 (1999).

60. Dunphy, W. G. & Kumagai, A. The cdc25 protein contains an intrinsic phosphatase activity. *Cell* **67**, 189–196 (1991).

61. Coulonval, K., Kooken, H. & Roger, P. P. Coupling of T161 and T14 phosphorylations protects cyclin B–CDK1 from premature activation. *Mol. Biol. Cell* **22**, 3971–3985 (2011).

62. Malumbres, M. & Barbacid, M. Mammalian cyclin-dependent kinases. *Trends Biochem. Sci.* **30**, 630–641 (2005).

63. Elia, A. E. H., Cantley, L. C. & Yaffe, M. B. Proteomic Screen Finds pSer/pThr-Binding Domain Localizing Plk1 to Mitotic Substrates. *Science* **299**, 1228–1231 (2003).

64. Elia, A. E. H. *et al.* The Molecular Basis for Phosphodependent Substrate Targeting and Regulation of Plks by the Polo-Box Domain. *Cell* **115**, 83–95 (2003).

65. Lindqvist, A., Rodríguez-Bravo, V. & Medema, R. H. The decision to enter mitosis: feedback and redundancy in the mitotic entry network. *J. Cell Biol.* **185**, 193–202 (2009).

66. Hutterer, A. *et al.* Mitotic Activation of the Kinase Aurora-A Requires Its Binding Partner Bora. *Dev. Cell* **11**, 147–157 (2006).

67. Chan, E. H. Y., Santamaria, A., Silljé, H. H. W. & Nigg, E. A. Plk1 regulates mitotic Aurora A function through βTrCP-dependent degradation of hBora. *Chromosoma* **117**, 457–469 (2008).

68. Fu, Z. *et al.* Plk1-dependent phosphorylation of FoxM1 regulates a transcriptional programme required for mitotic progression. *Nat. Cell Biol.* **10**, 1076–1082 (2008).

69. Laoukili, J. *et al.* FoxM1 is required for execution of the mitotic programme and chromosome stability. *Nat. Cell Biol.* **7**, 126–136 (2005).

70. Massacci, G., Perfetto, L. & Sacco, F. The Cyclin-dependent kinase 1: more than a cell cycle regulator. *Br. J. Cancer* **129**, 1707–1716 (2023).

71. Palozola, K. C. *et al.* Mitotic transcription and waves of gene reactivation during mitotic exit. *Science* **358**, 119–122 (2017).

72. Abe, S. *et al.* The initial phase of chromosome condensation requires Cdk1-mediated phosphorylation of the CAP-D3 subunit of condensin II. *Genes Dev.* **25**, 863–874 (2011).

73. De Castro, I. J., Gil, R. S., Ligammari, L., Di Giacinto, M. L. & Vagnarelli, P. CDK1 and PLK1 coordinate the disassembly and reassembly of the nuclear envelope in vertebrate mitosis. *Oncotarget* **9**, 7763–7773 (2018).

74. Hayward, D., Alfonso-Pérez, T. & Gruneberg, U. Orchestration of the spindle assembly checkpoint by CDK1-cyclin B1. *FEBS Lett.* **593**, 2889–2907 (2019).

75. Enserink, J. M. & Kolodner, R. D. An overview of Cdk1-controlled targets and processes. *Cell Div.* **5**, 11 (2010).

76. Wang, Y. A direct role for GRASP65 as a mitotically regulated Golgi stacking factor. *EMBO J.* **22**, 3279–3290 (2003).

77. Bourne, Y. *et al.* Crystal Structure and Mutational Analysis of the Human CDK2 Kinase Complex with Cell Cycle–Regulatory Protein CksHs1. *Cell* **84**, 863–874 (1996).

78. Wolthuis, R. *et al.* Cdc20 and Cks Direct the Spindle Checkpoint-Independent Destruction of Cyclin A. *Mol. Cell* **30**, 290–302 (2008).

79. Linder, M. I. *et al.* Mitotic Disassembly of Nuclear Pore Complexes Involves CDK1- and PLK1-Mediated Phosphorylation of Key Interconnecting Nucleoporins. *Dev. Cell* **43**, 141-156.e7 (2017).

80. Ward, G. E. & Kirschner, M. W. Identification of cell cycle-regulated phosphorylation sites on nuclear lamin C. *Cell* **61**, 561–577 (1990).

81. Heald, R. & McKeon, F. Mutations of phosphorylation sites in lamin A that prevent nuclear lamina disassembly in mitosis. *Cell* **61**, 579–589 (1990).

82. Naetar, N. *et al.* LAP2alpha maintains a mobile and low assembly state of A-type lamins in the nuclear interior. *eLife* **10**, e63476 (2021).

83. Serpico, A. F., Febbraro, F., Pisauro, C. & Grieco, D. Compartmentalized control of Cdk1 drives mitotic spindle assembly. *Cell Rep.* **38**, 110305 (2022).

84. Mchedlishvili, N., Matthews, H. K., Corrigan, A. & Baum, B. Two-step interphase microtubule disassembly aids spindle morphogenesis. *BMC Biol.* **16**, 14 (2018).

85. Guo, L. *et al.* Phosphorylation of importin-α1 by CDK1–cyclin B1 controls mitotic spindle assembly. *J. Cell Sci.* **132**, jcs232314 (2019).

86. Clarke, P. R. & Zhang, C. Spatial and temporal coordination of mitosis by Ran GTPase. *Nat. Rev. Mol. Cell Biol.* **9**, 464–477 (2008).

87. Clute, P. & Pines, J. Temporal and spatial control of cyclin B1 destruction in metaphase. *Nat. Cell Biol.* **1**, 82–87 (1999).

88. Fujimitsu, K., Grimaldi, M. & Yamano, H. Cyclin-dependent kinase 1–dependent activation of APC/C ubiquitin ligase. *Science* **352**, 1121–1124 (2016).

89. Shevah-Sitry, D., Miniowitz-Shemtov, S., Teichner, A., Kaisari, S. & Hershko, A. Role of phosphorylation of Cdc20 in the regulation of the action of APC/C in mitosis. *Proc. Natl. Acad. Sci.* **119**, e2210367119 (2022).

90. Kabeche, L. & Compton, D. A. Cyclin A regulates kinetochore microtubules to promote faithful chromosome segregation. *Nature* **502**, 110–113 (2013).

91. Hayward, D. *et al.* CDK1-CCNB1 creates a spindle checkpoint–permissive state by enabling MPS1 kinetochore localization. *J. Cell Biol.* **218**, 1182–1199 (2019).

92. Basu, S. *et al.* The Hydrophobic Patch Directs Cyclin B to Centrosomes to Promote Global CDK Phosphorylation at Mitosis. *Curr. Biol.* **30**, 883-892.e4 (2020).

93. Takizawa, C. G. & Morgan, D. O. Control of mitosis by changes in the subcellular location of cyclin-B1–Cdk1 and Cdc25C. *Curr. Opin. Cell Biol.* **12**, 658–665 (2000).

94. Gavet, O. & Pines, J. Activation of cyclin B1–Cdk1 synchronizes events in the nucleus and the cytoplasm at mitosis. *J. Cell Biol.* **189**, 247–259 (2010).

95. Glotzer, M., Murray, A. W. & Kirschner, M. W. Cyclin is degraded by the ubiquitin pathway. *Nature* **349**, 132–138 (1991).

96. Jin, L., Williamson, A., Banerjee, S., Philipp, I. & Rape, M. Mechanism of Ubiquitin-Chain Formation by the Human Anaphase-Promoting Complex. *Cell* **133**, 653–665 (2008).

97. Schreiber, A. *et al.* Structural basis for the subunit assembly of the anaphase-promoting complex. *Nature* **470**, 227–232 (2011).

98. Kramer, E. R., Scheuringer, N., Podtelejnikov, A. V., Mann, M. & Peters, J.-M. Mitotic Regulation of the APC Activator Proteins CDC20 and CDH1. *Mol. Biol. Cell* **11**, 1555–1569 (2000).

99. Davey, N. E. & Morgan, D. O. Building a Regulatory Network with Short Linear Sequence Motifs: Lessons from the Degrons of the Anaphase-Promoting Complex. *Mol. Cell* **64**, 12–23 (2016).

100. Xu, C. & Min, J. Structure and function of WD40 domain proteins. *Protein Cell* **2**, 202–214 (2011).

101. Tian, W. *et al.* Structural analysis of human Cdc20 supports multisite degron recognition by APC/C. *Proc. Natl. Acad. Sci.* **109**, 18419–18424 (2012).

102. Di Fiore, B. *et al.* The ABBA Motif Binds APC/C Activators and Is Shared by APC/C Substrates and Regulators. *Dev. Cell* **32**, 358–372 (2015).

103. Diella, F. Understanding eukaryotic linear motifs and their role in cell signaling and regulation. *Front. Biosci.* **Volume**, 6580 (2008).

104. Burton, J. L. & Solomon, M. J. D box and KEN box motifs in budding yeast Hsl1p are required for APC-mediated degradation and direct binding to Cdc20p and Cdh1p. *Genes Dev.* **15**, 2381–2395 (2001).

105. Alfieri, C., Zhang, S. & Barford, D. Visualizing the complex functions and mechanisms of the anaphase promoting complex/cyclosome (APC/C). *Open Biol.* **7**, 170204 (2017).

106. Yamano, H. The role of the destruction box and its neighbouring lysine residues in cyclin B for anaphase ubiquitin-dependent proteolysis in fission yeast: defining the D-box receptor. *EMBO J.* **17**, 5670–5678 (1998).

107. Chao, W. C. H., Kulkarni, K., Zhang, Z., Kong, E. H. & Barford, D. Structure of the mitotic checkpoint complex. *Nature* **484**, 208–213 (2012).

108. He, J. *et al.* Insights into Degron Recognition by APC/C Coactivators from the Structure of an Acm1-Cdh1 Complex. *Mol. Cell* **50**, 649–660 (2013).

109. Pfleger, C. M. & Kirschner, M. W. The KEN box: an APC recognition signal distinct from the D box targeted by Cdh1. *Genes Dev.* **14**, 655–665 (2000).

110. Lu, D. *et al.* Multiple mechanisms determine the order of APC/C substrate degradation in mitosis. *J. Cell Biol.* **207**, 23–39 (2014).

111. Guharoy, M., Lazar, T., Macossay-Castillo, M. & Tompa, P. Degron masking outlines degronons, co-degrading functional modules in the proteome. *Commun. Biol.* **5**, 445 (2022).

112. Zhang, Z. *et al.* Recombinant expression, reconstitution and structure of human anaphase-promoting complex (APC/C). *Biochem. J.* **449**, 365–371 (2013).

113. Barford, D. Structural insights into anaphase-promoting complex function and mechanism. *Philos. Trans. R. Soc. B Biol. Sci.* **366**, 3605–3624 (2011).

114. Chang, L., Zhang, Z., Yang, J., McLaughlin, S. H. & Barford, D. Atomic structure of the APC/C and its mechanism of protein ubiquitination. *Nature* **522**, 450–454 (2015).

115. Zhang, S. *et al.* Molecular mechanism of APC/C activation by mitotic phosphorylation. *Nature* **533**, 260–264 (2016).

116. Alfieri, C., Tischer, T. & Barford, D. A unique binding mode of Nek2A to the APC /C allows its ubiquitination during prometaphase. *EMBO Rep.* **21**, e49831 (2020).

117. Perez-Riba, A. & Itzhaki, L. S. The tetratricopeptide-repeat motif is a versatile platform that enables diverse modes of molecular recognition. *Curr. Opin. Struct. Biol.* **54**, 43–49 (2019).

118. Bruno, S. *et al.* CDC20 in and out of mitosis: a prognostic factor and therapeutic target in hematological malignancies. *J. Exp. Clin. Cancer Res.* **41**, 159 (2022).

119. Suganuma, T., Pattenden, S. G. & Workman, J. L. Diverse functions of WD40 repeat proteins in histone recognition: Figure 1. *Genes Dev.* **22**, 1265–1268 (2008).

120. Izawa, D. & Pines, J. How APC/C–Cdc20 changes its substrate specificity in mitosis. *Nat. Cell Biol.* **13**, 223–233 (2011).

121. Darling, S. *et al.* The C-terminal disordered loop domain of Apc8 unlocks APC/C mitotic activation. *Cell Rep.* **43**, 114262 (2024).

122. Chang, L., Zhang, Z., Yang, J., McLaughlin, S. H. & Barford, D. Molecular architecture and mechanism of the anaphase-promoting complex. *Nature* **513**, 388–393 (2014).

123. Kimata, Y., Baxter, J. E., Fry, A. M. & Yamano, H. A Role for the Fizzy/Cdc20 Family of Proteins in Activation of the APC/C Distinct from Substrate Recruitment. *Mol. Cell* **32**, 576–583 (2008).

124. Floyd, S., Pines, J. & Lindon, C. APC/CCdh1 Targets Aurora Kinase to Control Reorganization of the Mitotic Spindle at Anaphase. *Curr. Biol.* **18**, 1649–1658 (2008).

125. Marangos, P., Verschuren, E. W., Chen, R., Jackson, P. K. & Carroll, J. Prophase I arrest and progression to metaphase I in mouse oocytes are controlled by Emi1-dependent regulation of APCCdh1. *J. Cell Biol.* **176**, 65–75 (2007).

126. Pesin, J. A. & Orr-Weaver, T. L. Regulation of APC/C Activators in Mitosis and Meiosis. *Annu. Rev. Cell Dev. Biol.* **24**, 475–499 (2008).

127. Yamano, H. APC/C: current understanding and future perspectives. *F1000Research* **8**, 725 (2019).

128. Fujimitsu, K. & Yamano, H. PP2A-B56 binds to Apc1 and promotes Cdc20 association with the APC/C ubiquitin ligase in mitosis. *EMBO Rep.* **21**, e48503 (2020).

129. Garnett, M. J. *et al.* UBE2S elongates ubiquitin chains on APC/C substrates to promote mitotic exit. *Nat. Cell Biol.* **11**, 1363–1369 (2009).

130. Yu, H., King, R. W., Peters, J.-M. & Kirschner, M. W. Identification of a novel ubiquitin-conjugating enzyme involved in mitotic cyclin degradation. *Curr. Biol.* **6**, 455–466 (1996).

131. Meyer, H.-J. & Rape, M. Enhanced Protein Degradation by Branched Ubiquitin Chains. *Cell* **157**, 910–921 (2014).

132. Zhou, Z., He, M., Shah, A. A. & Wan, Y. Insights into APC/C: from cellular function to diseases and therapeutics. *Cell Div.* **11**, 9 (2016).

133. Cavazza, T., Malgaretti, P. & Vernos, I. The sequential activation of the mitotic microtubule assembly pathways favors bipolar spindle formation. *Mol. Biol. Cell* **27**, 2935–2945 (2016).

134. Beswick, R. W., Ambrose, H. E. & Wagner, S. D. Nocodazole, a microtubule depolymerising agent, induces apoptosis of chronic lymphocytic leukaemia cells associated with changes in Bcl-2 phosphorylation and expression. *Leuk. Res.* **30**, 427–436 (2006).

135. Kelly, A., Wickliffe, K. E., Song, L., Fedrigo, I. & Rape, M. Ubiquitin Chain Elongation Requires E3-Dependent Tracking of the Emerging Conjugate. *Mol. Cell* **56**, 232–245 (2014).

136. Liu, S.-T., Zhang, H., & Department of Biological Sciences, University of Toledo, 2801 West Bancroft St., Toledo, OH 43606, USA. The mitotic checkpoint complex (MCC): looking back and forth after 15 years. *AIMS Mol. Sci.* **3**, 597–634 (2016).

137. Yamaguchi, M. *et al.* Cryo-EM of Mitotic Checkpoint Complex-Bound APC/C Reveals Reciprocal and Conformational Regulation of Ubiquitin Ligation. *Mol. Cell* **63**, 593–607 (2016).

138. Bansal, S. & Tiwari, S. Mechanisms for the temporal regulation of substrate ubiquitination by the anaphase-promoting complex/cyclosome. *Cell Div.* **14**, 14 (2019).

139. Stewart, S. & Fang, G. Anaphase-Promoting Complex/Cyclosome Controls the Stability of TPX2 during Mitotic Exit. *Mol. Cell. Biol.* **25**, 10516–10527 (2005).

140. Hein, J. B., Hertz, E. P. T., Garvanska, D. H., Kruse, T. & Nilsson, J. Distinct kinetics of serine and threonine dephosphorylation are essential for mitosis. *Nat. Cell Biol.* **19**, 1433–1440 (2017).

141. Labit, H. *et al.* Dephosphorylation of Cdc20 is required for its C-box-dependent activation of the APC/C: Dephosphorylation-driven activation of the APC/C. *EMBO J.* **31**, 3351–3362 (2012).

142. Jones, K. T. Meiosis in oocytes: predisposition to aneuploidy and its increased incidence with age. *Hum. Reprod. Update* **14**, 143–158 (2008).

143. Rieder, C. L., Cole, R. W., Khodjakov, A. & Sluder, G. The checkpoint delaying anaphase in response to chromosome monoorientation is mediated by an inhibitory signal produced by unattached kinetochores. *J. Cell Biol.* **130**, 941–948 (1995).

144. Fischer, E. S. KINETOCHORE-CATALYZED MCC formation: A structural perspective. *IUBMB Life* **75**, 289–310 (2023).

145. London, N., Ceto, S., Ranish, J. A. & Biggins, S. Phosphoregulation of Spc105 by Mps1 and PP1 Regulates Bub1 Localization to Kinetochores. *Curr. Biol.* **22**, 900–906 (2012).

146. Vleugel, M. *et al.* Arrayed BUB recruitment modules in the kinetochore scaffold KNL1 promote accurate chromosome segregation. *J. Cell Biol.* **203**, 943–955 (2013).

147. London, N. & Biggins, S. Mad1 kinetochore recruitment by Mps1-mediated phosphorylation of Bub1 signals the spindle checkpoint. *Genes Dev.* **28**, 140–152 (2014).

148. Faesen, A. C. *et al.* Basis of catalytic assembly of the mitotic checkpoint complex. *Nature* **542**, 498–502 (2017).

149. Tipton, A. R. *et al.* BUBR1 and Closed MAD2 (C-MAD2) Interact Directly to Assemble a Functional Mitotic Checkpoint Complex. *J. Biol. Chem.* **286**, 21173–21179 (2011).

150. Tang, Z., Bharadwaj, R., Li, B. & Yu, H. Mad2-Independent Inhibition of APCCdc20 by the Mitotic Checkpoint Protein BubR1. *Dev. Cell* **1**, 227–237 (2001).

151. Kulukian, A., Han, J. S. & Cleveland, D. W. Unattached Kinetochores Catalyze Production of an Anaphase Inhibitor that Requires a Mad2 Template to Prime Cdc20 for BubR1 Binding. *Dev. Cell* **16**, 105–117 (2009).

152. Alfieri, C. *et al.* Molecular basis of APC/C regulation by the spindle assembly checkpoint. *Nature* **536**, 431–436 (2016).

153. Choi, E. *et al.* BubR1 acetylation at prometaphase is required for modulating APC/C activity and timing of mitosis. *EMBO J.* **28**, 2077–2089 (2009).

154. Kraft, C., Vodermaier, H. C., Maurer-Stroh, S., Eisenhaber, F. & Peters, J.-M. The WD40 Propeller Domain of Cdh1 Functions as a Destruction Box Receptor for APC/C Substrates. *Mol. Cell* **18**, 543–553 (2005).

155. Qin, L., Guimarães, D. S. P. S. F., Melesse, M. & Hall, M. C. Substrate Recognition by the Cdh1 Destruction Box Receptor Is a General Requirement for APC/CCdh1-mediated Proteolysis. *J. Biol. Chem.* **291**, 15564–15574 (2016).

156. Thomas, C. *et al.* A prometaphase mechanism of securin destruction is essential for meiotic progression in mouse oocytes. *Nat. Commun.* **12**, 4322 (2021).

157. Di Fiore, B. & Pines, J. How cyclin A destruction escapes the spindle assembly checkpoint. *J. Cell Biol.* **190**, 501–509 (2010).

158. Lara-Gonzalez, P., Westhorpe, F. G. & Taylor, S. S. The Spindle Assembly Checkpoint. *Curr. Biol.* **22**, R966–R980 (2012).

159. Den Elzen, N. & Pines, J. Cyclin a Is Destroyed in Prometaphase and Can Delay Chromosome Alignment and Anaphase. *J. Cell Biol.* **153**, 121–136 (2001).

160. Levasseur, M. D., Thomas, C., Davies, O. R., Higgins, J. M. G. & Madgwick, S. Aneuploidy in Oocytes Is Prevented by Sustained CDK1 Activity through Degron Masking in Cyclin B1. *Dev. Cell* **48**, 672-684.e5 (2019).

161. Arooz, T. *et al.* On the Concentrations of Cyclins and Cyclin-Dependent Kinases in Extracts of Cultured Human Cells. *Biochemistry* **39**, 9494–9501 (2000).

162. Bentley, A. M., Normand, G., Hoyt, J. & King, R. W. Distinct Sequence Elements of Cyclin B1 Promote Localization to Chromatin, Centrosomes, and Kinetochores during Mitosis. *Mol. Biol. Cell* **18**, 4847–4858 (2007).

163. Goda, T., Funakoshi, M., Suhara, H., Nishimoto, T. & Kobayashi, H. The N-terminal Helix of Xenopus Cyclins A and B Contributes to Binding Specificity of the Cyclin-CDK Complex. *J. Biol. Chem.* **276**, 15415–15422 (2001).

164. Petri, E. T., Errico, A., Escobedo, L., Hunt, T. & Basavappa, R. The Crystal Structure of Human Cyclin B. *Cell Cycle* **6**, 1342–1349 (2007).

165. Cho, K. F. *et al.* Split-TurboID enables contact-dependent proximity labeling in cells. *Proc. Natl. Acad. Sci.* **117**, 12143–12154 (2020).

166. Holland, A. J., Fachinetti, D., Han, J. S. & Cleveland, D. W. Inducible, reversible system for the rapid and complete degradation of proteins in mammalian cells. *Proc. Natl. Acad. Sci.* **109**, (2012).

167. Song, L. & Rape, M. Substrate-specific regulation of ubiquitination by the anaphase-promoting complex. *Cell Cycle* **10**, 52–56 (2011).

168. Zhang, Y. *et al.* Functional analysis of Cdc20 reveals a critical role of CRY box in mitotic checkpoint signaling. *Commun. Biol.* **7**, 164 (2024).

169. The UniProt Consortium. UniProt: the Universal Protein Knowledgebase in 2023.

170. Lane, S. I. R. & Jones, K. T. Non-canonical function of spindle assembly checkpoint proteins after APC activation reduces aneuploidy in mouse oocytes. *Nat. Commun.* **5**, 3444 (2014).

171. Touati, S. A. & Wassmann, K. How oocytes try to get it right: spindle checkpoint control in meiosis. *Chromosoma* **125**, 321–335 (2016).

172. Fang, G., Yu, H. & Kirschner, M. W. Direct Binding of CDC20 Protein Family Members Activates the Anaphase-Promoting Complex in Mitosis and G1. *Mol. Cell* **2**, 163–171 (1998).

173. Zeng, X. *et al.* Pharmacologic Inhibition of the Anaphase-Promoting Complex Induces A Spindle Checkpoint-Dependent Mitotic Arrest in the Absence of Spindle Damage. *Cancer Cell* **18**, 382–395 (2010).

174. Lub, S. *et al.* Inhibiting the anaphase promoting complex/cyclosome induces a metaphase arrest and cell death in multiple myeloma cells. *Oncotarget* **7**, 4062–4076 (2016).

175. Wang, M. & Casey, P. J. Protein prenylation: unique fats make their mark on biology. *Nat. Rev. Mol. Cell Biol.* **17**, 110–122 (2016).

176. Patra, D., Wang, S. X., Kumagai, A. & Dunphy, W. G. The Xenopus Suc1/Cks Protein Promotes the Phosphorylation of G2/M Regulators. *J. Biol. Chem.* **274**, 36839–36842 (1999).

177. Pines, J. Cell cycle: Reaching for a role for the Cks proteins. *Curr. Biol.* **6**, 1399–1402 (1996).

178. Wu, T. *et al.* The mechanism of acentrosomal spindle assembly in human oocytes. *Science* **378**, eabq7361 (2022).

179. Horakova, A., Konecna, M., Radonova, L. & Anger, M. Early onset of APC/C activity renders SAC inefficient in mouse embryos. *Front. Cell Dev. Biol.* **12**, 1355979 (2024).

180. Lu, D., Girard, J. R., Li, W., Mizrak, A. & Morgan, D. O. Quantitative framework for ordered degradation of APC/C substrates. *BMC Biol.* **13**, 96 (2015).

181. Brown, N. R. *et al.* Cyclin B and Cyclin A Confer Different Substrate Recognition Properties on CDK2. *Cell Cycle* **6**, 1350–1359 (2007).

182. Corey, D. R. & Abrams, J. M. Morpholino antisense oligonucleotides: tools for investigating vertebrate development. *Genome Biol.* **2**, REVIEWS1015 (2001).

183. Homer, H., Gui, L. & Carroll, J. A Spindle Assembly Checkpoint Protein Functions in Prophase I Arrest and Prometaphase Progression. *Science* **326**, 991–994 (2009).

184. Wei, L. *et al.* BubR1 is a spindle assembly checkpoint protein regulating meiotic cell cycle progression of mouse oocyte. *Cell Cycle* **9**, 1112–1121 (2010).

185. Chen, C. *et al.* The structural flexibility of MAD1 facilitates the assembly of the Mitotic Checkpoint Complex. *Nat. Commun.* **14**, 1529 (2023).

186. Van Zon, W. *et al.* The APC/C recruits cyclin B1–Cdk1–Cks in prometaphase before D box recognition to control mitotic exit. *J. Cell Biol.* **190**, 587–602 (2010).

187. Sears, R. M., May, D. G. & Roux, K. J. BioID as a Tool for Protein-Proximity Labeling in Living Cells. in *Enzyme-Mediated Ligation Methods* (eds. Nuijens, T. & Schmidt, M.) vol. 2012 299–313 (Springer New York, New York, NY, 2019).

188. Choi-Rhee, E., Schulman, H. & Cronan, J. E. Promiscuous protein biotinylation by *Escherichia coli* biotin protein ligase. *Protein Sci.* **13**, 3043–3050 (2004).

189. Schopp, I. M. *et al.* Split-BioID a conditional proteomics approach to monitor the composition of spatiotemporally defined protein complexes. *Nat. Commun.* **8**, 15690 (2017).

190. Kim, D. I. *et al.* An improved smaller biotin ligase for BioID proximity labeling. *Mol. Biol. Cell* **27**, 1188–1196 (2016).

191. Cho, K. F. *et al.* Proximity labeling in mammalian cells with TurboID and split-TurboID. *Nat. Protoc.* **15**, 3971–3999 (2020).

192. Green, N. Thermodynamics of the binding of biotin and some analogues by avidin. *Biochem. J.* **101**, 774–780 (1966).

193. Hubrecht, R. C. & Carter, E. The 3Rs and Humane Experimental Technique: Implementing Change. *Animals* **9**, 754 (2019).

194. Kim, D. I. & Roux, K. J. Filling the Void: Proximity-Based Labeling of Proteins in Living Cells. *Trends Cell Biol.* **26**, 804–817 (2016).

195. Ambekar, S. V., Beck, J. R. & Mair, G. R. TurboID Identification of Evolutionarily Divergent Components of the Nuclear Pore Complex in the Malaria Model Plasmodium berghei. *mBio* **13**, e01815-22 (2022).

196. Tsuji, A., Nakamura, T. & Shibata, K. Biotin-deficient diet induces chromosome misalignment and spindle defects in mouse oocytes. *Biosci. Biotechnol. Biochem.* **79**, 292–299 (2015).

197. Glotzer, M., Murray, A. W. & Kirschner, M. W. Cyclin is degraded by the ubiquitin pathway. *Nature* **349**, 132–138 (1991).

198. King, R. W., Glotzer, M. & Kirschner, M. W. Mutagenic analysis of the destruction signal of mitotic cyclins and structural characterization of ubiquitinated intermediates. *Mol. Biol. Cell* **7**, 1343–1357 (1996).

199. Aristarkhov, A. *et al.* E2-C, a cyclin-selective ubiquitin carrier protein required for the destruction of mitotic cyclins. *Proc. Natl. Acad. Sci.* **93**, 4294–4299 (1996).

200. Wickliffe, K. E., Lorenz, S., Wemmer, D. E., Kuriyan, J. & Rape, M. The Mechanism of Linkage-Specific Ubiquitin Chain Elongation by a Single-Subunit E2. *Cell* **144**, 769–781 (2011).

201. Au, S. W. N., Leng, X., Harper, J. W. & Barford, D. Implications for the Ubiquitination Reaction of the Anaphase-promoting Complex from the Crystal Structure of the Doc1/Apc10 Subunit. *J. Mol. Biol.* **316**, 955–968 (2002).

202. Wendt, K. S. *et al.* Crystal structure of the APC10/DOC1 subunit of the human anaphase-promoting complex. *Nat. Struct. Biol.* **8**, 784–788 (2001).

203. Santaguida, S., Tighe, A., D'Alise, A. M., Taylor, S. S. & Musacchio, A. Dissecting the role of MPS1 in chromosome biorientation and the spindle checkpoint through the small molecule inhibitor reversine. *J. Cell Biol.* **190**, 73–87 (2010).

204. Clift, D., So, C., McEwan, W. A., James, L. C. & Schuh, M. Acute and rapid degradation of endogenous proteins by Trim-Away. *Nat. Protoc.* **13**, 2149–2175 (2018).

205. Peters, J.-M. The anaphase promoting complex/cyclosome: a machine designed to destroy. *Nat. Rev. Mol. Cell Biol.* **7**, 644–656 (2006).

206. Kitajima, T. S., Ohsugi, M. & Ellenberg, J. Complete Kinetochore Tracking Reveals Error-Prone Homologous Chromosome Biorientation in Mammalian Oocytes. *Cell* **146**, 568–581 (2011).

207. McLean, J. R., Chaix, D., Ohi, M. D. & Gould, K. L. State of the APC/C: Organization, function, and structure. *Crit. Rev. Biochem. Mol. Biol.* **46**, 118–136 (2011).